ROLLING BEARING VIBRATIONS - THE EFFECTS OF VARYING COMPLIANCE, MANUFACTURING TOLERANCES AND WEAR

by

CURT STAFFAN SUNNERSJÖ

A Thesis Submitted in Fulfilment of the

Requirement for the degree of

Doctor of Philosophy

Faculty of Engineering

The University of Aston in Birmingham

AUGUST 1976

SUMMARY

In this study some common types of Rolling Bearing vibrations are analysed in depth both theoretically and experimentally. The study is restricted to vibrations in the radial direction of bearings having pure radial load and a positive radial clearance. The general vibrational behaviour of such bearings has been investigated with respect to the effects of varying compliance, manufacturing tolerances and the interaction between the bearing and the machine structure into which it is fitted. The equations of motion for a rotor supported by a bearing in which the stiffness varies with cage position has been set up and examples of solutions,obtained by digital simulation, is given. A method to calculate amplitudes and frequencies of vibration components due to out of roundness of the inner ring and varying roller diameters has been developed. The results from these investigations have been combined with a theory for bearing/machine frame interaction using mechanical impedance technique, thereby facilitating prediction of the vibrational behaviour of the whole set up. Finally, the effects of bearing fatigue and wear have been studied with particular emphasis on the use of vibration analysis for condition monitoring purposes. A number of monitoring methods have been tried and their effectiveness discussed.

The experimental investigation was carried out using two purpose-built rigs. For the purpose of analysis of the experimental measurements a digital mini computer was adapted for signal processing and a suite of programs was written. The program package performs several of the commonly used signal analysis processes and include all necessary input and output functions.

ACKNOWLEDGEMENTS

The author wishes to express his gratitude to the Department of Mechanical Engineering at the University of Aston for supplying funds and facilities to carry out this project. In particular I would like to thank my supervisor Professor E. Downham for his experienced advice and his readiness to offer assistance and encouragement throughout the course of the project. I would also like to thank all other academic and technical staff of the department who have in one way or another been involved in the work. Last but not least I would like to thank Mrs. D. Scott for her expert typing of my sadly untidy manuscript.

CONTENTS

NOTATION

A - Area of contact ellipse

a - Minor axis of contact ellipse

AM - Apparent mass

b - Major axis of contact ellipse

BP - Ball passage

d - Approach of two elastic bodies

D_c - Cage diameter

D_i - Inner ring diameter

D_o - Outer ring diameter

D_r - Rolling element diameter

DS - Dynamic stiffness

E - Elasticity modulus

e - Radial clearance

f_c - $2\pi\omega_c$

f_i - $2\pi\omega_i$

f_r - $2\pi\omega_r$

f_{rp} - Roller passage frequency

G - Shear modulus

h - Oil film thickness

K - Local stiffness

k - Eccentricity of contact zone

l - Roller length

LAG - Time lag in autocorrelation analysis

M - Rotor mass

MPAR - Monitoring parameter

N - No. of rolling elements

NODS - No. of data points .

NOS - No. of samples

NOTATION. continued...

o - Osculation

p - Pressure function

PCO - Probability of correct operation

Q - External force

q = $MPAR_{damaged}/MPAR_{good}$

Q_x - Horizontal reaction force

Q_y - Vertical reaction force

RP - Roller passage

SFREQ - Sampling frequency

TL - Trigger level

V - $2\pi/N$

V - Speed of roller over plane (in Chapter 3)

V_c - Speed of cage

V_i - Speed of inner ring

V_o - Speed of outer ring

W - Robustness of monitoring method

Z - Mechanical Impedance

α - Inclination of track

δ_x - Horizontal shaft centre displacement

δ_y - Vertical shaft centre displacement

η - Lubricant viscosity

ν - Poisson's ratio

ω_c - Angular cage speed

ω_i - Angular inner ring speed

ω_o - Angular outer ring speed

ω_{rp} - $f_{rp}/2\pi$

CHAPTER 1

INTRODUCTION

In recent years there has been a growing interest in techniques for condition monitoring of key components of mechanical systems. There exists a number of methods, based on vibration analysis, by which the condition of rolling element bearings can be monitored with some success. It was felt however, that in order to improve or replace existing techniques and for the user to feel confidence in using such techniques, there was a need for a more thorough understanding of the fundamental mechanisms relating the state of wear of a bearing to the vibrations this wear gives rise to. Having embarked upon such a line of study it soon became obvious, that a reliable understanding of the way in which a sound bearing excites vibrations, was a necessity, both for the understanding of the wear-vibration relationships in a worn bearing and also to avoid confusion between vibration components which occur naturally in a good bearing and vibrations due to deterioration of a worn bearing. A literature survey of papers concerned with various types of vibrations in rolling bearings revealed that there exists gaps on several important points in the knowledge of such vibrations. The fact that comparably little research effort has gone into this field (compare the very detailed investigation done on rolling bearing lubrication) is somewhat surprising, since the dynamic behaviour of the bearing is of vital importance for the quiet running properties of the bearing, and also for the accuracy with which a shaft or spindle supported by rolling bearings will run. There are even indications that the length of operational life of the bearing can be considerably

affected by dynamic effects, which is a fact not previously recognised. A further reason to improve the knowledge of vibration generation of rolling bearings is that if this process is well understood it provides a means with which to study the operation of the assembled bearing, both from the point of view of quality control and from the point of view of studying the effects of various design parameters such as radial clearance, number of rolling elements, cage pocket clearance and so on. Hence, the original aim of improving monitoring techniques for rolling bearings has been widened into a study of vibrations generated also in new bearings. This is done partly as a necessary and logical extension of the original scope, partly because of the interest in and importance of these phenomena in their own rights.

In this study attention has been concentrated on radial vibrations of bearings having radial loads. The bearing is assumed to be mounted in an application where the outer ring is stationary and the inner ring supports some sort of rotor or spindle, the movements of which near the bearing are restricted only by the actions of the bearing investigated, see Fig.1.1. This is obviously not an exhaustive treatment, but the described application is certainly a very common one, and one which allows analytical treatment. To get an overall view of the various types of vibrations occurring in rolling bearings, the types of vibrations can be divided into certain groups, see Fig. 1.3. An attempt to distinguish and define the elements in the process of vibration excitation and propagation is done in the block diagram of Fig. 1.2. This diagram should not be taken too literally, the boxes do not represent Transfer function in the strictly mathematical sense and there might be equally correct alternative ways of setting up the diagram.

It does however highlight what elements in the vibratory process that can be distinguished and which could be studied in more detail. The various types of vibrations of Fig. 1.3 will be discussed below and references to Fig. 1.2 will then be made and the meaning and properties of the block diagram discussed in more detail.

The first distinction to make is between externally excited vibrations and self excited vibrations, see Fig. 1.3. In the case of externally excited vibrations the bearing is not the origin of the exciting forces, which instead can come from for instance unbalance of the rotor or time varying rotor load. The properties of the bearing have an influence over what vibrations these external forces will excite and in Fig. 1.2 the boxes A and B are the ones of importance for this type of vibration. The way in which the external forces are transmitted through the bearing (box A) is discussed in Chapter 6, while the Mechanical Impedance of the bearing holder (box B) is investigated in Chapter 8.

Self excited vibrations can be defined as "Vibrations in which the alternating force that sustains the motion is created or controlled by the motion itself; when the motion stops the alternating force disappears" (den Hartog). The most fundamental type of self excited vibrations in rolling bearings is the so called Varying Compliance (VC) vibrations which arise due to the inherent properties of the bearing type and would occur also in ideal bearings being geometrically and elastically perfect. VC vibrations can crudely be said to arise because the stiffness of the bearing assembly varies according to the angular position of the cage. As will be

further explained in Chapter 2 the previous theory (Meldau) for VC vibrations is valid only for static or very slowly rotating bearings, i.e. for conditions where the rotor is always in static equilibrium. It was previously assumed that for a bearing running at normal speeds, the inertia of the rotor would only reduce the shaft movements compared to the static case, but that it would otherwise behave in much the same way as Meldau's theory predicts. As will be shown in Chapter 6, which investigates box C in Fig. 1.2, the inclusion of inertia forces in the VC vibration model gives an entirely different character to the solutions. In Chapter 6 a computer program, DYNSIM, was written to simulate the movements of a rotor supported by rolling bearings. The dynamic loads predicted can for normal operating conditions be of the same order as the static weight of the rotor. It has been possible to substantiate the theoretical model with several experimental runs.

An approximate model for VC vibrations can be set up if the rollers and raceways of the bearing are assumed to be absolutely rigid. Due to the geometry of the bearing assembly,the centre of the shaft supported by a bearing with positive clearance will move up and down relative to the outer ring,as the rollers pass under the load. Since this theory does not include inertia forces and flexibility of the components,it is called a Kinematic model. The Kinematic model for VC vibrations emerges as a special case of the theory for vibrations in real bearings described below. To summarise the three models for self excited vibrations in idealized bearings,one should note that the Kinematic model is valid only for small loads and low speeds (otherwise the assumption of zero elastic deflection does not hold true), Meldau's theory is valid for all loads but only low

speeds and the Dynamic model presented in Chapter 6 is valid for all loads and speeds. Meldau's theory reveals characteristics that cannot be explained by the Kinematic model and the Dynamic model reveals characteristics which cannot be explained by Meldau's theory.

The prime reason to develop the Kinematic theory was however not to describe VC vibrations but for the purpose of analysing vibrations due to form errors. In real bearings there inevitably exists form deviations from the theoretical design and the vibrations due to these form deviations will add to the previously described VC vibrations. The problem of calculating what vibrations these form deviations give rise to becomes very complex if the complete Dynamic model is used. It is for this reason that the Kinematic model was developed. It corresponds to box D in Fig. 1.2 and has successfully been applied to the vibration types within the dashed line in Fig. 1.3. The Kinematic model works best for low speeds and loads and where the displacement function of the rotor is smooth and continuous. Unlike the Dynamic model and Meldau's model it always gives a statically determinatesituation, i.e. only two rollers at a time carry the load.

Vibrations as a function of form deviations have been studied in a number of papers, see Chapter 2, but the results of the investigation given in Chapter 7 adds considerable new information to this subject. Only two types of form errors, which seem particularly important in practice, namely waviness of inner ring and non uniform roller diameters, have been studied. Most previous papers study bearings in rather artificial situations like "free" bearings having no bearing house and loaded only with a small, axial load. In fact, no paper has been found that studies effects of form

deviations in radially loaded bearings and takes into account the important effect of clearance. This effect is included in the Kinematic model developed in Chapter 7 for vibrations due to inner ring out of roundness. The idea of describing the out of roundness in terms of a Fourier series has been taken up from a previous paper, but by using digital technique to analyse the form deviations, the accuracy has been greatly improved. In earlier works it has in some cases been possible to discover a correlation between inner ring waviness and bearing vibrations for the uncomplicated case of lightly axially loaded bearings, but with the methods used in Chapter 7 it has been possible to repeatedly predict the frequencies and relative amplitudes of vibration components arising from inner ring waviness for cases of realistic loads and speeds and for bearings with radial clearance.

The effect of non-uniform roller diameters is a much simpler theoretical problem than the effect of inner ring waviness. It is studied in Chapter 7 using a simplified, almost intuitive, Kinematic model. Several previous papers have paid attention to the possibility that varying roller diameters could cause vibrations. Some of these employ highly theoretical methods where the effects of varying stiffness in different directions due to varying roller diameters in pre-loaded bearings can be shown to excite vibrations. It seems however that the most obvious way in which to analyse this effect has been overlooked. It is shown in Chapter 7 how the frequencies and relative amplitudes of these vibration components can be accurately calculated if the size of the diameter differences and the order in which the rollers are located in the cage is known.

In airborne noise from rotating bearings the rattle of the cage is often a prominent part. The sounds emanate from transient loads between the cage and individual rollers. Since these loads are directed tangentially only a small part of them are propagated through the structure in which the bearing is mounted. Because of its transient nature and erratic occurrence this phenomena is not well suited for analytical treatment and is not investigated in this thesis.

In a new bearing all the previously described vibration types occur. As the bearing becomes worn during operation, the surfaces of its components will deteriorate and the vibration characteristics of the bearing change. If the relationships between surface damages and vibrations generated are known, it is possible to determine the state of wear of the bearing by measuring and analysing the vibrations excited during operation. Such methods of inspection, which do not interfere with the normal operation of the bearing is of great interest in applications where sudden breakdowns can be catastrophic such as bearings in aircraft engines, bearings in navigational gyroscopes and so on. Also in applications where breakdowns do not put life at risk the commercial gain of knowing beforehand when a bearing is getting near the end of its life can be very considerable. The obvious example is continuously operating process plants where an unexpected breakdown can mean days of lost production before a spare bearing has been obtained and fitted. Prior knowledge of the state of the bearing would allow for the replacement of the bearing to take place at some regular shutdown for maintenance. One reason why monitoring of bearings is so useful is that prediction of bearing life is difficult. Rolling bearings

have an extremely wide scatter of operational life - a factor of ten between the best and worst 10% of a batch running under the same conditions is normal. This means that for the designer to be reasonably confident of trouble free operation of a set of bearings, he must over dimension the bearings considerably. By choosing smaller bearings combined with an adequate monitoring system, it might in many cases be possible to obtain higher reliability to a lower total cost.

The same sort of general model applies, whether the surface imperfections of a particular bearing are due to manufacturing errors, or arise as an effect of wear. Thus, box D in fig. 1.2 governs the vibration generation also for vibrations due to wear. Chapter 9 is devoted to such vibrations and condition monitoring methods based on vibration analysis. Subsurface fatigue (flaking and pitting), as well as deterioration due to abrasive wear, have been investigated. Worn bearings have been obtained by running bearings under heavy load in a purpose built wear rig (see Chapter 4). The bearing surfaces have been inspected regularly during these runs, and when signs of wear have occurred, the bearings have been mounted in a vibration test rig (see Chapter 4) and run under various loads and speeds. It has been possible to detect characteristic changes of the vibrations emitted, which are correlated with the occurrence of damage to the components of the bearings.

Just as wear causes vibrations, vibrations might cause wear. It seems reasonable to assume that the oscillating forces between rings and rollers significantly affect the rate of wear progression. There

is thus a feed back loop to box E, (fig.1.2) determining the increase of the parameter X, which represents the surface irregularities in some suitable way. A systematic investigation of box E would require wearing out large series of bearings, and this is not a practical proposition with the sort of facilities available. Hence, box E has not been included in the study of the wear-vibration properties of bearings in this thesis. There are however practical experiences that support the assumption of the type of model used. It is often observed that wear in bearings, once started, progresses in an accelerative way, and this is exactly the sort of result one would expect in the presence of a feed back loop (increase of wear, causes increase of vibration, causes increase of wear, and so on).

The mounting of bearings in a machine structure has a fundamental effect on both the generation and propagation of vibrations (box B in fig. 1.2). An approximate way of studying this problem is presented in Chapter 8. The method is based on experimentally determined functions of Mechanical Impedance of the bearing pedestal. These functions have been obtained by use of transient excitation techniques. Although this method of measuring impedance is not new, the occurrence of commercially available digital recorders gives the method added attraction as regards accuracy and speed.

The signal processing is obviously a crucial part of this work. This has been done mainly with a digital mini computer adapted for signal analysis. A program package for this purpose was written, and is presented in Appendix II. Some special aspects of signal processing

with digital techniques is discussed in Chapter 5, and the theoretical background to Spectral Analysis is described in Appendix I.

Dimensions are in SI units throughout the thesis, unless otherwise is explicitly stated.

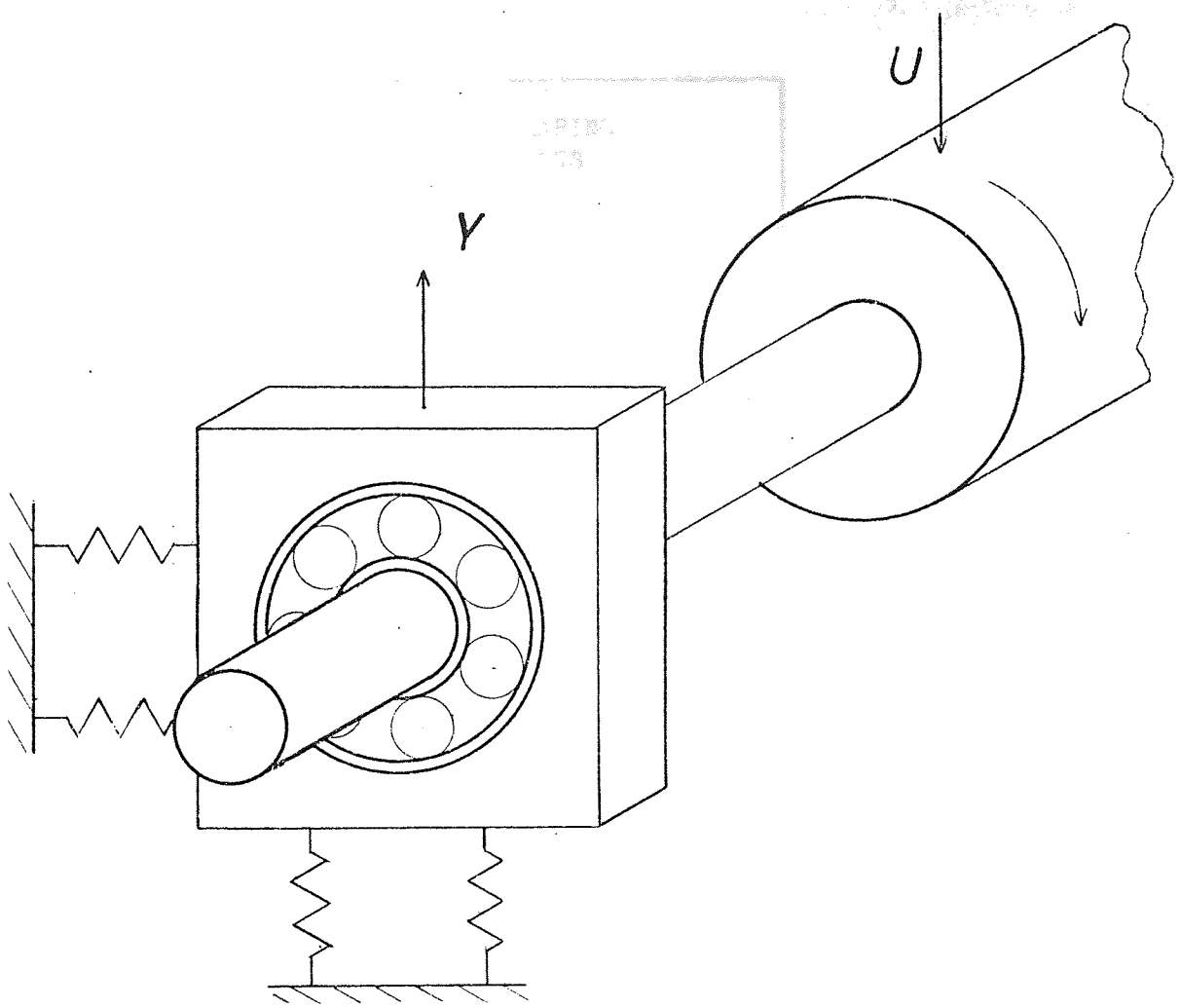

Fig 1.1 The type of rotor - bearing - pedestal arrangement studied in this thesis.

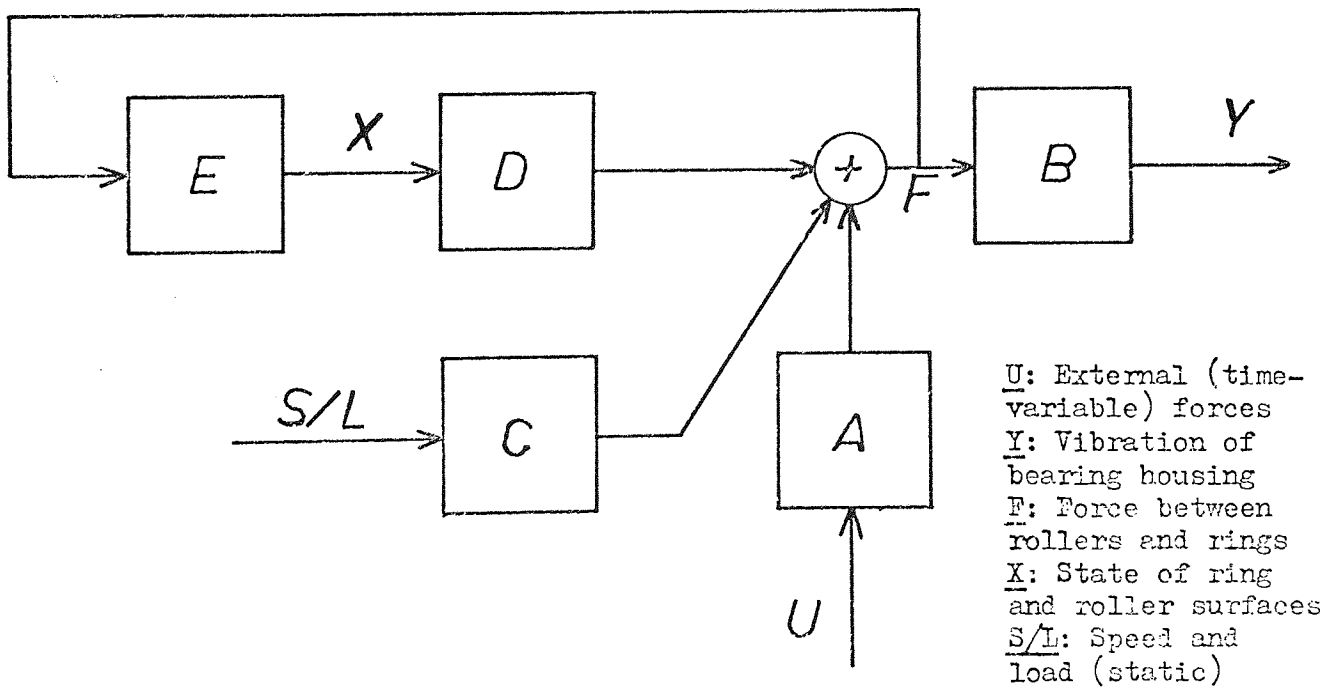

Fig 1.2 Factors and relationships in the vibratory process.

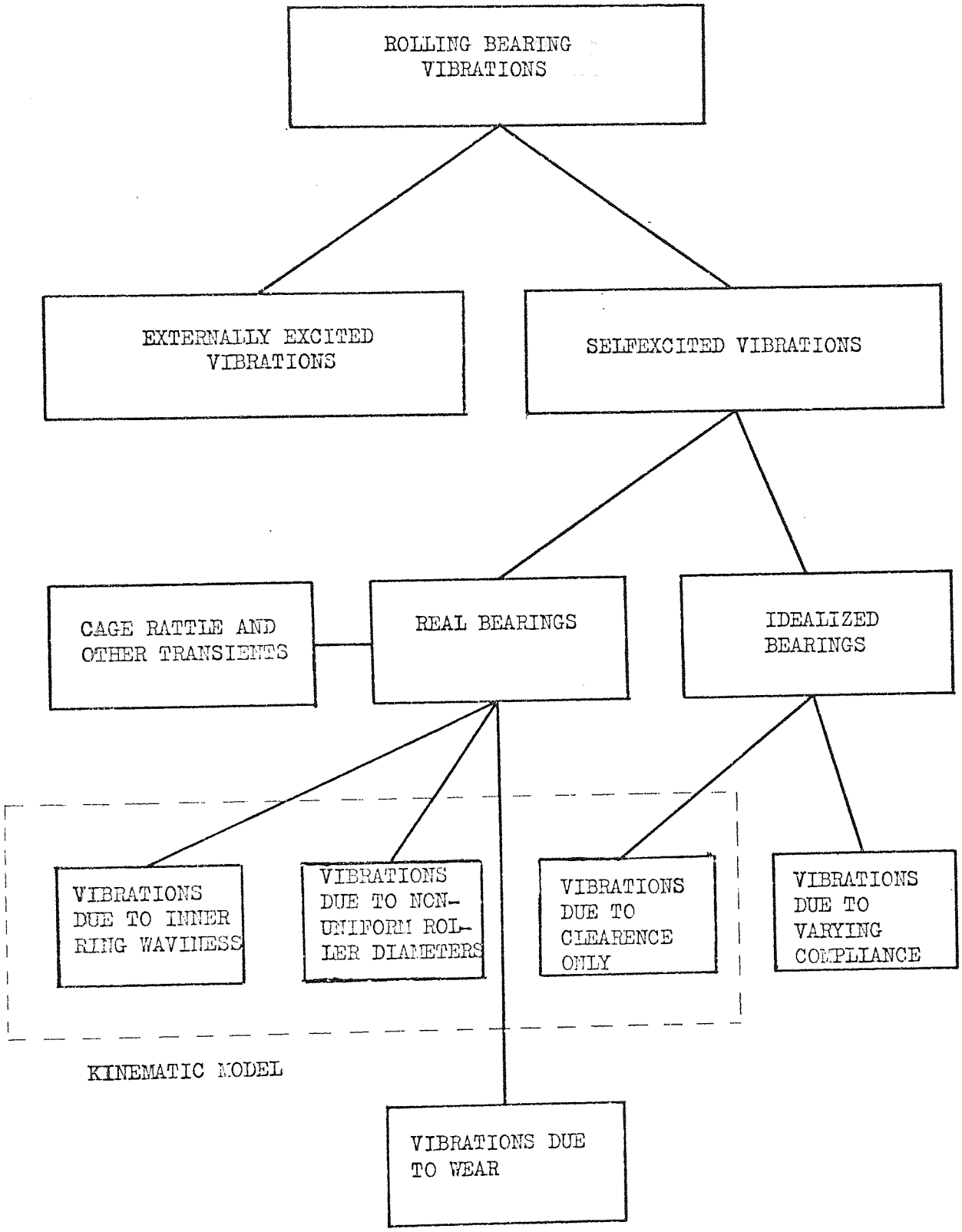

Fig 1.3 Breakdown of Rolling Bearing vibrations.

CHAPTER 2

SOME PREVIOUS STUDIES OF ROLLING BEARING VIBRATIONS

This review, which is not claimed to be exhaustive, means to show how the knowledge of rolling bearing vibrations has evolved up to the present state of the art. In the same way as in the rest of the thesis, it will be distinguished between vibrations in idealized bearing, vibrations in real bearings and vibrations due to wear, the latter being essentially of interest from the point of view of condition monitoring.

The most fundamental type of rolling bearing vibration is the Varying Compliance vibration. It arises because the geometric and elastic characteristics of the bearing assembly varies according to the cage position. This effect was studied in a report by Perret published in 1950, see ref (19). Perret's investigation is purely theoretical and deals with a deep groove ball bearing having ten balls. To calculate the local deformations (as opposed to bending of the rings) he makes use of the force-deformation relationships given by the Hertzian theory, see Chapter 3. The Hertzian theory gives a stiffness coefficient that depends on deformation, i.e. a non-linear force-deformation relationship. An additional cause of non-linearity, which remains also when the local stiffness coefficient is constant (as in roller bearings), emerges if a complete bearing assembly with radial clearance is considered. In such a bearing a varying number of rollers carry the load, so that the assembly stiffness changes step wise when a rolling element enters or leaves the load carrying zone. The assembly stiffness will be a

function of the local stiffness, the clearance, the external load and the angular position of the cage. Perret calculated the displacement of the centre of the inner ring with a constant external load for cage positions such that either a ball or a gap between two balls were directly under the load line. The calculation showed that generally the position of the inner ring centre would not be the same at these two cage positions. Thus, as the bearing rotates the centre of the shaft will move up and down as the balls pass under the load. The period of the movement will be $2\pi/N$, where N is the number of balls in the bearing. Perret found that at certain combinations of load, clearance and N, the vertical movement could be made zero. These combinations would then give a particularly steady and silent running bearing.

Perret's approach is however incomplete in that he only studies the bearing at the instants when the balls are arranged symmetrically around the load line, i.e. with either a ball or a ball gap directly under the load. In the intermediate cage positions however, the balls are non-symmetrically arranged, which means that when loaded with a vertical load, the centre of the inner ring will undergo a horizontal as well as a vertical displacement. Thus, generally the shaft centre will follow a closed trace or locus in a plane perpendicular to the axis around which the shaft rotates. A complete treatment of these shaft movements was given by Meldau in 1951, see ref (20). The case where horizontal movements are also considered is a great deal more complicated than the case treated by Perret. Meldau has developed expressions for vertical and horizontal displacements as functions of external load, radial clearance and local stiffness for a bearing having ten rollers or ten balls. The operating

parameters are combined into one parameter, with which the resulting displacements can be obtained as a function of cage position from a graph. By reading this graph for consecutive values of cage positions ,the locus of the shaft centre can be constructed. Examples of this is shown for a number of parameter combinations both for ball and roller bearings. As could be expected, it appears that in general the locii for roller bearings have sharper corners and undergo more abrupt changes than in the case of the ball bearings. The graph covers most normal operating conditions but is valid only for bearings with ten rolling bodies.

Since both Perret and Meldau made their calculations on bearings with ten balls, it is possible to compare their results. Perret claims that for certain combinations of load and clearance no vertical movement and a particularly silent and steady running bearing would result. For such a combination of load and clearance Meldau's method gives a similar result, no vertical movement, but Perret's claim for particular steadiness of running is not fulfilled because Meldau's graphs show that this combination of parameters would instead give a large horizontal movement. A study of Meldau's results shows that there exists no parameter combinations giving zero both vertical and horizontal movements although, there are combination giving zero vertical or zero horizontal movements. Meldau underlines that his method applies only to static cases or cases where the shaft rotates extremely slowly. Meldau's paper is an important work and has become something of a classic in the study of rolling bearing vibrations.

A special case of VC vibrations,which is easier to treat analytically was investigated by Perret in 1952, see ref (21). In bearings having large clearances, few rollers and moderate load,it will be quite common that only two rollers at a time carry the load. This makes the system statically determinate which simplifies the theory, and Perret gives a more detailed account of the shaft movements for this case. A further simplification of this statically determinate case was made by Barakov and Shavrin in 1969, see ref(22). In this paper the rings and rollers are assumed to be absolutely rigid so that no local deformations occur. Due to the geometrical changes that occur when the cage rotates,there will still be a vertical and horizontal movement of the shaft centre at roller passage (RP) frequency. Barakov and Shavrin also show how the displacement functions can be expanded into Fourier series, thereby demonstrating that vibrations can be expected, except for at RP frequency also at harmonics thereof. Unfurtunately there appears to be an arithmetic error in the calculation of the Fourier coefficients although the main character of the solutions is correct. The approximation with rigid components has been used in this thesis in Chapter 7 to study effects of form errors of bearing components on vibrations, where a complete,statically undeterminate model would have been too cumbersome to use. Tallian and Gustafsson published a survey of research done on bearing vibrations in 1964, ref (23), which to a large extent is based on a report by Gustafsson in 1963, ref (24). This report is an ambitious investigation of the whole problem of bearing noise and vibration, see also below. For the part that deals with VC vibrations, Gustafsson has used a digital computer to calculate the shaft movements according to Meldau's theory. Analogous to in Barakov and Shavrin's work, the Fourier coefficients are then calculated by computer.

It is claimed that the curves presented are valid for any number of rolling bodies in the bearing. There is no detailed motivation of this in refs. (23) or (24) and with reference to Meldau's paper it is difficult to see how this could be the case.

None of the above mentioned references give any experimental verification of VC vibrations. In a paper from 1962, ref.(25), Tamura and Taniguchi have measured the position of a shaft supported by a ball bearing for different cage positions and found movements that correspond to those predicted by Meldau. With the shaft running at normal speed they also found vibrations of the bearing fundament at ball passage frequency. Unfortunately no line spectrum of the vibrations was presented so the results are difficult to interpret.

Except for the radial VC vibrations a few other types of vibrations can occur in idealized bearings. Tamura and Taniguchi have published a series of papers, refs. (26) to (28), dealing with self excited vibrations in the axial direction of rotors supported by deep groove ball bearings. These vibrations are said to be of particular importance in small electrical machines. Gustafsson, ref.(24) has studied the flexural vibrations of the outer ring of a bearing which is not clamped in a bearing housing but where the outer ring is allowed to bend freely. It is then assumed that the outer ring will deform into a polygon with a number of corners equal to the number of rolling bodies, and that this polygon will rotate with the ball or roller set.

In previous sections attention was focussed on the vibrational properties of idealized bearings. In a real bearing there will always exist deviations from the theoretical design as regards dimensions and surface properties. These inaccuracies are widely regarded as being of major importance to the noise generation of rolling bearings. In the context of bending vibrations of the outer ring the concept of "free" bearings was mentioned in the previous paragraph. A lot of work done on vibrations due to form deviations have been done on free bearings, i.e. bearings mounted on a smooth running shaft with no real bearing house and usually only with a very light axial load. This is probably so because running bearings in this way is a much used means of quality control within the industry. Originally the vibrations were checked by hand or by listening to the bearing, later electronic instruments have been introduced. This is an appealing form of quality control because it is fast and cheap and it allows testing of the complete assembly. The investigation of relationships between form errors and vibrations in free bearings are therefore important from the manufacturers' point of view, but for the bearing user it is more interesting to be able to predict vibrational behaviour of a bearing which is properly mounted (clamped or press fitted) and run with realistic load and speed. A bearing which is noisy when run as a free bearing is likely to be noisy also in a practical application, but generally one must conclude that results from free bearing tests can not easily be applied to any other running conditions in a detailed way.

An early experimental study of the correlation between vibrations and bearing accuracy was done by Lohman in 1953, ref.(29). Contrary to

earlier standards for bearing noise and accuracy, Lohman showed that for free bearings the relative maximum displacement between inner and outer rings is not a critical factor, but that instead the high frequency movements generated by waviness and imperfections of the bearing surfaces have a direct effect on noise generation. Lohman also measured and analysed the frequency composition of noise generated by bearings mounted in electrical motors. He found that the frequency spectra were rather unstable and could change considerably after a period of time. Attempts to reduce the noise level by changing the clearance of the bearings were not successful, but by stiffening the endplates of the motor, where the bearings were fitted, a drastic reduction of noise was achieved. A further noise reduction followed the fitting of the bearings into sleeves of hard rubber.

In free bearings large amplitudes of vibrations occur at the natural frequency of the outer ring. Gustafsson in ref.(24) and Halm & Woithe in ref.(30) have shown methods of calculating these natural frequencies. It was also shown in both reports by use of spectrograms, that these vibrations actually occur at the calculated frequencies. These natural frequencies do however become irrelevant when the bearing is fitted in a mechanical structure. Not only do the position of the resonances move drastically, but Dowson in ref.(4) shows that, when a bearing is press fitted in a solid steel fundament, the only significant deformations that occur, are the local ones.

Tallian & Gustafsson made a study of noise due to waviness both for free bearings and for bearings in electrical machines, see ref.(23) & (24). They found that the characteristics of noise (measured with a microphone)

was fairly well correlated with that of vibrations of the bearing housing (measured with an accelerometer). The prime source of vibrations was found to be geometrical irregularities of the bearing components. In order to measure and characterise the form deviations, the inner ring was mounted on a smooth running spindle and a pickup was made to slide against the ring as the spindle rotated at high speed. The output of the pickup was fed through a filter having a few broad bands, so that the frequency distribution of the waviness of the ring could be studied. Sizeable waves of up to 100 cycles per circumference were found. Bearings classified in this way were mounted in electrical motors, and it was shown conclusively that the vibrations generated by the motors were dependent on the accuracy of the bearing components. An attempt to identify individual peaks in spectrograms from free bearings does not appear to be successful. The two reports represent an ambitious attempt to describe rolling bearing vibrations and gives valuable information on how over all noise levels are related to bearing quality, but it does not give any detailed insight into the mechanisms that relate form deviations with vibrations.

According to ref.(23) the tightness of the fit of mounting of the bearing does not have a great influence on vibration levels. In a more detailed study of this effect by Kutchev & Pavlov in 1974, ref.(32), the authors studied vibrations of bearings with adjustable fit mounted in electrical motors. The results are not entirely consistent for all motors tested, but generally the vibration level increased with increased clearance. For bearings with negative clearance(preloaded bearings) the vibrations increased with increasing preload. This latter effect was explained by the increasing effect of out of roundness of the bores into

which the bearings are press fitted. Hence, minimum vibrations occurred when the tightness of the fit was such that zero clearance of the bearing was obtained.

The correlation Tallian & Gustafsson found between form deviations of components and noise and vibrations of the bearing, is confirmed in a paper by Lura & Walker in 1972, ref.(31). Lura & Walker demonstrated that bearings with form deviations of few (5 - 11) cycles per circumference produce a comparably high level of low frequency vibrations, while bearings having coarse surface finish produced higher levels of high frequency vibrations. Lura & Walker also give descriptions of a number of commercial bearing vibration testers.

A paper along the same lines was published by Scanlan in 1965., (ref.53). This paper deals mainly with airborne noise from bearings and is chiefly concerned with the experimental apparatus required for its measurement. Scanlan points out that results from free bearing tests are not applicable to mounted bearings. When used for quality control purposes, however, free bearing tests are shown to be relevant and well repeatable.

A refinement of the methods of correlating vibrations and surface irregularities of bearings was presented by Yhland in 1968, ref.(33). Instead of feeding the output from the velocity pickup (sliding against the inner ring track) to a few broad bands as was done by Tallian & Gustafsson and Lura & Walker, he instead made a narrow band spectral analysis of the velocity signal. The peaks in the spectrogram represent the Fourier coefficients that make up the velocity signal. This is an appealing

approach because it allows identification of the individual waves of the track, and Yhland was able to show how a bearing with an inner ring track, having a characteristic spectrogram, generated vibrations that had a spectrogram, where these characteristics were apparent. This method thus allows for a detailed correlation between the inner ring form deviations and the vibrations generated in a free bearing. The fact that a velocity pick up was used gives the form deviations the dimension of velocity and the size of the amplitudes of the waves are thus dependant on the speed with which the spindle was rotating. This is somewhat unfortunate and it is felt that this kind of freak units with no direct physical interpretation should be avoided. Further, the method of measurement is open to some criticism. The pickup might lose contact with the track on some points, and there is always a risk that the measurements will be disturbed by resonances of the spindle or pickup. The results show conclusively that the predicted vibrations occur, but the accuracy of the method is poor and the measurements were done on a bearing having artificially accentuated waviness.

Another investigation of vibrations due to inner ring waviness was done by Halm & Woithe 1970, see ref.(30). It does not add any new information in principal to previous results, but by analysing a large number of bearings (50) it shows that the variation of vibration levels are consistent with the variation of form errors of the individual bearings. An investigation of the effect of clearance of free, radially loaded bearings show a small but steady increase with clearance of vibration levels for several bearing types and bearing individuals.

A different type of form errors, with an effect on vibrations, is the variation of roller or ball diameters. Yamamoto demonstrated in a paper from 1959 ref.(1), that large vibrations were excited, when the cage speed of the bearing coincided with the natural frequency of the rotor supported by the bearing. The size of the vibrations were dependant on how much smaller one undersized ball was compared to the rest of the ball set. The experiments were carried out with a vertical rotor, so that the bearing was axially loaded and all balls always in contact with the races. Another type of vibrations were found, where the non-uniformity of rolling body diameters was assumed to create a radial stiffness having an elliptic variation that rotated with cage speed. Also this type of vibration was found experimentally. In a subsequent paper in 1974, ref.(34), Yamamoto and Ishido made a more detailed analysis of how similar rotating anisotropies of stiffness and non-linearities due to misalignments, can cause resonant effects. A paper by Tamura in 1968, ref.(35), studies the effect of two undersized balls in a bearing. Attention is concentrated mainly on axial vibrations which is somewhat outside the scope of this thesis.

A number of papers have been written on methods of early detection of rolling bearing damage by vibration analysis. The most elementary method for such condition monitoring is by listening to the sound emitted by the bearing in operation. The listener then uses a screw driver or a stethoscope held against the bearing holder and tries to distinguish characteristic sounds associated with damage. For instance, repeating hammering sounds indicate spalling, high pitch noise and whining indicate poor lubrication and so on.

This type of subjective assessment has obvious disadvantages and one has therefore tried to develop electronic systems for vibration analysis. It should be pointed out that there are no standards for assessing the efficiency of such monitoring methods, and they are therefore difficult to compare. A method which goes some way towards such an assessment is given in Chapter 9.

The simplest method of electronic vibration monitoring of bearings is to measure the broadband RMS level or the peak to peak values of the generated vibrations. Usually it is necessary to use some sort of band pass filter to exclude vibrations not originating directly from the bearings, such as vibrations due to unbalance. A description of instruments for this purpose, together with some comments on their application, is given by Furness in 1967, ref.(36). Such a method does however often not have a sufficient selectivity and more sophisticated methods of signal analysis have therefore been employed. These generally fall into two categories: Frequency domain analysis and Time domain analysis. The analysis is usually concerned with detecting discrete surface irregularities such as cracks or fatigue flaking rather than abrasive type of wear or smear of the surfaces. In three papers, Balderstone 1968, ref.(37), Ballas 1969, ref.(38) and Yhland-Johansson 1970, ref.(39), frequency analysis by narrow band filtering has been tried. The underlying idea is that, as the rolling bodies roll over a surface defect, they will create a periodically occurring transient vibration. In all papers it has been demonstrated that defects of the bearing components give rise to changes of the spectrograms. Balderstone studies the changes occurring at high frequency (up to 100 kHz) resonances of the bearing, where effects of poor lubrication can also be detected.

The selective power of the methods is however poor because the transient is of very short duration and often near the level of random noise of the bearing, so that the impact on the spectrograms is not as significant as would be desired.

For this reason a number of time domain analysis techniques have been developed. One such technique was described in 1962 by Tallian-Gustafsson, ref.(40). It employs two parallel gates to which the vibration signal is fed. The gates are synchronised, so that when one is open the other is closed. Each gate is connected to a counter, that counts all vibration peaks exceeding a threshold level. By adjusting the length of time that the gates are open, one can tune the system to a periodicity at which the transients can be expected to occur, i.e. for outer ring defect, at ball passage frequency, for the inner ring, at shaft frequency minus cage speed times the number of balls, and for rolling bodies, at the rolling bodies' rotational frequency. If this is done, one gate will count peaks from random noise only, while the other will count peaks from the random noise plus peaks from the transients originating from the defect. For a bearing with a defect the ratio between the two counters will exceed one. It was demonstrated that very small surface defects could be detected with this method. How efficient the method would be in the presence of other noise sources is however open to question. Further, the methods obviously involves the use of very specialised equipment and rather complicated operation, and as far as it has been possible to find out, the method has not reached much practical application.

Another form of time domain analysis is described by Weichbrodt ref.(41). It is known as summation analysis and has the ability of detecting repeating events of the vibration signal, even if these are hidden by other vibration components. In the same way as was the case for the Tallian-Gustafsson method, it is tuned to certain frequencies at which the transients are expected to occur. When the calculated length of time between transients is set, a gate is opened, and a part of the vibration signal is recorded. The gate is then closed and opened again after the set time constant, and the new samples are added to the previously recorded. This process is repeated a large number of times, and in the sum thus stored, the vibration components occurring at the set frequency will be accentuated, while all others will average out. The method was tried on a bearing with cracks, mounted in a noisy machine, and was found to have a good selectivity. A comparison done with a straightforward spectral analysis by conventional narrow band filtering confirms the conclusion, that such filtering is not an effective means of monitoring. The main drawback of the method seems to be, that a very exact knowledge of the period of the transients is required. This will generally be very difficult to obtain, because even if the dimensions of the bearing to be tested is known, the relative speeds of the shaft, cage and rolling bodies calculated from these dimensions will also be affected by slippage and elastic deformations of the components.

Auto correlation analysis also falls in the group of Time domain analysis methods. It does not require any prior knowledge of periodicity

of the transients. A report published by Gershman & Povarkov in 1968, ref.(42), describes the use of Auto correlation analysis for ball bearing monitoring. Unfortunately the results show a low sensitivity to defects of the tested bearings.

With the occurrence of commercially available real time Fourier analysers the interest for monitoring in Frequency domain has been revived. The extremely short processing time required (fractions of a second) makes it practically possible to calculate a number of spectrograms and then add them together point by point. This has a similar effect as Time domain Summation in that it supresses random noise, but it does of course not require prior exact knowledge of cage speed, roller speed and so on. The use of real time Fourier analysers for crack detection in ball bearings has been described by Babkin-Anderson 1973, ref.(43) and Bannister-Donato 1971,ref(44). A considerable improvement of signal to noise ratio compared to standard narrow band filtering was achieved in both these reports. Although these spectrograms thus form a suitable basis for condition monitoring, the interpretation of the spectrograms is a subject which deserves careful consideration.

A method using measurements in the ultrasonic range seems to have reached a state of commercial application. The method, which is called the Shock Pulse Method, is described by Botoe 1971, ref(45), and several examples of its application by Howard in 1974, ref.(46). The basic principle of the method is to excite the natural frequency of the accelerometer used as vibration pick up by the transient pulse or shock

wave, generated when a rolling body rolls over a bearing defect. Since the shock wave is of short duration it contains high frequency components which could "ring" the single degree of freedom system, that an accelerometer constitutes. The accelerometer thus functions not only as a vibration sensor, but also as a filter and an amplifier. The maximum amplitude of the accelerometer signal is then used as an indicator of the severity of the defect. The natural frequency of the accelerometer used is 38 KHz, so that the frequencies measured lies in the ultrasonic range. The attraction of this lies in the fact that high frequency vibrations attenuate quickly, so that the noise from other bearings or machines does not interfere with the vibrations from the tested bearing. On the other hand, it seems likely that for the same reason, the way the accelerometer is attached to the bearing house and the distance between bearing and accelerometer might have a considerable influence on the readings. The attraction of the method is that no sophisticated instrumentation is required, but since it does not make use of the repetative nature of the occurrence of the transients, it cannot be expected to have the same discrimination power as the more elaborate methods previously described. An extension of the same basic method was described by Broderick in 1972, ref.(47), where a frequency analyser was used to determine the periodicity of the shock pulse. From this information it is then possible to determine if the damaged part is the inner or outer ring or a ball.

CHAPTER 3

FUNDAMENTALS OF ROLLING BEARING OPERATION

Before concentrating on the special aspect of bearing operation with which this thesis is concerned it is necessary to summarise some of the established theories and results dealing with general mechanics of rolling bearings. Particular emphasis is put on aspects which are important to wear and vibration characteristics of the bearing.

Traditionally the magnitude of the local stresses arising due to the external load has been considered as the main wear parameter, but recent research has shown that the oilfilm thickness is also of vital importance. From the vibration point of view, the relative velocities of the bearing-components and the stiffness of the bearing assembly are crucial factors. When it comes to effect on vibration of irregularities in the bearing surfaces, the oilfilm thickness is again of importance together with size and form of the contact zones. Methods of calculating these fundamental parameters will be reviewed in this chapter and in Chapter 6, where some special aspects of the stiffness of the bearing assembly will be studied in detail. When using these equations one must bear in mind the often far reaching approximations that have been made in the derivation of them in order to simplify the highly complex mechanical system that a real bearing constitutes. As far as experimental results are concerned accurate readings are made difficult by the very small dimensions of the

contact zones, displacements and oilfilm thicknesses. The resulting values should therefore be looked upon as giving orders of magnitude and insight into phenomena occurring in the bearing, rather than accurate quantities.

3.1 BEARING TYPES AND BEARING COMPONENTS

A rolling bearing consists of outer and inner rings (races, tracks), a set of rolling bodies and a cage (retainer) to hold the rolling bodies in position and prevent them from sliding against each other. Rings and rolling elements are made of steel alloys which have been hardened, ground and polished. The cage is usually made of some softer material like bronze or mild steel to avoid wear on the rolling bodies. There are basically three types of rolling elements : Spherical balls for ball bearings, cylindrical rollers (usually crowned at the edges to avoid edge pressure) for cylindrical roller bearings and needle roller bearings and barrel-shaped rollers for self aligning roller bearings. The load capacity of a bearing can be increased by using more than one row of rolling bodies. Ball bearings are used as a general purpose bearing type up to moderate loads. Roller bearings are preferred at higher loads and when a particularly stiff bearing is needed like in machine tool spindles. Self aligning (spherical) roller bearings are not suitable for high speeds but have the advantage of allowing a slight misalignment of the shaft. This is made possible by giving the outer track the shape of a portion of a sphere. The traces of the balls or rollers do therefore not have to be parallel to the end surfaces of the outer track or, in other words, the axis of symmetry of the outer and inner ring do not have to be absolutely parallel.

The basic idea behind rolling bearings is to replace sliding contact with rolling contact and thereby reduce friction and wear. The difference of radius of the contacting bodies is much greater for a rolling bearing than for a journal bearing. The load carrying areas are therefore much smaller and consequently the stresses in the contact points are much higher. The high pressure together with the rolling motion also means that the oilfilm separating the components of the bearing is very thin. Both these factors are highly undesirable from the aspect of wear. Therefore many bearing types are given a close conformity between rolling elements and tracks in a plane parallel to the bearing axis, thereby increasing the area that carries the load. The degree of conformity is called osculation and defined as (see Fig. 3.1.6.)

$$o = R_r / R_t \qquad \ldots\ldots\ldots\ldots\ldots\ldots \qquad (3.1)$$

Bearings (a), (b) and (c) in Fig. 3.1 are high osculation bearings while (d) is a low osculation bearing.

3.2 RELATIVE SPEED OF ROLLING BEARING COMPONENTS

In order to determine the relative angular speeds of the outer and inner rings, the cage and the rolling elements of the bearing assembly, the bearing is looked upon as if it operated in a similar way as an epicyclic gear. This assumption presupposes dry contacts, stiff components and a pure, rolling motion. Although these assumptions are neither consistent with the presence of an oilfilm separating tracks and rollers, nor with the deformations that occur in operation under heavy load, many authors e.g. Yamamoto in ref(1), have shown that for bearings operating under normal conditions a good working approximation is obtained through this method. Using the general formula relating the speeds

of sunwheel, planetwheels and planetwheel carrier , the relationships between inner and outer ring speeds and cage speeds can be written as

$$\frac{\omega_i - \omega_c}{\omega_o - \omega_c} = -\frac{D_o}{D_i} \qquad \ldots\ldots\ldots\ldots\ldots\ldots \quad (3.2)$$

re-arranging gives

$$\omega_c = \frac{D_o\omega_o + D_i\omega_i}{D_i + D_o} \qquad \ldots\ldots\ldots\ldots\ldots\ldots \quad (3.3)$$

Define the cage diameter as

$$D_c = \frac{D_i + D_o}{2} \qquad \ldots\ldots\ldots\ldots\ldots\ldots \quad (3.4)$$

The velocities are given by

$$V_c = \frac{\omega_c D_c}{2}$$

$$V_i = \frac{\omega_i D_i}{2}$$

$$V_o = \frac{\omega_o D_o}{2} \qquad \ldots\ldots\ldots\ldots\ldots\ldots \quad (3.5)$$

then

$$V_c = (V_o + V_i)/2 \qquad \ldots\ldots\ldots\ldots\ldots\ldots \quad (3.6)$$

If the outer ring of the bearing is stationary ($\omega_o = 0$), eq(3.3) becomes

$$\omega_c = \frac{D_i\omega_i}{D_i + D_o} \qquad \ldots\ldots\ldots\ldots\ldots\ldots \quad (3.7)$$

and eq(3.6) reduces to

$$V_c = V_i/2 \qquad \ldots\ldots\ldots\ldots\ldots\ldots \quad (3.8)$$

or

$$V_c = \frac{D_i\omega_i}{4} \qquad \ldots\ldots\ldots\ldots\ldots\ldots \quad (3.9)$$

If the axis of rotation of the roller or the ball is not parallel to the axis of rotation of the inner race (inclination of α), eg. (3.7) and(3.9) take the form:

$$\omega_c = \frac{D_i\omega_i}{D_i + D_o} \cos\alpha \qquad \ldots\ldots\ldots\ldots\ldots\ldots\ldots\ldots \quad (3.10)$$

$$V_c = \frac{D_i\omega_i}{4} \cos\alpha \qquad \ldots\ldots\ldots\ldots\ldots\ldots\ldots\ldots \quad (3.11)$$

The angular speed of the ball or roller is

$$\omega_r = 2\,\frac{V_c}{D_r} \qquad \ldots\ldots\ldots\ldots\ldots\ldots\ldots\ldots \quad (3.12)$$

3.3 STRESS AND DEFORMATION IN ELASTIC CONTACTS

The rigorous theory for describing states of stress and deformation in the contacting points of a rolling bearing is a rather complicated application of the theory of elasticity. Only main lines together with results needed further on in this study will be given here.

Starting by combining the two basic conditions of elasticity (Hooke's Law) and continuity the "General boundary problem of the theory of elasticity" can be written, using vector notation, as

$$\Delta\bar{u} + \frac{1}{1-2\nu} \text{ grad div } \bar{u} = 0$$

where $\bar{u}$ is the displacement vector. The solution to this equation has the form

$$\bar{u} = \text{grad } (\phi + \bar{r}\bar{\psi}) - 4(1-\nu)\bar{\psi} \qquad \ldots\ldots\ldots\ldots\ldots\ldots \quad (3.13)$$

where ϕ and $\bar{\psi}$ are potential functions composed so that

$$\begin{cases} \Delta\phi = 0 \\ \Delta\bar{\psi} = 0 \end{cases} \qquad \ldots\ldots\ldots\ldots\ldots\ldots\ldots\ldots \quad (3.14)$$

and $\bar{r}$ is the vector from origin. From this general formulation, the solution of a specific problem can be obtained by applying the appropriate boundary conditions as regards displacements and stresses. Thus, if a point load is applied perpendicular to the surface of a semi-infinite half plane the displacement of the surface in a direction parallel to the force becomes

$$u = \frac{(1-\nu^2)Q}{\pi E r} \qquad \ldots\ldots\ldots\ldots\ldots\ldots\ldots \quad (3.15)$$

where r is the distance from the point where the load is applied to the point of displacement u. A point load is of course a mathematical abstraction which does not occur in practice. Equation (3.15) can however be modified so as to calculate displacements due to distributed loads which is more interesting from a practical view-point. Rewrite (3.15) in differential form with $dQ = pdA$ (p is the pressure function) and integrate over the contact zone

$$u = \frac{1-\nu^2}{\pi E} \iint_A \frac{pdA}{r} \qquad \ldots\ldots\ldots\ldots\ldots\ldots\ldots \quad (3.16)$$

For a uniform pressure function acting on a strip with width 2b, Eq.(3.16) gives the expression for the displacement u at a distance x from the strip to

$$u = P \frac{(1-\nu^2)}{\pi E} \int_{-b}^{b} \ell n(x-s)^2 ds + \text{const} \ldots\ldots\ldots\ldots\ldots \quad (3.17)$$

Now, consider the general case of two elastic bodies being pressed against each other, see Fig.(3.2). The solution of this problem is due to H Herz. The Hertzian theory applied to rolling bearings is described in for instance ref.(2) and ref.(3). A small area of contact will form over which the pressure is distributed. It follows from the geometry of the bodies that the projection of the contact zone

will be elliptic and that the eccentricity of the ellipse (k = a/b) can be determined from the curvature of bodies I and II. Define the function F(r) known as curvature difference as

$$F(r) = \frac{(r_{I1}-r_{I2})+(r_{III}-r_{II2})}{\Sigma r} \quad \ldots\ldots\ldots\ldots\ldots\ldots \quad (3.18)$$

where Σr is the curvature sum

$$\Sigma r = \frac{1}{r_{I1}} + \frac{1}{r_{I2}} + \frac{1}{r_{III}} + \frac{1}{r_{II2}} \quad \ldots\ldots\ldots\ldots\ldots\ldots \quad (3.19)$$

It can however be shown that F(r) can also be calculated from the following expression

$$F(r) = \frac{(k^2-1)\Lambda-2\Gamma}{(k^2-1)\Lambda} \quad \ldots\ldots\ldots\ldots\ldots\ldots \quad (3.20)$$

where Γ and Λ are the elliptic integrals

$$\begin{cases} \Gamma = \int_0^{\pi/2} [1-(1-1/k^2)\sin^2\phi]^{-\frac{1}{2}} d\phi \\ \Lambda = \int_0^{\pi/2} [1-(1-1/k^2)\sin^2\phi]^{\frac{1}{2}} d\phi \end{cases}$$

It is now possible to calculate values for F(r) both from eq.(3.18) and eq.(3.20). For equal values of F(r) given by the two equations, k corresponds to a certain curvature difference and thus, the eccentricity of the contact zone can be obtained from the geometry of the mating bodies. To calculate the deformation of the bodies (i.e. the distance with which two from each other remote points in the two bodies will approach each other) when the load is applied, an approximation essential to the Hertzian theory is made. If the dimensions of the contact zone

is small compared to the radii of the mating bodies, and the contact zone is near flat, then the two bodies can be looked upon as two semi-infinite planes upon which forces are acting perpendicular to the surfaces. When this approximation is justified eq.(3.16) may be applied to calculate the deformation arising due to the pressure function which arises when bodies I and II are pressed against each other. To carry out the integration it is necessary to know the shapes and sizes of the contact area and the pressure function. The shape of the contact zone is given by the eccentricity of the contact ellipse, k, calculated from eq.(3.18) and eq.(3.20). Further it can be shown that the only pressure-distribution function to fulfill the boundary conditions has the form of a half ellipsoid given by the following equation

$$p = \frac{3Q}{2\pi ab} \left[1 - \left(\frac{x}{a}\right)^2 - \left(\frac{y}{b}\right)^2\right]^{\frac{1}{2}} \quad \ldots\ldots\ldots\ldots\ldots\ldots \quad (3.21)$$

The integral of this function over the contact ellipse equals the external load and since the eccentricity, k = a/b, is known, the values of a and b can now be determined. All necessary information is thus available to make use of eq.(3.16) to calculate the deformation due to the pressure ellipsoid. The resulting expressions for a, b and d can be written as

$$a = a^* \left(\frac{3Q}{2\Sigma r} \left[\frac{1-\nu_I^2}{E_I} + \frac{1-\nu_{II}^2}{E_{II}}\right]\right)^{1/3} \quad \ldots\ldots\ldots\ldots\ldots\ldots \quad (3.22)$$

$$b = b^* \left(\frac{3Q}{2\Sigma r} \left[\frac{1-\nu_I^2}{E_I} + \frac{1-\nu_{II}^2}{E_{II}}\right]\right)^{1/3} \quad \ldots\ldots\ldots\ldots\ldots\ldots \quad (3.23)$$

$$d = d^* \frac{\Sigma r}{2} \left(\frac{3Q}{2\Sigma r} \left[\frac{1-\nu_I^2}{E_I} + \frac{1-\nu_{II}^2}{E_{II}}\right]\right)^{2/3} \quad \ldots\ldots\ldots\ldots\ldots\ldots \quad (3.24)$$

where

$$a^* = \left(\frac{2k^2\Lambda}{\pi}\right)^{1/3} \qquad \ldots\ldots\ldots\ldots\ldots\ldots \quad (3.25)$$

$$b^* = \left(\frac{2\Lambda}{\pi k}\right)^{1/3} \qquad \ldots\ldots\ldots\ldots\ldots\ldots \quad (3.26)$$

$$d^* = \frac{2\Gamma}{\pi}\left(\frac{\pi}{2k^2\Lambda}\right)^{1/3} \qquad \ldots\ldots\ldots\ldots\ldots\ldots \quad (3.27)$$

The dimensionless quantities a*, b* and d* can be found tabulated or plotted as functions of F(r) in for instance ref.(2) or ref.(3). In the case where the contacting bodies are made of steel eq.(3.22), (3.23) and (3.24) simplifies to

$$a = 0.101a^* \left(\frac{Q}{\Sigma r}\right) \qquad \ldots\ldots\ldots\ldots\ldots\ldots \quad (3.28)$$

$$b = 0.101\, b^* \left(\frac{Q}{\Sigma r}\right) \qquad \ldots\ldots\ldots\ldots\ldots\ldots \quad (3.29)$$

$$d = 1.28 \cdot 10^{-3} d^* \left(\Sigma r\, (Q)^2\right)^{1/3} \qquad \ldots\ldots\ldots\ldots\ldots\ldots \quad (3.30)$$

with dimensions in mm and kg.

In a similar fashion but starting from eq.(3.17) corresponding expressions can be derived for line contacts, which occur in cylindrical roller bearings and heavily loaded spherical roller bearings. For two rollers of equal length, ℓ_1, Harris in ref.(2) gives the following expressions for the width of the contact strip and for the contact deformation using Imperial dimensions

$$b = 2.78 \cdot 10^{-4} \left(\frac{Q}{\ell \Sigma r}\right) \quad [\text{Imp}] \qquad \ldots\ldots\ldots\ldots\ldots\ldots \quad (3.31)$$

$$d = 7.36 \cdot 10^{-7} \frac{Q^{0.9}}{\ell^{0.8}} \quad [\text{Imp}] \qquad \ldots\ldots\ldots\ldots\ldots\ldots \quad (3.32)$$

Dowson has shown in ref.(4) that a good working approximation of the total deflection for the case of a roller between two tracks of typical dimensions are given by

$$2d = 17.5 \cdot \frac{2(1-\nu^2)}{\pi E} \cdot \frac{Q}{\ell} \qquad [\text{Imp}] \ldots\ldots\ldots\ldots\ldots\ldots \quad (3.33)$$

Or for steel components and converted to SI units

$$2d = 9.37 \cdot 10^{-5} \cdot \frac{Q}{\ell} \qquad [\mu M] \ldots\ldots\ldots\ldots\ldots\ldots \quad (3.34)$$

This equation conforms well with empirical results given in ref.(3).

In cases of close osculation it might be difficult to determine whether point or line contact should be assumed. Ref.(3) gives as a rule of thumb, that if a value for the major axis, a, results from the calculation using point contact assumption, such that $2a > \ell$ then line contact should be assumed as the best approximation.

The Hertzian theory deals only with deformations and stresses on the surface of the contacting bodies. It is known however, that the most common cause of failure of rolling bearings is subsurface fatigue causing spalling. It has also been shown by Palmgren and Lundberg in Ref.(5) that the maximum shear stress arises beneath the surface. In this reference the maximum shear stress is given as a function of the maximum pressure in the contact-ellipse. Also the depth below the surface at which this shear stress arises can be calculated. For point contacts the maximum pressure occurs at the geometrical centre of the contact ellipse and is given from eq.(3.21) to

$$P_{max} = \frac{3Q}{2\pi ab} \qquad \ldots\ldots\ldots\ldots\ldots\ldots\ldots\ldots \quad (3.35)$$

For line contact the maximum pressure becomes

$$P_{max} = \frac{2Q}{\pi \ell b} \qquad \ldots\ldots\ldots\ldots\ldots\ldots\ldots\ldots \quad (3.36)$$

For line contact the maximum shear stress will be

$$\tau_{max} = 0.159 \cdot \frac{Q}{\ell B} \qquad \ldots\ldots\ldots\ldots\ldots\ldots\ldots \quad (3.37)$$

and occurs the distance z_o below the surface

$$z_o \simeq 0.5b \qquad \ldots\ldots\ldots\ldots\ldots\ldots\ldots \quad (3.38)$$

The applicability of these results for point and load contact is of course dependant on how well the approximations of the theory conforms with the real situation. The formulas (3.32) to (3.38) should only be used where

1. All deformation occurs within the elastic range.
2. Only normal stresses are applied.
3. The contact surface is near flat.
4. The dimensions of the contact zone is small compared to the radii of the mating bodies.

It is clear that in many practical cases none of these conditions are completely satisfied. A small degree of plastic deformation often occurs, traction will cause some shear forces and for close osculation type bearings conditions (3) and (4) will often be violated. However, many experiments (see for instance Ref.(6) and Ref.(3)) have shown that good working estimates of the dimensions of the contact zone, the pressure function and the deformations can be obtained with these methods. For low to moderate loads in a bearing having a low value of osculation the conditions (1) to (4) are best fulfilled and consequently the best correspondence between theory and experiments are obtained in these cases. This is demonstrated in Ref.(3) where theoretical and experimental results are compared.

3.4 LUBRICATION OF ROLLER BEARINGS

In the previous sections of this chapter the rolling bearing has been treated as consisting of elastic components in dry, rolling contact with each other. The presence of lubricant is however of fundamental importance for the operation of a bearing. It is not until relatively recently that the mechanisms of this lubrication have been clearly understood and much research work still remains to be done in this field. Only some results of particular relevance to this thesis and some of the main lines of the theory are given here. For a fuller presentation see Ref.(7) which gives a comprehensive and authoritative review of theoretical as well as experimental progress in this field up to 1965.

The purely elastic model, which neglects the effect of lubrication, gives a relevant theory for one extreme case of rolling bearing operation, namely bearings operating under heavy loads and low speeds. Under these conditions the lubricant will be squeezed out of the contact zone and the Hertzian theory can be used to calculate deflection, pressure distribution and so on. The other extreme is represented by a bearing operating at very high speed and light load. In this case it is assumed that the elastic deflections of the bearing components are insignificant and that an oilfilm will form between rollers and tracks. The solution to this problem was given as early as 1916 by Martin. Martin's solution is founded on the Reynold equation which is a general formulation of the problem of hydrodynamical lubrication. The Reynold equation is derived directly from the two basic concepts of continuity and equilibrium of an element of the fluid. Assuming that

1. Body and inertia forces of the lubricant can be neglected.

2. All velocity gradients except across the oilfilm can be neglected.
3. The pressure, viscosity and density of the fluid are constant across the oilfilm.
4. The lubricant behaves as a Newtonian fluid.

Further, restrict the boundary conditions to the case where one body moves over another stationary body in a translatory motion with the speed V. The general form of the Reynold equation can then be written

$$\frac{\partial}{\partial x}\left(\frac{\delta h^3}{12\eta}\frac{\partial p}{\partial x}\right) + \frac{\partial}{\partial z}\left(\frac{\delta h^3}{12\eta}\frac{\partial p}{\partial z}\right) = \frac{\partial}{\partial x}(\delta V h) \quad \ldots\ldots\ldots\ldots\ldots\ldots \quad (3.39)$$

Eq.(3.39) can be further simplified by

5. Neglecting side leakage, and considering fluids which are
6. Isoviscous, and
7. Incompressible

as they pass through the load carrying zone. After integration, eq.(3.39) can be written

$$\frac{dP}{dx} = 12\eta V\left(\frac{h-h_m}{h^3}\right) \quad \ldots\ldots\ldots\ldots\ldots\ldots \quad (3.40)$$

where h_m denotes the oilfilm thickness at the point of maximum pressure. By applying the appropriate boundary conditions Martin could use this version of Reynold's equation to solve the problem of a cylinder rolling over a lubricated plane. To simplify the mathematics of the solution Martin considered a "cylinder" with parabolic cross section instead of a circular one. Because the width of the contact zone is very small compared to the roller diameter this gives a very good approximation. The results are given in the form of a set of dimensionless parameters giving all forces acting on the two bodies. By re-arranging these expressions the minimum oilfilm thickness as a function of external force and speed can be obtained:

$$h_{min} = 4.88 \cdot \frac{\eta V}{\Sigma r \cdot Q} \quad [Imp] \quad \ldots\ldots\ldots\ldots\ldots\ldots \quad (3.41)$$

The minimum oilfilm thickness for a typical roller bearing arrangement operating under normal loads and speeds will, according to eq.(3.41), have a value which is many times smaller than the surface roughness of the bearing components. This would indicate that no fully developed oilfilm forms in roller bearings under operation. However, from practical experience it was clear that there actually existed an oilfilm separating rollers and tracks and thereby avoiding metal to metal contact. This conflict between theory and experience gave rise to a re-examination of the assumptions made in Martin's theory.

The assumptions (1) to (7) are quite justifiable for lubrication of journal bearings,but there is a significant difference in lubrication of journal bearings and lubrication of roller bearings in that in the latter case,the load is carried by a very small area of the oilfilm and consequently the pressure in this area is correspondingly much higher. Therefore, since the viscosity of oil is pressure dependant, the viscosity of an oil element will change considerably as it passes through the contact zone. Therefore assumption (6) is not valid for roller/plane lubrication. In fact, for typical bearings and loads, the pressure in the load zone is so high that the oil practically solidifies. This points to the second alteration one has to make of Martin's theory. Since the lubricant becomes so viscous that it resembles a solid,it is also necessary to take into account the elastic deformations of roller and plane. Consequently, this type of lubrication is called Elasto Hydrodynamic (EHD) lubrication. An early attempt towards

the EHD problem was made by Grubin and although his solution was really no more than an inspired guess the results have later been shown to be reasonably accurate and able to predict the special phenomena associated with EHD lubrication. The EHD problem is constituted by three equations, one describing the pressure distribution of the lubricant, one giving the resulting elastic deflections due to this pressure function and the last giving the viscosity of the oil as a function of the pressure. These three equations are obviously inter-related and must be solved simultaneously. The equation governing the pressure build up is given by eq.(3.39), which if side leakage and compressibility is neglected is written:

$$\frac{d}{dx}\left(\frac{h^3}{\eta}\frac{dp}{dx}\right) = 12V\frac{dh}{dx} \quad \ldots\ldots\ldots\ldots\ldots\ldots \quad (3.42)$$

The oilfilm thickness, including effects of elastic deformation of roller and plane (see eq.(3.17)), is given by

$$h = \frac{x^2}{2R} - \frac{2}{\pi E}\int_{s_1}^{s_2} p(s)\ln(x-s)^2 ds + \text{const} \ldots\ldots\ldots \quad (3.43)$$

The viscosity dependancy of pressure can be approximated by

$$\eta = \eta_o e^{\alpha p} \quad \ldots\ldots\ldots\ldots\ldots\ldots \quad (3.44)$$

This system of equations fills the gap between the two extreme cases of roller bearing operation and covers the conditions under which most bearings would normally operate. No analytical solution to eqs.(3.42), (3.43) and (3.44) exists at present, but Dowson and Higginson in 1959 and 1960 have given numerical solutions for pressure distribution and film profile, for some common cases which have been of great importance in the understanding of the role of lubrication in roller bearings. These results have been verified by later experimental

measurements using X-ray and other methods to determine the shape of the oil film. The numerical method employed by Dowson and Higginson is fairly complex using different methods to solve the set of equations for different parts of the load zone. One striking feature of the solution is the presence of a pressure peak in the outlet of the load zone. For the purpose of this thesis knowledge of the entire pressure distribution and film shape is not important. The minimum oilfilm thickness is however of importance for the wear progression of the bearing and also for its vibration characteristics. Dowson and Higginson give an approximate formula for the minimum oilfilm thickness

$$h_{min} = \frac{1.6 \cdot G^{0.6} V^{0.7}}{W^{0.13}} \quad [\text{Imp}] \quad \ldots\ldots\ldots\ldots\ldots\ldots \quad (3.45)$$

where G is the shear modulus and V and W the dimensionless parameters

$$\begin{cases} V = \eta_o V(1-\nu^2)/ER_r \\ W = Q(1-\nu^2)/ER_r \end{cases} \quad \ldots\ldots\ldots\ldots\ldots\ldots \quad (3.46)$$

Minimum oilfilm thickness calculated by eq.(3.45) will, for cases of normal operation of roller bearings, give a value for h_{min} that is clearly greater than the surface roughness of the bearing components. The EHD theory therefore conforms with practical experience in that it predicts the existence of an uninterrupted oilfilm separating rollers and tracks. For high speeds and light loads h_{min} calculated by EHD theory approaches the value of h_{min} given in Martin's theory.

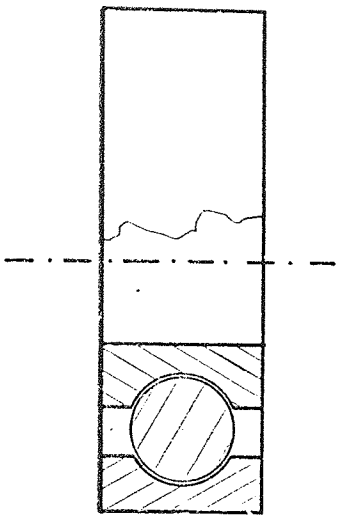

a. Deep-groove ball bearing

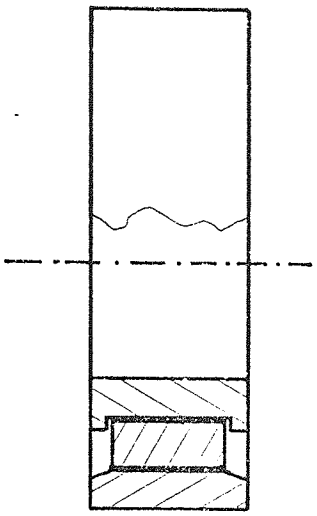

b. Cylindrical roller bearing

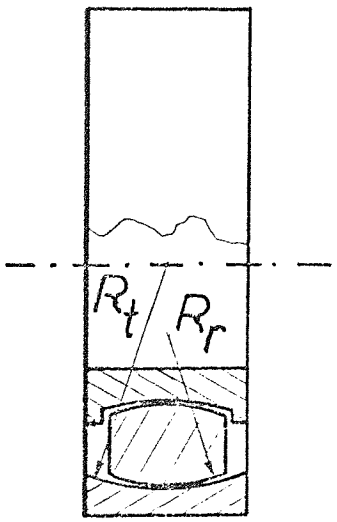

c. Spherical roller bearing, selfaligning

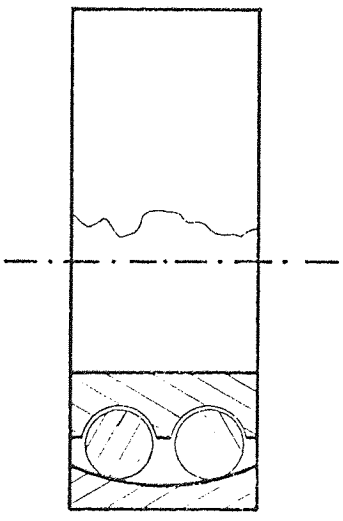

d. Double row, spherical ball bearing, selfaligning

Fig 3.1 Some common types of Rolling Bearings.

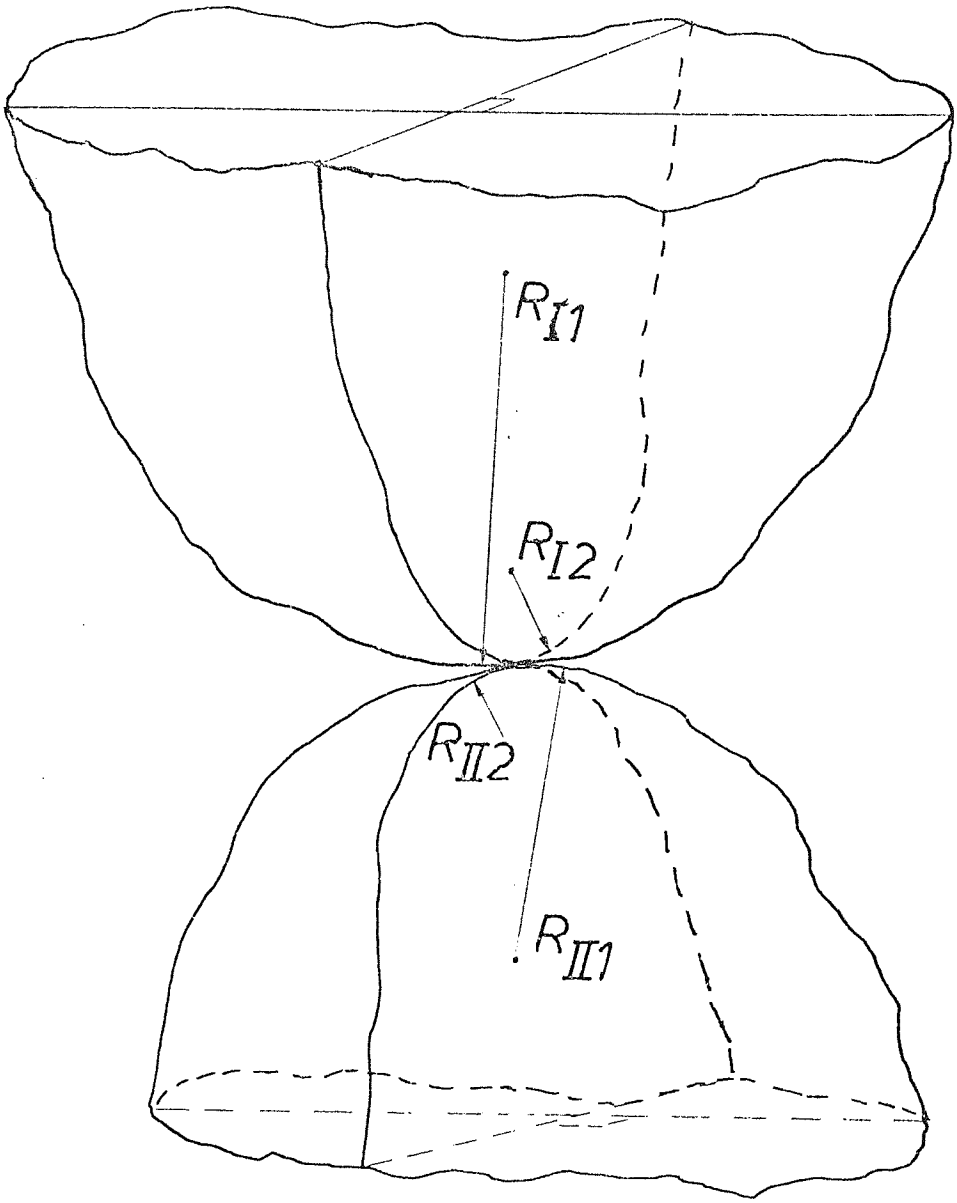

Fig 3.2 Two elastic bodies in contact. Near the contact-point each body is assumed to be defined by two, to each other perpendicular, circle segments. Thus, near the contact-point both bodies have elliptic cross sections (the bodies being assumed to be sliced in planes parallell to the contact zone).

CHAPTER 4

DESCRIPTION OF EXPERIMENTAL APPARATUS

The complexity of the problems concerning rolling bearing vibrations necessitates thorough experimental investigations before attempting to formulate any theoretical theories, and subsequently, to verify such theories and establish under which conditions they are valid. The experimental investigation consists firstly of obtaining measurements from bearings running under various operating parameters, and secondly, of analysing these measurements. The signal processing part will be discussed in Chapter 5 and Appendix II. This chapter is devoted to a description of the two rigs that have been used in obtaining the measurements.

At the outset of this project it was felt that it was essential to keep as many options as possible, concerning running conditions and bearing types, open. Thus, it was necessary to design the bearing test rig such that it allowed the bearings to be run with different loads and speeds and having a variable stiffness of the bearing mounting. Further, for the investigation of the effect of wear on vibration, it was necessary to be able to wear out bearings, and during this process, measure the vibrations at progressive stages of wear. The latter requirement means, that to achieve significant wear during reasonable time, the bearing had to be run with very heavy load. This requires a rugged construction of the rig

and its driving mechanisms. On the other hand, when the vibration measurements were carried out, it was essential that no disturbing vibrations from other bearings or drive components should occur. It was concluded that these conflicting requirements could not be met by the same rig, and it was therefore decided to build two rigs, one designed solely for vibration measurements, and one solely to wear out bearings.

4.1 BEARING WEAR RIG

It is essential that the wear occurring in the bearings should be of a similar type as wear developing under normal operating conditions. This excludes methods like mixing abrasives in the lubricant, running at an elevated temperature and the like. Since it is necessary to in some way achieve a high wear rate, the bearing is instead run under a load that is considerably higher than it would normally be used for. The loads used are however well below (about 30 - 40%) the loads at which plastic deformation would occur. To further increase the wear rate, the lubricants chosen usually have a viscosity which is somewhat below the manufacturers' recommendation.

The design of the rig is shown in picture 4.1. The main shaft (1) is supported by two double row self aligning roller bearings seated in plummer-blocks (2).The estimated operational life of the main bearings is such that about forty test bearings could be worn out before replacement of the main bearings. Either one or two test bearings can be run at the same time. The test bearings are positioned at the bearing seats (3) on the shaft and held in position by lock nuts. In picture 4.1 a test bearing is positioned at the right end of the shaft while the left end is

empty. The shaft is subjected to high bending moments due to the heavy loads, and calculations showed, that only by using high alloy steel with particular strength and toughness could the shaft be expected to survive. To further reduce the risk of fatigue, the shaft was given rounded transitions between sections and a careful surface treatment. Another problem caused by high loads was fretting corrosion. To overcome this problem, the seats of the main bearings had to be chromium plated and eventually, the seats of the test bearings, which were originally cylindrical, were changed to tapers. The test bearings are held by a semi circular bearing house combined with oil bath (4). Via two rods and a cross bar the bearing houses are connected to a hydraulic cylinder (5) which supplies the load on the bearings. The purpose of using a hydraulic system, instead of loading the bearings with weights, was to eliminate the risk of exciting resonant frequencies of the loading system. The high stiffness of the hydraulic system caused problems, because the thermal expansion of the bearing, as it gets warmed up, gives a steep rise in the load exerted on the bearing. To reduce the stiffness of the loading system, a bundle of leaf springs were positioned above the cylinder and a gas accumulator (6) was integrated in the system. The pressure in the cylinders is supplied by the hand pump (7) and can be read on the gauges (8). By use of the valves (9), the two cylinders can be operated independently of each other. A shear coupling is inserted between the main shaft and the drive shaft (10) in case a bearing should seize. The drive shaft is in turn driven by an adjustable pulley arrangement, which allows for variations of speed. The torque is supplied by a 3 phase induction motor. A hole is drilled through the bearing house, to allow for a thermometer to be inserted close to the outer ring of the test bearing. A blower unit has been used to regulate the temperature of the test bearings.

4.2 VIBRATION TEST RIG

The purpose of this rig is to run various types of bearings under different load and speed conditions, and measure the vibrations these bearings generate under operation. Obviously it is of the greatest importance, that the signal measured actually does originate from the test bearing and not from other bearings or components of the rig. The prime objective in the design of the rig has thus been, to minimize other sources of vibrations in the rig and, to make the influence of the rig on the vibrations measured as uncomplicated as possible. The rotor, which is supported at one end by the test bearing, has therefore been made so that its centre of gravity is very close to the geometrical centre of the test bearing. The rotor is supported in the opposite end by a self aligning double row ball bearing. The load on (and therefore vibrations from) this bearing is negligible, since the c.g. of the rotor coincides with the geometrical centre of the test bearing.

Further, since the reaction force at the test bearing side of the rotor goes through its c.g., this time varying force will be counteracted by the rotors inertia only and not give rise to bending vibrations of the rotor shaft. The rotor has therefore been considered as a rigid body acting as a pure mass. Gyroscopic effects have been neglected, since the speeds are relatively low and the displacement very small.

The test rig set up is shown in picture 4.2, and the three different configurations possible shown in Fig. 4.3a, b and c. The effective load exerted on the test bearing is for configuration a: 12 kg, b: 85 kg and c: 205 kg. It is obviously only in configurations b and c the c.g. coincides with the test bearing centre, but for configuration a, the

occurring forces are so small, that the rotor can still be considered rigid. Changing the rig from one configuration to another can be done in a matter of minutes. In configuration a, the three guard bearings(1) encompass the rotor disc (2) to limit violent vibrations. To change from 12 kg load to 85 kg load, the block (3) is slid away from the rotor on the bed plate(4). The 85 kg disc (5), which has an accurately machined seat, is bolted to the face of the 12 kg disc. When the block (3) is slid back against the rotor, the three guard bearings fit into a groove on the face of the disc (5). To increase the load to 205 kg, the tapered ring (6) can be driven up on the taper of disc (5), thereby firmly attaching it to the rotor. The short shaft (7), which carries the test bearing (8), is exchangeable so that bearings with either cylindrical or tapered bores may be fitted. The test bearing is secured in a bearing holder, having a tight sliding fit, by a lock nut. The bearing holder is in turn bolted to the tube (9). The two brackets (10) holding the tube, can be slid to different positions on the block, thereby making it possible to vary the stiffness of the bearing mounting. Henceforth, bracket positions as far apart as possible will be referred to as "hard" mounting, brackets 15 and 33 cm from the bearing, "medium stiffness" mounting, and brackets 25 and 33 cm from the bearing, "soft" mounting. A number of planes have been machined on the bearing holder. On these planes, holes are drilled and threaded to allow for mounting of accelerometers and attachment of vibrator and load cells. The acceleration of the bearing holder is measured with a piezo-electric accelerometer, having a natural frequency (unmounted) of 39 KHz. The acceleration signal is fed to a normalising charge amplifier, and the voltage output of this is fed to a recording device, either a magnetic tape recorder or a digital recorder. In the latter case, the signal is first fed through a low pass filter to make the signal

comply with the Nyquist sampling criteria (see Chapter 5). The tape recorder, which is of FM type, has a linear (within 0.5 dB) response from DC to 20 KHz. The rotor is driven by an induction motor via a magnetic clutch and a pulley arrangement. The magnetic clutch allows for wide variations of the speed of the rotor shaft, and this speed is accurately controlled by a feed back system. To measure the speed of the rotor a tachometer wheel is mounted on the shaft. The tachometer signal is fed to an electronic counter.

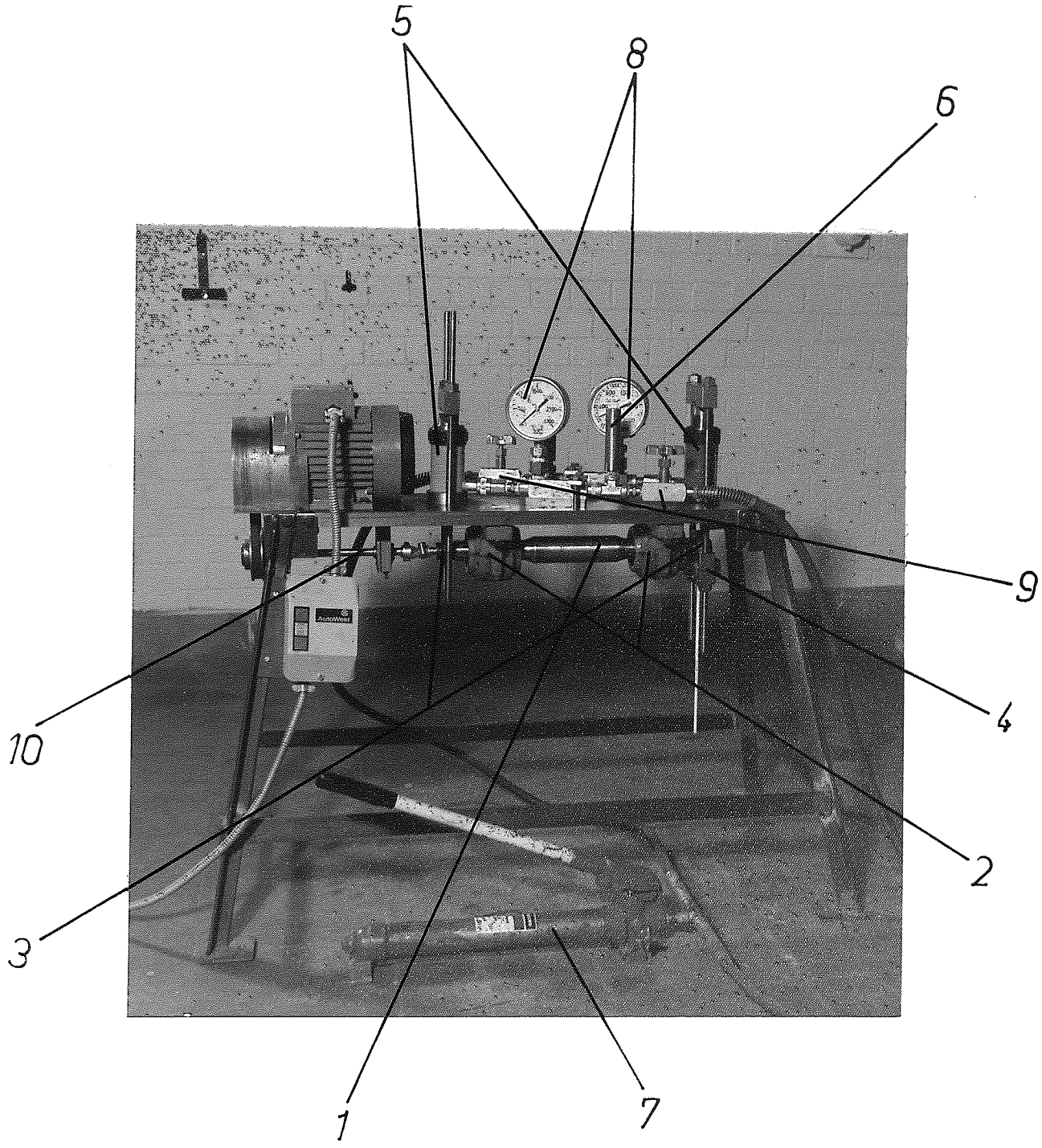

FIG 4.1 WEAR RIG

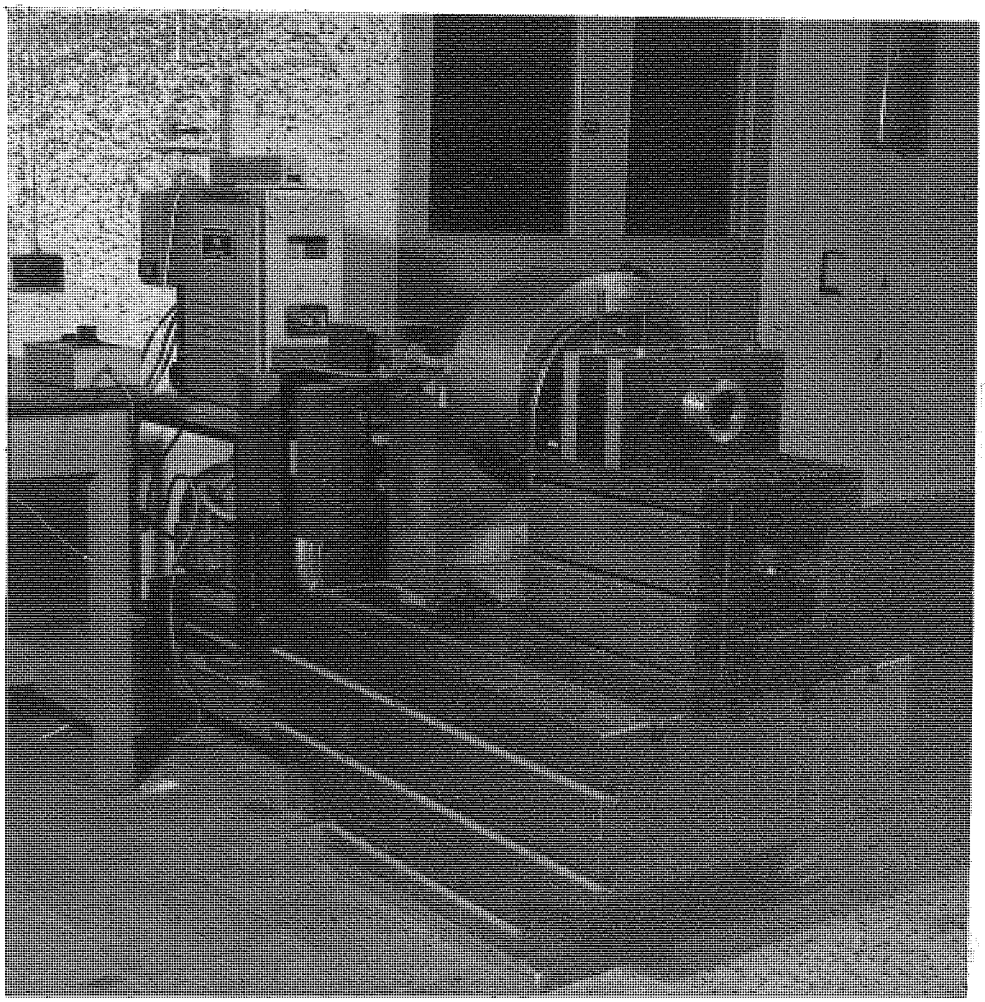

FIG 4.2 VIBRATION TEST RIG

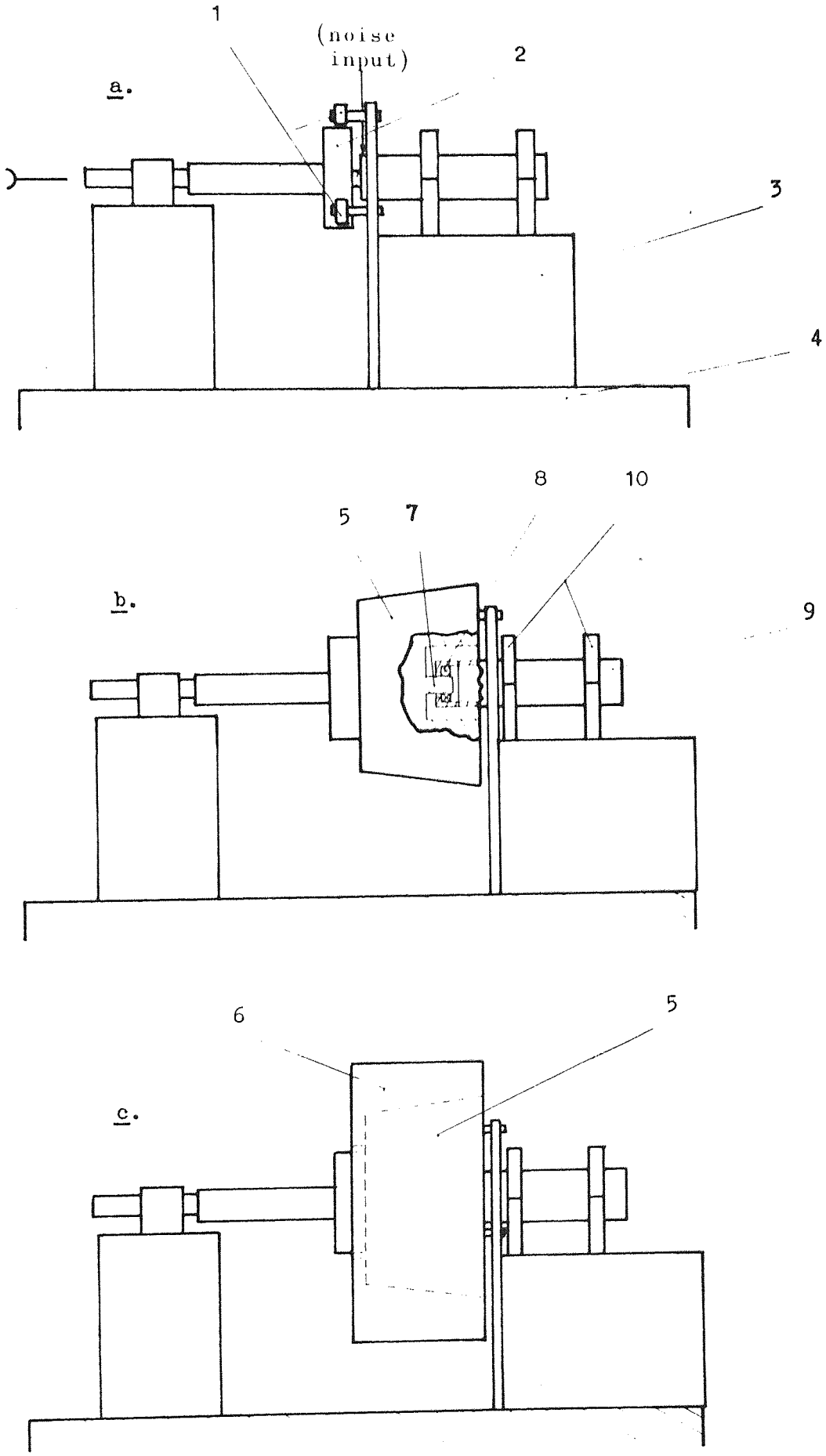

Fig 4.3 The bearing vibration test rig with 12, 85 and 205 kg rotors.

CHAPTER 5

METHODS OF SIGNAL PROCESSING

The time-history signal, representing vibrations generated by bearings run in the test rig, is very complex and not much useful information can be derived directly from it. Further analysis is therefore necessary and serves to investigate specific aspects of the signal and thereby revealing characteristics of the bearing's vibrational behaviour. The signal processing might be carried out either with conventional analog methods or by using digital techniques. Both methods have their own advantages, analog equipment can be connected directly to the test rig and the results obtained at the time the experiment is carried out. The analysis times are however often long, narrow band spectral analysis over a wide frequency range, is a matter of hours. Also, the accuracy of the results is better when digital techniques are used. This is particularly true of the accuracy of the frequency axis in spectral analysis, and this is of great importance when determining the origin of frequency components occurring close to each other, which is often the case in roller bearing vibrations. Probably the most valuable advantage of digital techniques is however, the flexibility of digital systems. Analog instruments will perform a certain predetermined analysis, while when a digital computer is used for analysis, modifications of and additions to the standard programmes can easily be done. For the above mentioned reasons, it was decided that a digital mini computer available in the department shouldbe adapted for signal processing purposes for this project. The setting up of such a system is a considerable

task, but if a large amount of processing is to be carried out, the faster processing timescompensate for this. During the evolution of the project, it has also been found possible to use the digital signal processing system for tasks not originally forseen, such as analysis of bearing component shapes and analysis of computer simulated vibrations and forces.

Signal analysis by computer involves 1) making the data accessible to the computer, 2) processing the data and 3) outputting the results in a presentable form. Inputting of data is done either by sampling from an analog signal or by reading the data punched on paper tape using an optical reader. In the first case, the signal is normally recorded on an FM magnetic tape recorder, while in the latter case the tape is punched by a data logger or a punch connected to a high speed digital recorder. The outputting of results are done either with a digital plotter or by printing on Teletype or fast character printer.

The suite of programs performing the analysis is called DAS, and is described in Appendix II, where examples of runs are also given. The available routines are:

1). Calculation of mean value, root mean square, variance and standard deviation.

2). Probability density function.

3). Probability distribution function.

4). Auto-correlation function.

5). Calculation of Fourier coefficients (frequency analysis by Fast Fourier transform).

6). Power spectral density.

Summing up the use of the routines it can be said that 1) to 3) determine the amplitude distribution of the signal (if the signal is Gaussian, Probability density and Probability distribution is fully determined by the signal's mean value and value for standard deviation) while 4) is a time domain analysis capable of distinguishing between random and periodic components. Processes 5) and 6) transform the time domain signal to frequency domain, thereby determining the frequency distribution (and if so desired, the phase distribution) of the signal. The frequency analysis functions are particularly useful, since they often make it possible to associate certain vibration components with events of the system generating the vibration. Since the purpose and properties of these processes are generally well known, no detailed discussion will be given here, except for where the use of digital analysis requires special consideration. Details of the processes are given in ref.(12) and Chapters 11, 21 and 22 of ref.(13).

The mathematical background to spectral analysis by Fourier transformation is described in Appendix I. If an infinite number of samples from an infinitely long signal are analysed, the transform gives a complete description of the frequency contents of the signal. When carrying out the process in practice, this is obviously not possible, and the fact that only a small part of the signal is analysed has some important implications. Leaving apart the influence of random components for the moment, it is assumed that the signal consists of periodic components. Using the "normalized" Fourier transform, see equation I.13, the line spectra resulting from the analysis of the signal should then consist of discrete lines with a height equal to the amplitude of the respective harmonic

components. The truncation of the signal makes the line spectra degenerate into a series of peaks appearing at the frequencies of the lines. The effect can be explained by studying the transformation of a pure sine wave. As illustrated in Fig. 5.1, the analysis of only a part of the sine wave is equivalent to multiplying the sine function with a square wave pulse, i.e. instead of transforming

$$y = A\sin\omega_o t \quad \ldots\ldots\ldots \quad (5.1)$$

then function actually transformed is

$$y' = A\sin\omega_o t \cdot [U(t) - U(t-t_o)] \quad \ldots\ldots\ldots \quad (5.2)$$

where t_o is the total sampling time. The square wave pulse function is called a window function, denoted w(t). The Fourier transform of the product of two time-varying functions is the convolution ("faltung") of the Fourier transforms of the functions. Thus, if, (see Ref.(11)),

$$FT(A\sin\omega_o t) = A\delta(\omega-\omega_o) \quad \ldots\ldots\ldots \quad (5.3)$$

and

$$FT(w(t)) = W(\omega) \quad \ldots\ldots\ldots \quad (5.4)$$

then the Fourier transform of equation (5.2) is

$$Y' = A \int_{-\infty}^{\infty} \delta((\omega-\omega_o) - x)\, W(x)dx \quad \ldots\ldots\ldots \quad (5.5)$$

But from Chapter 4 of ref.(10), for any function I

$$\int_{-\infty}^{\infty} \delta(a-t)\, I(t)dt = I(a) \quad \ldots\ldots\ldots \quad (5.6)$$

And thus, equation (5.5) gives

$$Y' = A \cdot W(\omega-\omega_o) \quad \ldots\ldots\ldots \quad (5.7)$$

The practical result of the analysis is thus, a function being proportional to the amplitude of the sine wave and the Fourier transform of the window function (in this case a square wave pulse), the latter being symmetrical around ω_o. The continuous curve of Fig. 5.2 will only result, if an infinite number of samples are analysed during the period t_o. If the number of points is limited, which it of course always will be, the effective output on the plotter will be the curve made up from discrete points of Fig. 5.2. The above implies two problems, the occurrence of large side lobes around the peak and the fact that there might not happen to be a point at the top of the window, in which case the height of the peak will be under-estimated. The spectrograms can however be improved by using another window function than the straight forward square wave pulse. There are a number of window functions described in the literature, the most common being the Hanning window. The transform of the Hanning window (defined under "window" in Appendix II) has a more favourable shape than the transform of the pulse function. It has smaller side lobes and a broader, flatter peak, which makes the readings more stable, see the schematic drawing in Fig. 5.2 and graphs 5 and 7 of Appendix II.

When running the FFT program of the DAS system, the two parameters NOS (number of samples) and SFREQ (sampling frequency) have to be set. The sampling frequency must be set according to the Nyquist sampling criteria, stating that more than two samples per cycle of the highest frequency component of the signal is required. To ensure that this criteria is fulfilled it is necessary to pass the signal through a low pass filter before feeding it to the A/D converter or digital recorder. If components of higher frequency are present in the signal, the resulting peaks will

"fold" back into the spectrogram and obscure the genuine peaks. Hence, the cut off frequency should always be set below half the sampling frequency. It is advisable to cut off also the lower end of the signal with a high pass filter so that a reasonable number of cycles (at least ten) are used to calculate the lowest non-zero frequency component.

From the Nyquist sampling criteria it follows that the spectrogram will cover the range zero to SFREQ/2. The Fourier coefficients making up this range are the first NOS/2 points produced by the FFT routine. The remainder of the points are the mirror image of these points since the coefficients are symmetrical. Thus the frequency increment between each coefficient is (SFREQ/2)/(NOS/2), and this increment is the counterpart to the filter bandwidth in an anolog filtering system.*

For signals having both random and periodic components, the random components can be suppressed by repetitive processing. The DAS package allows for all routines to be repeated an unlimited number of times and the average of the results taken. This technique proved particularly useful for monitoring purposes, where periodic components were buried in random noise, but could be detected by repeated frequency analysis.

A technique for averaging out random noise in the time domain was described in Chapter 2. The method is called Summation analysis and requires detailed knowledge of the signal's characteristics beforehand. An alternative way of noise reduction is by use of the Auto-correlation

---

* By bandwidth is then understood the effective frequency resolution rather than the stringent definition referring to the half power points.

process. Since it has not been possible to find any comparisons between the two methods' discrimination power, such an investigation was carried out and is presented in Appendix III. It is shown there, that Summation analysis is generally a more efficient means of noise suppression than Auto-correlation. For signals of the kinds considered here however, the signal to noise ratio by Auto-correlation analysis has been considered satisfactory and it has not been felt, that the expected improvement when using Summation analysis would motivate the much more cumbersome processing methods required.

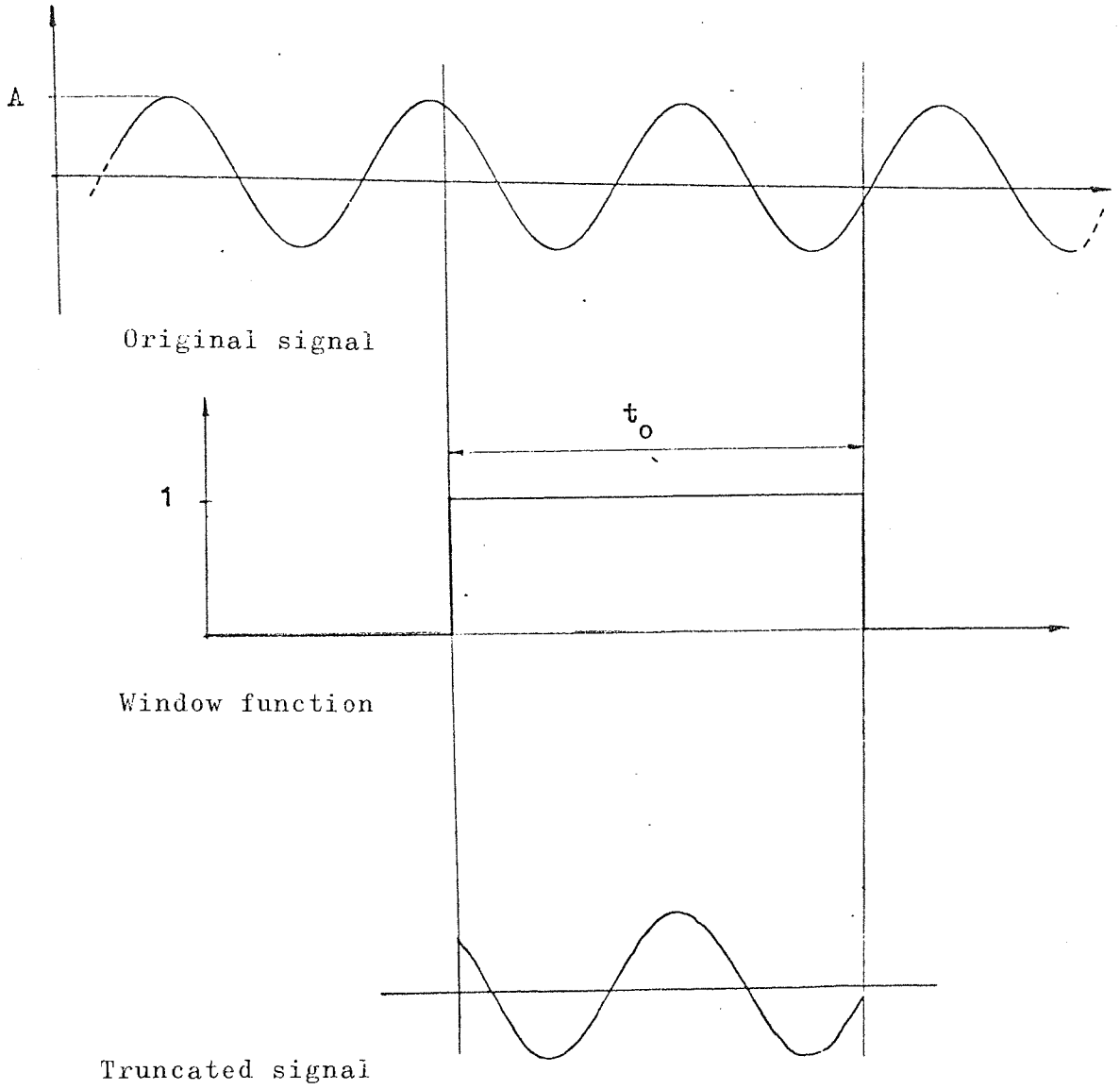

Fig 5.1 Truncation of time-history signal

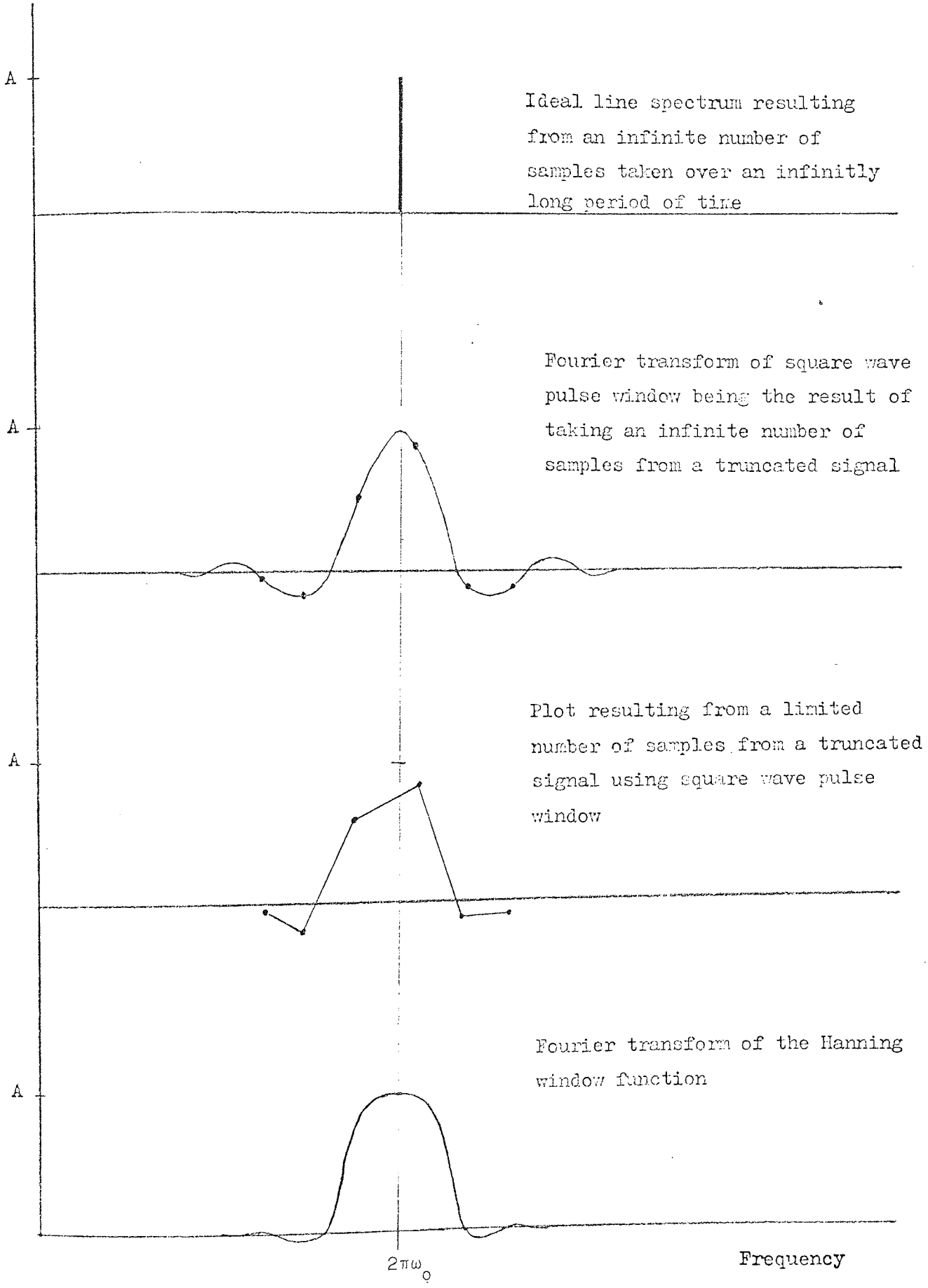

Fig 5.2 Sketches showing the effect of various window functions

CHAPTER 6

VIBRATIONS GENERATED BY IDEALISED ROLLING BEARINGS

Rolling element bearings will generate vibrations during operation even if they are geometrically and elastically perfect. This is an inherent feature of the bearing type and is due to the use of a finite number of rolling elements to carry the external load. A study of a realistic bearing arrangement shows that the number of rolling elements under load varies with the cage position. This gives rise to a periodical variation of the total stiffness of the bearing assembly and consequently generates vibrations. The number of rolling bodies under load also depends on the vertical and horizontal position of the inner ring relative to the outer ring, which is assumed to be stationary. The bearing assembly thus constitutes a statically undeterminate system with time varying and non-linear stiffness coefficients where vertical and horizontal displacements are strongly coupled. The most convenient way of tackling such a problem is to assume displacements and subsequently calculate the arising reaction forces. This force-deformation relationship will be derived in Section 6.1. A derivation has previously been presented by Meldau, see Chapter 2, but by using unit step functions and writing the relationship in the form of a finite sum, it has in this study been possible to obtain the result in closed form, which was not the case in Meldau's work. To calculate the relative movements between inner and outer rings, that results from the stiffness variation, Meldau assumed constant external vertical load and zero external horizontal load.

This assumption is valid only for very slowly rotating bearings, as Meldau also points out. In a bearing operating at normal speed, the displacements generated by the bearing will cause the occurrence of inertia forces proportional to the mass of the external load. For a typical bearing assembly a cage speed of only four radians per second (approximately 90 revs per minute shaft speed), gives an oscillating force in the horizontal direction of about 40 N and in the vertical direction of about 30 N for a 75 kg load. For higher speeds dynamic forces of the same order of magnitude as the dead weight of the load occur. These dynamic effects have been analysed by including the previously described stiffness function in the equations of motion of a rotor supported on roller bearings.

6.1 THE FORCE-DEFORMATION RELATIONSHIP FOR ROLLER BEARING ASSEMBLIES

Consider the roller bearing in Fig. 6.1. The angular position of the cage is defined by ψ and the gaps between the rollers by $V(V = 2\pi/N$, where N is the number of rollers). The bearing has a radial clearance of 2e so that when the inner and outer ringsare concentric, there is no contact between the rollers and the outer ring. In Fig.6.2, circle I represents the dashed circle (radius R) of Fig. 6.1 and circle II is the track of the outer ring (radius R + e). Now assume that the centre of the inner ring is moved from O to O' along $\bar{A}$ as shown in Fig.6.2. This will cause the two circles to interfere with each other over a part of the circumference. Returning to Fig. 6.1, it becomes clear that this interference will cause an elastic (for small displacements) deformation of the rollers and rings. Dowson has shown in reference (4), that for rings mounted firmly against solid steel shaft and bearing house, the only

significant deformations are the local deformations at the contact points between rollers and rings. He also showed that the local stiffness is near linear and can be well approximated with eq.(3.34). These deformations will give rise to the reaction force of the bearing. The zone over which the circles I and II interfere will therefore be called the load carrying zone. To calculate the reaction forces, it is necessary to know the function $\delta(v)$, or since $v \simeq \phi$, ($|\bar{A}| << |\bar{B}|$, $|\bar{C}|$), the function $\delta(\phi)$ as indicated in Fig. 6.2. The vectors $\bar{A}$ and $\bar{C}$ can be written in parameter form

$$\begin{cases} \bar{A} = [A_x; A_y] = [\delta_x; \delta_y] = [\delta_o \cos\alpha; \delta_o \sin\alpha] \\ \bar{C} = [(R+e)\cos\phi;\ (R+e)\sin\phi] \end{cases} \quad \ldots\ldots\ldots \quad (6.1)$$

From Fig. 6.2

$$\bar{A} + \bar{B} = \bar{C} \quad \ldots\ldots\ldots \quad (6.2)$$

so that

$$\bar{B} = \bar{C} - \bar{A} \quad \ldots\ldots\ldots \quad (6.3)$$

and thus

$$|\bar{B}| = |\bar{C} - \bar{A}| \quad \ldots\ldots\ldots \quad (6.4)$$

or in coordinate form

$$|\bar{B}| = \sqrt{(C_x - A_x)^2 + (C_y - A_y)^2} \quad \ldots\ldots\ldots \quad (6.4)$$

With the coordinates from eq.(6.1) substituted into eq.(6.4) the length of vector $\bar{B}$ can be calculated,

$$|\bar{B}| = \sqrt{[(R+e)\cos\phi-\delta_o\cos\alpha]^2 + [(R+e)\sin\phi-\delta_o\sin\alpha]^2} =$$

$$= \sqrt{(R+e)^2+\delta_o^2-2\delta_o(R+e)(\sin\alpha\sin\phi+\cos\alpha\cos\phi)} =$$

$$= \sqrt{[(R+e)-\delta_o(\sin\alpha\sin\phi+\cos\alpha\cos\phi)]^2+\delta_o^2[1-(\sin\alpha\sin\phi +}$$

$$\overline{+ \cos\alpha\cos\phi)^2]} \qquad \ldots\ldots\ldots \qquad (6.5)$$

For a medium sized bearing with realistic load, the second term under the root sign will be about a millionth of the first term. Thus eq.(6.5) can be rewritten as

$$|\bar{B}| = R+e-\delta_o\sin\alpha\sin\phi-\delta_o\cos\alpha\cos\phi \qquad \ldots\ldots\ldots \qquad (6.6)$$

Substituting eq.(6.1) into eq.(6.6) gives

$$|\bar{B}| = R+e-\delta_y\sin\phi-\delta_x\cos\phi \qquad \ldots\ldots\ldots \qquad (6.7)$$

where δ_x and δ_y are the horizontal and vertical displacements respectively of the inner ring centre. The expression for $\delta(\phi)$ now follows directly, see Fig. 6.2,

$$\delta(\phi) = R-|\bar{B}| = \delta_x\cos\phi+\delta_y\sin\phi-e \qquad \ldots\ldots\ldots \qquad (6.8)$$

If the local stiffness between two rings and one roller is called K, the reaction force from one roller in position ϕ, see Fig.6.2, can be written as

$$\bar{P}(\phi) = K\cdot\bar{\delta}(\phi) \qquad \ldots\ldots\ldots \qquad (6.9)$$

or rewritten in component form,

$$\begin{cases} P_x(\phi) = -K|\delta(\phi)|\cos\phi \\ P_y(\phi) = -K|\delta(\phi)|\sin\phi \end{cases} \qquad \ldots\ldots\ldots \qquad (6.10)$$

Obviously a roller can only support compression forces, so for negative values of $\delta(\phi)$, P_x and P_y should equal zero. Therefore, multiply the right membra of eq.(6.10) with $U(\delta(\phi))$, where U is the Heaviside unit step function having the value one for positive arguments and the value zero for negative arguments.

$$\begin{cases} P_x(\phi) = -K\,\delta(\phi)\cos\phi \cdot U[\delta(\phi)] \\ P_y(\phi) = -K\,\delta(\phi)\sin\phi \cdot U[\delta(\phi)] \end{cases} \quad \ldots\ldots\ldots \quad (6.11)$$

Now define

$$\phi_k = \psi + (k-1)V \quad \ldots\ldots\ldots \quad (6.12)$$

and

$$\begin{cases} Q_x = \Sigma\, P_x \\ Q_y = \Sigma\, P_y \end{cases} \quad \ldots\ldots\ldots \quad (6.13)$$

By combining equations (6.13), (6.11) and (6.12), the reaction forces resulting from the displacement of the inner ring centre from O to O' can now be calculated

$$\begin{cases} Q_x = -K \sum_{k=1}^{N} \delta(\phi_k)\cos\phi_k \cdot U[\delta(\phi_k)] \\ Q_y = -K \sum_{k=1}^{N} \delta(\phi_k)\sin\phi_k \cdot U[\delta(\phi_k)] \end{cases} \quad \ldots\ldots\ldots \quad (6.14)$$

Substituting eq.(6.8) into eq.(6.14) gives the full expression

$$\begin{cases} Q_x(\delta_x;\delta_y;\psi) = -K \sum_{k=1}^{N} (\delta_x\cos\phi_k + \delta_y\sin\phi_k - e)\cos\phi_k \cdot U[\delta(\phi_k)] \\ Q_y(\delta_x;\delta_y;\psi) = -K \sum_{k=1}^{N} (\delta_x\cos\phi_k + \delta_y\sin\phi_k - e)\sin\phi_k \cdot U[\delta(\phi_k)] \end{cases}$$

$$\ldots\ldots\ldots \quad (6.15)$$

Note that for constant values of δ_x and δ_y, Q_x and Q_y will vary with ψ and this is what is known as the varying compliance effect. Fig.6.3 shows the vertical reaction force as a function of δ_y for cage positions of $\psi = 0°$ and $\psi = 15°$ for a bearing having 12 rollers. For both these cage positions the rollers are symmetrically arranged, which makes $\delta_x = Q_x = 0$ for all values of δ_y.

6.2 ROTOR SUPPORTED BY ROLLING BEARINGS

Having derived an expression for the force - deformation relationship for the bearing assembly, it is now possible to proceed to considering a rotor - bearing system. In the set up of Fig. 6.4, it is assumed that all components except the bearing investigated, are absolutely rigid. The left hand side of the rotor is supported by a self aligning bearing. If the rotor is turned very slowly, no inertia forces occur, which makes $Q_x = 0$ and $Q_y = M \cdot g$. Inserting these values in equation (6.15) and calculating δ_x and δ_y as functions of ψ, will give the static VC shaft locus. Even at very low speeds however, the inertia forces have a significant effect. To solve the then occuring dynamic VC vibration problem, the equations of motion for the mass of the rotor for horizontal and vertical movements are set up.

$$\begin{cases} M\ddot{\delta}_x = Q_x(\psi;\delta_x;\delta_y) \\ M\ddot{\delta}_y = Q_y(\psi;\delta_x;\delta_y) - M \cdot g \end{cases} \quad \ldots\ldots\ldots \quad (6.16)$$

For a rotor running at steady speed, $\psi = \omega_c t$ and equation (6.16) is rewritten

$$\begin{cases} M\ddot{\delta}_x - Q_x(\omega_c t;\delta_x;\delta_y) = 0 \\ M\ddot{\delta}_y - Q_y(\omega_c t;\delta_x;\delta_y) + M \cdot g = 0 \end{cases} \quad \ldots\ldots \quad (6.17)$$

Equation (6.17) forms a coupled system of secondary differential equations with time varying coefficients and with terms that are only piecewise analytic (differentiable).

It has not been possible to find a general analytical solution to equation (6.17), but for two important special cases, such solutions can easily be obtained. For high accuracy applications, roller bearings are often preloaded, i.e. they have a negative radial clearance. If the preload and the shaft movements occurring are such that

$$|e| > \sqrt{\delta_x^2 + \delta_y^2} \qquad \ldots\ldots\ldots \qquad (6.18)$$

then all rollers will always be in contact with both races and, the term $U(\delta(\phi))$ of equation (6.15) is always one. Thus equation (6.15) becomes

$$\begin{cases} Q_x = -K \sum_{k=1}^{N} (\delta_x \cos\phi_k + \delta_y \sin\phi_k - e)\cos\phi_k \\ Q_y = -K \sum_{k=1}^{N} (\delta_x \cos\phi_k + \delta_y \sin\phi_k - e)\sin\phi_k \end{cases} \ldots\ldots\ldots \qquad (6.19)$$

Since the summation is carried out over the whole circumference of the bearing, equation (6.19) reduces to

$$\begin{cases} Q_x = -K \sum_{k=1}^{N} \delta_x \cos^2\phi_k = -K \sum_{k=1}^{N} \delta_x \frac{1+\cos 2\phi_k}{2} = \\ \quad = -\delta_x \frac{KN}{2} \\ Q_y = -K \sum_{k=1}^{N} \delta_y \sin^2\phi_k = -K \sum_{k=1}^{N} \delta_y \frac{1-\cos 2\phi_k}{2} \\ \quad = -\delta_y \frac{KN}{2} \end{cases} \ldots\ldots\ldots \qquad (6.20)$$

Thus, for such a preloaded bearing, the stiffness is constant and time invariant and no VC vibrations would be generated. Equation (6.20) also shows that the stiffness does not increase with the preload, once the condition (6.18) is fulfilled. One should therefore avoid excessive preload since this can cause problems of over-heating and increased friction, while no increase of the assembly stiffness is gained.

In a similar way, the case for e = 0 can be analysed. From Fig.6.2 it is clear that if e = 0 the contact zone will cover exactly half the circumference of the outer race for all (small) displacements. If the bearing has an even number of rollers, then N/2 rollers will always be in contact with both rings. Equation (6.15) becomes

$$\begin{cases} Q_x = -K \sum_{k=1}^{N/2} (\delta_x \cos\phi_k + \delta_y \sin\phi_k)\cos\phi_k = \\ \quad = -K \sum_{k=1}^{N/2} \delta_x \cos^2\delta_x + \delta_y \frac{\sin 2\phi_k}{2} = -\delta_x \frac{KN}{4} \\ Q_y = -K \sum_{k=1}^{N/2} (\delta_x \cos\phi_k + \delta_y \sin\phi_k)\sin\phi_k = \\ \quad = -K \sum_{k=1}^{N/2} \delta_x \frac{\sin 2\phi_k}{2} + \delta_y \sin^2\phi_k = -\delta_y \frac{KN}{4} \end{cases} \quad \ldots\ldots\ldots \quad (6.21)$$

Hence, also in this case the force - deformation relationship is linear and time invariant and no VC vibrations would be generated. The stiffness is half that of the fully preloaded case.

For other than these two special cases, solutions to equation (6.17) have been obtained by simulation on a digital computer. The simulation

has been carried out using a modelling package called SLANG, which has been written for use on ICL computers by Hawker Siddeley Dynamics Limited, see ref.(8). The integration routine is a third order Runge-Kutta and the package is used in a similar way as an analog computer. Thus, Fig. 6.5 shows the analog circuit diagram using the notation below

$$\begin{cases} x_1 = \delta_x \\ x_2 = \dot{\delta}_x \\ x_3 = \delta_y \\ x_4 = \dot{\delta}_y \end{cases} \qquad \ldots\ldots\ldots \qquad (6.22)$$

Combining equation (6.22) and equation (6.17) gives

$$\begin{cases} \dot{x}_1 = x_2 \\ \dot{x}_2 = -\frac{Q_x}{M} \\ \dot{x}_3 = x_4 \\ \dot{x}_4 = -\frac{Q_y}{M} - g \end{cases} \qquad \ldots\ldots\ldots \qquad (6.23)$$

Using the values of Q_x and Q_y from equation (6. 15), equation (6.23) has been represented in a computer program, DYNSIM, using the SLANG package.

6.3 COMPUTATIONAL CONSIDERATIONS

By use of digital simulation techniques, problems like scaling and saturation of amplifiers, associated with analog simulation, are avoided. When using digital simulation it is however necessary to specify the step length of the simulation, i.e. the increment of the time variable between each consecutive value of the simulated variables. For a non-linear

system of this type, the only way to determine a suitable step length is by trial and error. If the step length is too long, the solution goes unstable, while if it is too short, it is not possible to cover a sufficient length of time in an economical way. For the range of loads which has been investigated, (225kg - 25kg), step times between 0.5 and 0.1 milliseconds have been used, the shorter step time for the lighter load.

A different kind of problem arises when it comes to choosing initial values for a particular run. DYNSIM requires the initial position and velocity of the shaft centre to be set before execution is started. If these values are not chosen so that the rotor is in static and dynamic equilibrium at the start of the run, a free vibration at the natural frequency of the system will result. Since it is impossible to calculate correct initial values, free vibrations will be superimposed on the VC vibrations. This is a considerable problem because the free vibrations can often be of greater magnitude than the VC vibrations, which are then obscured. Further, the free vibrations will interact with the VC vibrations and change these in an uncontrolled way. The problem has been overcome by using a specific start up procedure and by introducing damping in the system. The static equilibrium position is calculated for a particular load and cage position by use of equation (6.15). These values are used as starting values, and the rotor speed is gradually increased from zero to the set speed, see Fig. 6.6. A damping term is included into equation (6.17), hence

$$\begin{cases} M\ddot{\delta}_x + C_x\dot{\delta}_x - Q_x = 0 \\ M\ddot{\delta}_y + C_y\dot{\delta}_y - Q_y + Mg = 0 \end{cases} \quad \ldots\ldots\ldots \quad (6.23)$$

The purpose of the damping is to attenuate the free vibrations generated during the start up ($t<T_s$) before the variables are output ($t>T_{op}$), without significantly affecting the forced VC vibrations. To investigate the effect on the steady state vibrations by damping, two trial runs were made. All parameters were identical except for the damping which had the ratio $C_{x,1}/C_{x,2} = C_{y,1}/C_{y,2} = 2$. The solutions were virtually identical, which demonstrates that the steady state vibrations are only marginally affected by damping if the damping coefficients are carefully chosen. The setting of the parameters T_s, T_{op} and the damping coefficients are obviously crucial to obtain meaningful solutions. Generally T_s has been set at $T/3$, T_{op} at $0.9T$ and C_x and C_y to values giving a 20% reduction of energy per cycle of free vibrations, a Q-factor of about 31. The setting of the damping requires calculation of the natural frequency of the system, which has been approximately calculated using the stiffness coefficients from Fig.6.3.

DYNSIM outputs the calculated sequence of values for δ_x, δ_y, Q_x and Q_y. The output can be fed to a program calculating the maximum range of displacements and forces, $DXR = \delta_{x,max} - \delta_{x,min}$; $DYR = \delta_{y,max} - \delta_{y,min}$; $QXR = Q_{x,max} - Q_{x,min}$; $QYR = Q_{y,max} - Q_{y,min}$. Alternatively, the output is punched on paper tape for further analysis. The analysis of the punched tape is done on the Nova minicomputer with a programme called DSAN (DynSim ANalysis). DSAN reads the papertape and stores the contents on a disk file. Subsequently, DSAN plots δ_x, δ_y, Q_x, and Q_y as functions of time. By calling polar plot, δ_x and δ_y are used to plot the shaft locus and Q_x and Q_y are used to plot the vector locus of the reaction forces. Finally, the displacements and forces are frequency analysed using a FFT routine. Thus

each DYNSIM run produces 10 plots. It has been possible to incorporate several of the routines used for the DAS package (see Appendix II) in DSAN. The organisation of DYNSIM and DSAN is shown in fig. 6.7.

To produce a record over 150 msecs, the total simulation time will be 600 msecs with T_{op} set at 0.75T. Using a step length of 0.1 msecs, the computation time required is about 2.5 minutes on the ICL 1904. When the simulated record is output on papertape and analysed with DSAN a complication arises, in that the ICL paper tape code is not directly compatible with the code used by DGC. The necessary editing (exchange of exponent symbol and line separator) is done automatically with the DGC editor using a short macro routine which is set up for this purpose. The editing of a record of 512 samples takes about 20 minutes of computing time, but must due to shortage of core storage capacity be divided into two batches making the effective time required about one hour. A further problem with transferring large amounts of data from one computer to another by use of paper tape is that with the very long tapes required, mispunches and misreads often occur, which have to be traced and rectified. For the above mentioned reasons, DYNSIM runs which are output on paper tape have generally been limited to 550 lines. The actual DYNSIM program is not reproduced here since it requires the use of a SLANG compiler, which is only one of a number of simulation packages available. The setting up of a program to simulate eq.(6.23) is however a fairly straight forward task - programmed in SLANG about 400 lines is required.

The previously derived analytical solutions, see eq.(6.20) and eq. (6.21) have been used toverify the correct operation of DYNSIM. An

example from a preloaded bearing is shown in fig.6.8. This bearing was started under the static equilibrium position and given an initial horizontal velocity. It thus performs harmonic oscillations in the directions of both axis, but with a 90° phase lag. As is seen in fig. 6.8, the system behaves purely linear in spite of the fact that the cage is running at 20 r/s. Because of the damping, the ellipse is degenerated into a spiral which approaches the static equilibrium position. The amplitudes, frequency and damping measured from the graphs agree with those calculated analytically. Several other trial runs have also been made to ensure that the program works in a correct way.

6.4 Characteristics of VC Vibrations

In this section examples of DYNSIM runs with typical operating parameters will be presented and some particular phenomena believed to be typical for VC vibrations will be discussed. The nature of the predicted vibrations is verified by experimental results presented in this section and in section 8.1.

The dynamic effects can be looked upon from two points of view: They can be characterized either by the displacement of the shaft centre relative to the bearing housing, or by the forces on the bearing pedestal from rotor and bearing. The occurring reaction forces influence the operational life of the bearing and determine the level of noise and vibrations generated during operation, while the displacement characteristics are of prime importance in applications where accuracy and steadiness of run is emphasized. Each DYNSIM run produces a sequence of δ_x, δ_y, Q_x and Q_y as functions of time. These sequencies can be analysed

in detail using DSAN, but it is practically possible to analyse only a small number of runs in this way. As a measure of the overall severity of vibrations two parameters are therefore defined: Dynamic Force Parameter, DFP = QYR/(Mg), and Dynamic Displacement Parameter, DDP = DXR + DYR, with QYR, DXR and DYR defined in section 6.3.

Values for DDP and DFP have been calculated for 40 realistic combinations of load (25 - 225 kg) and speed (715 - 5710 RPM shaft speed). The bearing simulated is a cylindrical roller bearing with twelve rollers, a local stiffness of $107 \cdot 10^6$ N/m (calculated with eq. 3.34 for a roller length of 10 mm) and with a radial clearance of e = 50 microns. The results are plotted in fig. 6.9 and fig. 6.10 respectively. One point to make about the DYNSIM runs is, that due to the highly nonlinear character of the system, slight changes of running conditions might cause drastic and abrupt changes of the solutions. Interpolation (and of course, extrapolation) is therefore hazardous. Hence, although the DDP and DFP surfaces are correct at the grid points, intermediate values should be used with caution. It has been necessary to economize with the number of grid points in order to keep computation time within reasonable limits - to calculate a complete surface of 40 points takes about one hour and forty minutes.

The main factors governing VC vibrations are speed, load and radial clearance. VC vibration variations with these parameters are exemplified with DSAN runs presented in figs. 6.11 to 6.25. Variation with speed is shown in figs 6.11 to 6.15, where load and clearance are kept constant (M = 75 kg; e = 50 microns) and the speed is varied between 0.6 and 35.0

cage revolutions per second (85 - 5000 RPM shaft speed). The shaft loci are given in fig. 6.11 during 150 msecs. Note that in all loci plots, the coordinate system is translated downwards a distance e in order to obtain suitable scaling. Fig. 6.12 gives vertical shaft displacement, $\delta_y(t)$, and fig. 6.14 gives vertical reaction force, $Q_y(t)$, both during 200 msecs. The spectral distribution of δ_y and Q_y are calculated by Fourier Transform and presented in figs 6.13 and 6.15. Variations with load are shown in figs. 6.16 to 6.20, where speed and clearance are kept constant (f_c = 8.0 Hz, corresponding to f_s = 1145 RPM; e = 50 microns) and the load varies between 25 and 225 kg. Finally, variations with clearance is given in figs. 6.21 to 6.25, where load and speed are kept constant (f_c = 8.0 Hz; M = 125 kg), while e varies between 25 and 100 microns. Except for the loci plots, only vertical displacements and forces have been analysed. The reason for this is, that the vertical dynamic force is superimposed on the static load and it therefore seems likely that vertical effects are more critical than horizontal ones, although quite large movements occur in the horizontal direction.

The experimental study of VC vibrations of a real bearing is made difficult by several factors. The existence of form errors of the bearing components causes vibrations, which have a magnitude comparable to those of the VC vibrations. Further, VC vibrations will be greatly affected by misalignment, unbalance and flexibility of rotor shaft and bearing pedestal. For these reasons it has not been considered realistic to aim at making quantitative comparisons between theoretical and experimental results, but merely to demonstrate that the predicted phenomena associated with VC vibrations actually occur in practice.

The experimental runs have been carried out with the bearing vibration test rig (see Chapter 4) using a cylindrical roller bearing type N206 having twelve rollers. The bearing was oil lubricated (Shell Carnea 31) and was carefully aligned using the method described in Chapter 9. For the runs referred to in Chapter 8, a single row, spherical roller bearing type 20206 was used. The generated vibrations were picked up by an accelerometer positioned on the bearing housing right under the bearing. The original vibrations from the bearing will obviously be coloured by the dynamic properties of the bearing housing and fundament, and due to the non-linearity of the system, there is no simple way of compensating for this (see section 8.1). Nevertheless, characteristic phenomena may still be recognised.

The DDP and DFP surfaces of figs. 6.9 and 6.10 show the overall dynamic behaviour of the rotor - bearing system. Large movements occur at low speed and heavy load. As is seen from fig. 6.16 these are mainly horizontal movements with the shaft rocking back and forward in the bearing. A ridge, most clearly seen in fig. 6.10, goes diagonally across the surface, starting at 32 Hz, 25 kg and leading to 15 Hz, 175 kg. The largest DFP value, 2.5, occurs at 33 Hz, 25 kg, i.e. at this point the dynamic load is as high as 125% of the static load. The loci plotted in fig. 6.11 represents running conditions along the 75 kg load line of fig. 6.9. At 25.0 Hz it crosses the ridge and at this point very large vibrations result. Due to the coupling between vertical and horizontal movements large displacements in one direction will also generate large displacements in the other direction. It is however clear that the locus at this load - speed combination has a much larger vertical component than

was the case for the low speed - heavy load cases. An indication of the underlying reason for the occurrence of large vibrations at certain load - speed combinations can be obtained by studying the stationary rotor - bearing assembly. For many typical combinations of load, speed and clearance only one and two, or two and three rollers will be loaded during one RP cycle. The stiffness of the bearing at the instants when the rollers are symmetrically arranged around the load line can be obtained from fig. 6.3. The stiffness at intermediate cage positions will not deviate substantially from these values. The assembly stiffness will remain constant over a certain range of displacements making the system linear for longer or shorter periods of the RP cycle. Fig. 6.26 shows the natural frequencies in vertical and horizontal directions for the instants with one, two or three rollers symmetrically arranged around the load line. Instead of scaling the abscissa axis in Hz, it has been scaled in the cage speeds giving a RP frequency coinciding with the natural frequency of the bearing, i.e. it gives the critical cage speed for a certain load and certain number of rollers under load. It is not possible to relate the stationary bearing and the rotating bearing to each other in a detailed, analytical way - with the rotor running and the number of rollers under load constantly changing, the rotating system does not have natural frequencies in the same way as a linear system does. It is however a reasonable hypothesis to assume that the rotating system will exhibit resonant like behaviour in the load - speed regions of the stationary natural frequencies. By the term "resonant like" is then simply meant that if the forcing frequency coincides with a natural frequency of the system, large but unspecified vibrations will result. The hypothesis was proved valid both by the results of the DYNSIM runs

and from experimental runs. Comparing fig. 6.9 and 6.10 with fig. 6.26 it is apparent that the diagonal ridge in fig. 6.10 coincides very well with the resonant region for vertical motion in fig. 6.26. Also the previously mentioned change from distinctively horizontal movements for the low speed - heavy load cases to loci with a larger component of vertical motion is consistent with the hypothesis. The points furthest away from the resonant region of fig. 6.26 are in the top right corner of the diagram. In fig. 6.9 and 6.10 it is also apparent that these parts of the surface are the ones least affected by dynamic effects (see also fig. 6.12 and 6.14). Running the bearing above the resonant region resembles running a flexible shaft over-critically, thereby stabilizing it. The DDP values approach zero for increasing speed, while the DFP values approach a small but non zero constant value for high speed. These characteristics are also analogous to the over-critically running flexible shaft. In Chapter 8 it is shown that whether the resonance is a property of the bearing itself or of the whole rotor - bearing - fundament system is irrelevant. Fig. 8.2 and 8.3 show response curves for cases where the bearing RP frequency is passing through a system resonance. In both cases the natural frequency of the resonance was measured on a stationary system.

One might think that since the stiffness variation causing VC vibrations is periodic, the resulting movements would also always be periodic. This is however not necessarily the case, because the system's initial conditions (position and velocity of shaft centre) might well be different at the start of each new cycle of stiffness variation. The set of starting values determine the character of the subsequent locus

cycle, and the way in which the starting values change from one cycle to the next determines the type of solution obtained. Hence, for a system where the initial conditions remain identical at the start of each new cycle, the solutions will be periodic with loci having essentially closed traces (6.11: 0.6, 2.7, 8.0 Hz; 6.16: 25, 75 kg; 6.21: 25 microns). As is seen in the loci plots, there also exists solutions which do not produce closed traces, but behave in a more unpredictable way. Although these solutions are non periodic, they have, with two exceptions, stable characteristics in that they have a constant RMS value and a constant and well defined spectral distribution if the averaging time is chosen long enough. These solutions could therefore be classed as non periodic, stationary. The manner in which the starting values change could be either random (e.g. 6.11: 25 Hz and 6.21; 75 microns) or more systematic. One example of the latter case is fig. 6.11: 15.0 Hz, where the shaft centre moves up and down along a near vertical line. Superimposed on this motion is a slow horizontal motion which makes the shaft wander slowly back and forward in the horizontal direction.

Among the DYNSIM runs two cases were found, which did not stabilize during the available simulation time, 6.16: 225 kg and 6.21: 100 microns. In the latter case, the shaft centre performs near circular motions for the first 25 cycles of the record and then whips out predominantly in the horizontal direction, see also fig. 6.24. No extensive analysis has been made of these non stationary cases, since this would require very long DYNSIM runs. Thus, the presented samples merely demonstrate the existence of such phenomena. The loci plots are not an ideal way of

representing slow changes with time. Instead a method which offers better clarity has been employed. By use of a special plotting routine (HELIPLOT) linked to the DSAN package, the locus of fig. 6.16: 225 kg, has been expanded into a helical in fig. 6.31. As this figure shows, the shaft swings back and forward in the horizontal direction with large and smooth movements for the first half of the record, but after about 0.1 secs, the motion becomes progressively more jerky with a diminishing amplitude. The two apparently non stationary cases that were found, seem to be examples where the initial conditions vary in a systematic way with cycle times much longer than the RP time. One way of explaining the phenomena is to assume that the starting values change from one RP cycle to the next in such a way that a positive increment of the starting values of one cycle causes a positive increment of the subsequent starting values and vice versa. The displacements build up until they are limited by non linearities of the system, then the trend reverses and the amplitudes start to decrease. Thus, the motion is characterized by beats having a time period which is much longer than the RP cycle time. The load - speed combination of fig. 6.16: 225 kg, is near a resonance and experimentally, slow beats of the type predicted have also been found when running a bearing with its RP frequency close to a system resonance, see the scope photographs of fig. 8.3.

The spectrograms obtained from the DYNSIM runs are mainly of line spectrum type, i.e. they have a well defined spectral content. The RP frequency is the fundamental and normally, dominating peak, but harmonics and also subharmonics occur. Fig. 6.27 shows an example from an experimental run with a large fundamental and several diminishing harmonics.

For some running conditions, a clean sinewave at RP frequency results, in which case no harmonics occur, see the experimental run in fig. 6.29 and the DYNSIM run in fig. 6.15: 35 Hz. Subharmonics seem to occur only for solutions having large horizontal movements, as is seen when comparing loci plots and spectrograms. This seems to be so irrespective of whether the large horizontal movements arise due to resonant excitation (6.18 and 6.20: 175 kg with subharmonics at 1/3 RP frequency) or because of a situation where a very light rotor bounces around on the rollers (6.18 and 6.20: 25 kg with subharmonics at 1/2 RP frequency). Fig. 6.30 shows an example of such a light rotor having subharmonics at 1/2 RP frequency. Figs. 8.4 to 8.7 show some cases of subharmonics arising at 1/5 RP frequency when large vibrations are excited during the passage of a system resonance. Due to resonances one of the first harmonics might have a greater magnitude than the fundamental. An example from the experimental runs is shown in fig. 6.28 and from the DYNSIM runs in fig. 6.20: 125 kg.

The subject of VC vibrations in the context of resonant excitation will be further discussed in section 8.1.

6.5 Generalization of the equation for VC vibrations

Previously in this chapter only bearings with a linear force-deformation relationship between rolling bodies and tracks have been considered. This linearization is adequate for bearings having line contact and also gives approximate solutions for other types of contacts provided the displacements are small. Generally, however, the linear relationship of eq. (6.9) does not hold true for any other type of

bearings than cylindrical roller bearings. Rolling bearings like spherical ball bearings, deep groove ball bearings, spherical roller bearings and so on, have local stiffnesses that are functions of the deformation. Hence, eq. (6.9) is modified to

$$P(\phi) = k\delta^{w}(\phi) \qquad \ldots\ldots\ldots (6.24)$$

For bearings having point contacts, the value for w is, according to eq. (3.30), 3/2. As was pointed out in Chapter 3, the Hertzian theory presupposes contact zones, which are small compared to the dimensions of the mating bodies. This condition is fulfilled for low osculation type bearings, but not for high osculation type bearings like deep groove ball bearings and spherical roller bearings. For such contact conditions the appropriate value for w is best obtained experimentally. Having obtained a value for w, eq.(6.9) is replaced by eq.(6.24) and the derivation of the force - displacement function for the bearing assembly is carried out in the same way as for cylindrical roller bearings. The counterpart to eq. (6.15) for cases of non linear local contact conditions then becomes

$$\begin{cases} Q_x(\delta_x;\delta_y;\psi) = -K \sum_{k=1}^{N} (\delta_x\cos\phi_k + \delta_y\sin\phi_k - e)^{w}\cos\phi_k \; U[\delta(\phi_k)] \\ Q_y(\delta_x;\delta_y;\psi) = -K \sum_{k=1}^{N} (\delta_x\cos\phi_k + \delta_y\sin\phi_k - e)^{w}\sin\phi_k \; U[\delta(\phi_k)] \end{cases}$$

$\ldots\ldots\ldots$ (6.25)

Equation (6.25) is then substituted in eq.(6.23) and solutions might be determined by simulation with a modified DYNSIM program. Also external forces, eg. due to unbalance, can easily be included.

One point of fundamental difference between bearings with linear contact characteristics and bearings with non linear contact characteristics is that, for the cases where the former type does not generate VC vibrations (either e = 0 or e larger than occurring displacements), the latter type will still generate such vibrations. Hence by adjusting the clearance of cylindrical roller bearings, VC vibrations might, at least in theory, be eliminated, which is not the case for other types of rolling bearings.

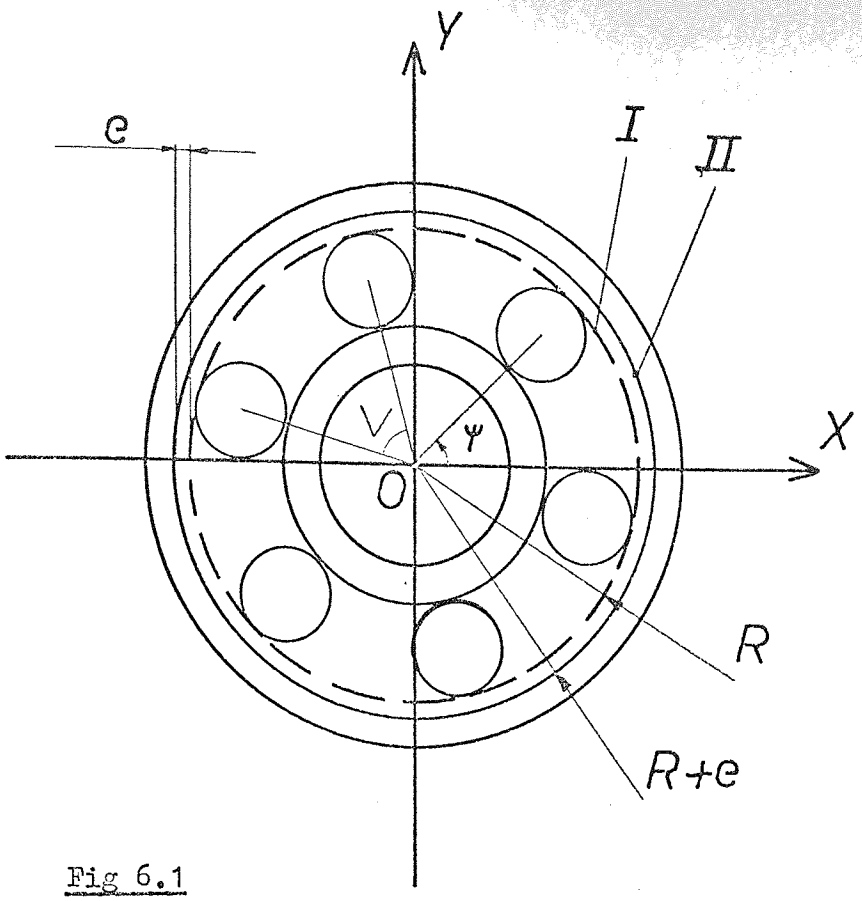

Fig 6.1

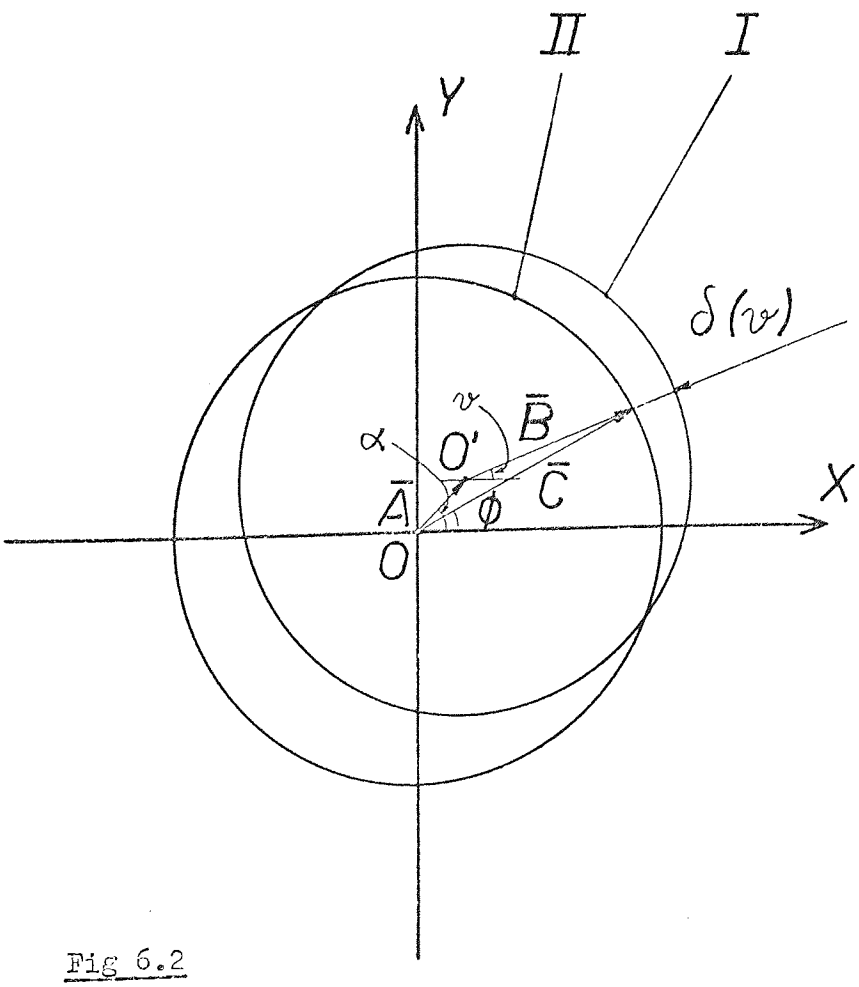

Fig 6.2

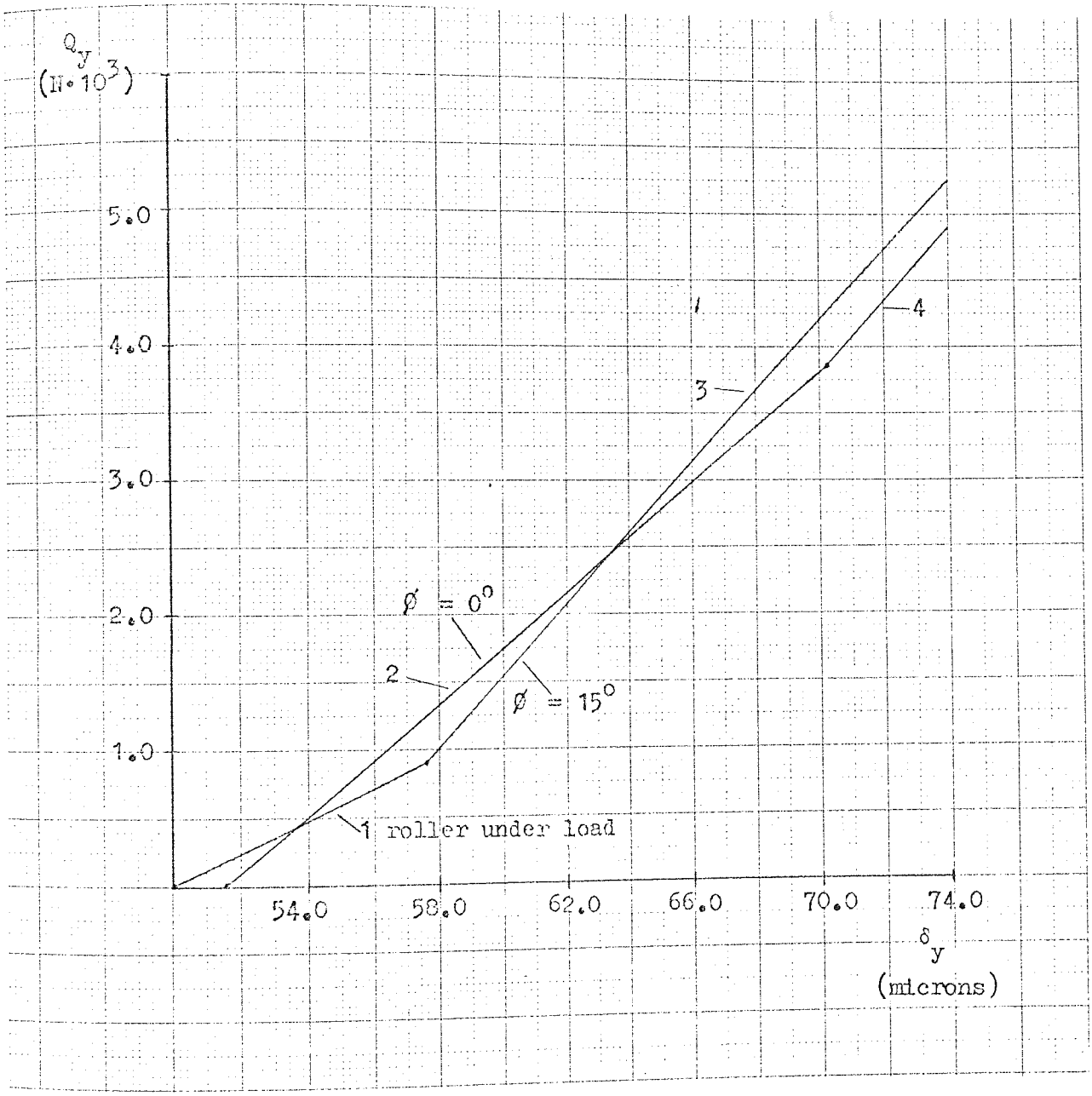

Fig.6.3. Force - deformation relationships for a cylindrical roller bearing with either a roller or a gap under the load line. N = 12; e = 50 microns; K = $109 \cdot 10^6$ N/m. The numbers 1 to 4 in the diagram refers to the number of rollers in the load carrying zone at a specific load.

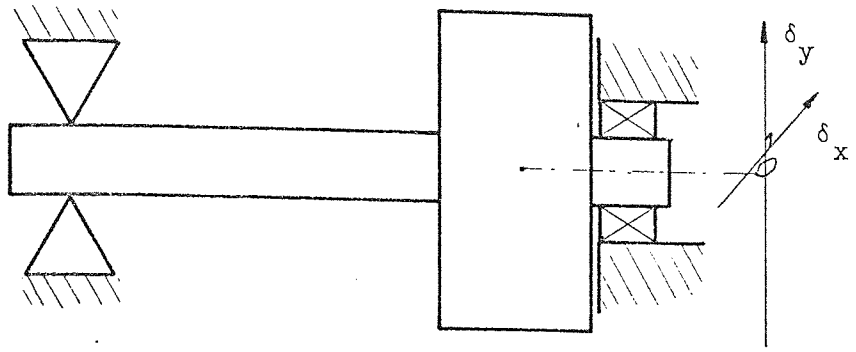

Fig 6.4 Rotor - bearing arrangement

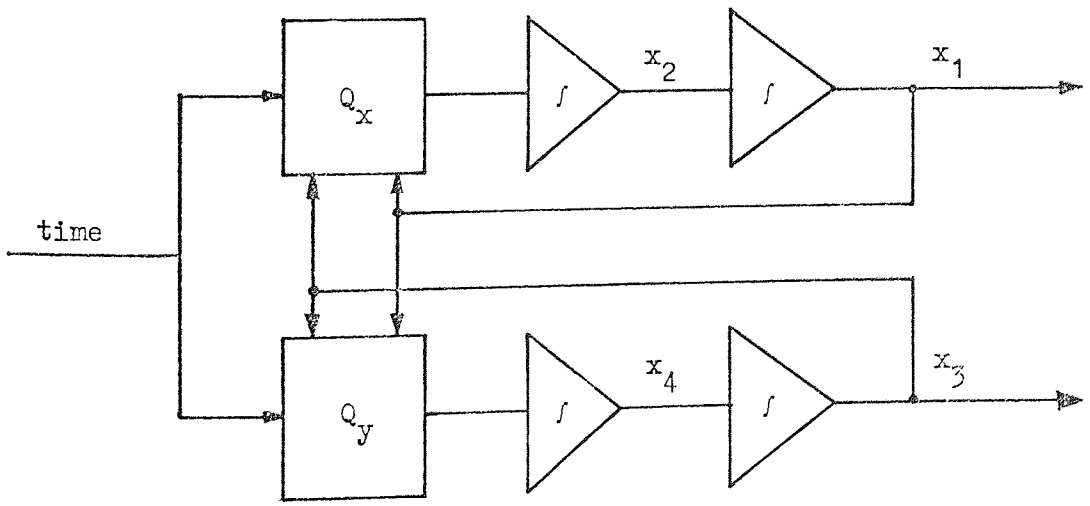

Fig 6.5 Analog circuit diagram for simulation of VC vibrations

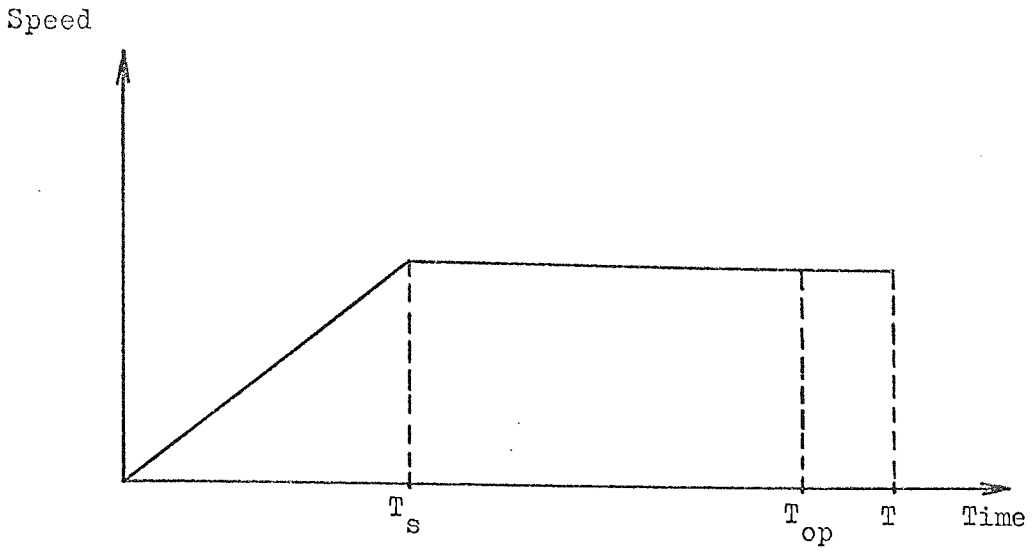

Fig 6.6 Starting up procedure of simulation

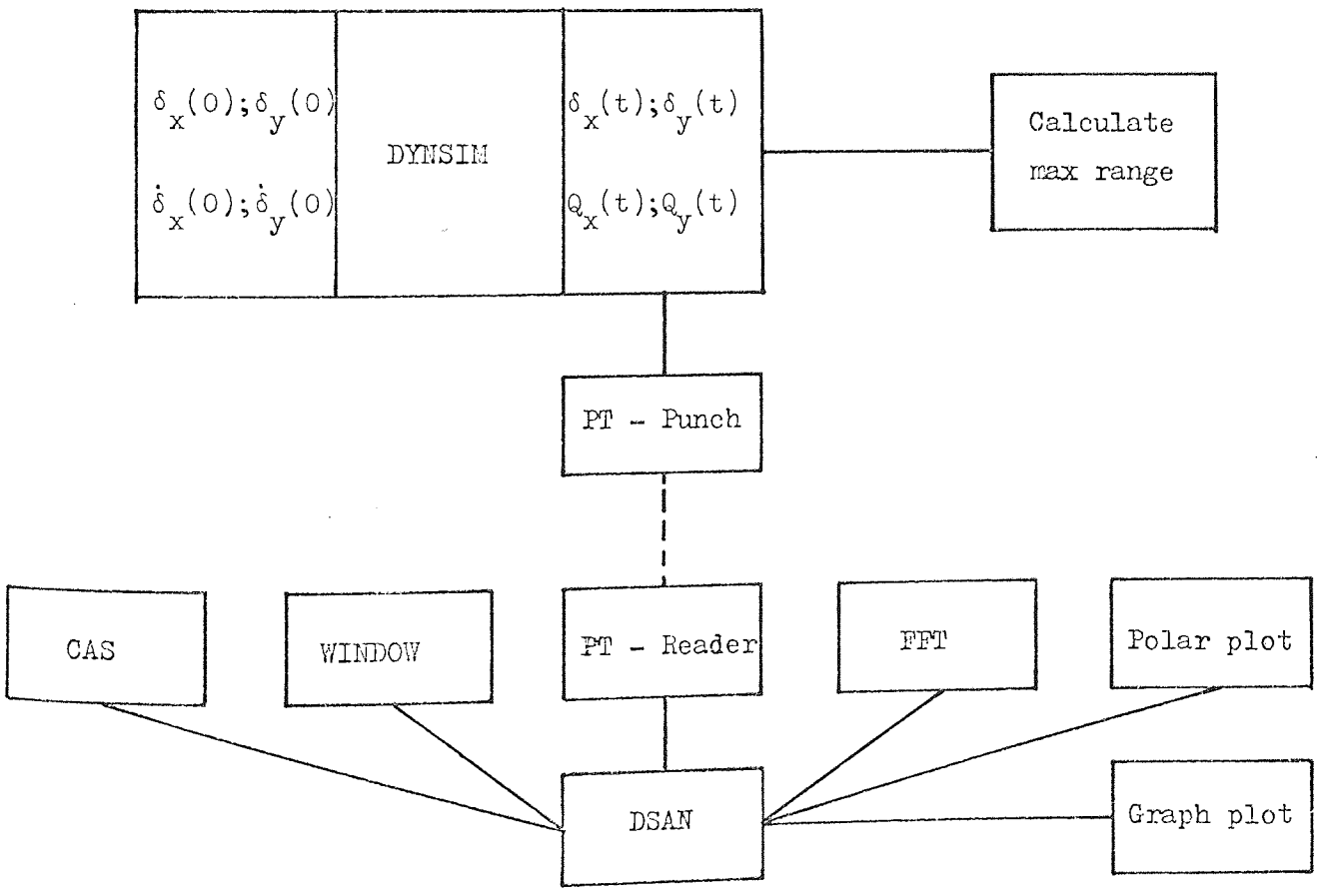

Fig 6.7 Organisation of simulation programs

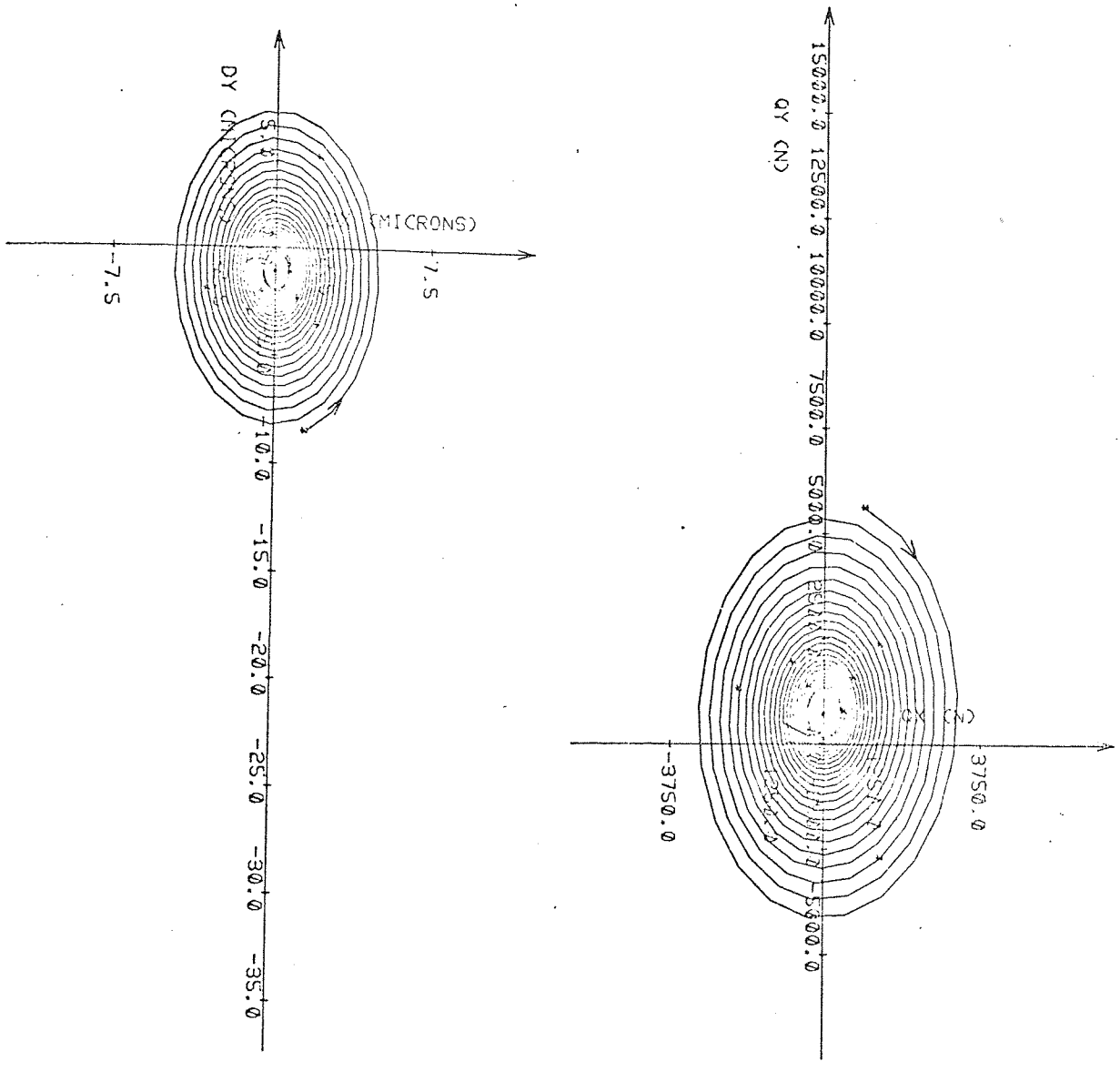

Fig 6.8 Shaft locus (see fig 6.4) and reaction force vector plots for preloaded bearing

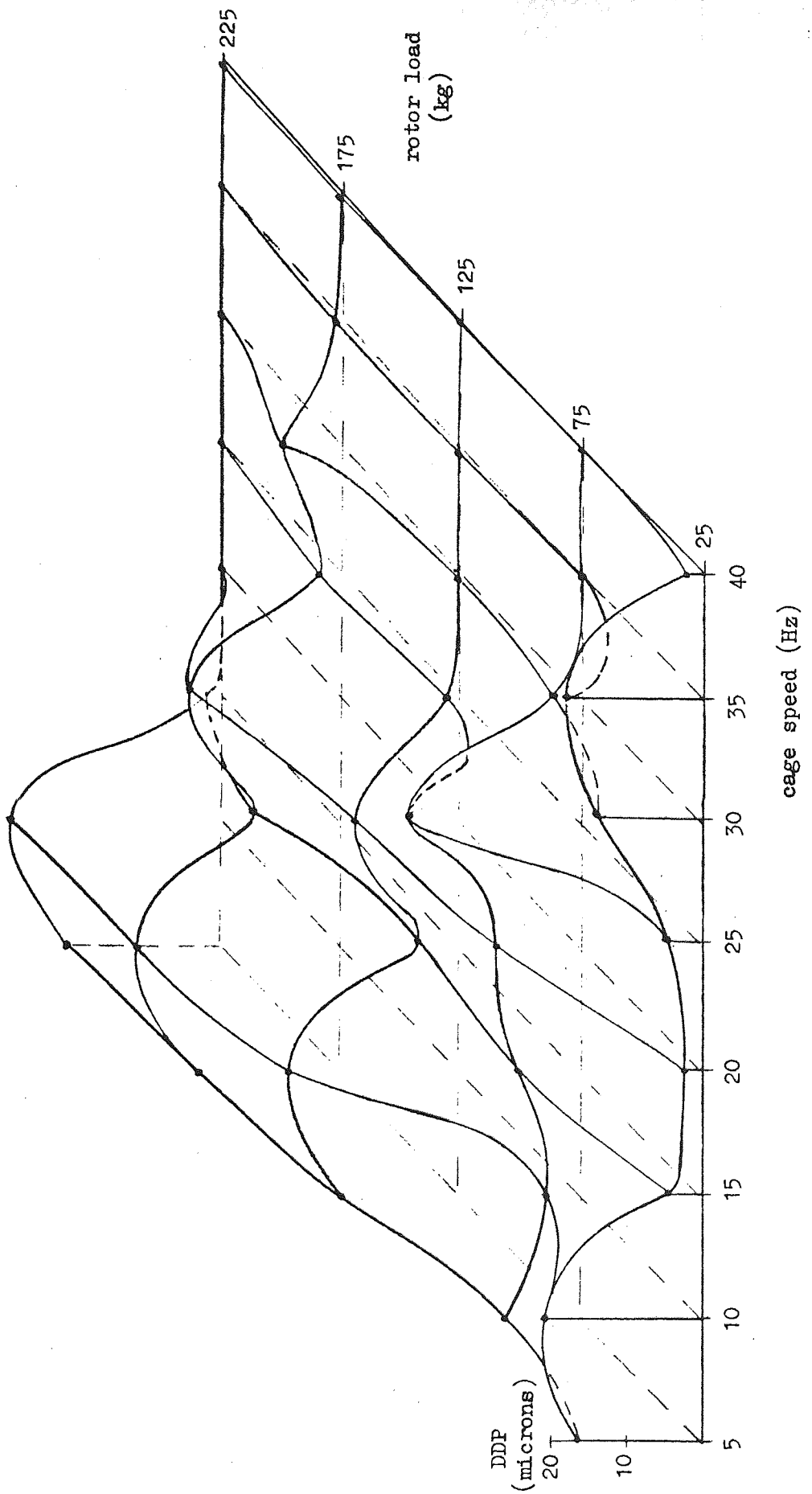

Fig 6.9 DDP surface for e = 50 microns.

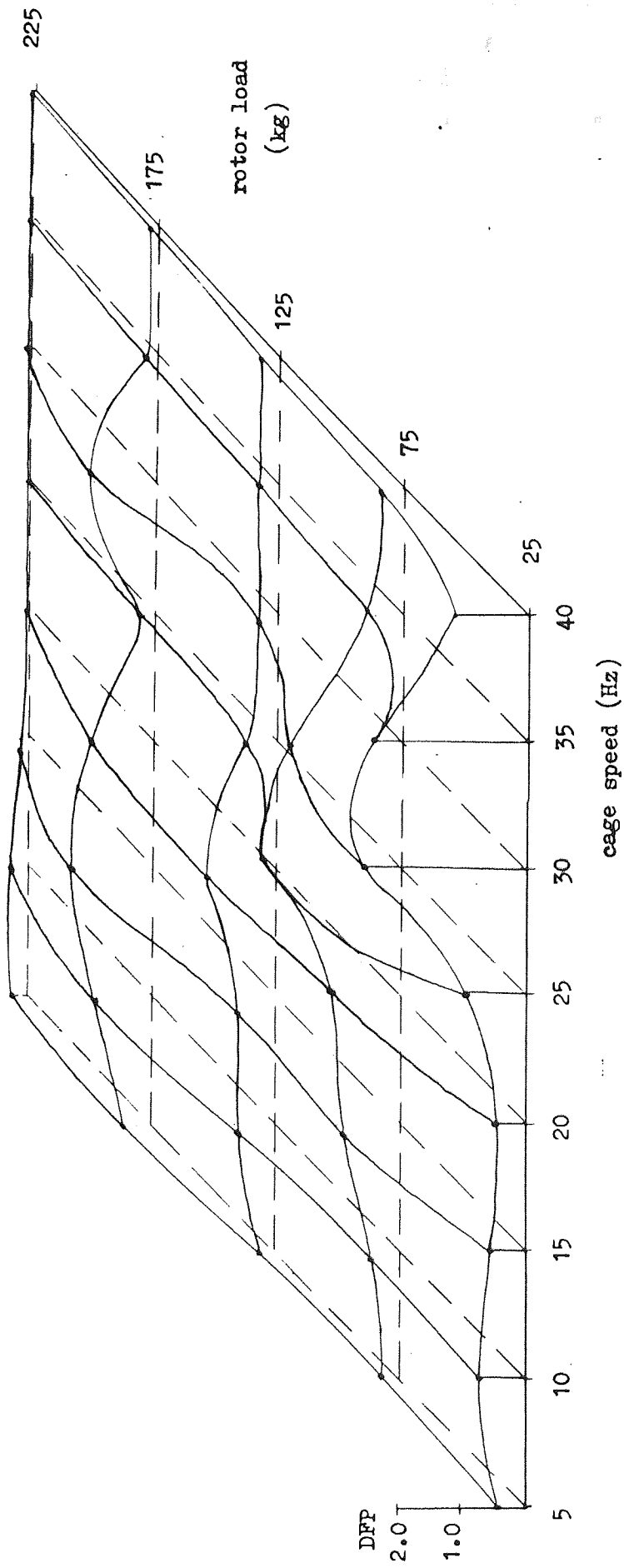

Fig 6.10 DFP surface for e = 50 microns.

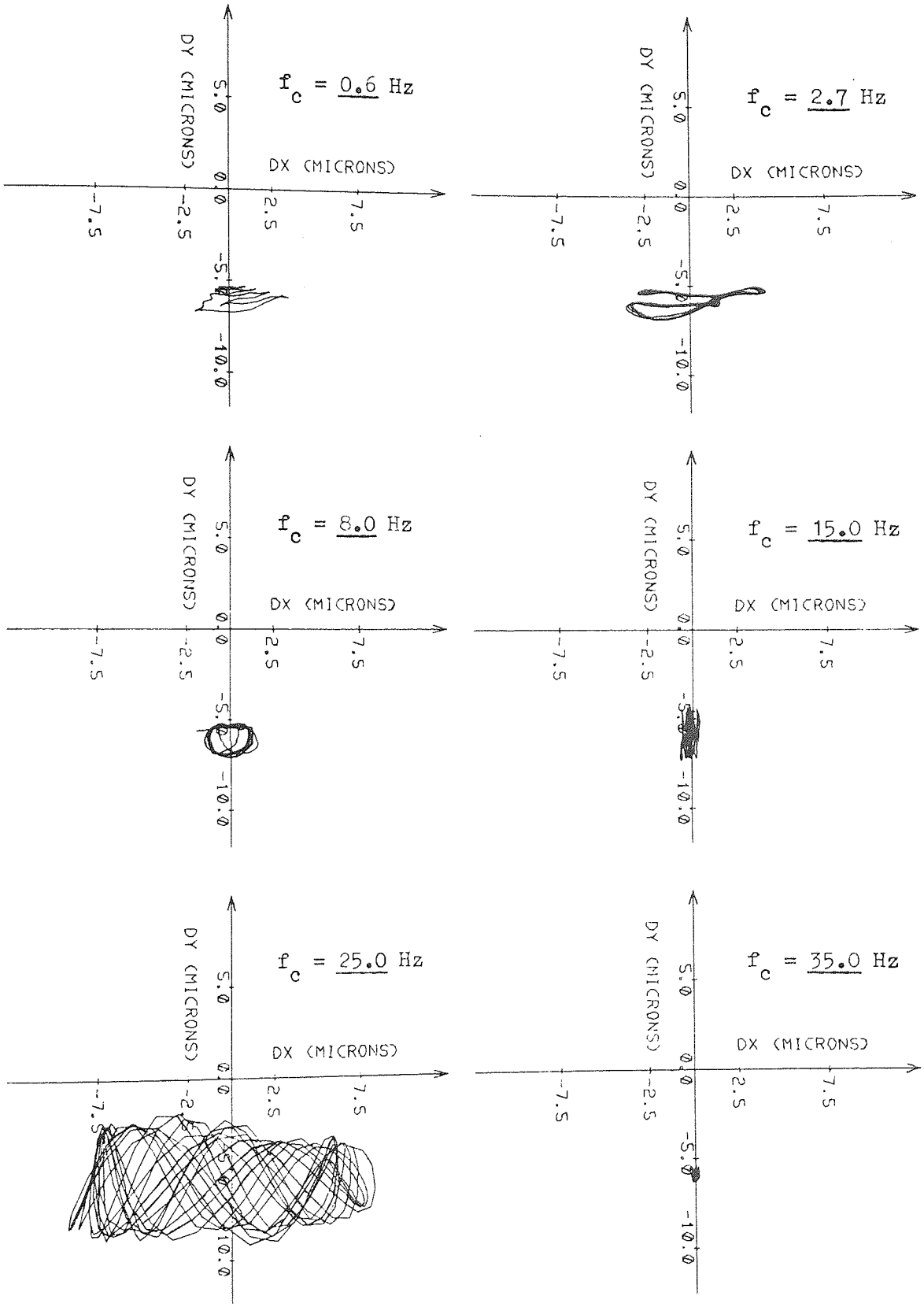

Fig 6.11 Shaft loci variations with speed. M = 75 kg; e = 50 microns.

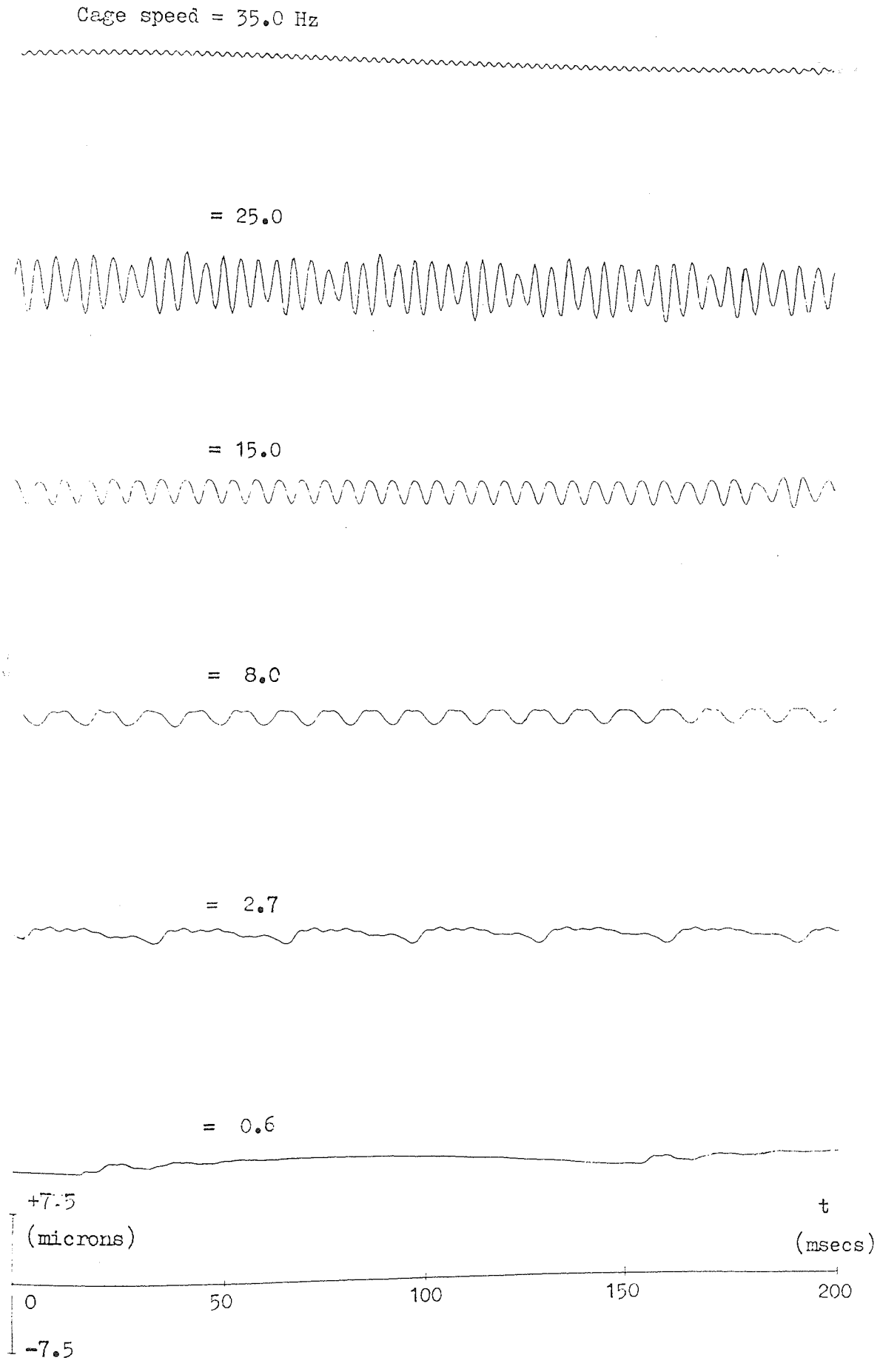

Fig 6.12 Vertical displacement of inner ring center. M = 75 kg; e = 50 microns.

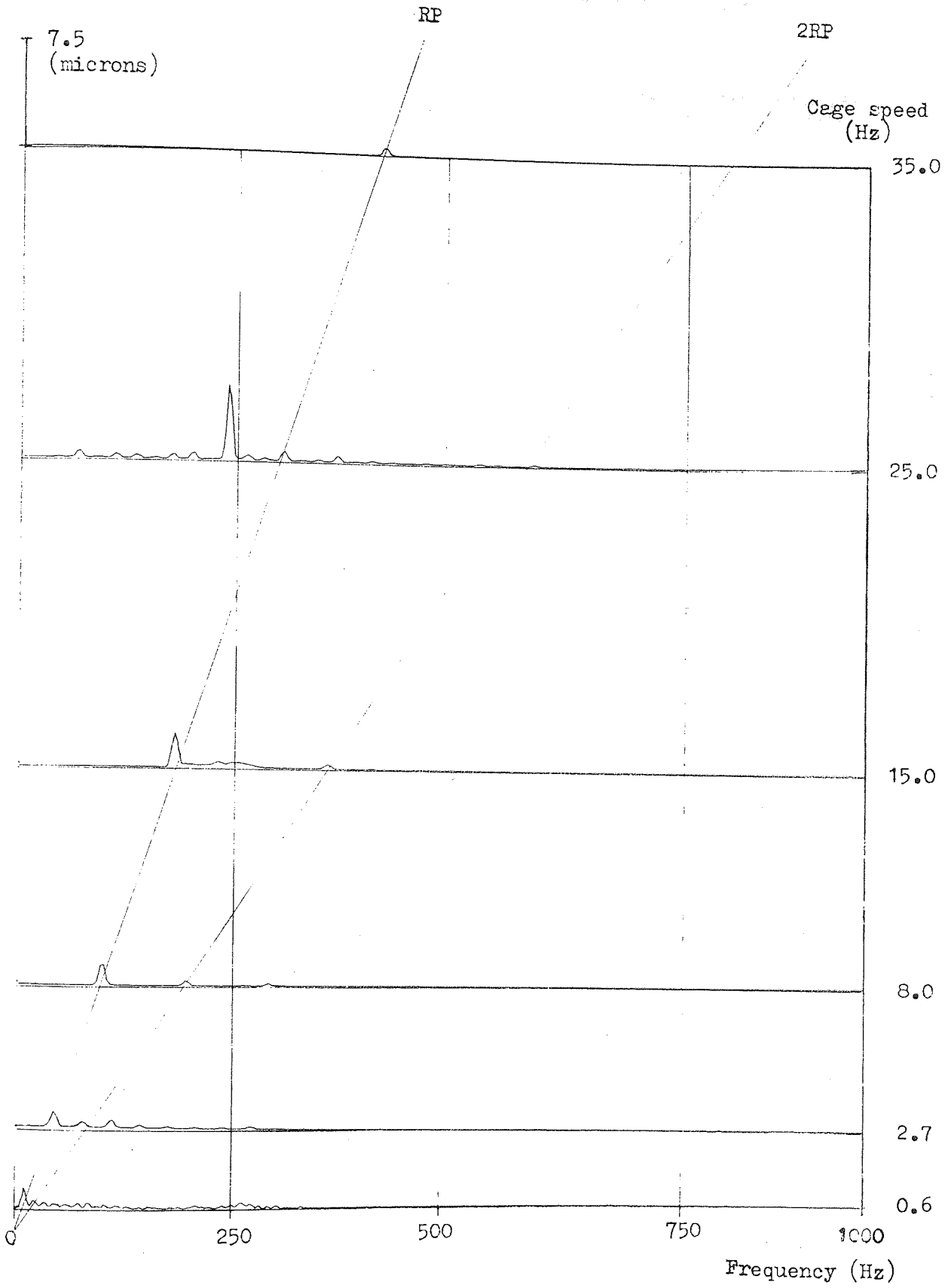

Fig 6.13 Spectral distribution of the displacement functions given in fig 6.12.

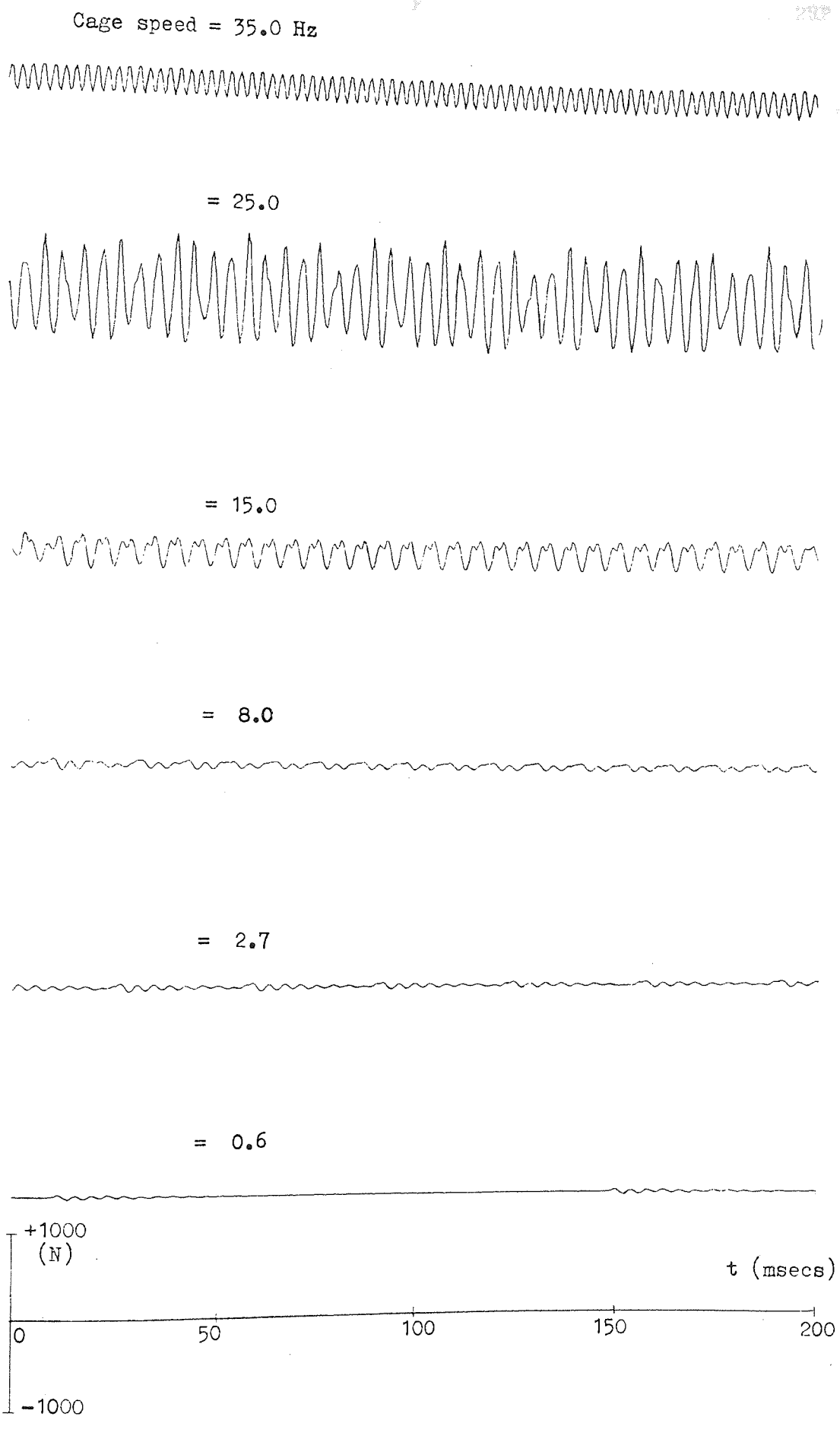

Fig 6.14 Vertical reaction force ($Q_y(t)$). M = 75 kg; e = 50 microns.

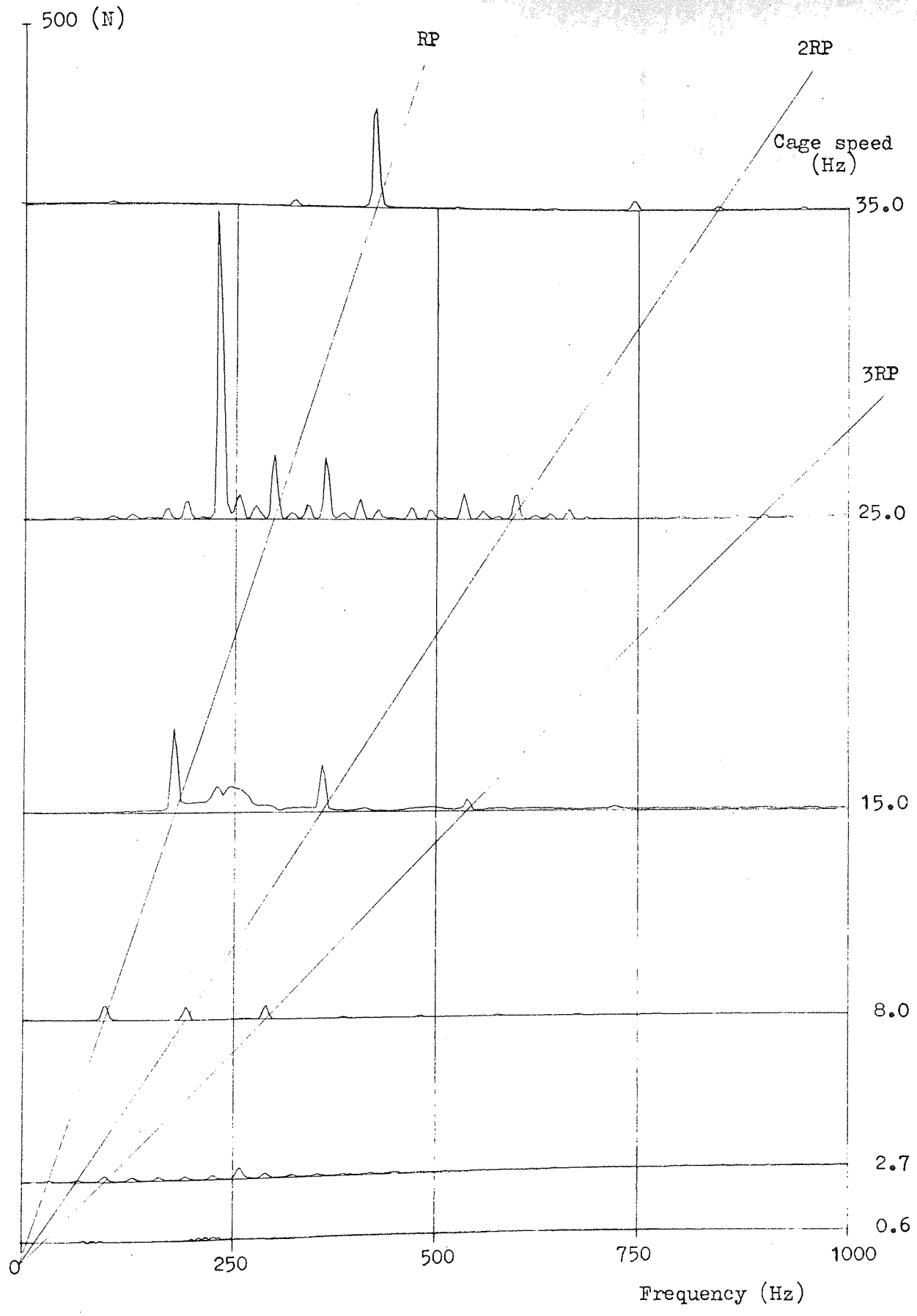

Fig 6.15 Spectral distribution of the force functions given in fig 6.14.

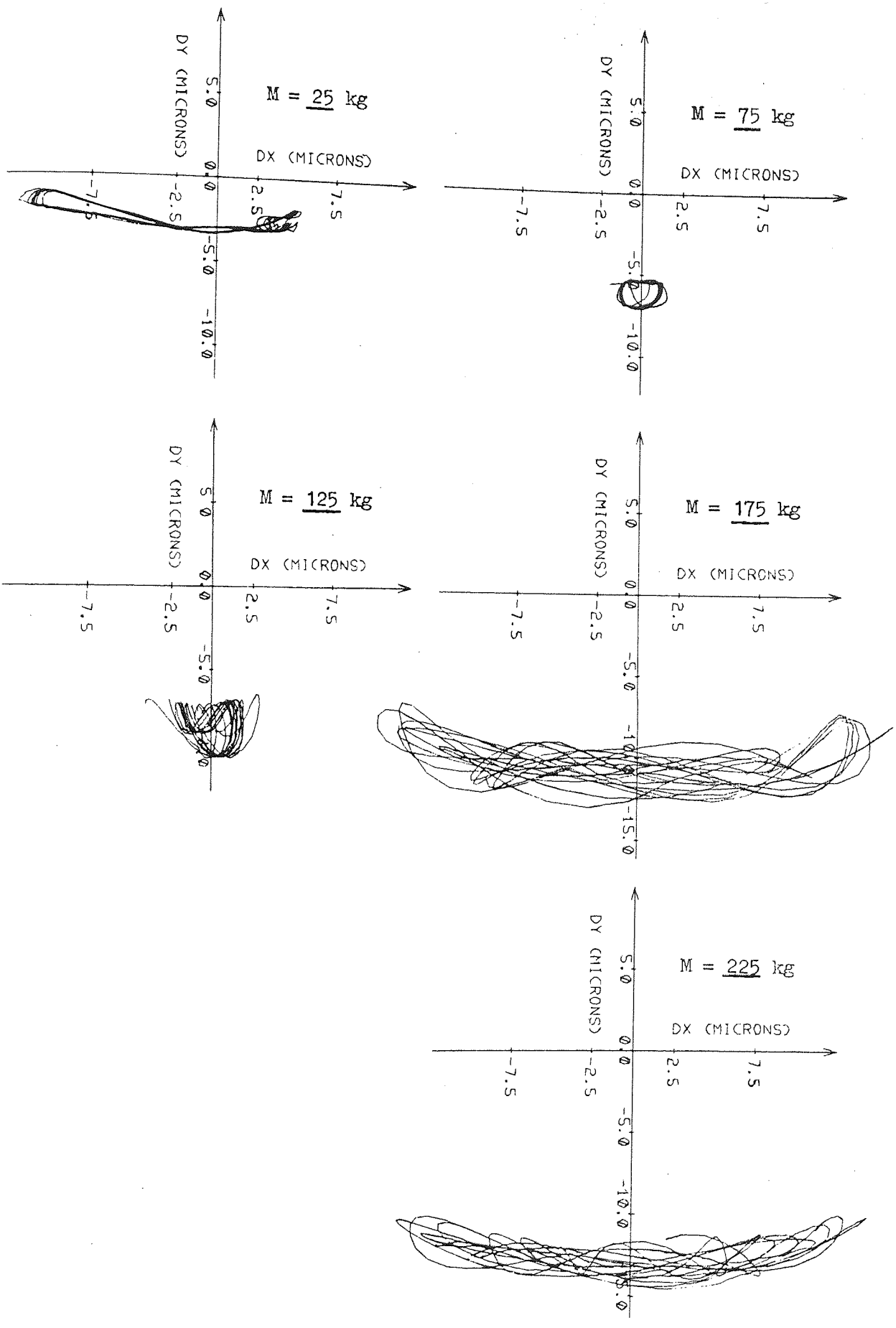

Fig 6.16 Shaft loci variations with load. f_c = 8.0 Hz; e = 50 microns

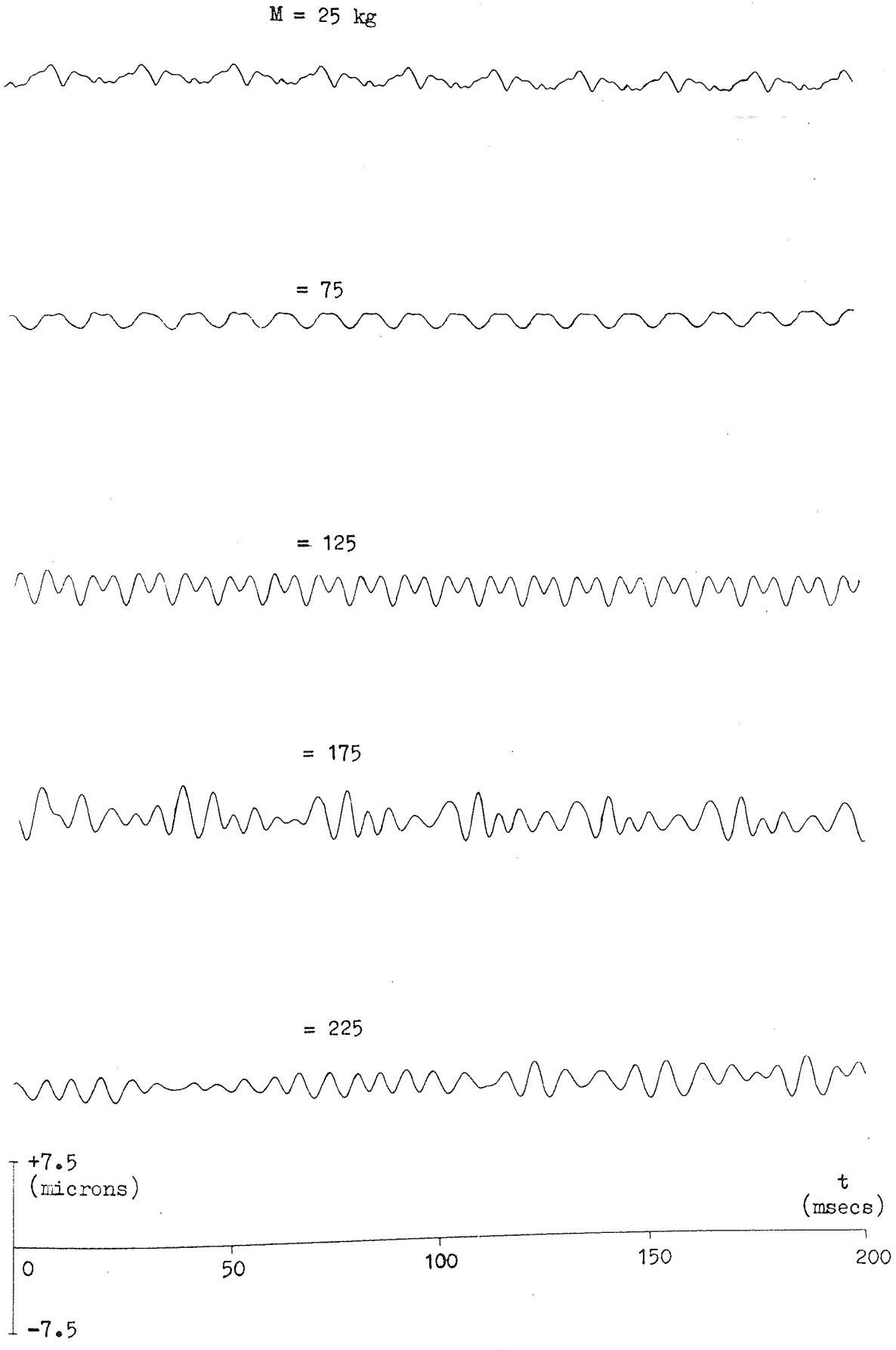

Fig 6.17 Vertical displacement of inner ring center. f_c = 8.0 Hz; e = 50 microns.

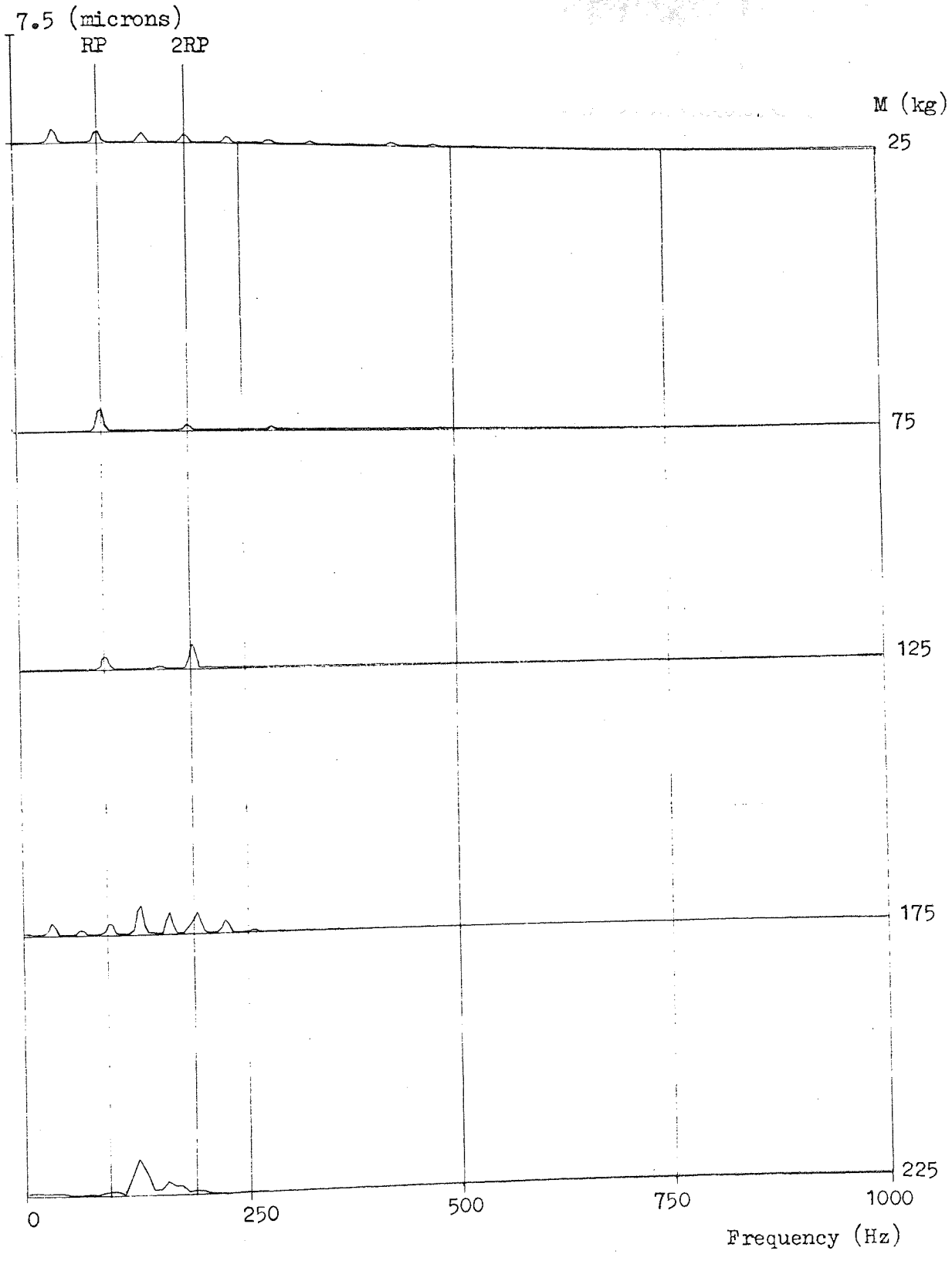

Fig 6.18 Spectral distribution of the displacement functions given in fig 6.17.

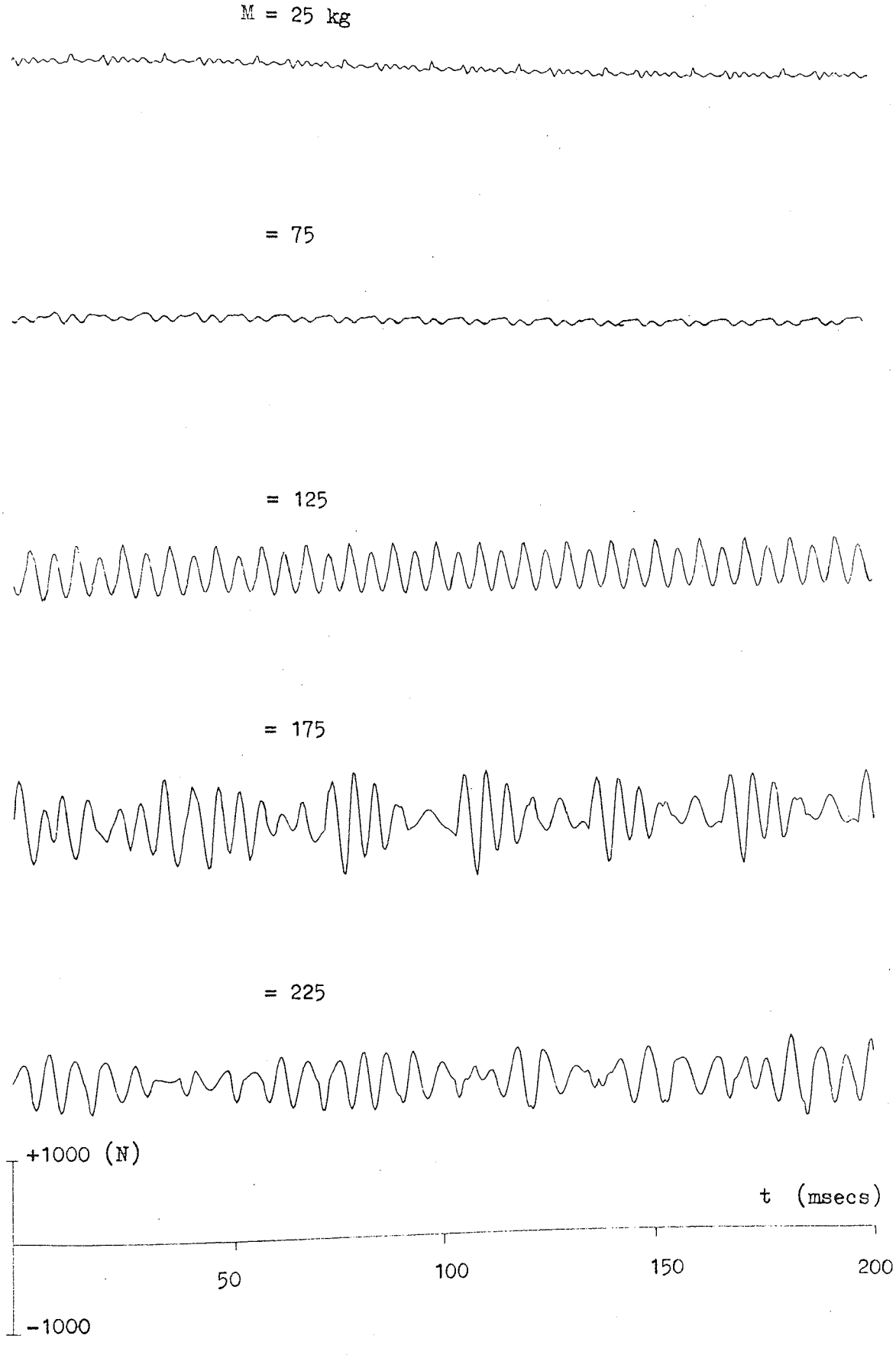

Fig 6.19 Vertical reaction force ($Q_y(t)$). f_c = 8.0 Hz; e = 50 microns.

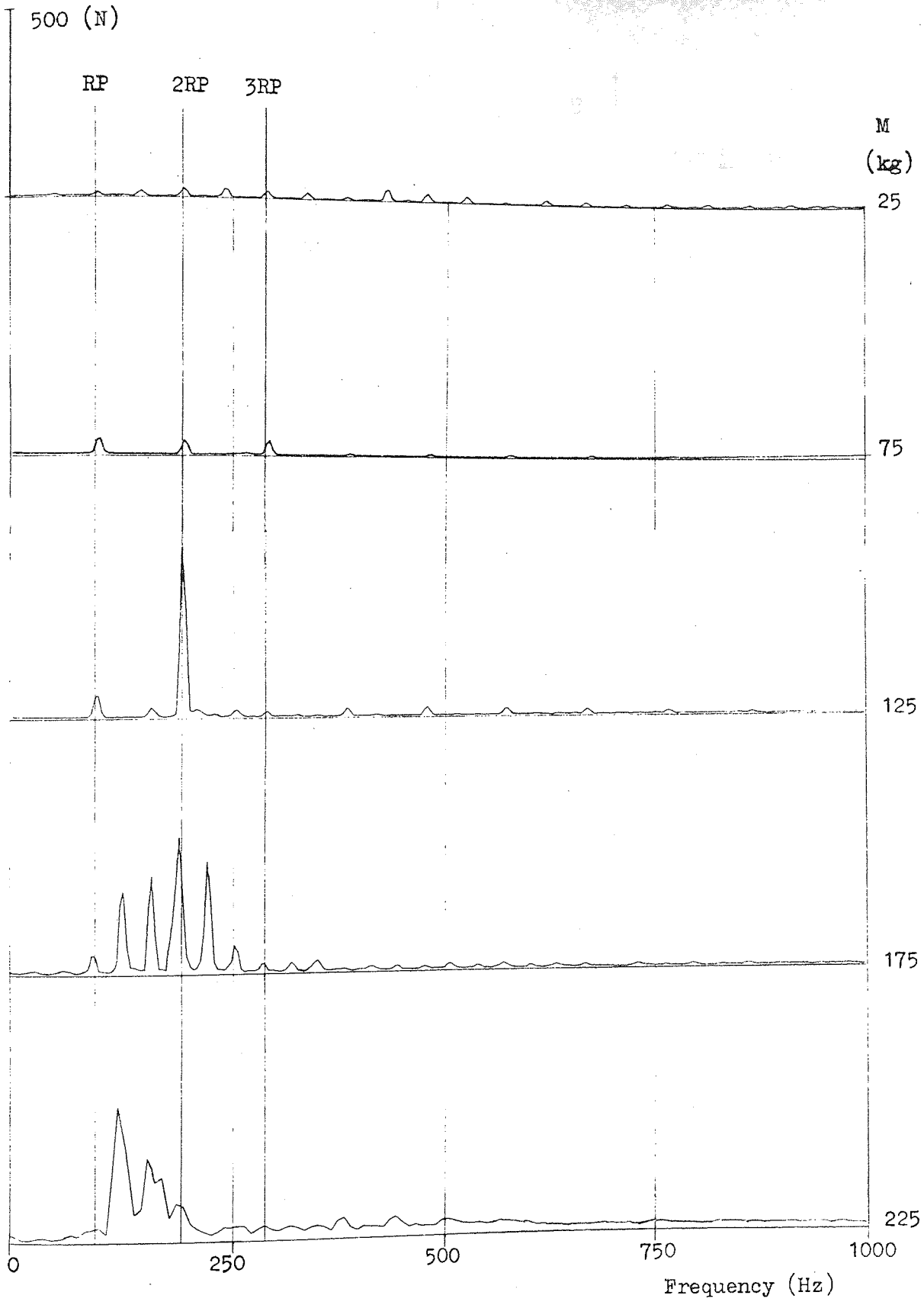

Fig 6.20 Spectral distribution of the force functions given in fig 6.20

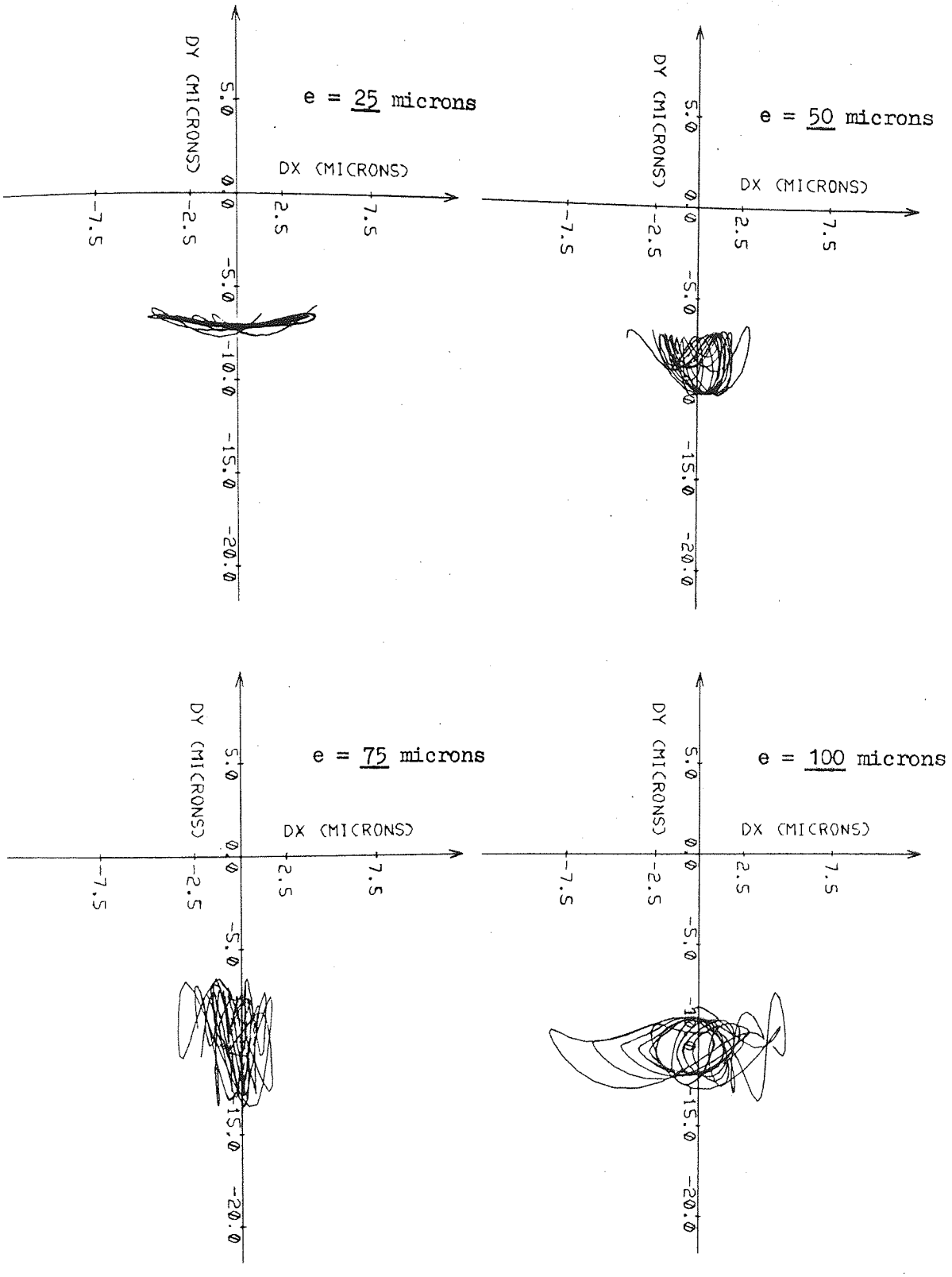

Fig 6.21 Shaft loci variations with clearence. f_c = 8.0 Hz; M = 125 kg.

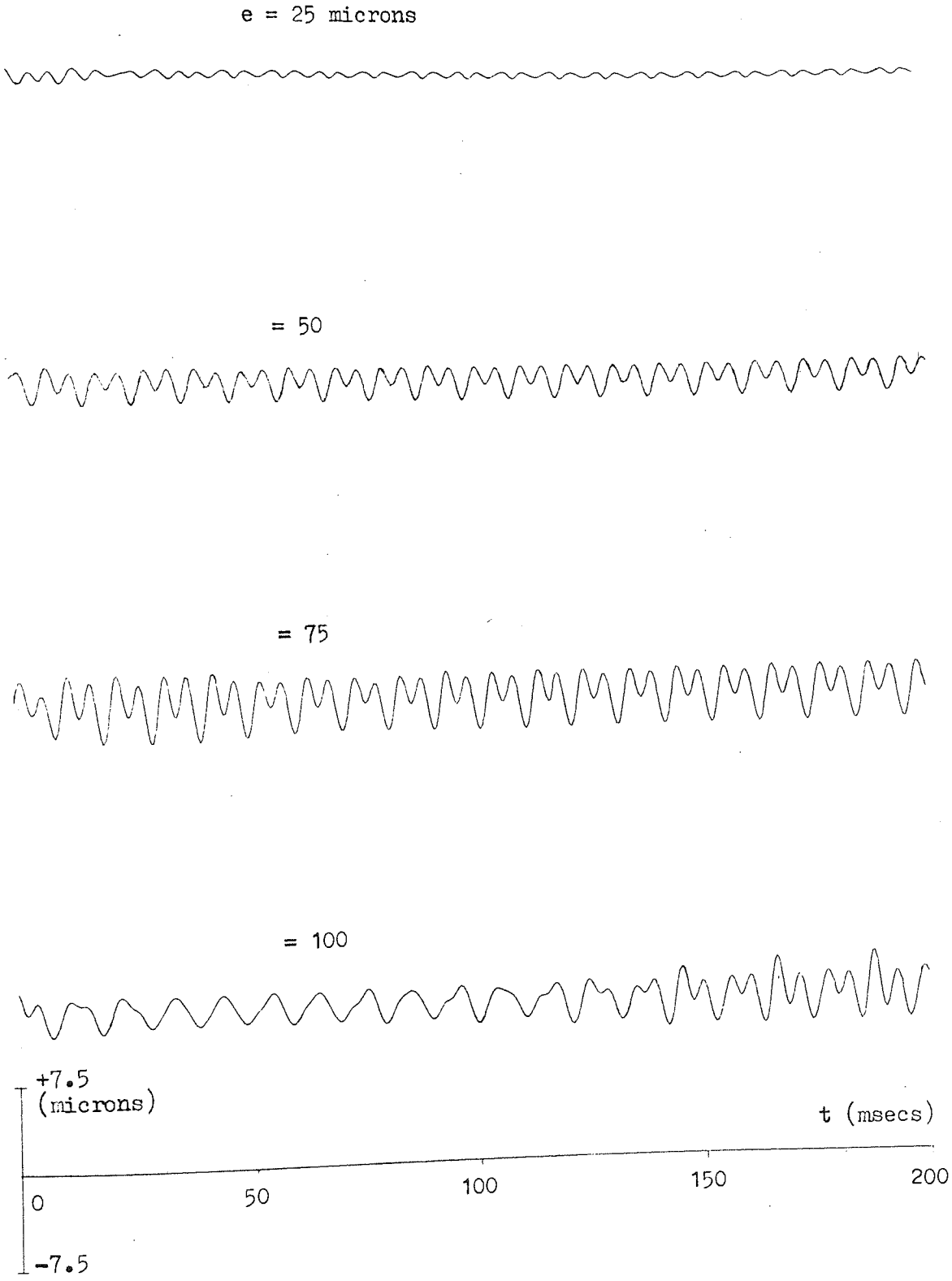

Fig 6.22 Vertical displacement of inner ring center. f_c = 8.0 Hz; M = 125 kg.

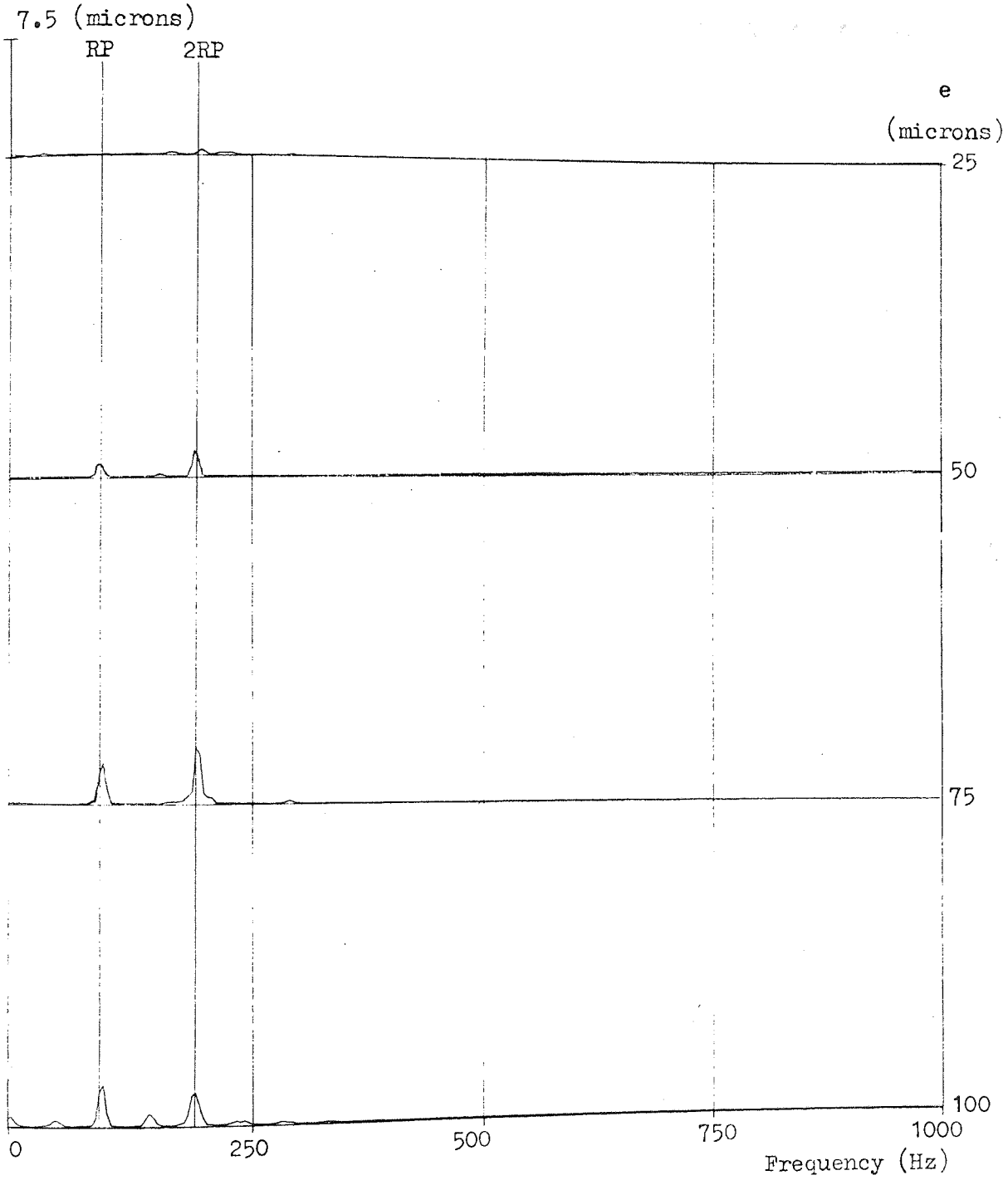

Fig 6.23 Spectral distribution of the displacement functions given in fig 6.22.

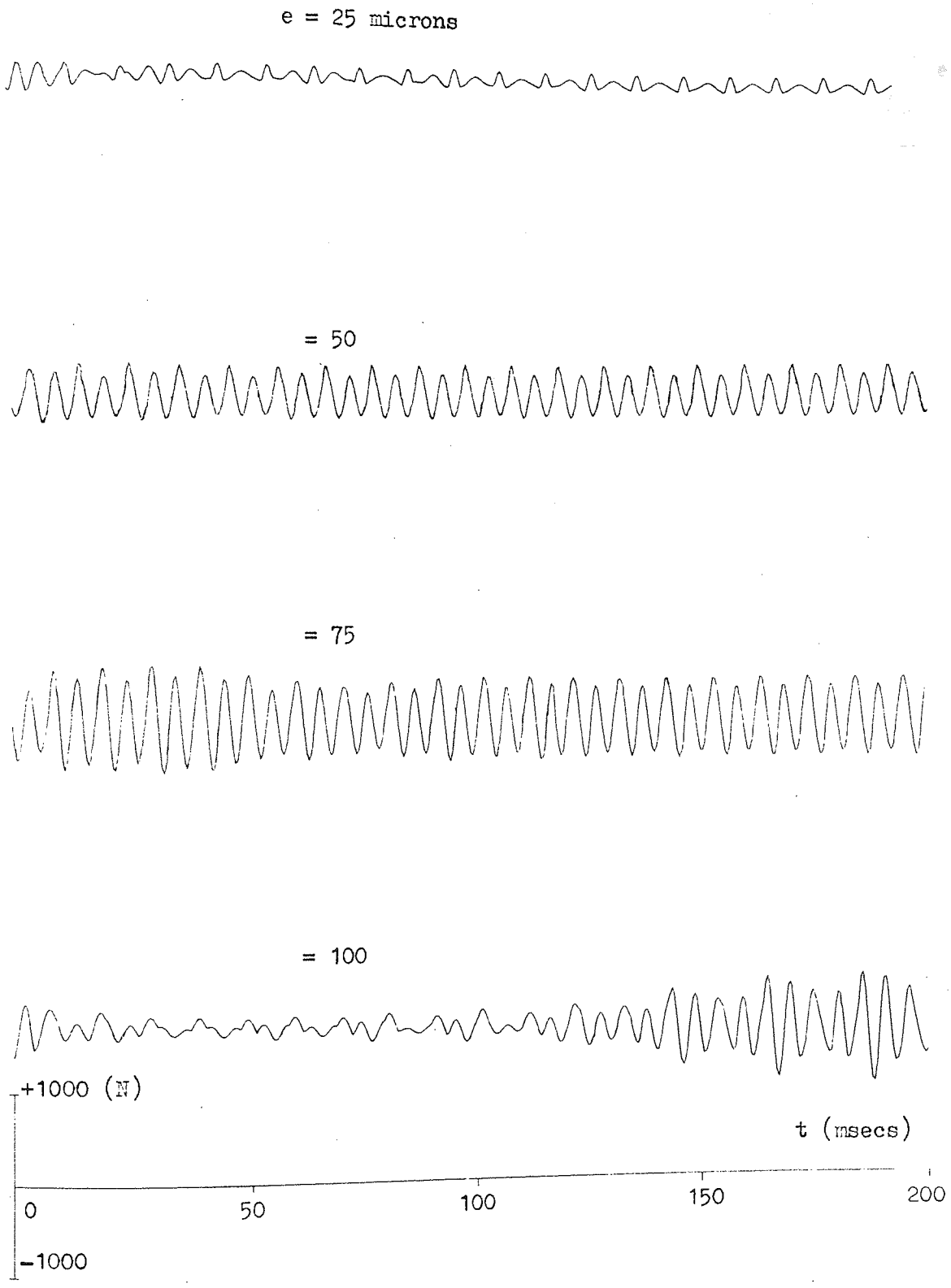

Fig 6.24 Vertical reaction force ($Q_y(t)$). f_c = 8.0 Hz; M = 125 kg.

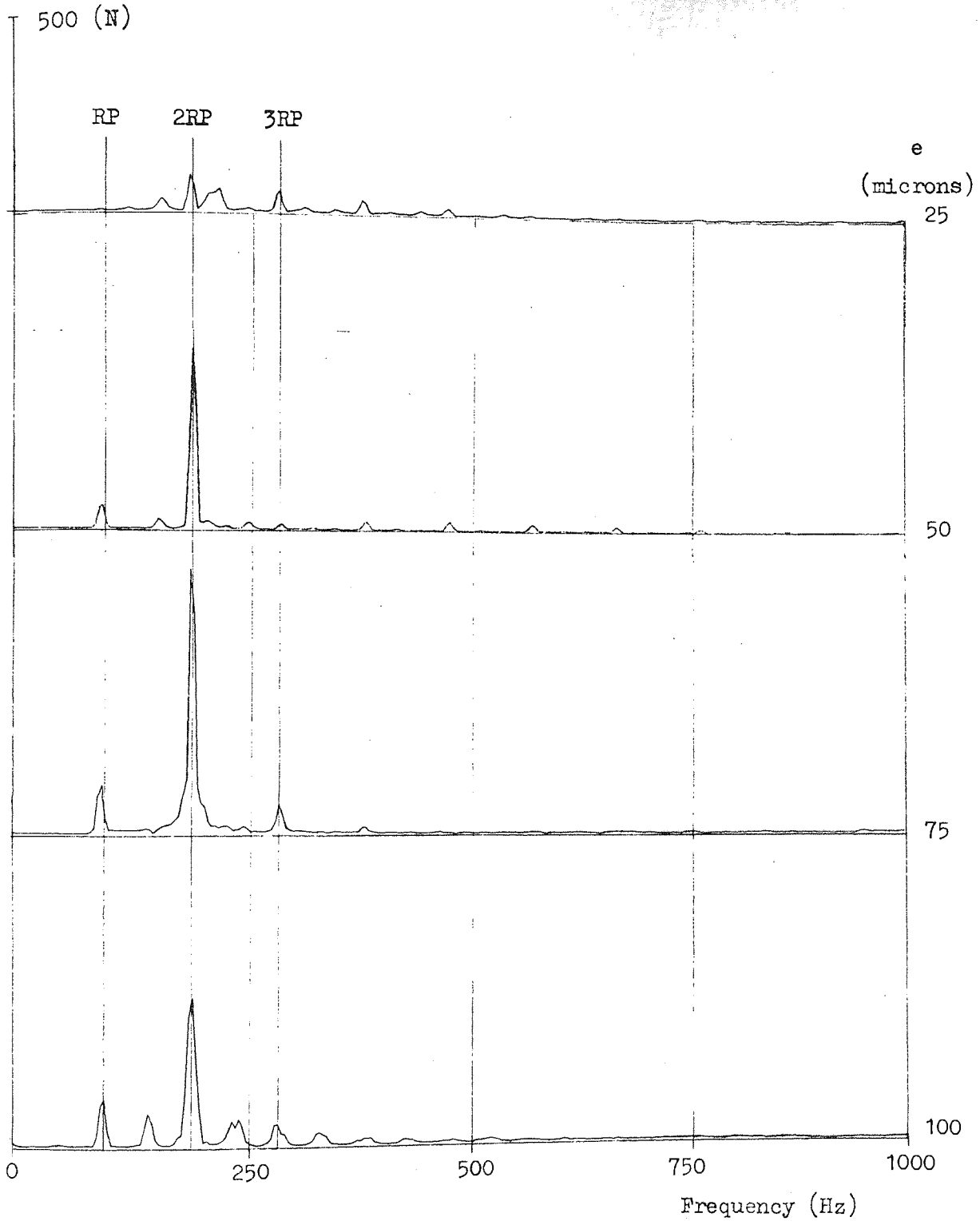

Fig 6.25 Spectral distribution of the force functions given in fig 6.24.

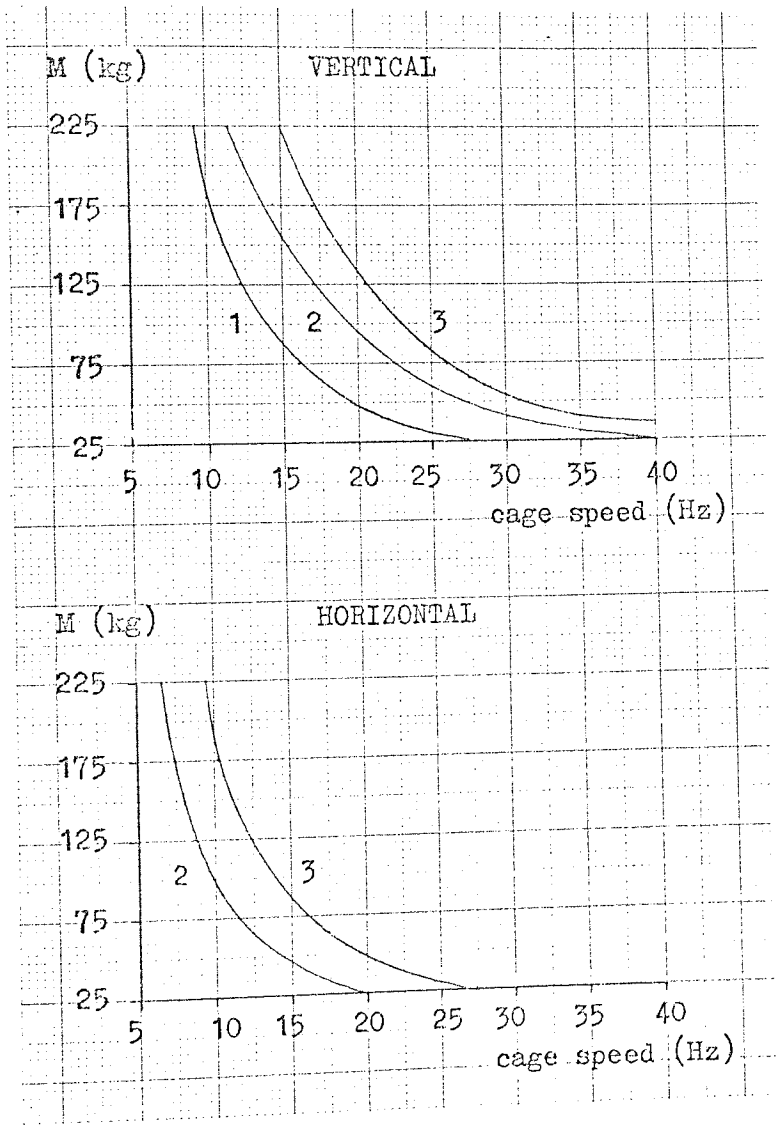

Fig 6.26 Estimation of critical cage speeds at rotor masses between 25 and 225 kg for motions in vertical and horizontal directions. The numbers in the diagrams denotes the number of rollers under load.

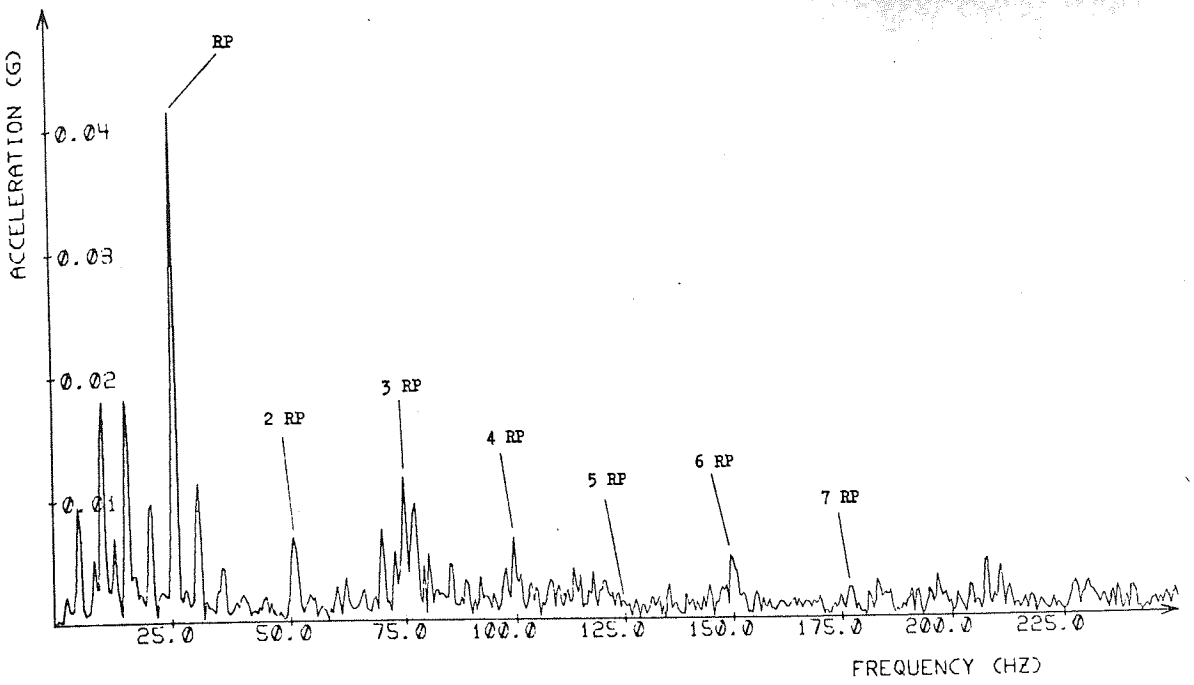

Fig 6.27 Spectrogram of roller bearing type N206 run in the vibration test rig. M = 205 kg; f_s = 300 RPM (corresponds to f_c = 2.1 Hz).

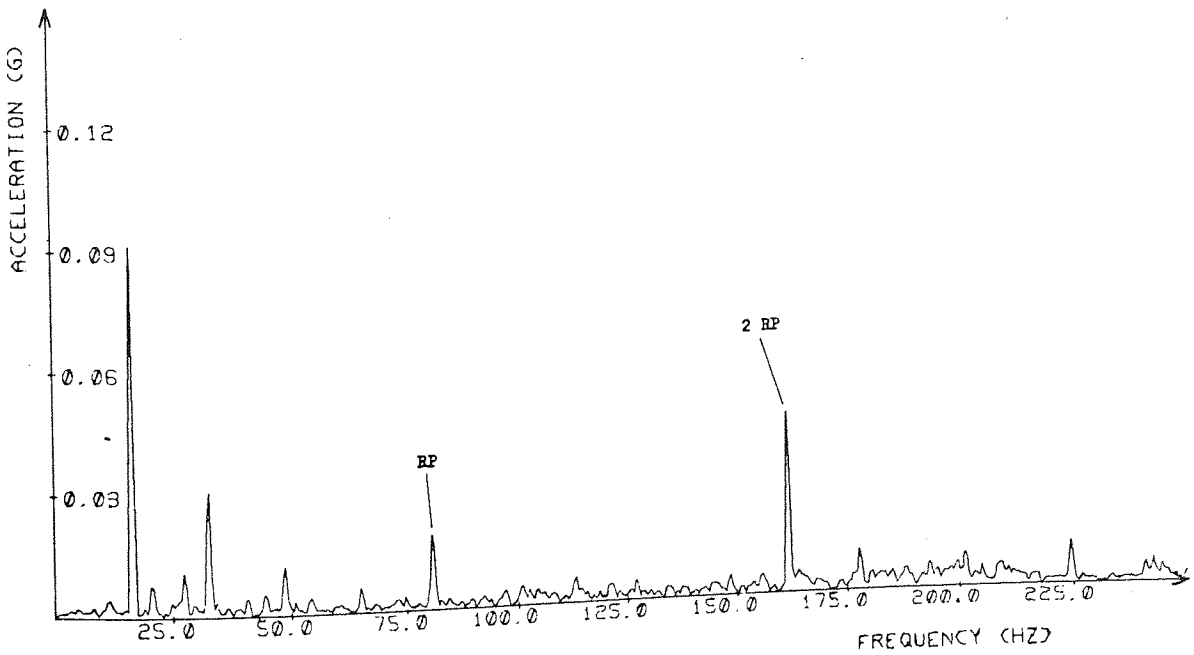

Fig 6.28 Spectrogram of roller bearing type N206 run in the vibration test rig. M = 85 kg; f_s = 945 RPM (corresponds to f_c = 6.6 Hz).

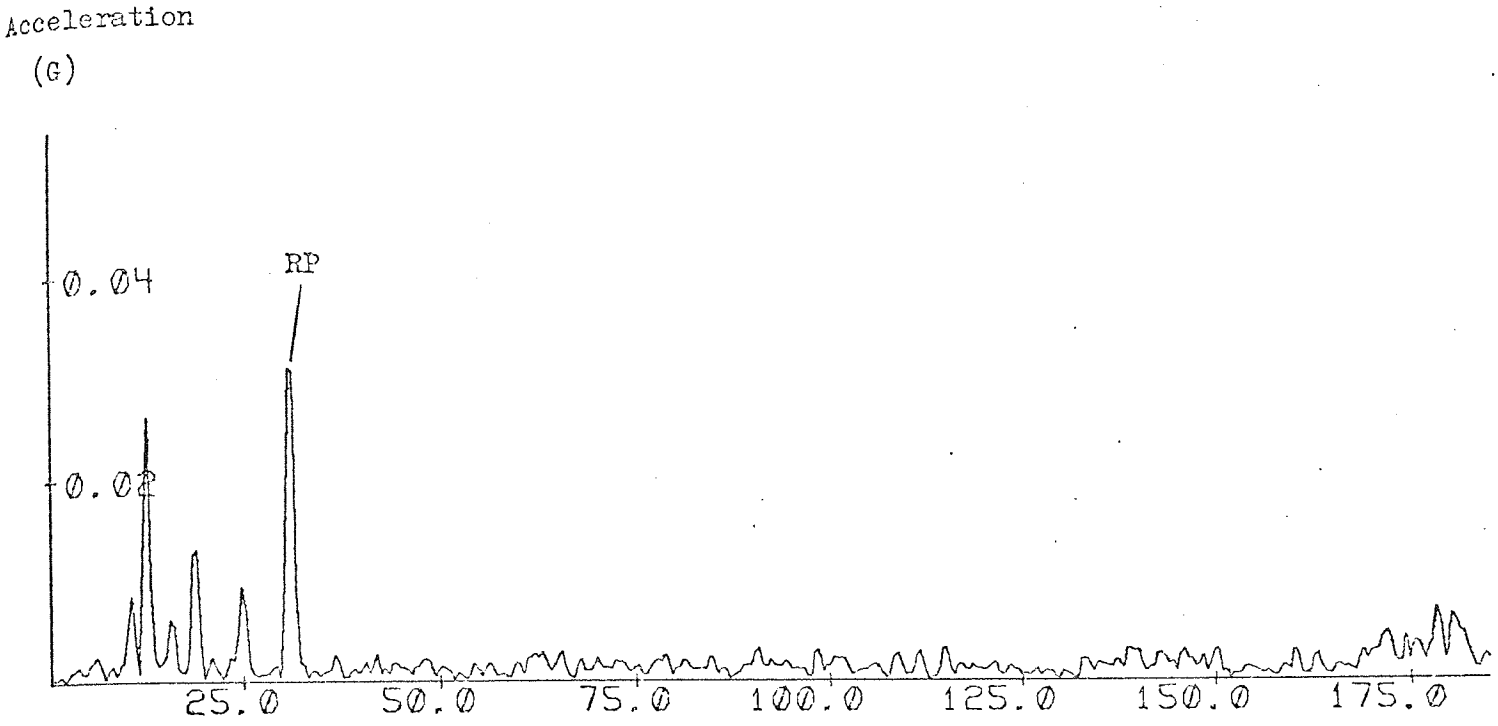

Fig 6.29 Spectrogram from a roller bearing type N206 run in the vibration test rig. M = 85 kg; f_s = 360 RPM (corresponds to f_c = 2.5 Hz).

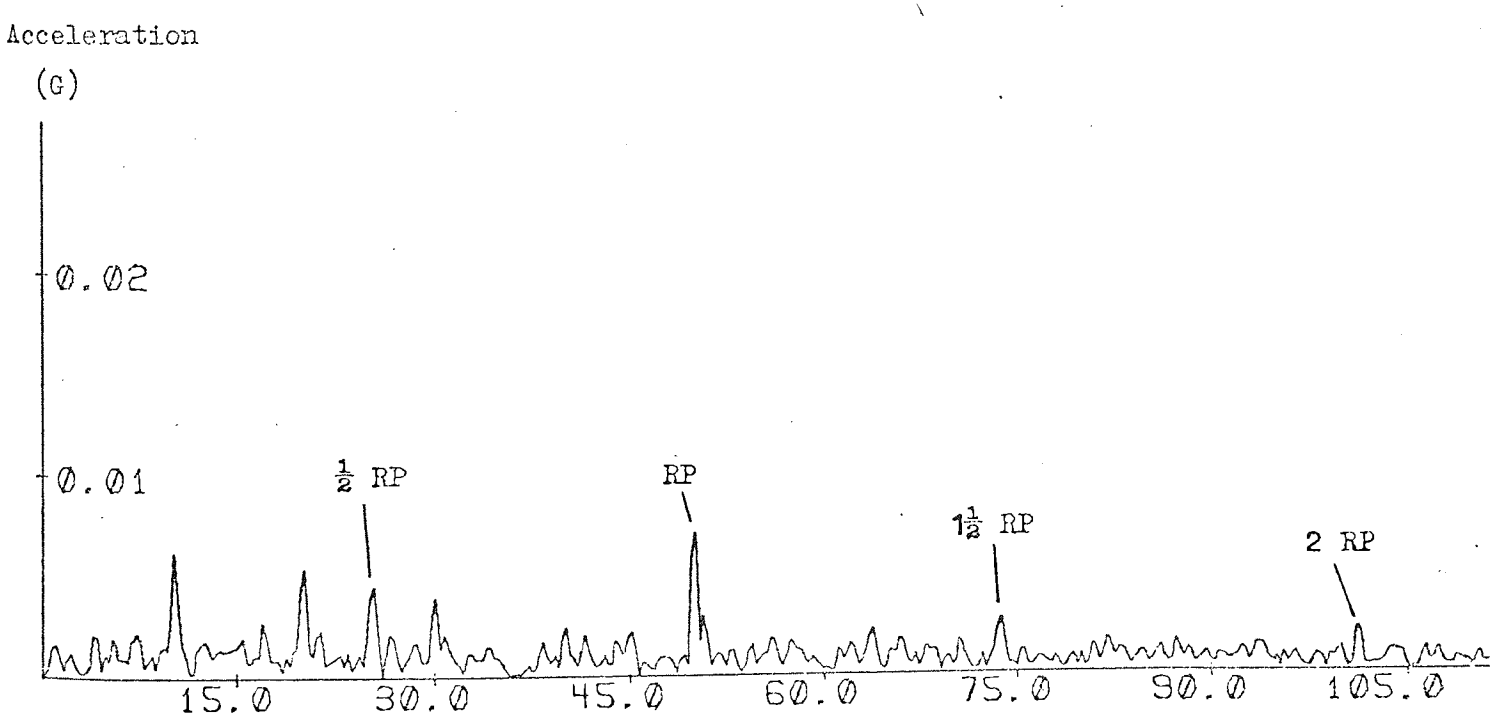

Fig 6.30 Spectrogram from a roller bearing type N206 run in the vibration test rig. M = 12 kg; f_s = 600 RPM (corresponds to f_c = 4.2 Hz).

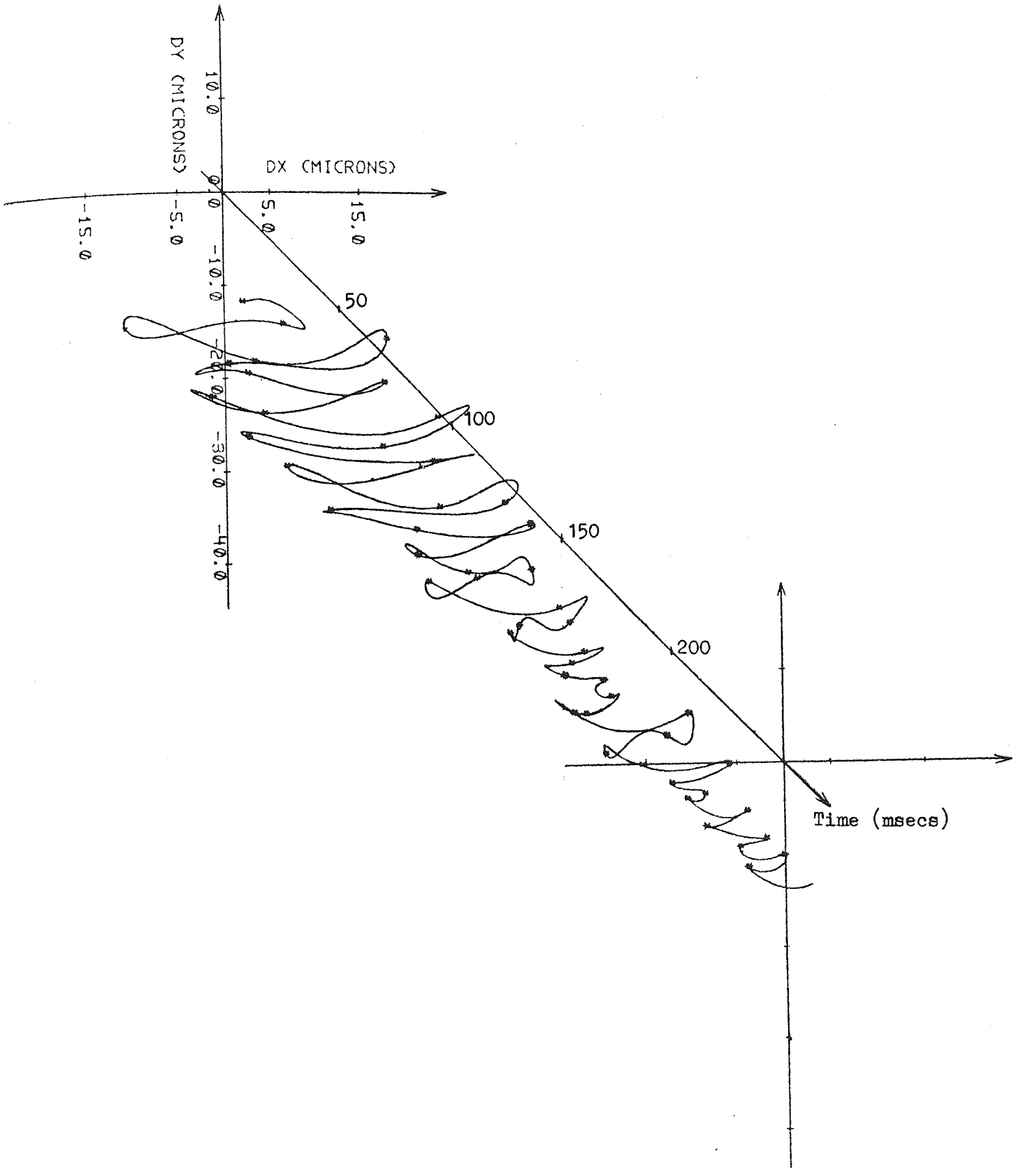

Fig 6.31 Expanded shaft locus from DYNSIM run with M = 225 kg, f_c = 8.0 Hz and e = 50 microns.

CHAPTER 7

EFFECTS OF MANUFACTURING TOLERANCES ON BEARING VIBRATIONS

In the previous chapter it was shown that vibrations in rolling bearings are generally excited because of the variation of assembly stiffness that occurs as the cage rotates. This type of vibration is inherent in the design of rolling element bearings and would occur also in a geometrically perfect bearing. The shapes of the components of a real bearing however, will of course always deviate to some extent from their theoretical design and the size of these deviations are determined by the tolerances with which the bearing is manufactured. For bearings of standard tolerances the vibrations generated by these form errors will often be of equally great importance as those generated by varying assembly stiffness. The unsteady, rumbling noise that many bearings generate while in operation is generally attributed to this source.

The purpose of this chapter is to show in some detail how the surface irregularities are related to the vibration characteristics of the running bearing. A complete theory describing the relative movement of inner and outer rings of the bearing arrangement becomes excessively complicated if it is to allow for flexibility between rollers and raceways except for the case of the idealized bearing treated in Chapter 6. It has however been found possible to obtain good qualitative predictions of bearing vibration characteristics due to form errors with a simplified theory

where rollers and raceways are assumed rigid. The equations of motions for the shaft centre then reduces to purely geometrical relationships and this theory is therefore called Kinematic. The fact that zero elastic deformation is assumed means that the bearing under consideration must have a positive clearance and be only lightly loaded. Only two rollers are assumed to carry the load except for the moment when one roller leaves the load carrying zone and a new roller enters it, i.e. for values of $\psi = n \cdot V$, $n = 0,1,2,\ldots$, see Fig. 7.1. A Kinematic model clearly constitutes a linear model, which means that effects of different form errors can be treated separately and the results superimposed to obtain the total movement of the shaft centre relative to the centre of the outer race and the bearing housing.

7.1 TYPES OF FORM ERRORS

Deviations from the theoretical design occurs in all components of the bearing and are of various types. For instance, the cross sections of the inner and outer rings will not be perfectly circular. The same is true of the contours of the rollers. Further, inaccuracies of the cage will make the rollers unevenly spaced and will make the cage unbalanced and finally, the diameters of the rollers will not be perfectly uniform. All the mentioned form errors could generate vibrations, but in the author's experience from this study of several common types and makes of bearings, it seems that in practice two types of form errors can be singled out as having particular effect on the bearing's vibration characteristics.

The roundness of the rollers is generally much better than the roundness of the tracks. This is probably so because the rollers are made out of solid, cast raw materials. Moreover, even if the rollers were non-circular

or wavy to an extent where significant vibrations could be expected, the relative phases of the waves on the roller surfaces would vary in a random manner as new rollers enter and leave the load carrying zone. This means that no sustained oscillating force of the type that could excite the fundament or shaft could occur. Vibrations due to out of roundness of rollers are therefore insignificant compared to other vibrations of the bearing and has not been found in any of the experimental runs. Different experiences, although relating to ball bearings, were reported by Tallian and Gustafsson in ref. (23), who claim that the surface quality of the balls has a direct influence on the vibrations of the bearing. It seems however likely that a set of balls with a poor surface quality will also have a less uniform diameter and it is believed that it is this latter property of the ball set that is the actual cause of the reported correlation between high vibration levels and poor ball surfaces.

The raceways are made out of cold drawn steel tube, which is cut and centreless ground. Internal stresses originating from the drawing are often present in the raw material and after subsequent heat treatment these stresses will manifest themselves in the form of lobes or waves around the circumference. Less than perfect grinding will give a similar result. The amplitude of the waves decrease quickly for wave numbers above 10 to 15 cycles per circumference. In ref. (24) it is claimed that waves up to approximately 100 cycles per circumference have been found, but one must then remember the difference of measurement methods used. In ref. (24) it is not the actual height of the waves that is measured, but the speed with which the probe moves in the radial direction, a method which emphasises the higher frequency components. The same ring generally

have several waves, each with a different number of cycles around the circumference so that the total shape of the ring is the superposition of these waves. The magnitude of these form errors is sufficient to generate significant vibrations from both outer and inner races. In an axially loaded bearing all the rollers are always in contact with both races. In such a case one would expect vibrations due to waviness from both races, shown in ref. (23). In a radially loaded bearing with stationary outer ring and having positive clearance however, often only two or three rollers carry the load. This means that for waviness of the outer ring to generate vibrations, the length of the waves must be rather short. The actual wavelength is however such that no significant vibrations are generated, although one would imagine that waviness of the outer race affects the load distribution between the rollers. For the inner ring the situation is different since the lobes there continuously roll over the contact points with the rollers as the ring rotates. Vibrations due to inner ring waviness have also been found in most experimental runs.

Unbalance of the cage would produce a rotating force of frequency equal to the cage speed, see Chapter 3. Components at this frequency sometimes occur in the experimental runs, but are generally small. A simple calculation shows that for the cage unbalance to give a vibration level equal to that produced by a one micron, two lobe wave of the inner ring, the unbalance must be about 40% of the total mass of the cage which is clearly impossible. It is then more realistic to consider the effect of varying roller diameters, which have a direct effect on the vertical position of the shaft. The size of the variations are of the same order as the out of roundness of the inner ring. Vibrations originating from this effect have been found in experimental runs and are often of the same

order of magnitude as the vibrations originating from waviness of the inner ring. As regards the variations of gaps between the rollers due to imperfections of the cage, it can be shown that although these variations are quite large they will have little effect on the movements of the shaft.

The conclusion of the above discussion is that for radially loaded bearings, attention should primarily be concentrated on vibrations due to inner ring waviness and varying roller diameter. This conclusion is also supported by practical experience from running bearings in the test rig. Fig. 7.3 shows a series of spectrograms of a spherical, single row, roller bearing, type 20206, running in the vibration test rig with the 12 kg rotor at speeds between 5 and 30 Hz (300 - 1800 RPM) and with the tube brackets in the "medium" stiffness position. The vibrations are picked up by an accelerometer positioned on the bearing holder, right under the test bearing and are analysed using the DAS system. Because of the complexity of the signal it is inevitable that at any single shaft speed, some vibration peaks will coincide. With a plot of the type of Fig. 7.3 however, it is possible to distinguish all important frequency components at at least one shaft speed. The spectrograms are dominated by two series of vibration harmonics, one with the shaft speed as the fundamental and one with the cage speed as the fundamental. The frequency components are notated with NS' for the N:th shaft harmonic and NC for the N:th cage harmonic. It will be shown that the origin of these groups of harmonics can be derived to waviness of inner track and non-uniform roller diameter respectively. The first shaft harmonic (the fundamental) is however due to unbalance of the rotor and not normally an effect of the

bearing, unless the unbalance is due to the bearing bore not being concentric. This can however not be distinguished from other types of unbalance. Except for the two main groups of harmonics there is also a frequency component at roller passage frequency (RP) which, although occurring at an integer multiple of cage speed is a VC type of vibration and not due to non-uniformity of the roller diameters. There are also two frequency components marked 6S'' and 7S'' which are secondary peaks, a form of nonsymmetrical side bands, to 6S' and 7S' and which are also an effect of form deviations of the inner track. For other types of bearings and operating conditions it might be necessary to include effects of roller and outer ring waviness and these effects could be studied along the same lines as will be used here.

7.2 VIBRATIONS DUE TO VARYING ROLLER DIAMETERS

To demonstrate experimentally form errors and vibrations originating from form errors three bearingsof type 20206 will be studied in this chapter. The three bearings are of similar design and tolerance class and are all sold commercially by well known manufacturers of quality bearings. The three bearings will be referred to as bearings A, B and C.

The rivets holding the two cage halves together were removed so that the bearings could be dismantled. The rollers were numbered with an engraver pen and their diameters measured using a Watt vertical measuring machine. The diameter differences are extremely small, often only fractions of a micron, which makes it difficult to obtain repeatable readings even with specialised measuring equipment. By measuring the sets several times and taking the mean values it was however possible to obtain reasonably consistent values for the diameters of the rollers.

The differences between the smallest and largest roller were for bearing A:1.3 μm, for bearing B:0.5 μm and for bearing C:3.1 μm. The standard deviations (the RMS value for a series of samples having been made to have a mean value of zero) of the roller diameter differences were for bearing A:0.45, for bearing B:0.1 and for bearing C:1.0. Thus the accuracy of the rollers is significantly poorer for bearing C than for bearings A and B, which do not differ much between themselves, although B is somewhat better than A. In fact, the differences of diameters measured for bearing B is probably within or near the accuracy of the measurement method. One would now expect that the size of the vibration components related to the cage speed of the bearings would show some sort of correlation with the amount of non-uniformity of roller diameters as expressed by the standard deviations of the respective bearings. The three bearings were run in the vibration test rig at 18 Hz (1080 RPM) speed, loaded by the 12 kg rotor and the spectrograms for these runs are shown in Fig. 7.12. The amplitudes of the first six cage harmonics were measured for the three bearings and their respective RMS values were calculated. Hence, the RMS values associated with cage speed and harmonics thereof were for bearing A:2.2 10^{-3}G, for bearing B:1.7 10^{-3}G and for bearing C:2.4 10^{-3}G. These measurements show that the standard deviations of roller diameter differences are related to the RMS values of the vibrations of the running bearing in such a way , that a high value of standard deviation will give a high value of RMS vibration at the frequencies concerned.

The method of the previous paragraph is rather crude, and the result is merely an indication of a correlation of some sort between roller diameter accuracy and vibration at cage harmonics. It is however not only the amount with which the roller diameters differ from each other

that matters,but also the order in which the rollers are positioned in the roller set. This will be shown in a more detailed analysis of this relationship between roller properties and vibration characteristics below. Consider again Fig. 7.1. For a slowly rotating bearing where no elastic deformations occur, the vertical position of the centre of the inner ring relative to the centre of the outer ring will, at the instant when a roller is right under the load line, be determined by the diameter of that roller. Thus, during one cage revolution of a twelve roller bearing, the position of the shaft centre will be known at twelve instants if the roller diameters of the roller set is known. The roller diameters of bearing C is represented by the twelve small circles in Fig. 7.4 a. For the cage positions where a roller is not directly under the load, the shaft position is not known, but for the accuracy needed here it is sufficient to assume that the vertical position is given by a smooth line drawn through the known twelve points as shown in Fig. 7.4a. A series of ordinates can now be taken from the displacement function of Fig. 7.4a, and since this function is periodic, with the cage speed as the fundamental, the function can be expanded into a Fourier series, see Appendix I. The calculation of the Fourier coefficients can be done by using for instance the Runge or Fischer-Hinnen and Lewis's rules, see Chapter 38 of ref.(13). Since a computer with a Fourier analysis program was available for the DAS system, in this case, the ordinates were simply punched on paper tape and read into the DAS system. The Fourier coefficients, C_i, are given in Fig. 7.5a. Neglecting phase difference between the components, the vertical shaft displacement function can now be written as

$$y(t) = C_1 \sin\omega_c t + C_2 \sin 2\omega_c t + C_3 \sin 3\omega_c t + \ldots \qquad \ldots.(7.1)$$

Remembering that the Kinematic model constitutes a linear model, each component gives rise to a shaft movement that is independent of the other components, so that the vertical acceleration of the rotor due to component i is

$$\ddot{y}_i(t) = -C_i\, i^2 \omega_c^2 \sin i\omega_c t \qquad \ldots\ldots\ldots\ldots\ldots\ldots \quad (7.2)$$

and the force exerted on the bearing holder due to the acceleration of the mass (M) of the rotor is

$$f(t) = C_i i^2 \omega_c^2 M \cdot \sin i\omega_c t \qquad \ldots\ldots\ldots\ldots\ldots\ldots \quad (7.3)$$

This force will give rise to an oscillation of the bearing holder at frequency $i \cdot \omega_c$, the amplitude of which depends on the dynamic properties of the set-up. Thus, the acceleration which is measured with an accelerometer on the bearing holder, is for a certain frequency directly proportional to the Fourier coefficient of the roller diameter variation function at that particular frequency. Note that the theory is restricted to making comparisons (not calculating absolute values) between vibration components of similar frequency. An extension of the theory will be made in Chapter 8, which takes into account the Mechanical Impedance of the system. The simplified derivation pre-supposes a non-flexible bearing holder tube, but the conclusion of the theory, that the vibration levels are proportional to their respective Fourier coefficients, is valid also for the case of a flexible tube. The hypthotesis is tested by arranging the roller set of the same bearing in two different sequences of rollers, thereby producing different series of Fourier coefficient. In Fig. 7.4a the rollers have been arranged to give a strong 3 cycle component and in Fig. 7.4b the

rollers have been arranged to give a 6 cycle effect. The Fourier coefficients of the displacement functions are shown in Fig. 7.5a and b respectively. Spectrograms of the bearing run in the test rig are shown in Fig. 7.6 for the two roller arrangements. According to the hypothesis the amplitude of the cage harmonics should vary in proportion to the magnitude of the Fourier coefficients. In the table below C_i are the Fourier coefficients as measured from Fig. 7.5a and b and A_i are the vibration amplitudes as measured in Fig. 7.6a and b.

i =	1	2	3	4	5	6
$\frac{C_{i,3}}{C_{i,6}}$	0.095	1.1	4.0	0.53	0.75	0.64
$\frac{A_{i,3}}{A_{i,6}}$	-	1.4	4.7	2.2	0.70	0.56

The table above, together with direct comparison between Fig. 7.6 and 7.5 seems to confirm the theory. The first harmonic occurs at a low frequency which gives too low a signal level to give measurable vibration amplitudes. As would be expected the 3 cycle arrangement has a large third harmonic vibration component and the six cycle arrangement has a large 6 cycle harmonic. The only deviation from the theory is the fourth harmonic but one must remember the measurement difficulties involved and the simplified way of treating a very complex problem. All in all, the experiment seems to verify the theory and showsits practicality in being able to predict the vibration characteristics as dependant on roller accuracy of a standard tolerance bearing run under realistic conditions.

It should be noted that the RMS values of the first six cage harmonics for the 3 cycle arrangement is about 2.6 times that of the 6 cycle arrangement. When particularly quiet running bearings are needed,it might thus be worthwhile to arrange the rollers in a way so as to give minimum vibrations. This could well be a more economical way of improving the running properties of the bearing than to improve the accuracy of the rollers. The possibility of moving large frequency components,which excite resonances of the set up, to other and less sensitive frequencies by arranging the rollers in a different order, should also be noted.

7.3 MEASUREMENT AND ANALYSIS OF RACEWAY SHAPES

The form deviations of the inner ring arerelated to the bearing's vibration characteristics in a somewhat more complicated way than was the case for the effect of non-uniformity of roller diameters. In this section it will be described how the contours of the races can be measured and analysed. The aim of the analyses is in principal the same as that of Yhland, ref.(33), described in Chapter 2. The method used here is however different and the results are much more accurate and they are expressed in the dimensions of length, contrary to Yhland's method which gives the out of roundness in the dimension of velocity.

The function of form deviation from perfect circle was obtained by the use of a Taylor Hobson Tallyrond instrument, see picture 7.7. The object to be measured is attached to the table with a vice (1) and carefully centred. A stylus (2) is brought into contact with the surface of the raceway and when rotating the spindle (3) to which the stylus is attached, the stylus will closely follow the shape of the surface under investigation.

The output from the instrument is a voltage proportional to the radial displacement of the stylus and this is, after being amplified, fed to a recording device. The most commonly used recorders are the polar plotter (4) and the rectilinear plotter (5), examples of which are shown in Fig.7.8. If a series of rectilinear plots are made across the raceway (i.e.the spindle is moved a short distance in the vertical direction between each measurement) a picture of the surface of the bearing track is obtained. The inner ring surfaces of the three bearings A, B and C are shown in Fig. 7.9. The magnification in vertical direction is 4000 and in horizontal direction 1. As can be seen,the waves and ridges of the surfacesgo across the track without much change. Thus,one trace in the middle of the surface is a fairly representative sample of the whole of the surface. Contrary to what was the case for accuracy of the rollers, bearing C has a considerably better accuracy of inner track than bearings A and B which are fairly similar although bearing A has a higher proportion of short waves. Fig.7.12 shows spectrograms from the three bearings run in the test rig at 18 Hz (1080 RPM) shaft speed with the 12 kg rotor. Knowing that bearings A and B have better rollers but less good inner rings than bearing C, one would expect to have a higher proportion of vibration components at shaft harmonics for A and B but less predominant vibrations at cage harmonics compared with bearing C. This is also clearly shown in Fig. 7.12 and it is quite easy to distinguish between the three bearings.

The type of plots of Fig. 7.9 give a general idea of the shape of the tracks, but if a more detailed analysis is to be carried out, the output of the Tallyrond can instead be fed to an A/D converter (6) connected to a paper tape punch (7). The form function can now be made available to a

digital computer and the DAS system has a program which reads this tape. The speeds of spindle rotation and sampling frequency are such that a maximum of 200 samples can be obtained per revolution of the spindle, i.e. per circumference of the ring. Thus, the samples are spaced with $360/200 = 1.8°$ between each sample. Fig. 7.10 shows the out of roundness of the inner raceways of bearings A, B and C around one circumference measured at the axial centre of the raceways. They are plotted using the DAS system and 7.10 is the digital counterpart to the rectilinear plot of Fig. 7.8. The form deviation function can be further analysed using the standard DAS routines. To obtain a digital counterpart to Yhland's lobe analyses, the FFT routine is used. Since the form function repeats each time the spindle starts a new revolution, the function is obviously periodic and the FFT routine will yield the Fourier coefficients that make up the out of roundness function. The Fourier coefficients of the three bearings are shown in Fig. 7.11 where the ordinates have been multiplied with the Hanning Window function before being Fourier analysed. The result of this analysis will be used in section 7.6, but first an expression for the relative movements between outer and inner ring centres will be derived.

7.4 POSITION OF SHAFT CENTRE AS A FUNCTION OF CAGE POSITION, INNER RING FORM DEVIATIONS AND CLEARANCE

Vibrations due to inner ring waviness have been investigated by several authors as was described in Chapter 2. These investigations were concerned with axially loaded bearings, mainly deep groove ball bearings. For many practical applications however, knowledge of the vibration characteristics of radially loaded bearings is more useful. In radially

loaded bearings with positive clearance, rollers continuously enter and leave the load-carrying zone as the cage rotates and this complicates the theory for vibration generation in such an application.

Consider Fig. 7.1. The X-Y coordinate system is fixed and positioned in the centre of the outer ring. The X'-Y' system rotates with the inner ring, the origin coinciding with the centre of the shaft. The angle ϕ defines the angular position of the shaft or the inner ring, and the shaft movements are defined by the x-y coordinates of the origin of the X'-Y' system. Now, assume that the shaft centre is moved along the circle segment A from origin to $(x_1; y_1)$ by shortening radius I from R to Z_1, see Fig. 7.2a. Since A<<R, the circle segment can be approximated to a straight line,which directly yields the following relationships,

$$B = R - Z_1 \quad \ldots\ldots\ldots\ldots\ldots\ldots \quad (7.4)$$

$$\gamma = 90° - V \quad \ldots\ldots\ldots\ldots\ldots\ldots \quad (7.5)$$

$$A = \frac{B}{\cos\gamma} \quad \ldots\ldots\ldots\ldots\ldots\ldots \quad (7.6)$$

Substitute (7.4) and (7.5) into (7.6) which gives

$$A = \frac{R-Z_1}{\sin V} \quad \ldots\ldots\ldots\ldots\ldots\ldots \quad (7.7)$$

The new position of the shaft centre can be calculated from

$$\begin{cases} x_1 = A\sin(\psi + \gamma) \\ y_1 = -A\cos(\psi+\gamma) \end{cases} \quad \ldots\ldots\ldots\ldots\ldots\ldots \quad (7.8)$$

However since $V + \gamma = 90° \quad \ldots\ldots\ldots\ldots\ldots\ldots \quad (7.9)$

and thus $\psi + \gamma = \psi + 90° - V \quad \ldots\ldots\ldots\ldots\ldots\ldots \quad (7.10)$

Equation (7.8) can be rewritten as

$$\begin{cases} x_1 = \dfrac{R-Z_1}{\sin V} \cdot \cos(\psi - V) \\ y_1 = \dfrac{R-Z_1}{\sin V} \cdot \sin(\psi - V) \end{cases} \quad \ldots\ldots\ldots\ldots\ldots\ldots \quad (7.11)$$

Radius I is now kept constant and instead radius II is shortened to Z_2 which moves the shaft centre from $(x_1; y_1)$ to $(x_o; y_o)$, Fig. 7.2b. The following relationships are obtained

$$C = R - Z_2 \quad \ldots\ldots\ldots\ldots\ldots\ldots \quad (7.12)$$

$$r = 90° - V \quad \ldots\ldots\ldots\ldots\ldots\ldots (7.13)$$

$$D = \frac{C}{\cos r} \quad \ldots\ldots\ldots\ldots\ldots\ldots \quad (7.14)$$

Substituting (7.12) and (7.13) into (7.14) gives

$$D = \frac{R-Z_2}{\sin V} \quad \ldots\ldots\ldots\ldots\ldots\ldots \quad (7.15)$$

The angle u is

$$u = 90° - 90° + \psi = \psi \quad \ldots\ldots\ldots\ldots\ldots\ldots \quad (7.16)$$

E and F are the horizontal and vertical projections of D, thus

$$\begin{cases} F = D\cos u \\ E = D\sin u \end{cases} \quad \ldots\ldots\ldots\ldots\ldots\ldots \quad (7.17)$$

Substitute (7.15) and (7.16) into (7.17) giving

$$\begin{cases} F = \dfrac{R-Z_2}{\sin V} \cdot \cos\psi \\ E = \dfrac{R-Z_2}{\sin V} \cdot \sin\psi \end{cases} \quad \ldots\ldots\ldots\ldots\ldots\ldots \quad (7.18)$$

The final position of the shaft is

$$\begin{cases} x_o = x_1 - F \\ y_o = y_1 - E \end{cases} \quad \ldots\ldots\ldots\ldots\ldots\ldots \quad (7.19)$$

And finally, substituting (7.11) and (7.18) into (7.19) the full expression of the shaft centre position as a function of Z_1, Z_2 and the cage position becomes

$$\begin{cases} x_o = \dfrac{(R-Z_1)\cos(\psi - V) - (R-Z_2)\cos\psi}{\sin V} \\ y_o = \dfrac{(R-Z_1)\sin(\psi - V) - (R-Z_2)\sin\psi}{\sin V} \end{cases} \quad \ldots\ldots\ldots\ldots \quad (7.20)$$

Equation (7.20) is valid only for $0 < \psi < V$, because when ψ exceeds V, the load of the shaft will shift to a new roller entering the load zone from the left. An expression valid for all ψ will be developed later.

From Fig. 7.1 it is seen that

$$\begin{cases} Z_1 = r_{i,nom} + dr + dev(\theta) & \ldots\ldots\ldots \quad (7.21) \\ Z_2 = r_{i,nom} + dr + dev(\theta+V) & \ldots\ldots\ldots \quad (7.22) \\ R = r_{i,nom} + dr + e & \ldots\ldots\ldots\ldots\ldots\ldots \quad (7.23) \end{cases}$$

where $dev(\theta)$ is the deviation from perfect roundness of the inner ring as shown in Fig. 7.10. It is assumed that the form function of Fig. 7.10 starts from point J in Fig. 7.1 and the trace is made in anti-clockwise direction. Subtracting (7.21) from (7.23) and (7.22) from (7.23) gives

$$\begin{cases} R-Z_1 = e - dev(\theta) \\ R-Z_2 = e - dev(\theta-V) \end{cases} \quad \ldots\ldots\ldots\ldots\ldots\ldots \quad (7.24)$$

Substituting (7.24) into (7.20) gives

$$\begin{cases} x_o = \dfrac{(e-dev(\theta))\cos(\psi-V) - (e-dev(\theta+V))\cos\psi}{\sin V} \\ y_o = \dfrac{(e-dev(\theta))\sin(\psi-V) - (e-dev(\theta-V))\sin\psi}{\sin V} \end{cases} \quad \ldots\ldots\ldots\ldots \quad (7.25)$$

Equation (7.25) is, being derived from equation (7.20), valid only for $0 < \psi < V$. When this value is exceeded the process will repeat again, but as a new roller becomes loaded the argument of the dev(θ) function will suddenly increase with the value of V. By use of the Heaviside unit step function U, having the value 1 for positive arguments and the value zero for negative arguments, eg.(7.25) can be rewritten as below in a form which is valid for all positive values of ψ.

$$\begin{cases} x_o = \dfrac{1}{\sin V} \sum_{k=o}^{\infty} [(e-dev(\theta+kV))\cos(\psi-(k+1)V) - (e-dev(\theta+ \\ \quad +(k+1)V))\cos(\psi-kV)]\cdot[U(\psi-kV)-U(\psi-(k+1)V)] \\ y_o = \dfrac{1}{\sin V} \sum_{k=o}^{\infty} [(e-dev(\theta+kV))\sin(\psi-(k+1)V) - (e-dev(\theta+ \\ \quad +(k+1)V))\sin(\psi-kV)]\cdot[U(\psi-kV)-U(\psi-(k+1)V)] \end{cases} \quad \ldots\ldots\ldots \quad (7.26)$$

From equation (7.26) the locus of the shaft centre can be calculated as a function of the angular position of the cage, ψ, provided the out of roundness function for the inner ring is known for all values of θ.

7.5 AN APPROXIMATE SOLUTION TO THE VC VIBRATION PROBLEM

In Chapter 2 a paper by Barakov & Shavrin, ref(22), was reviewed, which gave an expression showing how the inner ring centre would move up and down as the rollers passed under the load. Note that this is a purely kinematic effect, which does not involve elastic deformation of rollers or rings and which could occur also in geometrically perfect bearings. The solution to this problem (it can easily be shown that Barakov's & Shavrin's solution is incorrect, although the main character of their solution agrees with the expressions given below) can be obtained from equation (7.26) simply by making dev(θ) = 0 for all values of θ. The y_o function of eq.(7.26) then reduces to

$$y_o = \frac{e}{\sin V} \sum_{k=\theta}^{\infty} [\sin(\psi-(k+1)V)-\sin(\psi-kV)][U(\psi-kV)-U(\psi-(k+1)V)] \quad .....(7.27)$$

which simplifies to

$$y_o = -\frac{e}{\cos V/2} \sum_{k=0}^{\infty} \cos(\psi-kV-V/2).[U(\psi-kV)-U(\psi-(k+1)V)] \quad ..... \quad (7.28)$$

The value of the sum (including the sign) is plotted as a function of ψ ($=\omega_c t$) in Fig. 7.13 . A comparison with Fig. 7.1 shows that it is at the peaks of the y_o function that the load is shifted to a new roller entering the load carrying zone from the left. The obtained expression for shaft movement indicates the limitations of the Kinematic theory. If y_o is made a function of time by substituting $\omega_c t$ for ψ, the function can be derivated twice with respect to time. Without actually carrying out this derivation, it is obvious that the sharp corners of the displacement function give delta functions of infinite height in the acceleration function. To accelerate the mass of the rotor very fast requires very large forces,

which is inconsistent with the assumptions of the Kinematic theory, namely, that no elastic deformations occur. Consequently, the Kinematic theory works best for smooth, continuous displacement functions, and this is so also when displacements arise due to form errors. Vibrations due to varying roller diameters are generated by such a continuous displacement function, and the accuracy of predictions of amplitudes for vibrations due to this effect are also more accurate than predictions of vibrations due to form errors of the inner race, which are generated by a discontinuous function. For both cases however, the Kinematic model is a useful approximation if its limitations are kept in mind.

The y_o function is obviously periodic with the RP frequency as its fundamental. To show what vibration components the calculated shaft movement gives rise to, the Fourier coefficients of the function y_o of eq.(7.28) are calculated. Since the phase is unimportant it is permissible to move the t=0 axis to the dashed line of Fig.7.13. For $-V/2\omega_c<t<V/2\omega_c$ the time varying part of the y_o function then is

$$y_o(t) = \cos\omega_c t \qquad \ldots\ldots\ldots\ldots \qquad (7.29)$$

The general expression for the Fourier coefficients (see Appendix I) is

$$a_n = \frac{1}{T}\int_b^{b+T} f(t)e^{-jn\omega t}dt \qquad \ldots\ldots\ldots \qquad (7.30$$

So with the expression for y_o and the applicable boundary conditions,

$$a_n = \frac{\omega_t}{V} \int_{-V/2\omega_c}^{V/2\omega_c} \cos\omega_c t \cdot e^{-jn\omega t}\, dt$$

$$= \frac{\omega_c}{V} \int_{-V/2\omega_c}^{V/2\omega_c} \cos\omega_c t\, (\cos n\omega t - j\sin n\omega t)\, dt$$

$$= \frac{\omega_c}{2V} \int_{-V/2\omega_c}^{V/2\omega_c} [\cos(\omega_c + n\omega)t + \cos(\omega_c - n\omega)t - j\sin(\omega_c + n\omega)t + j\sin(\omega_c - n\omega)t]\, dt$$

$$= \frac{\omega_c}{2V} \left[\frac{\sin(\omega_c+n\omega)t}{\omega_c+n\omega} + \frac{\sin(\omega_c-n\omega)t}{\omega_c-n\omega} + j\frac{\cos(\omega_c+n\omega)t}{\omega_c+n\omega} - j\frac{\cos(\omega_c-n\omega)t}{\omega_c-n\omega} \right] \Bigg|_{-V/2\omega_c}^{V/2\omega_c}$$

$$= \frac{\omega_c}{V} \left[\frac{\sin(\omega_c+n\omega)V/2\omega_c}{\omega_c+n\omega} + \frac{\sin(\omega_c-n\omega)V/2\omega_c}{\omega_c-n\omega} \right] \quad \ldots\ldots\ldots (7.31)$$

Since ω is the angular speed of the fundamental, it can be written as

$$\omega = \frac{2\pi}{T} = \frac{2\pi\omega_c}{V} \quad \ldots\ldots\ldots (7.32)$$

Substitute eq.(7.32) into eq.(7.31) gives

$$a_n = \frac{\omega_c}{V} \left[\frac{\sin(\omega_c+2\pi n\omega_c/V)\ V/2\omega_c}{\omega_c+2\pi n\omega_c/V} + \frac{\sin(\omega_c-2\pi n\omega_c/V)\ V/2\omega_c}{\omega_c-2\pi n\omega_c/V} \right]$$

$$= \frac{\sin(V/2+\pi n)}{V+2\pi n} + \frac{\sin(V/2-\pi n)}{V-2\pi n}$$

$$= \frac{\sin V/2\cos\pi n}{V+2\pi n} + \frac{\sin V/2\cos\pi n}{V-2\pi n}$$

$$= (-1)^n \sin V/2 . \frac{V-2\pi n + V+2\pi n}{V^2-4\pi^2 n^2}$$

$$= \frac{2(-1)^n \sin V/2 . V}{V^2-4\pi^2 n^2} \qquad \ldots\ldots\ldots \qquad (7.33)$$

Eq. (7.28) can now be rewritten in analytical form as

$$y_o = -\frac{e}{\cos V/2} \sum_{n=-\infty}^{\infty} a_n e^{jn \frac{2\pi\omega_c}{V} t} \qquad \ldots\ldots\ldots \qquad (7.34)$$

Since the left membrum of eq. (7.34) is real, the coefficients a_n must be such that no imaginary terms occur in the right membrum. This is so only if $a_n = a_{-n}$ (see eq. (7.33)), thus

$$y_o = -\frac{e}{\cos V/2} \sum_{n=-\infty}^{\infty} a_n \cos n \frac{2\pi\omega_c}{V} t$$

$$= -\frac{e}{\cos V/2} \left[a_o + 2 \sum_{n=1}^{\infty} a_n \cos n \frac{2\pi\omega_c}{V} t \right]$$

$$= -\frac{e}{\cos V/2} \left[a_o + 2 \sum_{n=1}^{\infty} a_n \cos n\omega_{rp} t \right] \qquad \ldots\ldots\ldots \qquad (7.35)$$

The modulus of the Fourier coefficients are

$$a_n = \frac{2\sin V/2 \cdot V}{V^2 - 4n^2\pi^2} \qquad \ldots\ldots\ldots \quad (7.36)$$

But since $V^2 << 4n^2\pi^2$ for all $n > 0$

$$a_n \simeq \frac{2\sin V/2 \cdot V}{2n^2\pi^2} \qquad \ldots\ldots\ldots \quad (7.37)$$

As an example, the first five components of the expansion for a bearing having twelve rolling elements ($V = \pi/6$) is given below

$n =$	0	1	2	3	4
$a_n =$	0.9886	0.00687	0.00172	0.000763	0.000429

So, neglecting phase, the Fourier expansion of $y_o(t)$ for this particular bearing is written

$$y_o(t) = -1.0353e(0.9886 + 0.01374\cos\omega_{rp}t + 0.00344\cos 2\omega_{rp}t + 0.00153\cos 3\omega_{rp}t + 0.000858\cos 4\omega_{rp}t + \ldots\ldots) \quad \ldots\ldots \quad (7.38)$$

To calculate the order of magnitude of these vibration components, a bearing with 50 microns radial clearance is considered. The vibration components given by eq.(7.38) then becomes: 0.71 microns amplitude at RP frequency, 0.18 microns at the first harmonic, 0.08 microns at the second harmonic and so on. The component at RP frequency is of the same order as the displacements caused by inner ring waviness, See Fig.7.11, or varying roller diameters, see Fig. 7.5. Consequently, the vibration component occuring at RP frequency is of the same order of magnitude as those generated by form errors, see Fig. 7.3.

The vibration line spectrum calculated with the approximate Kinematic model should be compared to the line spectrum calculated with the DYNSIM program of Chapter 6. For many cases of small to moderate speeds and loads the general characteristics agree, but effects like sub-harmonics, resonance excitation, and beating are not predicted by the Kinematic model. The sharp corners of the displacement function of Fig. 7.13, will be rounded due to elastic deformation of rollers and rings. This tends to attenuate higher harmonics and make y_o resemble a sine wave with RP frequency. The more flexible the rolling bodies are, the more pronounced will this smoothing of the displacement function become. Thus, bearings with essentially point contact, like ball bearings or lightly loaded spherical roller bearings, will have fewer and smaller harmonics than bearings with line contact, like cylindrical roller bearings. The validity of this statement is borne out by a comparison between Figs. 6.27 and 7.3. The spectrogram of Fig. 6.27 originating from a cylindrical roller bearing, has several sizeable harmonics, while virtually no harmonics occur in the spectrograms of Fig. 7.3 from a spherical roller bearing.

7.6 VIBRATIONS DUE TO INNER RING WAVINESS

By use of eq.(7.26) the vertical and horizontal movements of the inner ring centre of a bearing having a non-circular inner ring can be calculated. Similarly to the case of vibrations due to clearance described above, but contrary to vibrations due to non-uniform roller diameters, eq.(7.26) will have discontinuities. The extent of these discontinuities depend on the type of form deviation, so that for some bearings eq.(7.26) will give very good predictions of the occurring

vibration components, while for other bearings the predictions are less accurate. As will be demonstrated however, the Kinematic model offers a simple and reliable method for obtaining the characteristics of vibrations associated with inner ring waviness.

As the mass of the rotor moves according to eq.(7.26), the inertia forces associated with this movement will cause forced vibrations of the bearing holder. Although eq.(7.26) gives a complete description of the shaft centre movements as a function of ψ, it is not possible to see from the expression directly what the characteristics of the generated vibrations are. When the summation is carried out, some terms will cancel out, while others will constitute the predominant vibrations. What is important, from the vibration point of view, is not so much instantaneous positions, as the components that persist during a length of time. Fourier analysis has such an averaging effect if the time during which the function is analysed, is made long enough.

To analyse the y_o function, a computer program, KINSIM (KINematic SIMulation), was written. This program is not a simulation program in the same sense as DYNSIM is, since eq.(7.26) is not a differential equation, and all that needs doing is to tabulate y_o for a series of ψ values. KINSIM is linked to the DAS system via one of the dummy file calls. When called, KINSIM will produce "samples" taken from the theoretical model of eq.(7.26) and write the ordinates on disk file ORDA, from where it can subsequently be read and analysed by the DAS routines. To produce the ordinates, values of the dev(θ)function, see Fig.7.10, must be fed into the program. The most obvious way of doing this is to

simply read a sufficient number of the out of roundness ordinates into KINSIM from the paper tape on which they are punched, see Section 7.3. However, it proved difficult to achieve accurate results in this way, the problem stemming from the digitization of the dev(θ) function. As the bearing rotates, one roller leaves the load carrying zone, and the next one enters it. At these instants, the argument of dev(θ + kV) is incremented by V. The argument is then by rounding matched to the sample on the paper tape which is nearest to this argument. This rounding can, especially for high frequency waves, cause significant errors. Therefore a different method was tried.

It was shown in Section 7.3 how the Fourier coefficients of the dev(θ) function could be calculated. By use of these coefficients the dev(θ) function can be expanded into a Fourier series, i.e. if phase is neglected, written as

$$dev(\theta) = c_o + \sum_{n=1}^{\infty} c_n \sin(n\theta) \qquad \ldots\ldots\ldots \qquad (.7.39)$$

However, c_o, is a calibration factor without any significance for the raceway shape and similarly, c_1 is only a function of how well the ring has been centered on the Tallyrond table and thus, the relevant part of the expansion is

$$dev(\theta) = \sum_{n=2}^{\infty} c_n \sin(n\theta) \qquad \ldots\ldots\ldots \qquad (7.40)$$

As seen from Fig. 7.11 showing the Fourier coefficients of inner ring waviness for the three bearings A, B and C, these tracks are well defined by the first twelve Fourier coefficients. The KINSIM program

allows for up to fifteen waves around the circumference to be specified. In a bearing rotating at a steady speed the angles ψ and θ can be written as functions of time

$$\begin{cases} y = \omega_c t \\ \theta = \phi - \psi = (\omega_s - \omega_c)t \end{cases} \quad \ldots\ldots\ldots \quad (7.41)$$

Now, substituting eq. (7.40) and (7.41) into eq.(7.26) gives

$$\begin{cases} x_o = \frac{1}{\sin V} \sum_{k=o}^{\infty} \sum_{n=2}^{\infty} [(e - c_n \sin n((\omega_s - \omega_c)t + kV))\cos(\omega_c t - (k+1)V) - \\ \qquad (e - c_n \sin n((\omega_s - \omega_c)t + (k+1)V)\cos(\omega_c t - kV)][U(t - \frac{kV}{\omega_c}) - U(t - \frac{(k+1)V}{\omega_c})] \\ y_o = \frac{1}{\sin V} \sum_{k=o}^{\infty} \sum_{n=2}^{\infty} [(e - c_n \sin n((\omega_s - \omega_c)t + kV))\sin(\omega_c t - (k+1)v) - \\ \qquad (e - c_n \sin n((\omega_s - \omega_c)t + (k+1)V)\sin(\omega_c t - kV)][U(t - \frac{kV}{\omega_c}) - U(t - \frac{(k+1)V}{\omega_c})] \end{cases}$$

$$\ldots\ldots\ldots \quad (7.42)$$

If KINSIM instead is made to simulate eq.(7.42), all information of the dev(θ) function is contained in its first 10 to 15 Fourier coefficients, c_n. This is not only in a considerable data reduction (about 1800 data points were required to read the dev(θ)function directly) but it also does away with the rounding problem previously described. As a demonstration of the KINSIM program, the vertical shaft movements of a bearing with eight lobes on the inner ring have been simulated and are shown in fig. 7.14.

Rembering that the Kinematic model constitutes a linear system a significant simplification can be made. The linearity implies that shaft movements due to a number of superimposed waves of the track can be calculated separately for each wave. Thus for L = 2 to 15, KINSIM was run with values of c_n as below.

$$c_n = \begin{cases} 1 \text{ if } n=L \\ 0 \text{ otherwise} \end{cases} \quad \ldots\ldots\ldots \quad (7.43)$$

The line spectra of these runs, for the first 15 components of the inner ring form function, are all dominated by two peaks. A number of small peaks also occur, but for the wave numbers investigated, the two predominant peaks contribute more than 99% of the total RMS value of the y_o function. The y_o function averaged over a long period of time can thus be written as

$$y_o(t) = A\sin 2\pi f_1 t + B\sin 2\pi f_2 t \quad \ldots\ldots\ldots \quad (7.44)$$

neglecting phase. The KINSIM runs are summarised in Fig. 7.15. As is shown in this diagram, the wave having n cycles per circumference gives,

$$\begin{cases} f_1 = n \cdot f_s \\ f_2 = |n \cdot f_s - f_{rp}| \end{cases} \quad \ldots\ldots\ldots \quad (7.45)$$

The coefficients A and B are obtained by multiplying the factors C_1 and C_2 of fig. 7.15 (obtained for a wave with an amplitude of one micron) with the coefficients c_n of fig. 7.11 representing the amplitude of the actual wave. Thus, if the Fourier coefficients of the form function are known these can be used in conjunction with the diagram of fig. 7.15 to calculate the stationary part of the movements of inner ring centre relative to the outer ring centre in a bearing having wavy inner race,

$$y_{o,n}(t) = c_n C_1(n)\sin(n\omega_s)t + c_n C_2(n)\sin|n\omega_s - \omega_{rp}|t$$

..... (7.46)

Due to the linearity, equation (7.46) can be used to determine the vibrations generated by waves having different values of n independantly.

Generally it is not practical to calculate the Fourier coefficients of $y_o(t)$ analytically. For the special cases when the numbers of wave cycles equals the number of rolling elements, n = N, however, an analytical solution can easily be obtained and this can be used as a corrolarium of the functioning of the KINSIM program. Thus substitute n = 12, e = 0 (the clearance does not significantly effect components due to waviness) and V = 30° into equation (7.42),

$$y_o(t) = \frac{1}{\sin 30^\circ} \sum_{k=o}^{\infty} [-1 \cdot \sin(12(\omega_s - \omega_c)t + 12k \cdot 30^\circ) \cdot \sin(\omega_c t - (k+1)\ 30^\circ)$$

$$+ \ 1 \cdot \sin(12(\omega_s - \omega_c)t + 12k\ 30^\circ + 360^\circ) \cdot \sin(\omega_c t - k \cdot 30^\circ)] \cdot$$

$$[U(t - \frac{k \cdot 30^\circ}{\omega_c}) - U(t - \frac{(k+1) \cdot 30^\circ}{\omega_c}\ ]$$

$$= \frac{\sin 12(\omega_s - \omega_c)t}{\sin 30^\circ} \sum_{k=o}^{\infty} [\sin(\omega_c t - k \cdot 30^\circ)$$

$$- \sin(\omega_c t - (k+1)\ 30^\circ)][(U(t - \frac{k \cdot 30^\circ}{\omega_c}) - U(t - \frac{(k+1) \cdot 30^\circ}{\omega_c}\ ]$$

$$= \frac{2\sin 12(\omega_s - \omega_c)t \cdot \sin 15^\circ}{\sin\ 30^\circ} \sum_{k=o}^{\infty} \cos(\omega_c t - 30^\circ \cdot k - 15^\circ)$$

$$[U(t - \frac{k\ 30^\circ}{\omega_c}) - U(t - \frac{(k+1)\ 30^\circ}{\omega_c})] \qquad \text{.....} \qquad (7.47)$$

A comparison with equation (7.28) shows that except for the term before the summation sign, eq.(7.28) and eq.(7147) are identtical. Thus, by the use of the table of Fourier coefficients on page 100, equation (7.47) can be written as

$$y_o(t) = 7.0353 \sin 12(\omega_s - \omega_c)t[0.9886 + 0.01374\cos\omega_{rp}$$

$$+ \quad 0.00344\cos 2\omega_{rp} + 0.00153\cos 3\omega_{rp} + ...]$$

$$= 1.0353\ [0.9886\sin(12\omega_s - \omega_{rp})t + 0.00687\sin(12\omega_s - \omega_{rp} \pm \omega_{rp})t$$

$$+ 0.00172\sin(12\omega_s - \omega_{rp} \pm 2\omega_{rp})t + ...] \qquad ..... \qquad (7.48)$$

According to equation (7.48) a twelve cycle wave would give rise to a predominant peak at frequency $2\pi(12\omega_s - \omega_{rp})$ and symmetrical side bands spaced with f_{rp} Hz from the main peak. The amplitudes of the side bands decrease very rapidly, the central peak having an amplitude of 1.0235, the first pair of sidebands having an amplitude of 0.0071, and thus only the first two terms of equation (7.48) has to be considered. A KINSIM run with the parameter for this case gives an identical result, which is also shown in fig.7.15, where however only one of the side bands are shown. For all other values of n, the side bands are non-symmetrical, so that except for the central peak, only one side band is large enough to have to be considered.

These results can now be applied to the three bearings A, B and C previously considered. Their inner race way shapes with respective Fourier coefficients are shown in figs.7.10 and 7.11 and the spectro-grams from the bearings run at 18 Hz shaft speed with 12 kg rotor are

shown in fig. 7.12. By use of fig. 7.11 and 7.15 it is now possible to determine at what frequencies and with what relative amplitudes, bearing vibrations are to be expected. Bearing A has large 6 and 7 lobe out of roundness. Fig. 7.15 shows that these will cause vibration components at 6 and 7 times shaft speed together with secondary peaks at frequencies f_{rp} below these. Primary and secondary peaks should be of about the same amplitude. These peaks are marked in fig. 7.12 with 6S', 7S' and 7S". The peak at 6S" coincides with the shaft fundamental and cannot be seen in fig. 7.12, but fig. 7.3, which is a run with the same bearing, shows such a peak at the higher speeds. The peaks 4S' and 5S' are small as could be expected from fig. 7.11. For out of roundness with only 2 or 3 cycles there is a risk that the race way shapes are affected by the mounting of the bearing in the test rig. This might explain the surprising absence of a peak at 3S' for bearing C. Otherwise the theory is valid and demonstrates the possibility of qualitative predictions of bearing vibrations due to inner ring out of roundness for typical bearings run under realistic conditions. To determine absolute values of frequency components the dynamics of rotor and bearing housing must also be considered. This will be discussed in section 8.2.

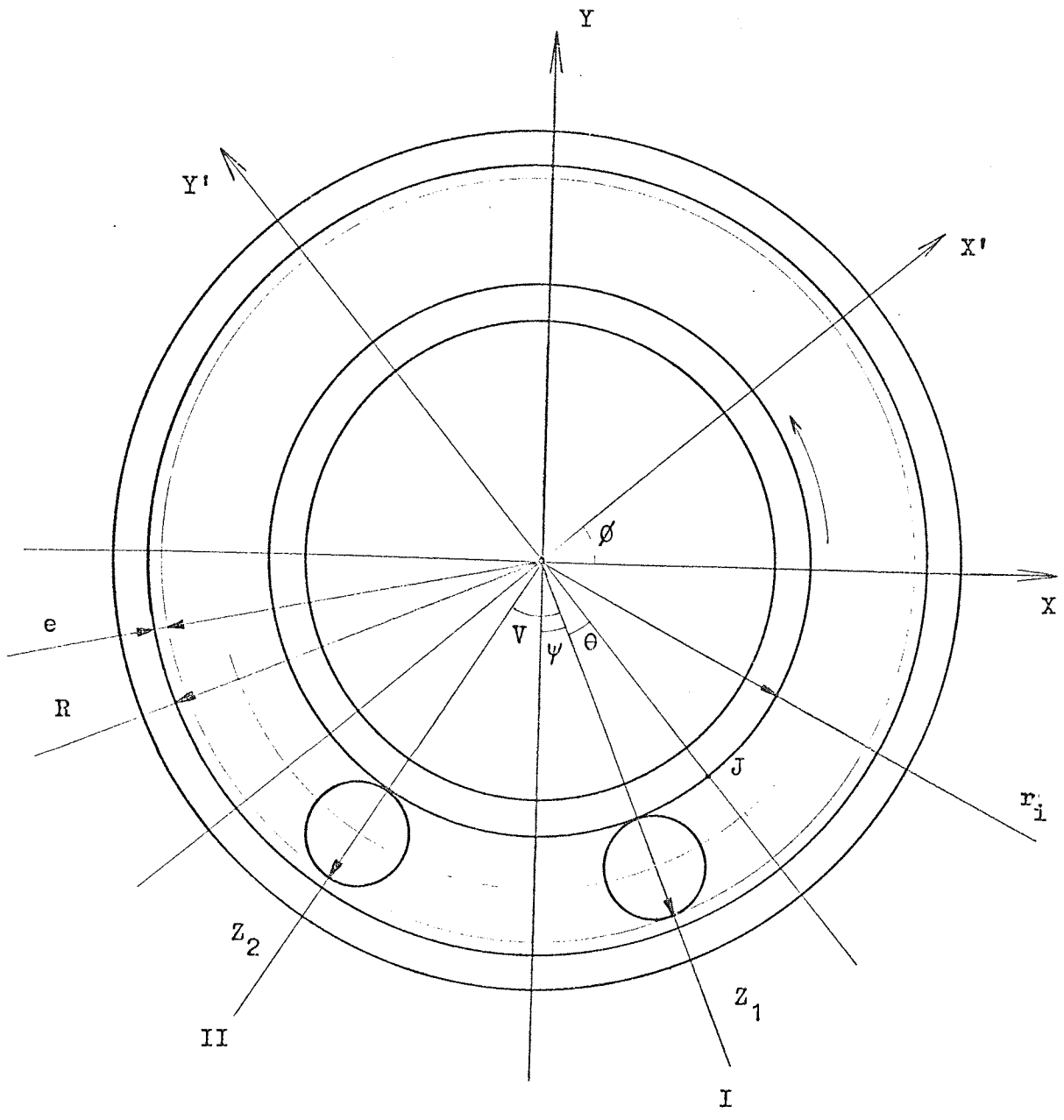

Fig 7.1.

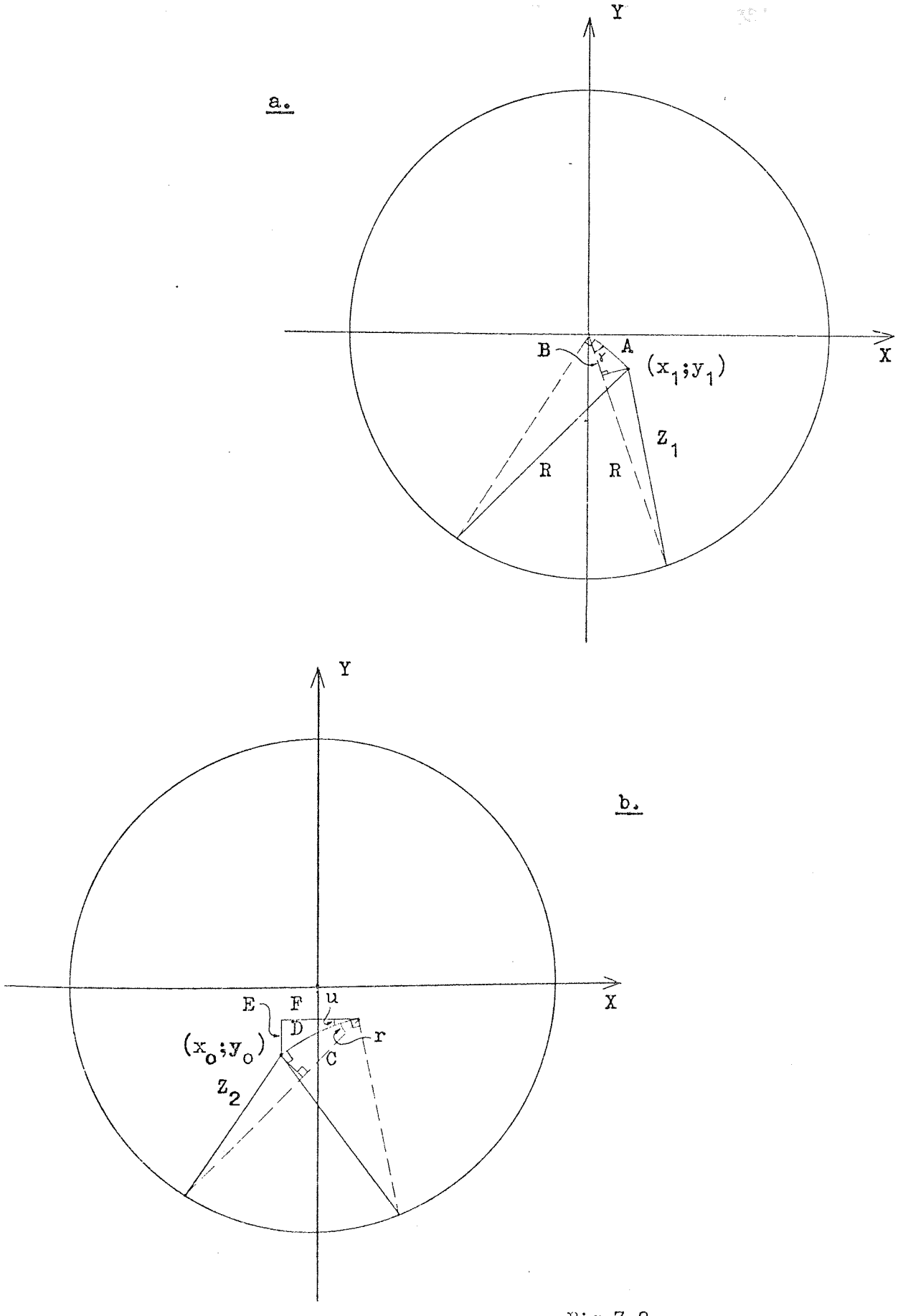

Fig 7.2.

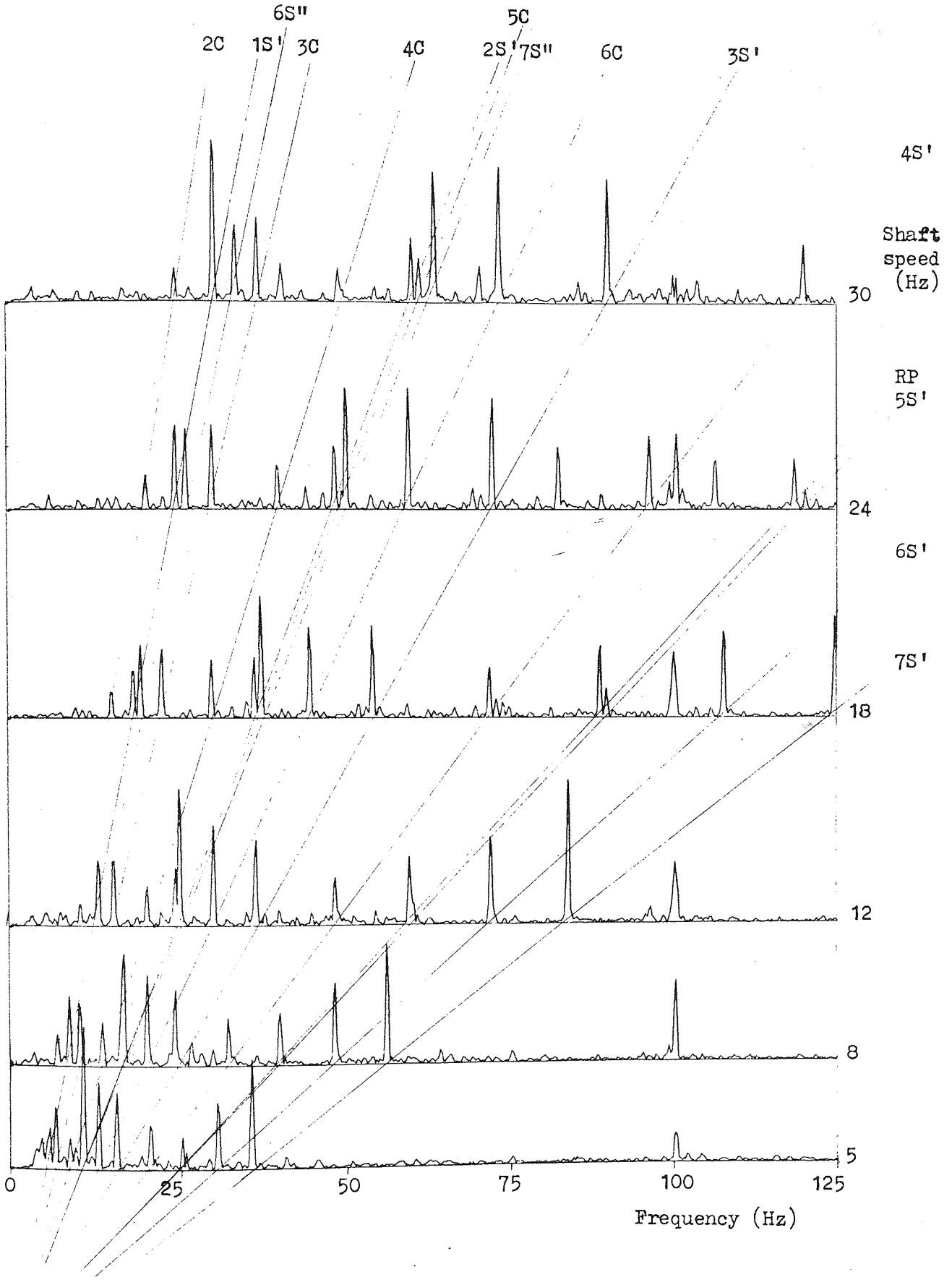

Fig 7.3. Cambell type diagram for a single row, spherical roller bearing (type 20206) run in the vibration test rig with M = 12 kg and "medium stiffness" mounting.

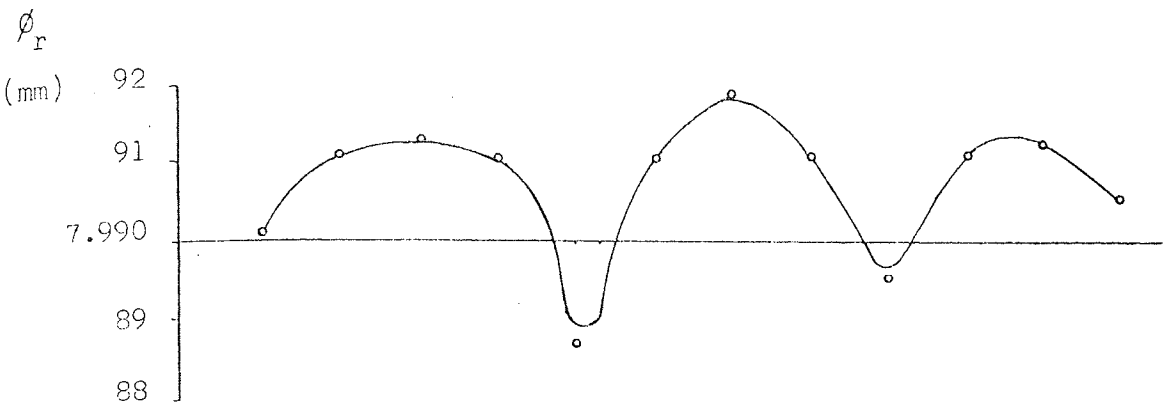

a.

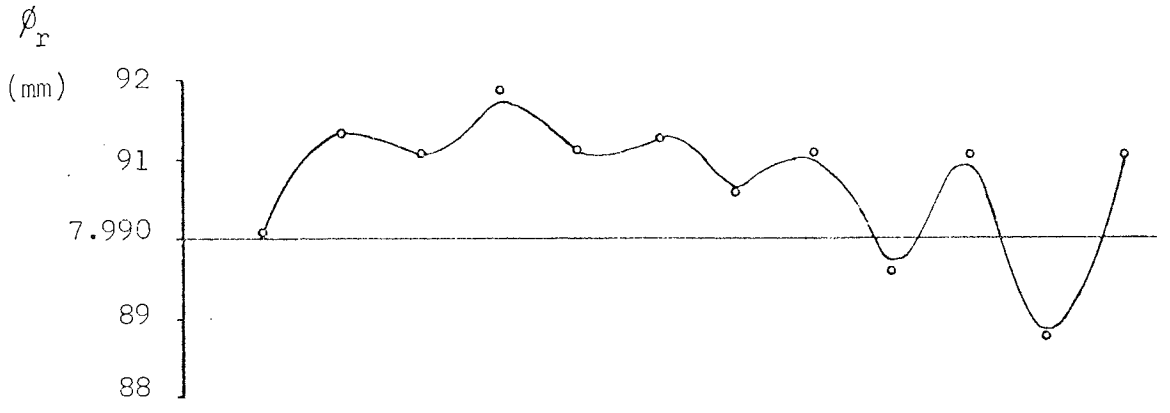

b.

Fig. 7.4. The rollers have been rearranged so as to give two different sequences of diameter variations.

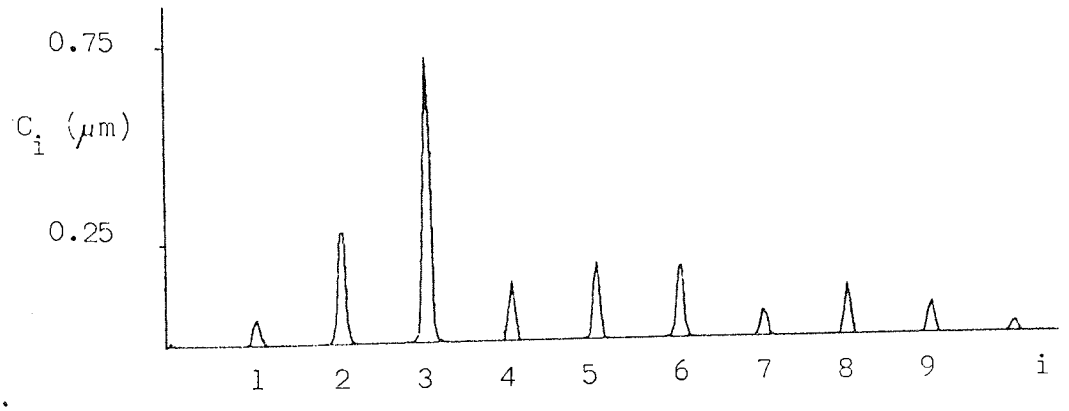

a.

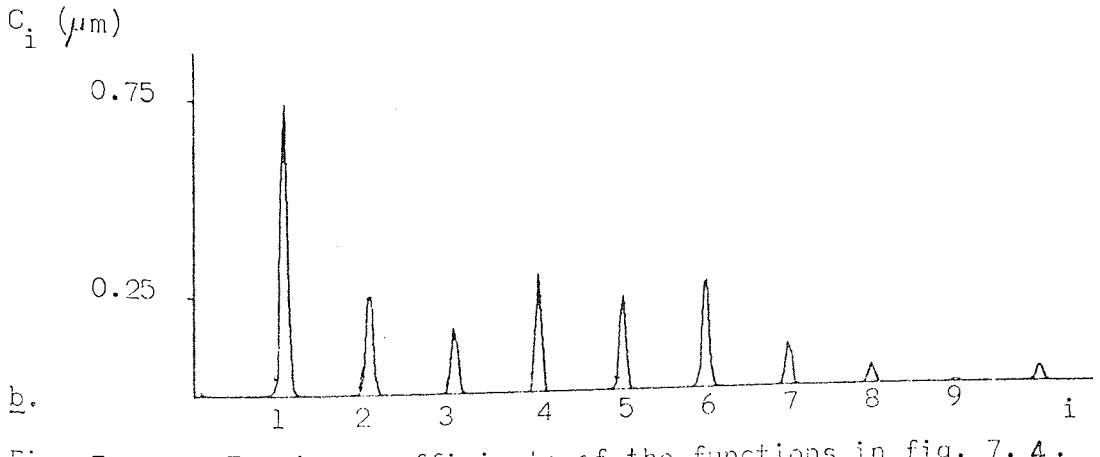

b.

Fig. 7.5. Fourier coefficients of the functions in fig. 7.4.

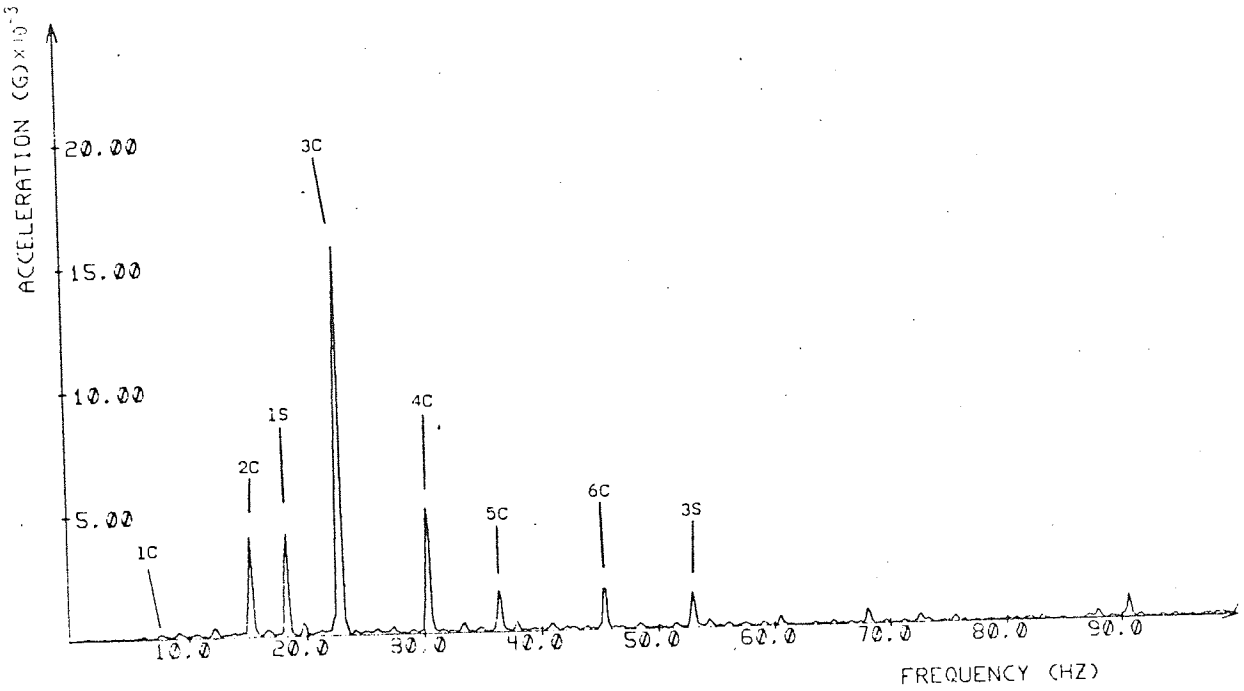

a.

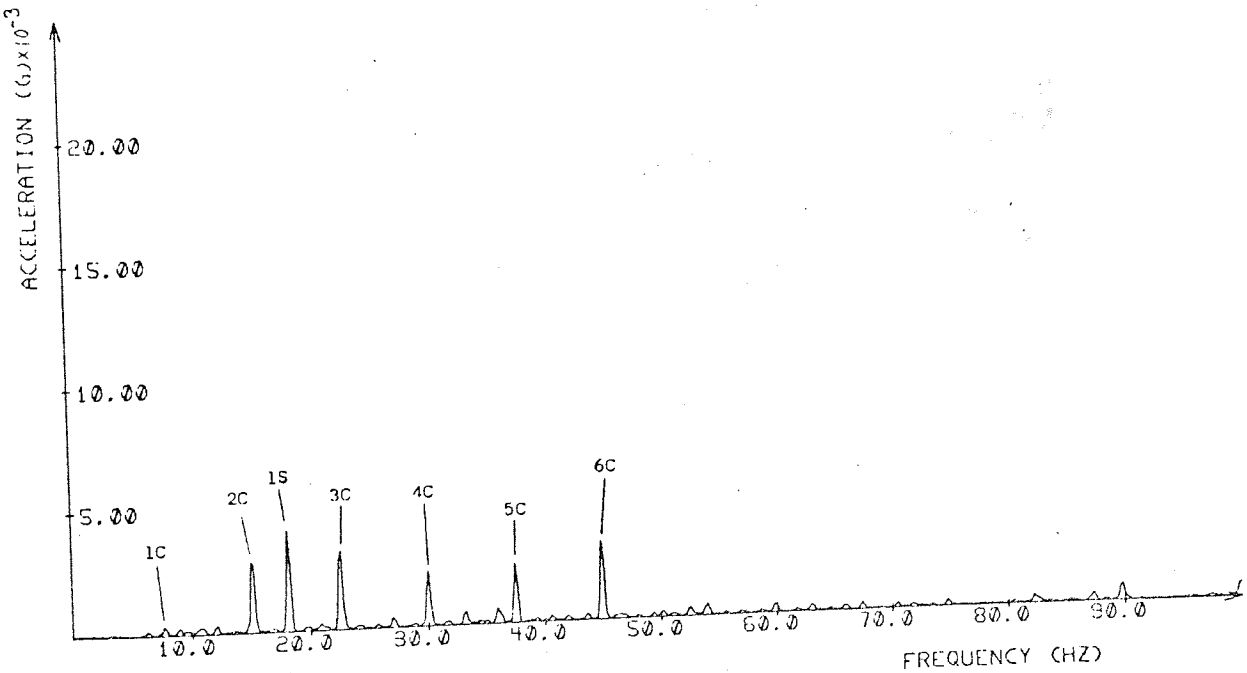

b.

Fig 7.6. Spectrograms from the vibration test rig from a type 20206 single row, spherical roller bearing with M = 12 kg and "medium stiffness" mounting. Both spectrograms are obtained from the same bearing, but in a. the rollers are arranged as in fig 7.4 a, while in b., the rollers have been rearranged in the sequence of fig 7.4 b.

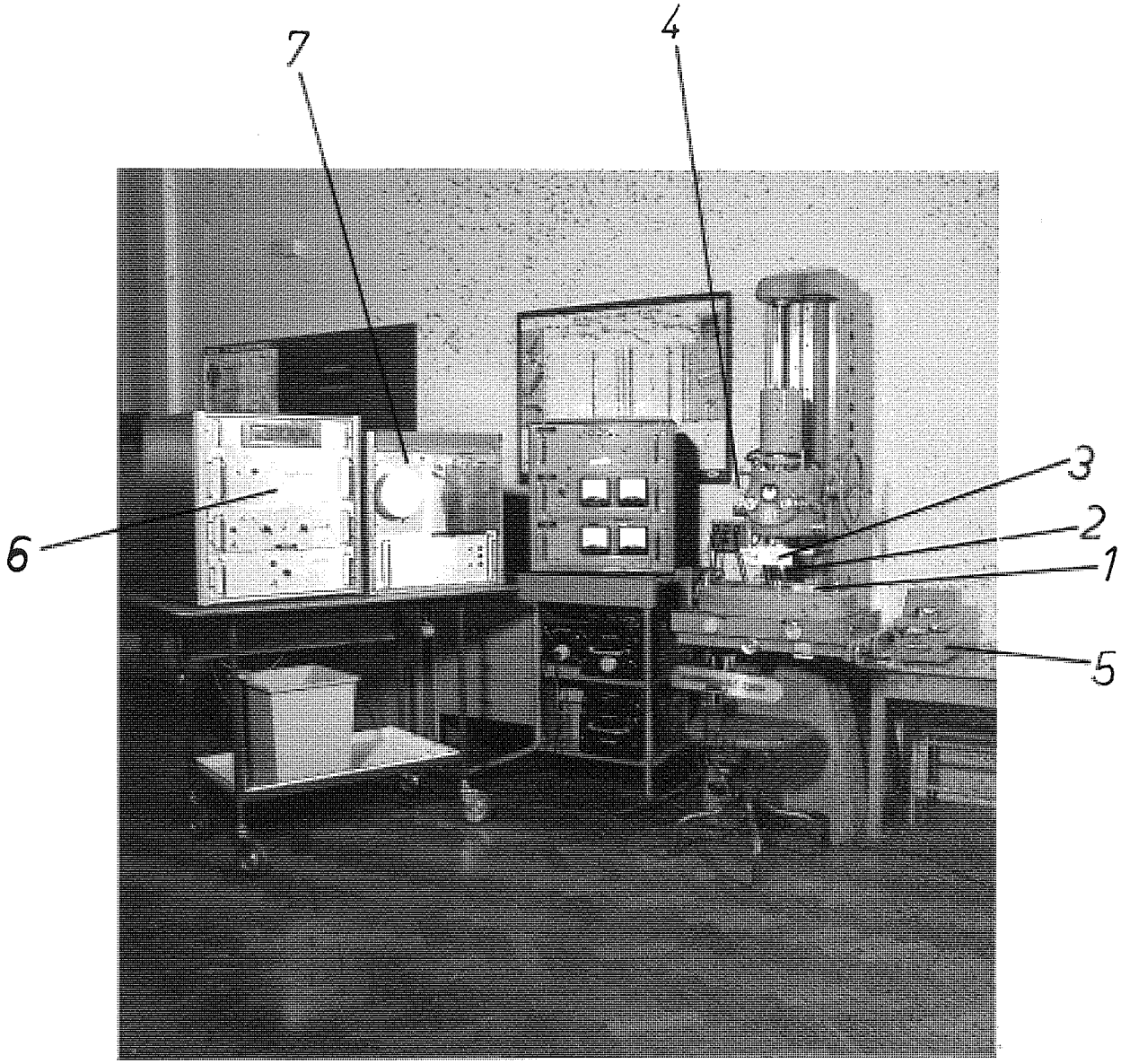

FIG 7.7

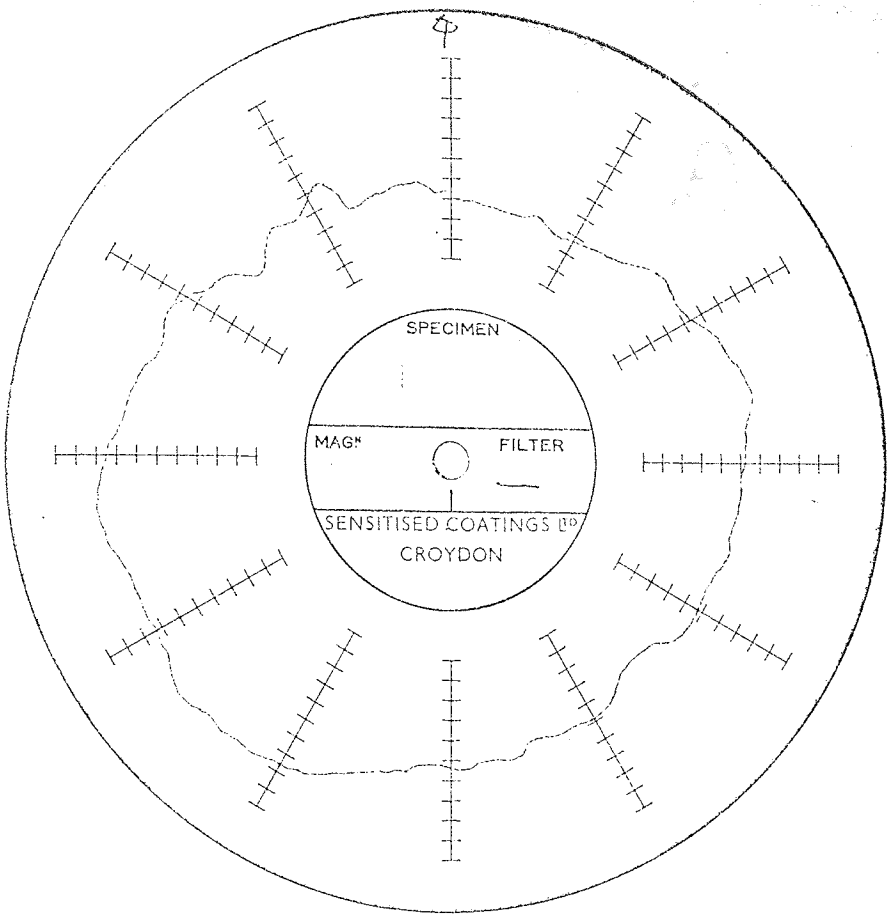

a. Polar plot.

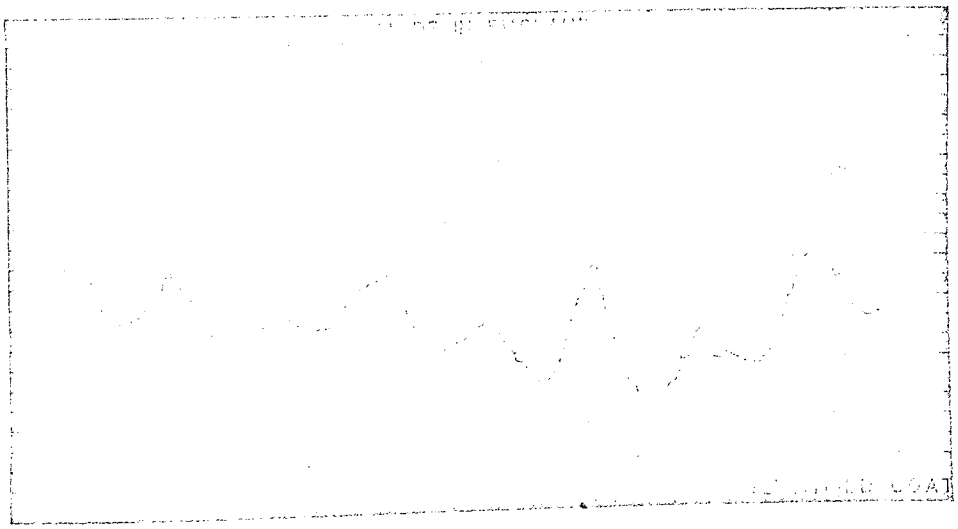

b. Rectiliner plot.

Fig 7.8 Types of plots normally used to record out of roundness measured with Tallyrond instrument.

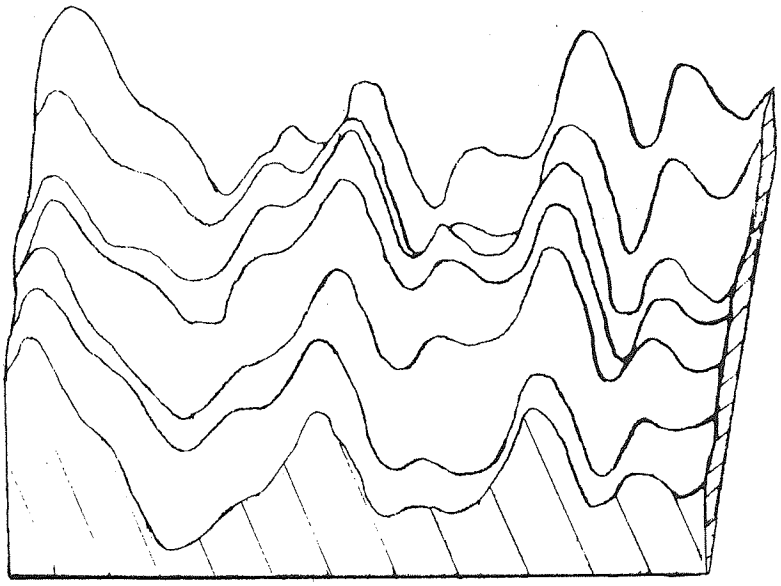

Bearing A

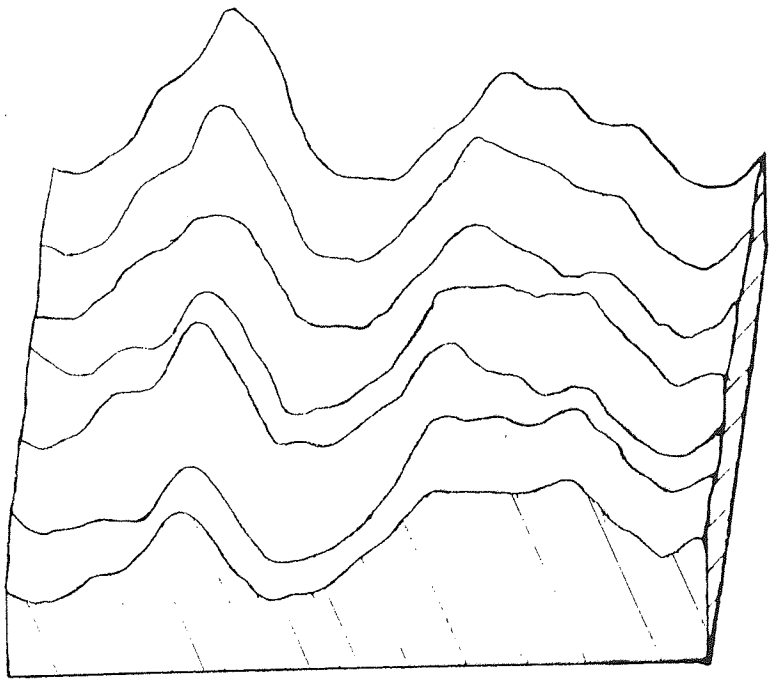

Fig. 7.9. Inner race surfaces of three 20206 type bearings. Vertical magnification is 4000X.

Bearing B

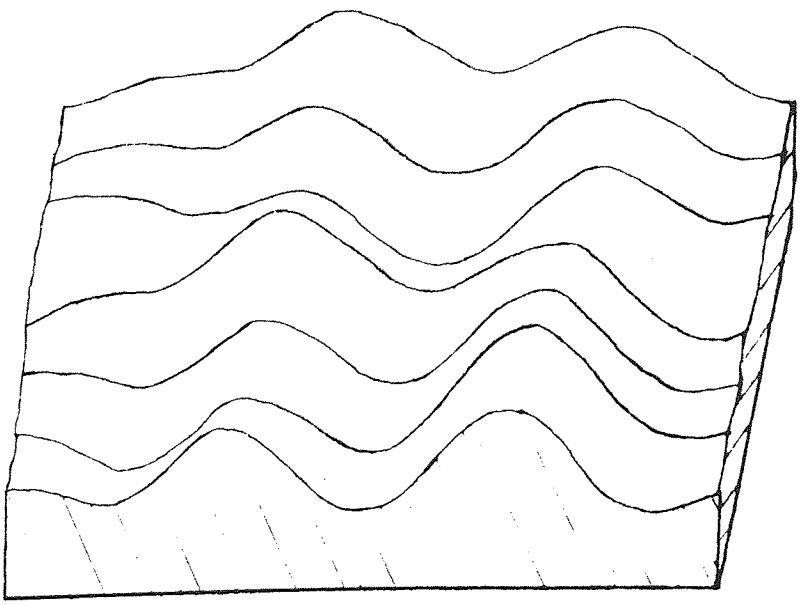

Bearing C

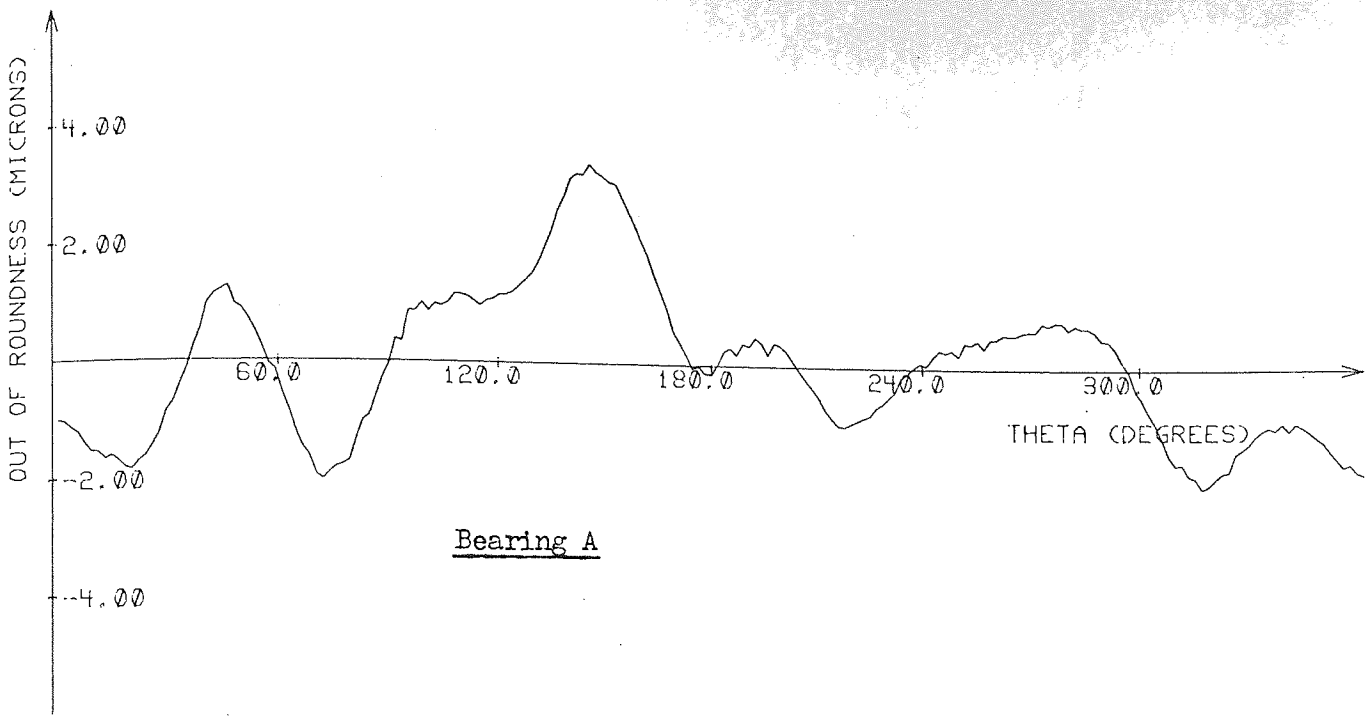

Bearing A

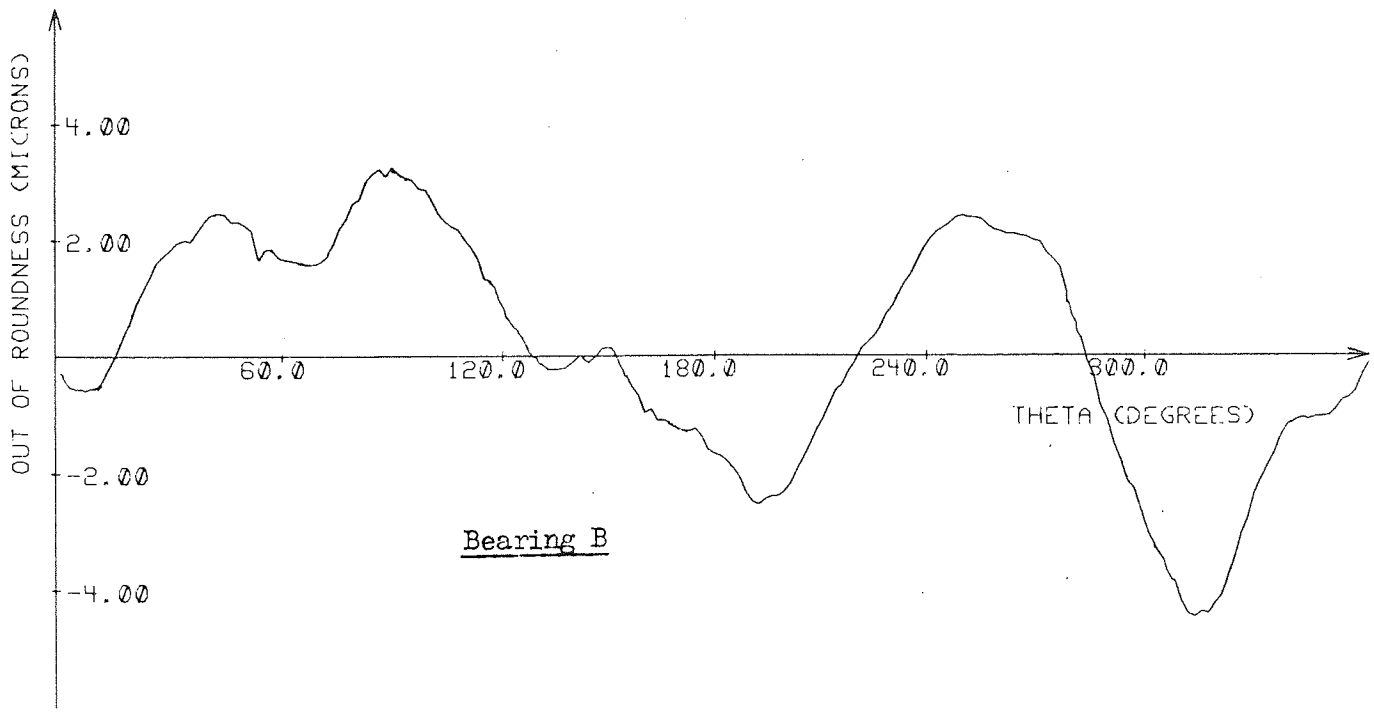

Bearing B

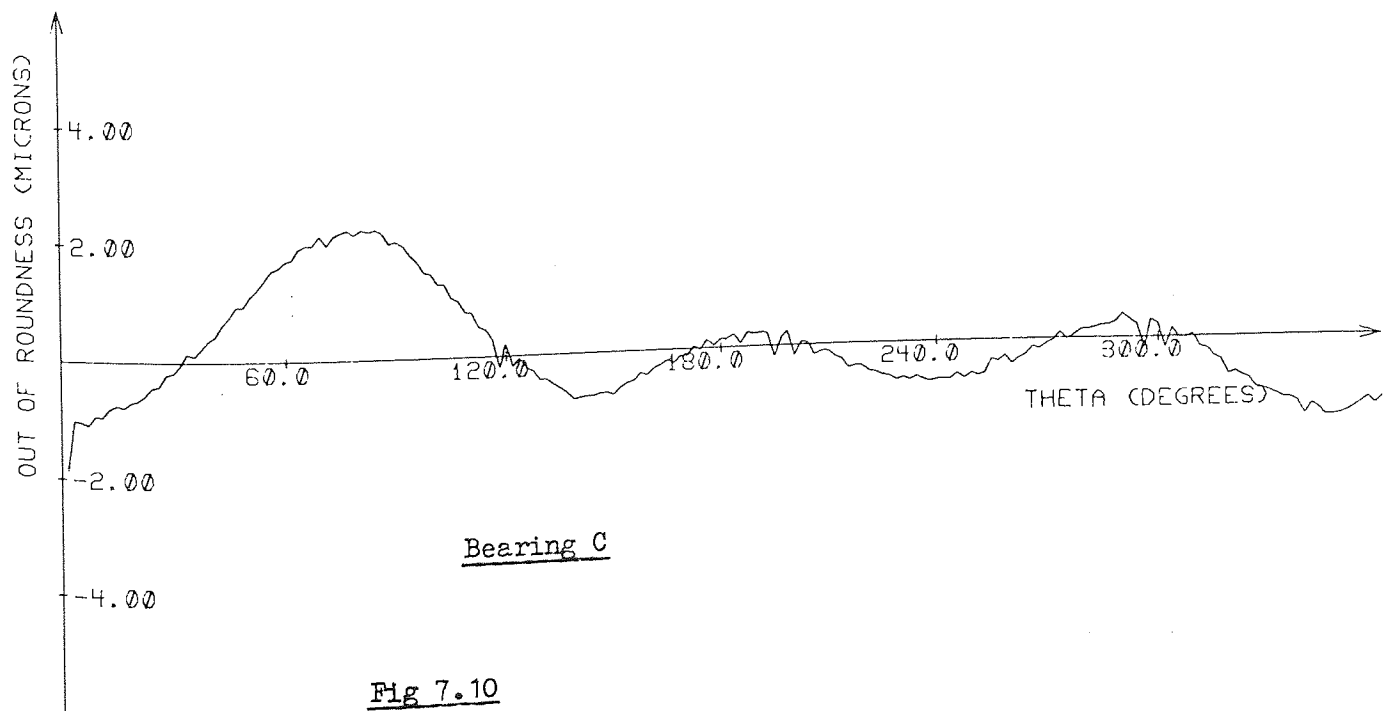

Bearing C

Fig 7.10

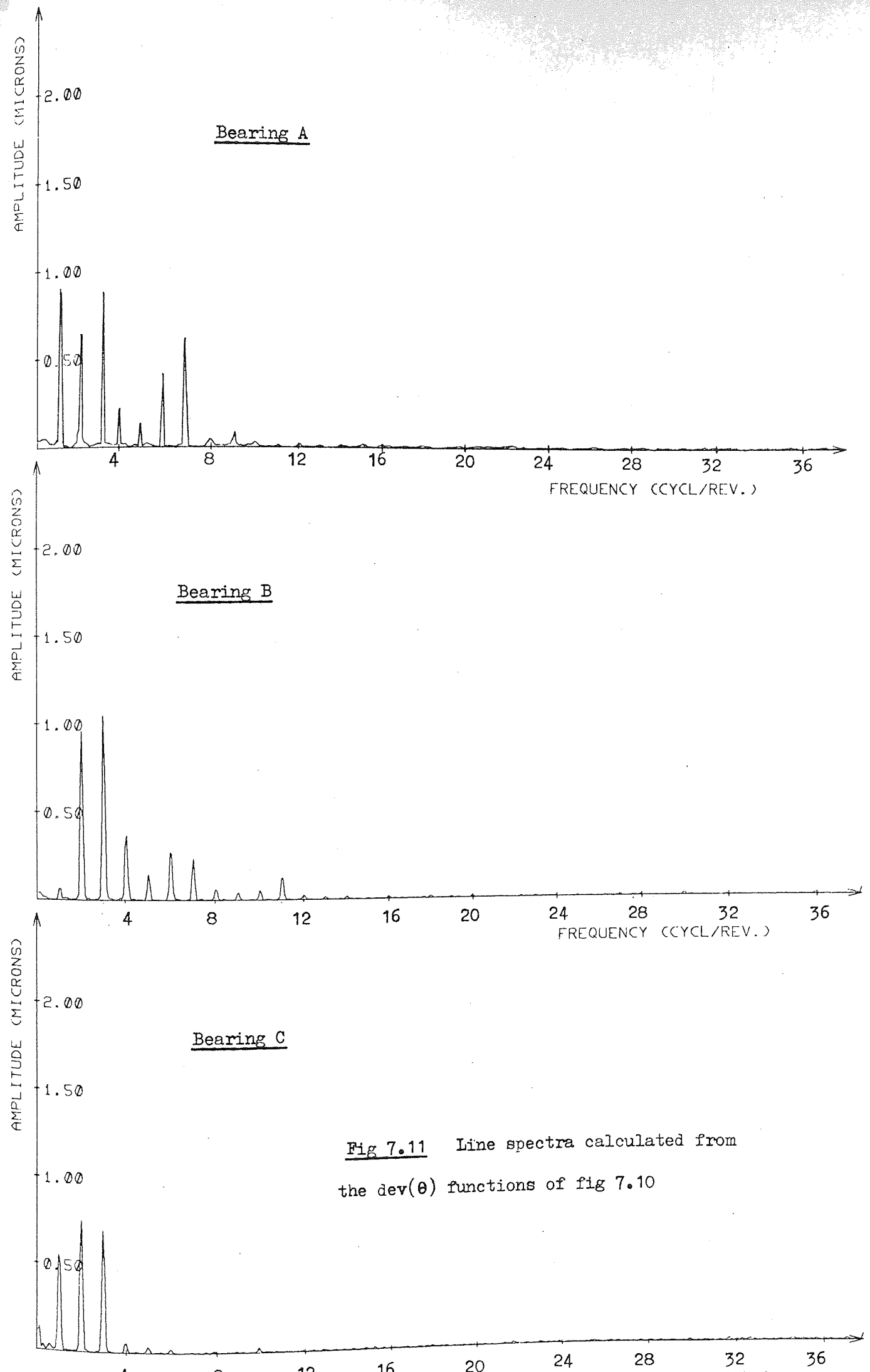

Fig 7.11 Line spectra calculated from the dev(θ) functions of fig 7.10

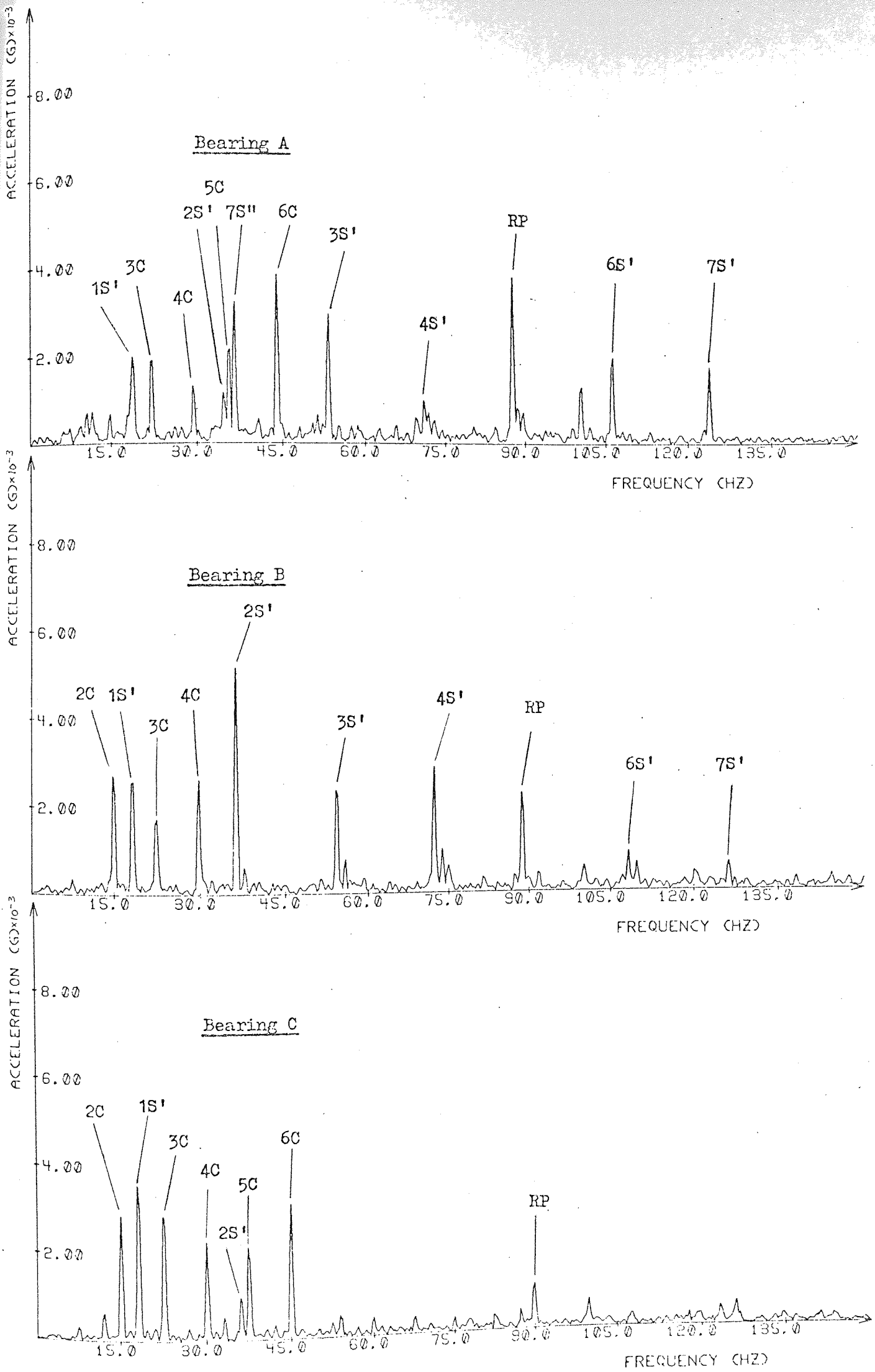
ACCELERATION (G)×10⁻³
8.00
6.00
4.00
2.00
Bearing A
1S'
3C
4C
5C
2S'
7S''
6C
3S'
4S'
RP
6S'
7S'
15.0
30.0
45.0
60.0
75.0
90.0
105.0
120.0
135.0
FREQUENCY (HZ)
ACCELERATION (G)×10⁻³
8.00
6.00
4.00
2.00
Bearing B
2C
1S'
3C
4C
2S'
3S'
4S'
RP
6S'
7S'
15.0
30.0
45.0
60.0
75.0
90.0
105.0
120.0
135.0
FREQUENCY (HZ)
ACCELERATION (G)×10⁻³
8.00
6.00
4.00
2.00
Bearing C
2C
1S'
3C
4C
5C
6C
2S'
RP
15.0
30.0
45.0
60.0
75.0
90.0
105.0
120.0
135.0
FREQUENCY (HZ)

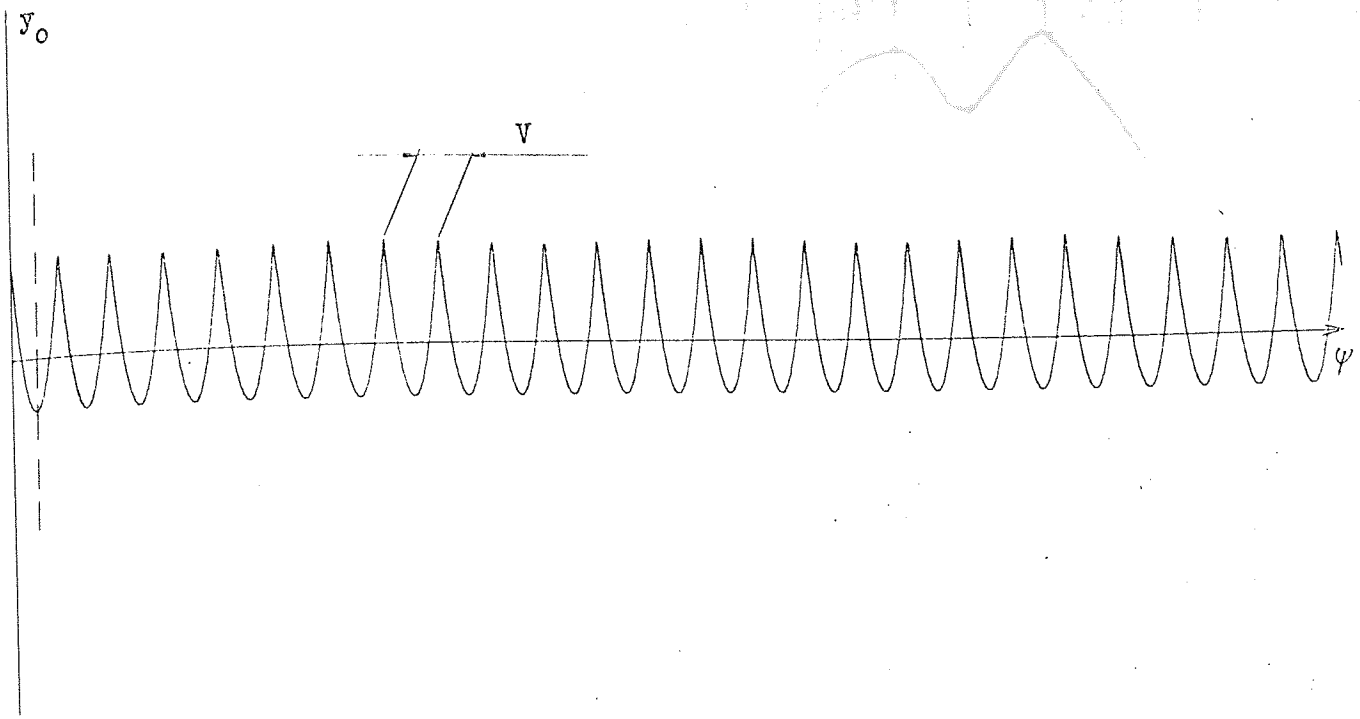

Fig 7.13 Vertical kinematic motion for bearing with positive clearence. The graph is obtained using the KINSIM program.

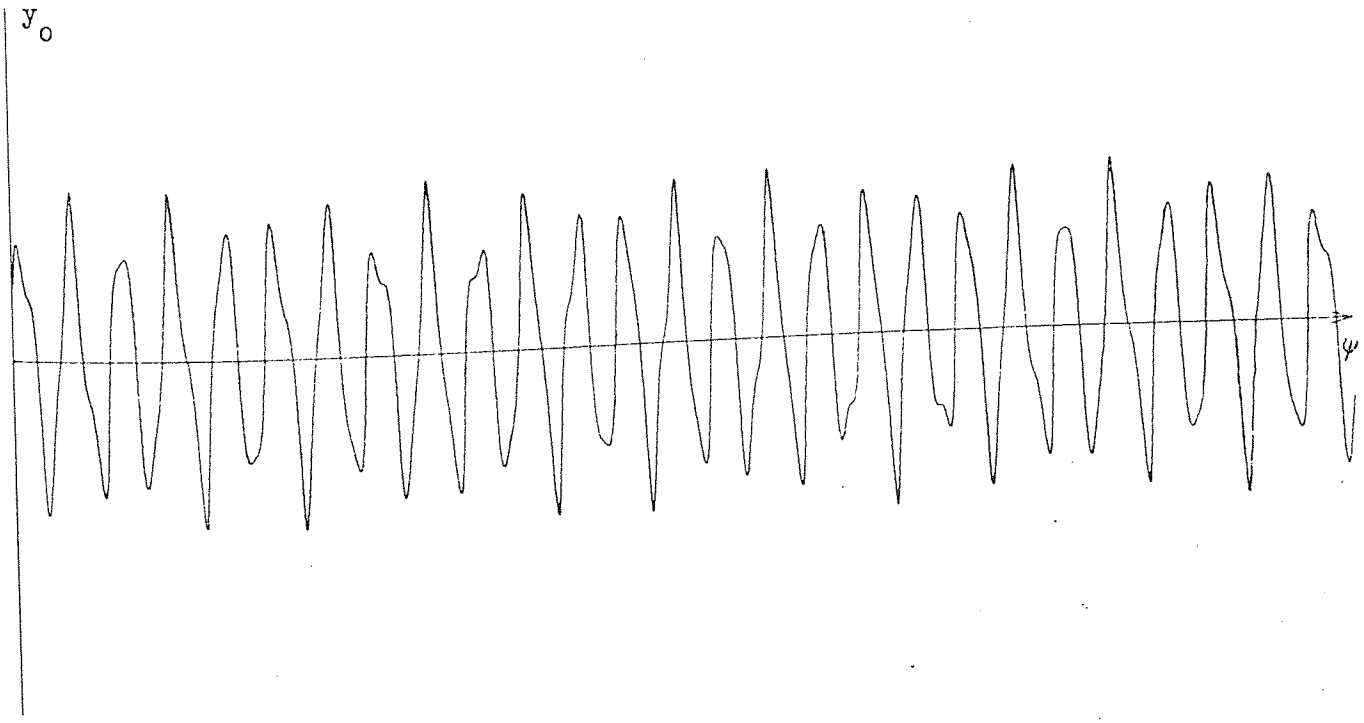

Fig 7.14 Example of KINSIM run.

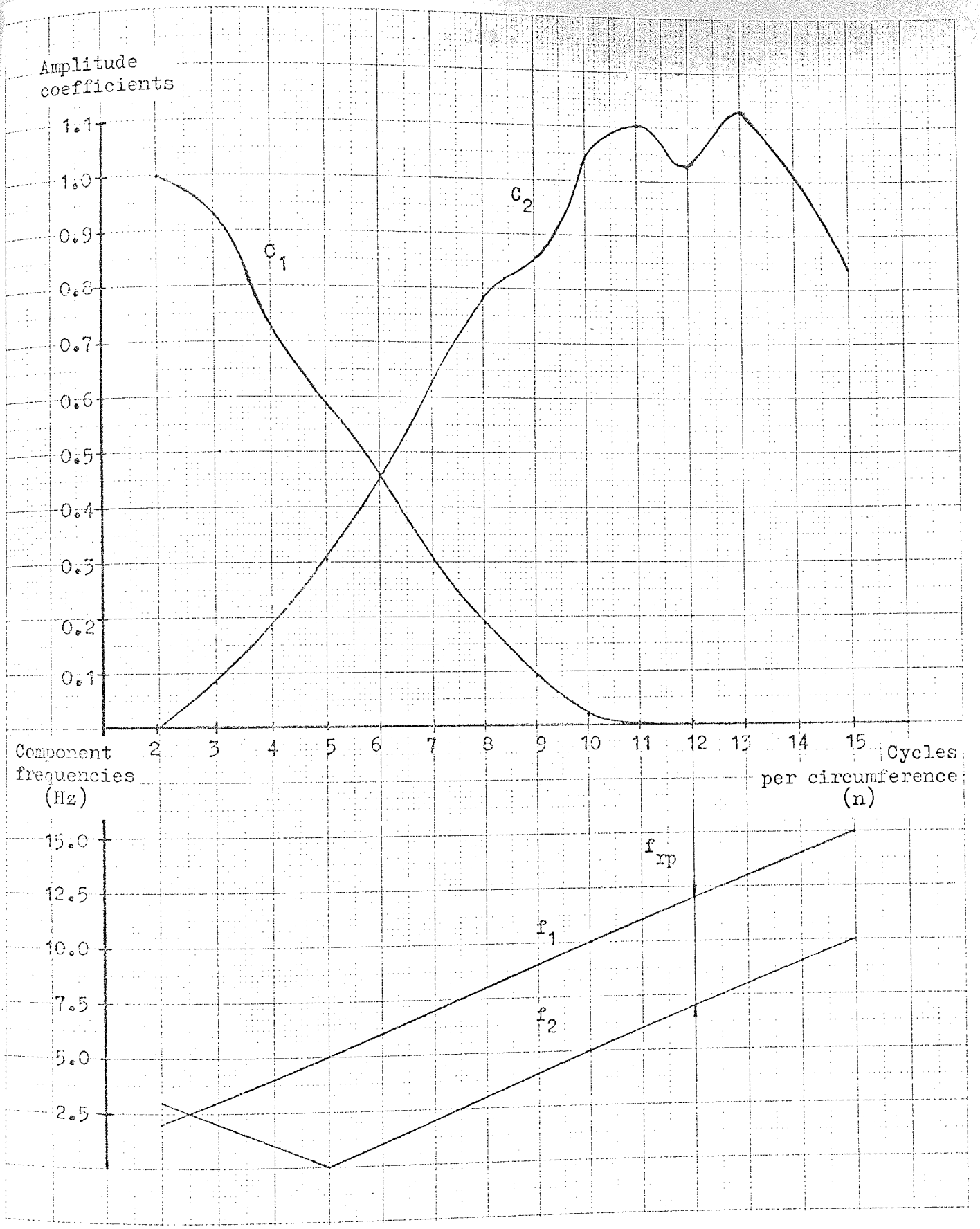

Fig. 7.15. The diagram shows the amplitudes and frequencies of the two predominant components generated by waviness of the inner track for waves having between 2 and 15 cycles per circumference. All waves have an amplitude of one micron and the shaft speed is one Hz. The diagram is valid only for bearings having 12 rolling elements.

CHAPTER 8

ROLLING BEARING INTERACTION WITH MACHINE STRUCTURES

In the two previous chapters the relative motion between inner and outer rings of a roller bearing has been studied as an effect of varying compliance and manufacturing tolerance. When a bearing is mounted in a machine structure of some sort it will however form an integrated part of this system, and the vibrations generated will depend not only on the properties of the bearing, but also on the dynamic properties of the rotor and fundament. It is important to realise that generally, the bearing is such a highly non-linear system, that it does not as such have independant vibration properties. This is the basic reason why the "free bearing" experiments described in Chapter 2 are useful mainly from the point of view of quality control, while the results do not say very much about how the bearing would behave in a practical application. In this chapter methods of treating a general rotor - bearing system will be briefly discussed, with a more detailed discussion of how an approximate method can be used to treat cases where it is permissible to assume an inflexible bearing.

8.1 FLEXIBLE BEARING AND STRUCTURE

In the general case elastic deformations will occur in rotor shaft, bearing and fundament. The theory derived for self excited vibrations in Chapter 6 assumes that the outer ring is held in a fixed position. If the

centre of the ring vibrates around its equilibrium, the restoring forces Q_x and Q_y will depend not only on cage and shaft position, but also on the position of the centre of the outer ring. Further, due to elastic bending of the shaft, the position of the centre of the mass of the rotor will not coincide with (or be proportional to) the position of the centre of the inner ring. To simulate the behaviour of the complete system, these effects must be taken into account. Although no such solution has been attempted, it will be shown very briefly along what lines a solution could be obtained.

The rotor and the fundament are substituted with lumped parameter systems consisting of masses, springs and dampers. For an approximate solution over a limited frequency range it would probably suffice with two degrees of freedom for x and y directions respectively plus coupling. The parameters of the lumped systems must then be assigned values so that they get dynamic properties similar to those of the original system. If the original systems are defined by their measured Mechanical Impedances, this information can be used to determine the optimal combination of parameters of the lumped system. An exhaustive account of digital techniques for the identification of such parameters is given in Ref.(48). Knowing these parameters, the whole dynamic system consisting of rotor substitute, bearing model and fundament substitute can then be simulated with a modified DYNSIM program, where the boundary conditions of the bearing movements and forces are determined by the lumped systems. Although this extention of DYNSIM would increase the number of degrees of freedom from 2 to 6, the increase of computer time would be small, since the linear, lumped systems are much easier to evaluate than

the bearing system. The setting up of such a system is a considerable task and it was felt that at present other aspects of bearing vibrations were of a higher priority.

Although the general problem of bearing - machine frame dynamics has been left unsolved, it has been found possible to determine at what shaft speeds there is a risk of exciting resonance of a given set up. The problem of resonance excitation by VC vibrations is a very complicated one, and the following does not offer stringent theoretical explanations, but is based mainly on intuition and experiments. It was shown in Chapter 6 that large vibrations resulted if the roller passage frequency or any of its first few harmonics coincided with the natural frequency of the bearing - rotor system. Unlike which is the case in resonant excitation of linear systems, the vibrations produced at resonance by the bearing assembly, was a cluster of components at or near the resonance or, the occurrence of subharmonics. Nevertheless, the essential point of resonance excitation is that when the frequency of the exciting force coincides with a natural frequency of the excited system, large vibrations result, and this general effect is common to both linear systems and the investigated bearing assembly system. In Chapter 6 the frequencies at which large vibrations were excited coincided with the natural frequencies of the stationary bearing. It is reasonable to expect a similar effect in a system where the bearing is combined with flexible rotor and fundament. The Mechanical Impedances for three configurations of the vibration test rig have been measured with the rotor stationary (see Section 8.3) and are presented in Fig.8.1. The deepest trough of Fig.8.1.A occurs at 80.5 Hz and in Fig. 8.1.B at 179.5 Hz. Thus two major natural frequencies are for configuration A: 80.5 Hz and for configuration B: 179.5 Hz.

The effects on vibration levels when running the roller passage frequency through these resonances have been investigated. In order to suppress vibrations due to unbalance and form deviations, the acceleration signal is for case A bandpass filtered between 50 and 100 Hz. The RMS value of the filtered signal is plotted against shaft speed and RP frequency (for this bearing, RP = $12 \cdot 0.42 \cdot f_s$) in Fig. 8.2, which shows a peak from 15.25 to 16.75 Hz shaft speed corresponding to 76.9 to 84.4 Hz RP frequency. Comparing Fig. 8.1A and Fig. 8.2 it seems clear that the resonance at 80.5 Hz is excited by the VC vibrations at roller passage frequency, and that the natural frequency of the system is the same whether the bearing is rotating or stationary. The resonance for configuration B has been investigated in more detail. The RMS value of the signal, filtered through 150 to 200 Hz, is plotted in Fig. 8.3. A sequence of scope photographs were taken during the passage through the resonance, and these are inserted in the diagram. The numbers I to VIII refer to spectrograms calculated from the unfiltered signal, which are presented in Figs. 8.4 - 8.7. Fig. 8.1B indicates that the stationary resonance occurs around 179.5 Hz but studying Fig. 8.4.I, it is apparent that the region having resonant like behaviour occur between 150 to 185 Hz for the rotating bearing, i.e. the natural frequency has shifted downwards approximately 10%. The reason might be, that the build up of an oilfilm (see Chapter 3) in the contact points between rollers and rings when the bearing runs, might diminish the total stiffness of the assembly. The occurrence of subharmonics in the context of resonance excitation was predicted in Chapter 6. Such subharmonics have also been found when running the RP frequency slightly above or below the resonance. Spectro-

grams IV,VII and VIII in figs.8.5 and 8.7 respectively have fairly large subharmonics at 1/5 of the RP frequency. The study of the subharmonics is complicated by the fact that RP frequency of this type of bearing, very nearly coincides with the fifth shaft harmonics, so that the subharmonics occur at the same frequencies as the shaft harmonic . Since there is no reason why the unbalance of the rotor or the waviness of the inner ring should change during the coasting down through the resonance, one must however conclude that the subharmonics are genuinely an effect of VC vibrations, possibly in some way interacting with other phenomena.

A resonant effect of a different kind was discovered when running the 12 kg rotor and a self aligning roller bearing with the tube brackets in "soft" position. The vibration components concerned appear in the region of the RP frequency, and the phenomena is therefore thought to be a type of VC vibrations. The overall level of vibrations undergoes a sudden jump to a much higher level for a very small increase of shaft speed. When the speed is slowly and continuously reduced, a similar jump back to a low level of vibrations occurrs with the jump in this direction occurring at a lower speed. Fig. 8.9 shows the drop in vibration level as the rotor is allowed to coast through the jump. The overall vibration level is plotted versus speed in Fig.8.10 for increasing and decreasing speed. In Fig. 8.11 two spectrograms showing frequency distribution just before and just after the jump is shown. It appears that the system has two stable modes of operation, the one resulting in a higher vibration level than the other. It seems that a certain surplus

energy is needed to make the system jump from the low vibration level mode to the high vibration level mode, and this is the reason why the system can run in either of the two modes for a small speed range, according to Fig. 8.10, between 30.4 and 30.9 Hz shaft speed. This type of phenomena has only been observed for very flexible mounting and light rotor. The combination of light rotor and flexible mounting allows for large movements without excessive forces, and it is thought that the jump phenomena only occurs when large displacements are possible.

8.2 RIGID BEARING AND FLEXIBLE FUNDAMENT.

The difficulty in treating the problem of a complete rotor - bearing - fundament system lies in the non-linearity of the bearing. In a system consisting only of linear components it is possible to analyse the components separately and then combine the results to give the characteristics of the complete system, see Appendix I. If the stiffness of the fundament is much less than the stiffness of the bearing, it is permissible to neglect elastic deformations of the bearing, making the bearing resemble a cam-drive acting on elastic components. The relative movements between inner and outer rings due to manufacturing tolerance was calculated using a Kinematic model (assuming non-flexible bearing components) in Chapter 7. The bearing can thus be integrated in the test rig structure using the Kinematic model in combination with the measured Mechanical Impedances of the fundament and the calculated Mechanical Impedance of the rotor. Fig. 8.12 shows the approximated model for a rigid bearing, acting as a displacement generator, positioned between the rotor (which can be assumed to act as a pure mass) and the bearing house bolted to the flexible tube. Now, let d_1 and d_2 be the

displacements of rotor and tube respectively, f_1 and f_2 the forces excerted on rotor and tube by the bearing and let DS_r be the Dynamic Stiffness of the rotor and DS_t be the Dynamic Stiffness of the tube. Then letting capital letters denote Fourier Transforms of respective variables

$$\frac{F_1(\omega)}{D_1(\omega)} = DS_r(\omega) \quad \ldots\ldots\ldots \quad (8.1)$$

$$\frac{F_2(\omega)}{D_2(\omega)} = DS_t(\omega) \quad \ldots\ldots\ldots \quad (8.2)$$

Let the total displacement between inner and outer ring calculated from the KINSIM model be d,

$$d_1(t) + d_2(t) = d(t) \quad \ldots\ldots\ldots \quad (8.3)$$

and since the bearing is assumed massless

$$f_1(t) = f_2(t) \quad \ldots\ldots\ldots \quad (8.4)$$

Combining equation (8.4) with equations (8.1) and (8.2) gives

$$DS_r(\omega)\, D_1(\omega) = DS_t(\omega)\, D_2(\omega) \quad \ldots\ldots\ldots \quad (8.5)$$

According to equation (8.3),

$$d_1(t) = d(t) - d_2(t) \quad \ldots\ldots\ldots \quad (8.6)$$

which gives*

$$D_1(\omega) = D(\omega) - D_2(\omega) \quad \ldots\ldots\ldots \quad (8.7)$$

Substituting equation (8.7) in equation (8.5) gives

$$D_2(\omega) = \frac{DS_r(\omega)}{DS_t(\omega)} [D(\omega) - D_2(\omega)] \quad \ldots\ldots\ldots \quad (8.8)$$

---

* $FT[f(t)+g(t)] = F(\omega)+G(\omega)$

Rearranging equation (8.8) gives

$$D_2(\omega) = \frac{DS_r(\omega)}{DS_r(\omega) + DS_t(\omega)} D(\omega) \quad \ldots\ldots\ldots \quad (8.9)$$

To demonstrate the characteristics of the system, assume for a moment that the tube acts as a massless spring. Then, according to Chapter 10 of Ref. (13)

$$DS_r(\omega) = Z_r(\omega) \cdot j\omega = -\omega^2 M \quad \ldots\ldots\ldots \quad (8.10)$$

and

$$DS_t(\omega) = Z_t(\omega) \cdot j\omega = k \quad \ldots\ldots\ldots \quad (8.11)$$

Substituting into equation (8.9) gives

$$D_2(\omega) = \frac{-\omega^2 M}{k-\omega^2 M} D(\omega) \quad \ldots\ldots\ldots \quad (8.12)$$

Thus, for small values of ω, the rotor will closely follow the function d(t) while the tube will remain stationary. For large values of ω, the inertia of the rotor prohibits movements of this, and the tube is forced to follow the function d(t). For excitation at the natural frequency of the system ($\omega_n^2 = k/M$), large vibrations are excited.

Since the measurements on the test rig are taken using accelerometers, equation (8.9) is transformed to the appropriate dimension by replacing D_1 with A_1, D_2 with A_2, and the Dynamic Stiffnesses with their corresponding Apparent Masses. Equation (8.9) then becomes

$$A_2(\omega) = \frac{AM_r(\omega)}{AM_r(\omega) + AM_t(\omega)} A(\omega) \quad \ldots\ldots\ldots \quad (8.13)$$

The rotor is still assumed to act as a pure mass, thus

$$AM_r(\omega) = M \qquad \ldots\ldots\ldots \qquad (8.14)$$

Now consider the system of Fig. 8.13. When excited at point O, the impedance of this system is the total driving point impedance of the test rig. The total impedance for parallel sub systems is the sum of the sub system, see Appendix I,

$$AM_{tot}(\omega) = AM_r(\omega) + AM_t(\omega) \qquad \ldots\ldots\ldots \qquad (8.15)$$

Hence, the denumerator of equation (8.13) can be measured directly from the rig, point O in Fig. 8.12, and inserted into the equation.

Methods of measuring this impedance are described in Section 8.3, and plots of the Apparent Mass for three configurations are given in Fig. 8.1. It is now possible to calculate quantitative values for vibrations of the bearing housing due to form deviations of the bearing components. The value for total displacement is given by coefficients of Fig. 7.11 and 7.15.

$$D(\omega) = c_i \cdot C_1 \qquad \ldots\ldots\ldots \qquad (8.16)$$

This displacement gives rise to the acceleration

$$A(\omega) = -D(\omega)\omega^2 \qquad \ldots\ldots\ldots \qquad (8.17)$$

So, substituting equations (8.17),(8.16),(8.15) and (8.14) into equation (8.13) gives

$$A_2(\omega) = \frac{M}{AM_{tot}} \cdot c_i \cdot C_1 \cdot \omega^2 \qquad \ldots\ldots\ldots \qquad (8.18)$$

where AM_{tot} is taken from Fig.8.1.

In the table below, the calculation of $A_2(\omega)$ has been carried out for bearing A in Fig. 7.9-7.11, run at 12 Hz shaft speed in configuration C of Fig. 8.1.

i =	2	3	4	5	6	7	
c_i =	0.26	0.9	0.25	0.15	0.45	0.6	(microns)
C_1 =	1	0.93	0.72	0.59	0.45	0.31	
f' =	24	36	48	60	72	84	(Hz)
AM_{tot} =	2.8	12.2	8.7	6.1	4.6	2.2	(kg)
A_2 =	3.9	4.3	2.3	2.5	11	28	$(g \cdot 10^{-3})$

The calculated values are compared to the experimental values, see Fig. 8.15A.

i =	2	3	4	5	6	7	
A_2 =	5.2	6.0	2.1	1.2	6.0	6.8	$(g \cdot 10^{-3})$

In a similar way, the sixth and seventh secondary peaks can be calculated (secondary peaks of lower order are suppressed by the low values of C_2).

i =	6	7	
c_i =	0.45	0.6	(microns)
C_2 =	0.45	0.63	
$f'' = f' - f_{rp}$ =	11.5	23.5	(Hz)
AM_{tot} =	1.6	2.8	(kg)
A_2 =	0.8	3.6	$(g \cdot 10^{-3})$

The secondary peaks in Fig. 8.15A coincide with other peaks and are not possible to distinguish. In Fig. 7.3 however, the secondary peaks appear clearly and seem to be of the order of magnitude predicted (compare with shaft harmonics). Calculation of vibration amplitudes due

to varying roller diameters can be done in a similar fashion, using the c_i values of Fig. 7.5. For this case $C_1 = 1$, and $f = 0.42\ f_s$. It was pointed out in Chapter 7 that the KINSIM model works best for small loads, otherwise the assumption of zero elastic deflection does not hold true. The A_2 values for the rotor run with 75kg and 225kg rotor on "medium" stiff mounting were also calculated and measured and are together with the previous results plotted in Fig.8.16. From this diagram it is apparent that the approximate model works with satisfactory accuracy for small load, but that the accuracy deteriorates for higher loads and stiffer mounting,and in particular tends to overestimate the higher frequency components, which is all consistent with the nature of the approximation.

An example of the different nature of linear and non-linear resonant excitation is shown in Fig. 8. 8. It is apparent from the fig. that a resonance exists around 145 Hz. The eigth shaft harmonic at 18 Hz shaft speed and the sixth shaft harmonic at 24 Hz shaft speed excites this resonance. The mechanisms of vibration generation are for these two components essentially linear (KINEMATIC model), and the effect of excitation is a considerable increase of the amplitude of the component at resonant frequency, while the rest of the plot remains unchanged. At 30 Hz shaft speed, the RP frequency coincides with the natural frequency. The amplitude of the RP component does not increase significantly compared to the previous shaft speed, instead a cluster of smaller peaks occur around the RP component.

8.3 MEASUREMENT OF MECHANICAL INPEDANCE

The theoretical background to the use and measurement of Mechanical Impedance is discussed in Appendix I. Measurement of Mechanical Impedance (or its derivatives such as Dynamic Stiffness, Apparent Mass, Mobility, Compliance) involves exciting the investigated system with a known input force and measuring the resulting vibrational movement. If the system is linear, its dynamic properties are then fully defined by the ratio of the Fourier Transform of the forcing function and the Fourier Transform of the displacement-, velocity- or acceleration-function. The most commonly used type of forcing function is a sine wave, because the ratio between input RMS force and output RMS vibration directly yields the modulus of the impedance without further processing. Where disturbances from the operation of the system occur, white noise force is sometimes employed. When using sinewave excitation, the force is normally supplied by an electro mechanical vibrator (although centrifugal and hydraulic vibrators are also used), fed by a power amplifier and sine wave generator. Both input and output signals have to be narrow band filtered, which is easiest done with a heterodyne filter tuned by the forcing signal. All in all, a considerable amount of sophisticated instrumentation is required and the setting up of particularly the bulky and heavy vibrator can be time consuming. A very quick and simple method of determining Mechanical Impedance is by use of transient excitation. The use of transient excitation for measurement of impedance in difficult environmental conditions was described in Ref.(49). In this paper, samples from force and acceleration functions were taken manually using a storage oscilloscope, and these samples were then used to calculate the Fourier Transforms.

This operation can be greatly simplified by using two parallel digital recorders connected to a paper tape punch. The recorders, which are triggered simultaneously, offers pretrigger facilities which are essential for capturing transients. Subsequent to each trigger, 1024 samples are taken from the signal (maximum sampling frequency is 200KHz) and stored in a core memory. The content of the core memory can then be punched on paper tape and thereby be made available to a digital computer for further processing. The set up for Mechanical Impedance testing by transient excitation is shown in Fig. 8.14. The program carrying out the Fourier Transformation is identical to that used in the DAS system for processing of stationary signals, the only difference being that the Hanning window is not used when analysing transients. After dividing the forcing function transform with the acceleration function transform point by point, the ratio is multiplied with a cal. factor and plotted on the digital plotter.

Fig. 8.17A shows the transient forcing and acceleration functions using the analog output of the digital recorders. The Fourier Transforms of the two functions are shown in Fig. 8.17B and the resulting impedance plot in Fig. 8.1.A. As is seen in Fig. 8.17B the signal to noise ratio can sometimes be a problem for the transform of the forcing function. This is so because the forcing function is of extremely short duration, so that on average, over the whole record, there is very little signal on which to base the calculations of the transform. It is possible to adjust the shape of the transform of the forcing function by using different methods of striking the load cell. Steel hammers with and without interfaces, wood blocks, copper hammers and rubber tubes have

been tried. By checking the shape and size of the force transform it is then possible to make sure that a sufficient force level exists for the frequency range investigated. For the low frequencies analysed here, it was found that the rubber tube gave the best results.

A number of impedance plots were obtained, three of which are shown in Fig. 8.1. All plots were very consistent as regards the position of resonances and anti-resonances for all excitation techniques used. They did however vary substantially between themselves as regards the signal to noise ratio and the absolute values of apparent mass. It is felt that the accuracy of Mechanical Impedance measurement by transient excitation is somewhat inferior to that achieved with sine-sweep excitation.

To obtain accurate measurements with transient excitation, the choice of correct means of excitation for a particular structure and frequency range is critical. The number of samples used, also have an influence on the accuracy of the result. It is felt that a more detailed investigation of these aspects is necessary in order to make accurate impedance measurements by transient excitation a matter of routine.

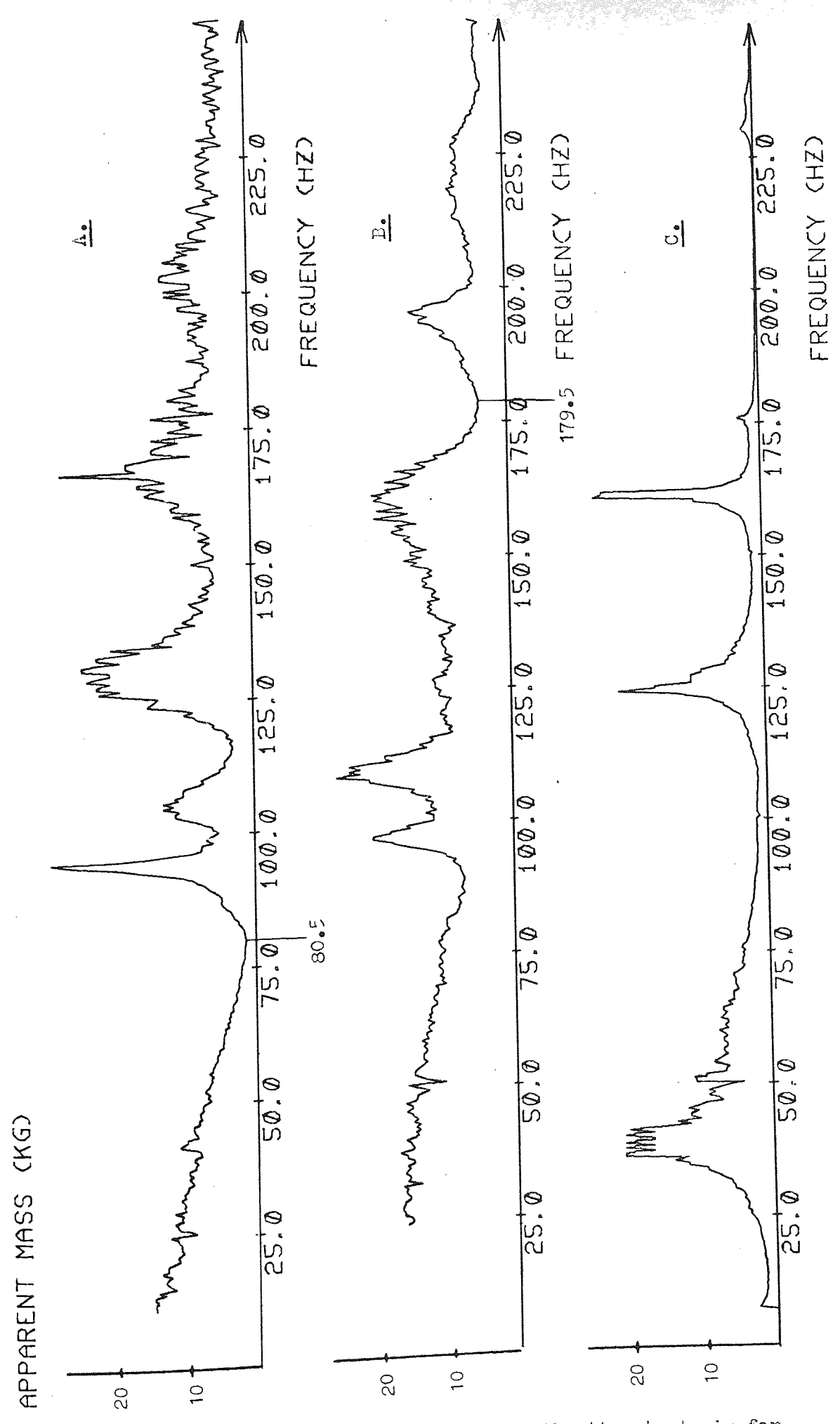

Fig. 8.1. Mechanical Impedance plots for the vibration test rig for A: 225 kg rotor and "hard" mounting, B: 75 kg rotor and "hard" mounting

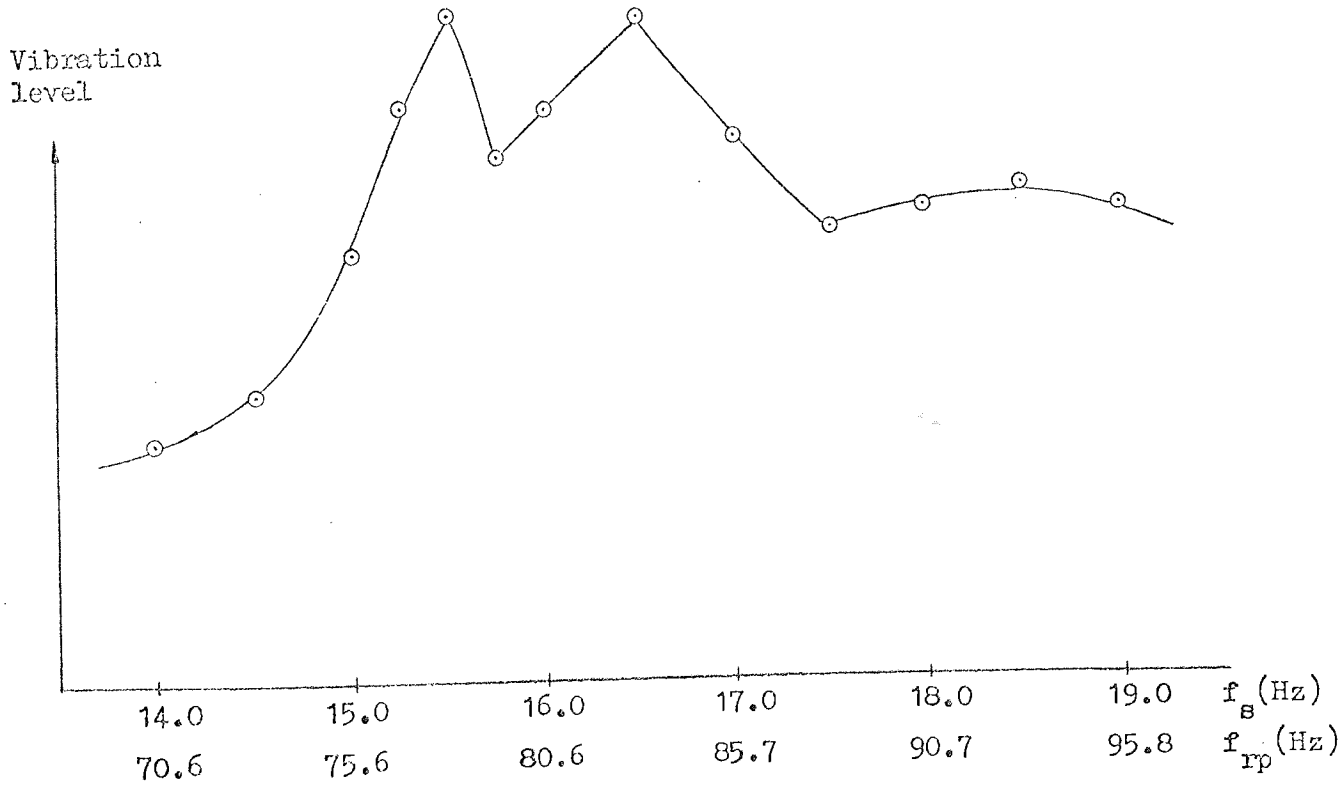

Fig. 8.2 225 kg rotor coasting down through the 80.5 Hz resonance of fig. 8.1 A.

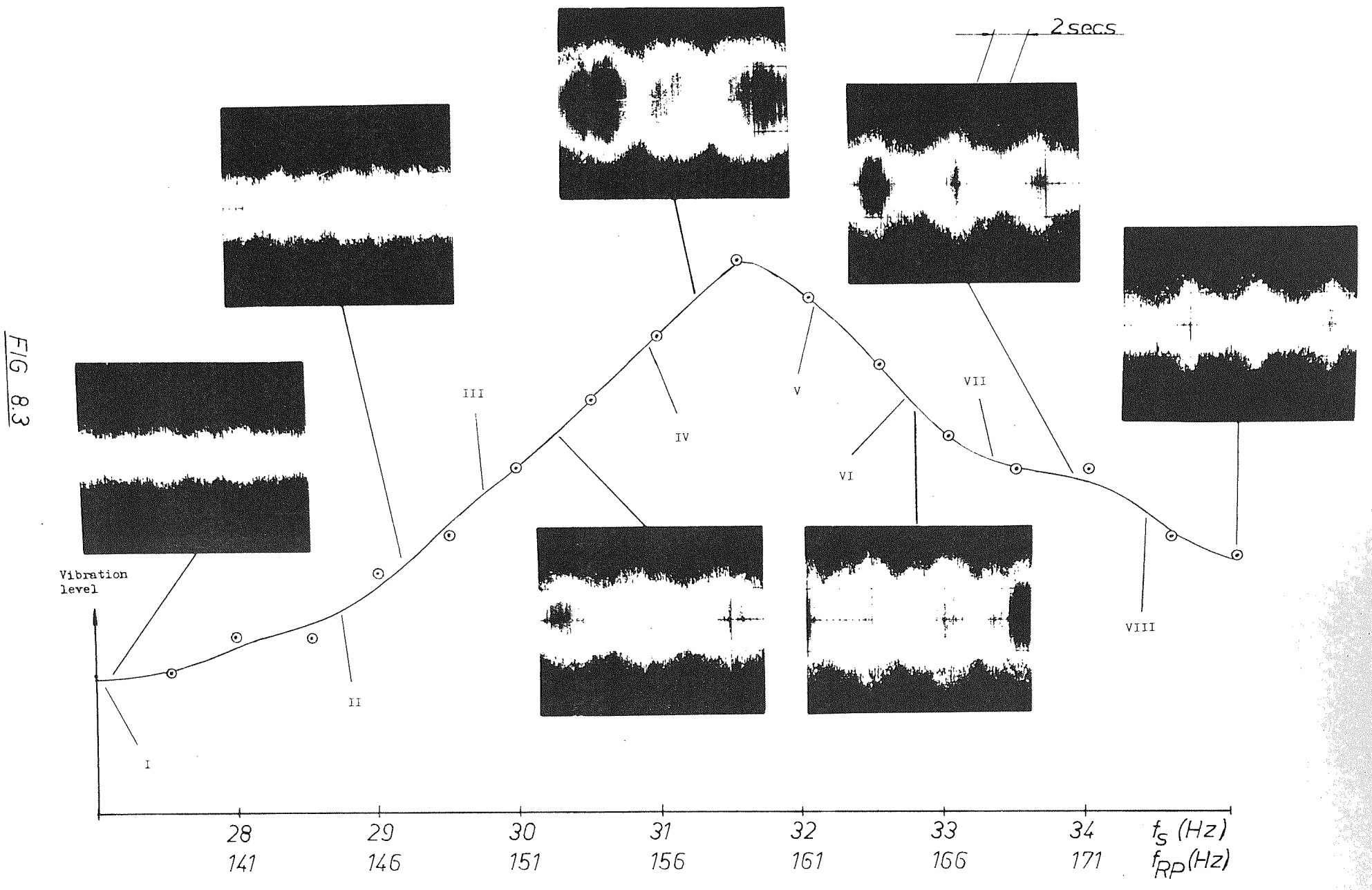
2 secs
Vibration level
I
II
III
IV
V
VI
VII
VIII
28
141
29
146
30
151
31
156
32
161
33
166
34
171
f_S (Hz)
f_{RP} (Hz)

FIG 8.3

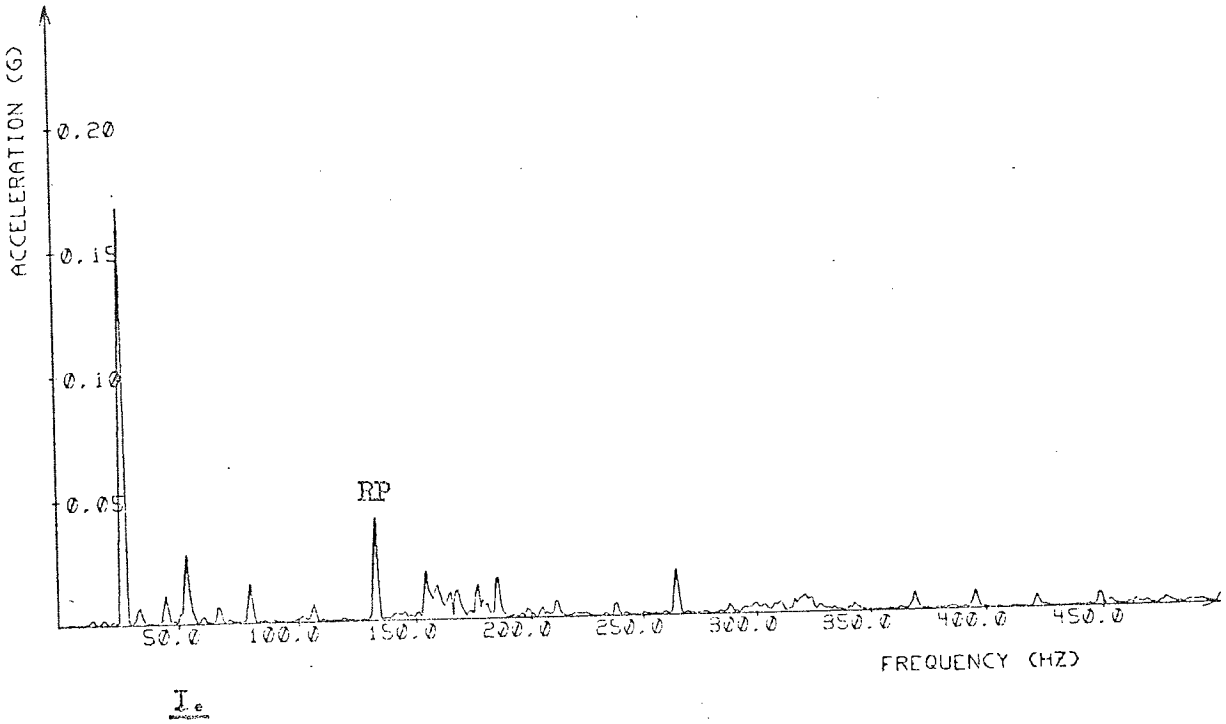
ACCELERATION (G)
0.20
0.15
0.10
0.05
RP
50.0
100.0
150.0
200.0
250.0
300.0
350.0
400.0
450.0
FREQUENCY (HZ)

I.e

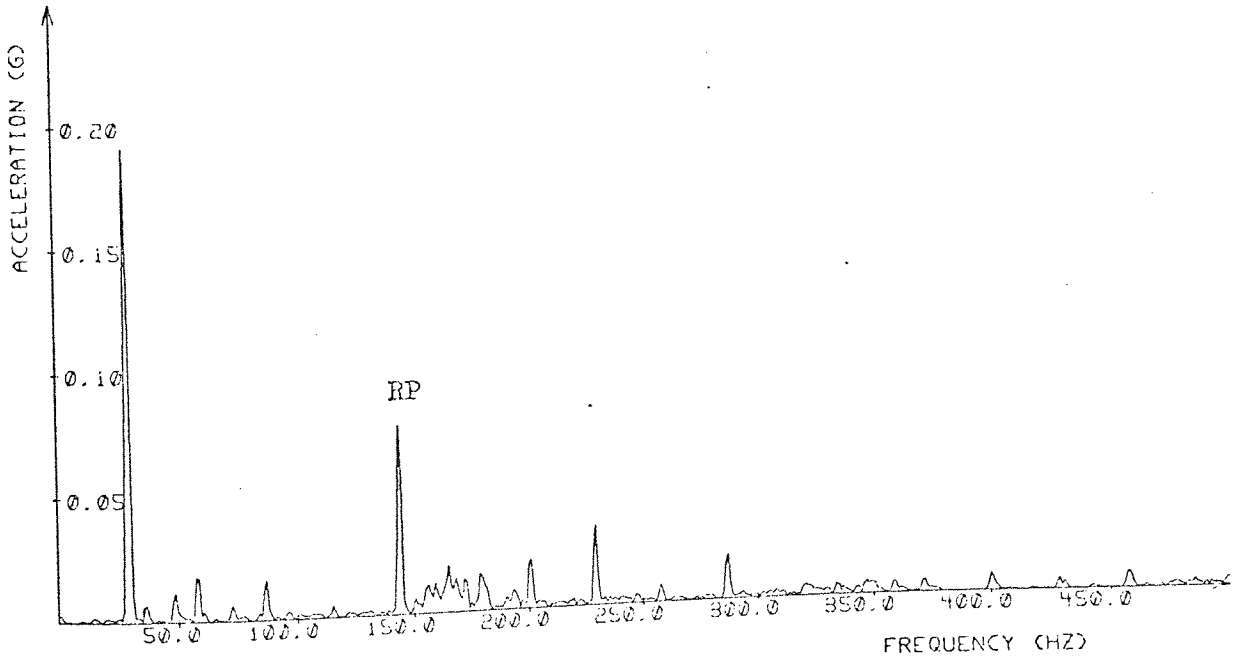
ACCELERATION (G)
0.20
0.15
0.10
0.05
RP
50.0
100.0
150.0
200.0
250.0
300.0
350.0
400.0
450.0
FREQUENCY (HZ)

II.

Fig. 8.4.

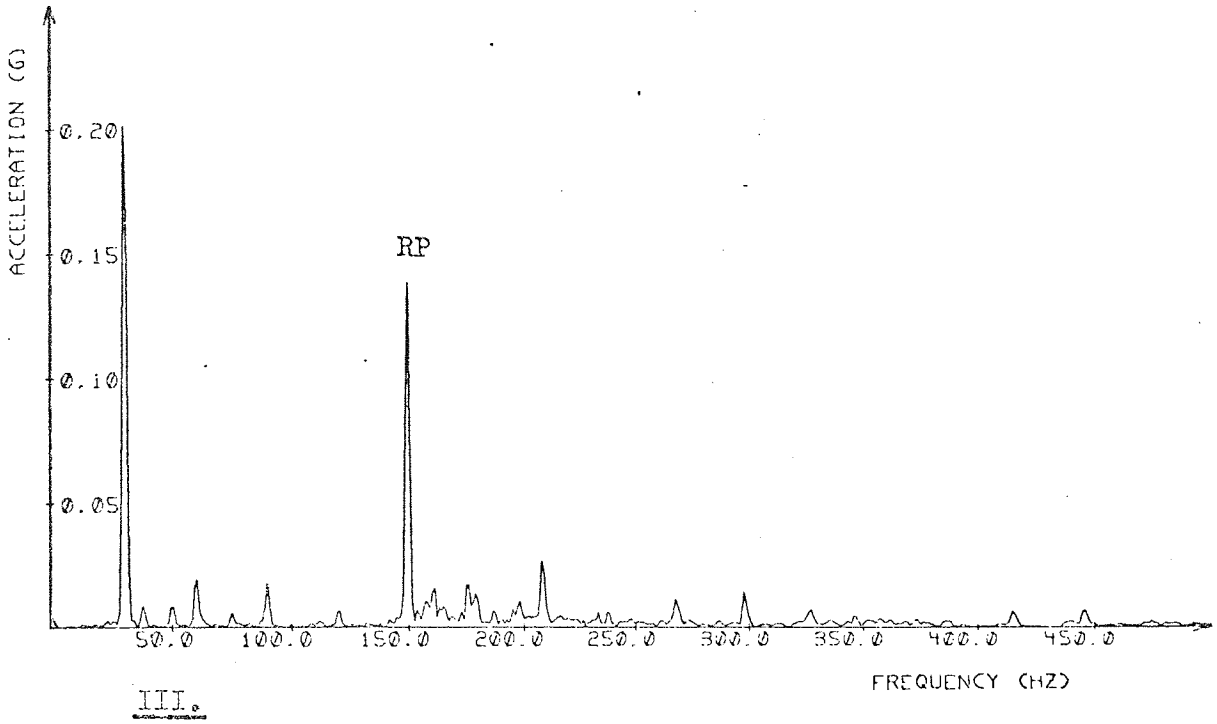
ACCELERATION (G)
0.20
0.15
0.10
0.05
RP
50.0
100.0
150.0
200.0
250.0
300.0
350.0
400.0
450.0
FREQUENCY (HZ)

III.

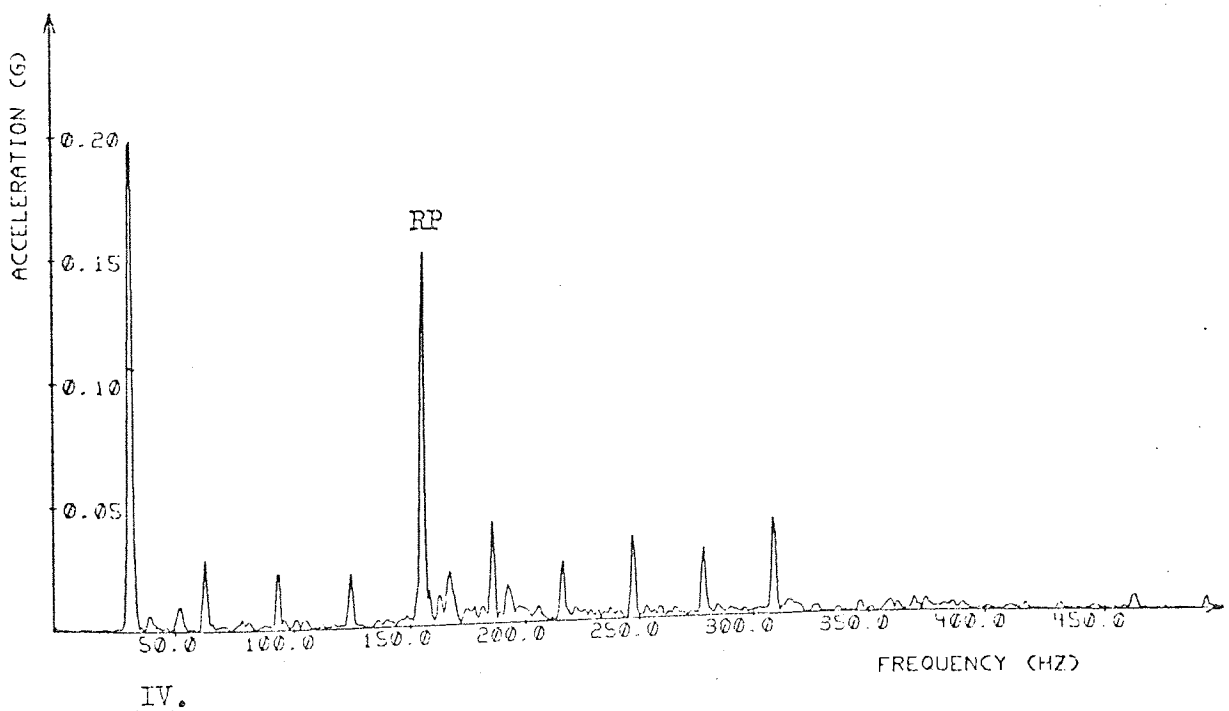
ACCELERATION (G)
0.20
0.15
0.10
0.05
RP
50.0
100.0
150.0
200.0
250.0
300.0
350.0
400.0
450.0
FREQUENCY (HZ)

IV.

Fig. 8.5.

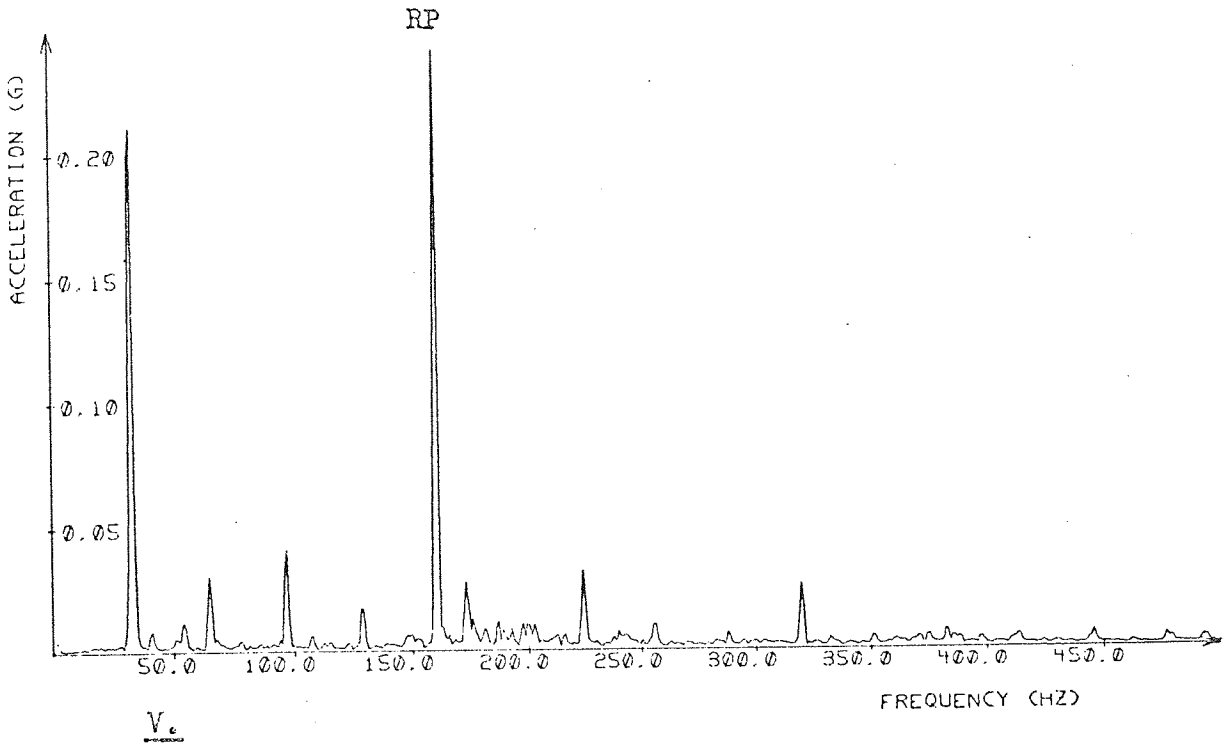
RP
ACCELERATION (G)
0.20
0.15
0.10
0.05
50.0
100.0
150.0
200.0
250.0
300.0
350.0
400.0
450.0
FREQUENCY (HZ)

V.

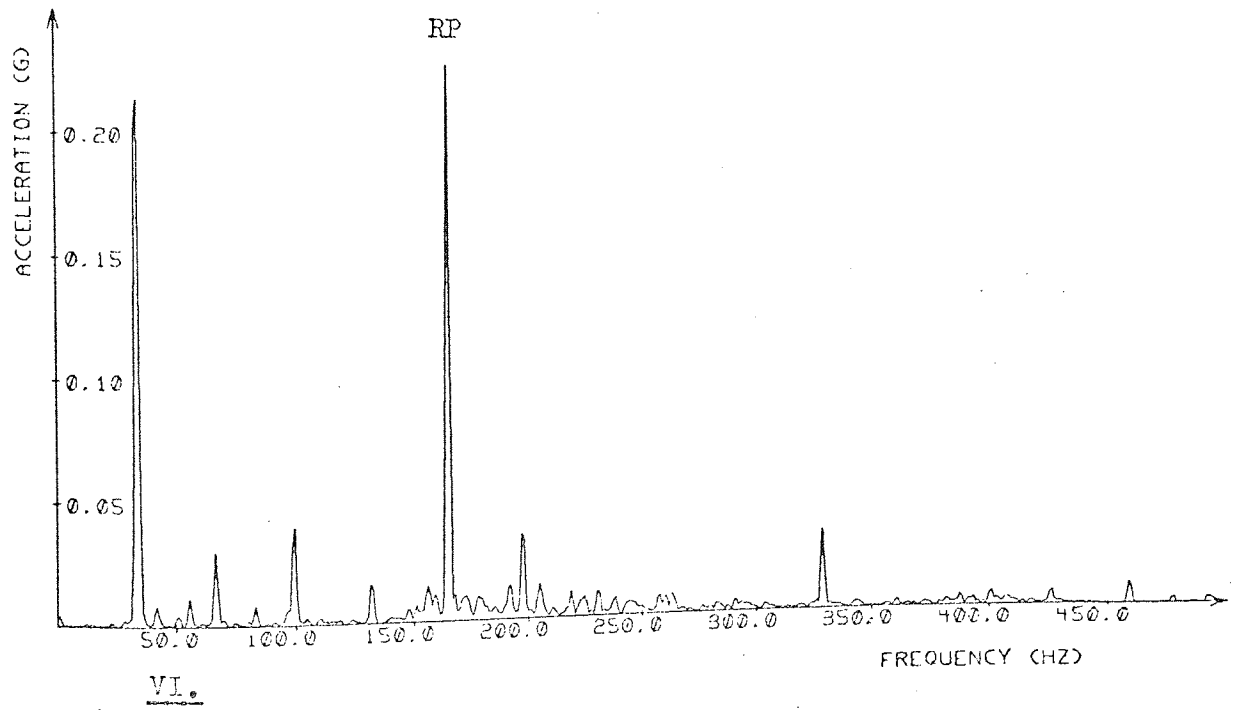
RP
ACCELERATION (G)
0.20
0.15
0.10
0.05
50.0
100.0
150.0
200.0
250.0
300.0
350.0
400.0
450.0
FREQUENCY (HZ)

VI.

Fig. 8.6.

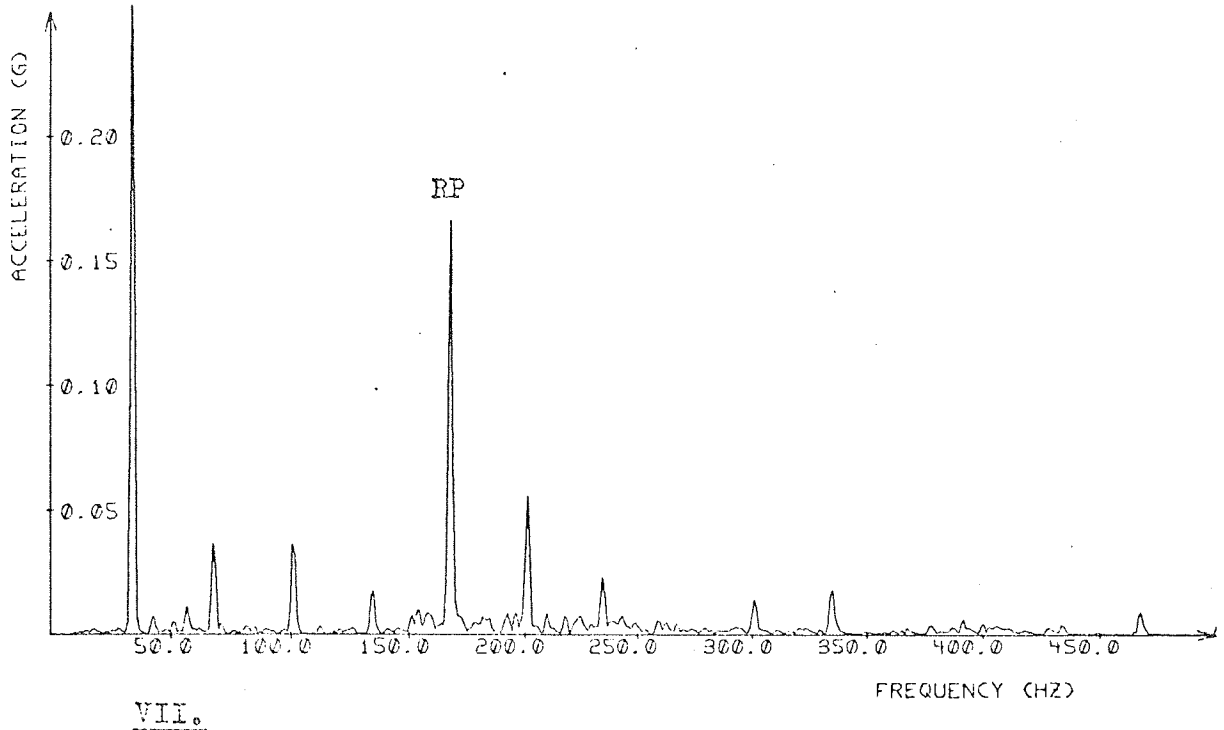

VII.

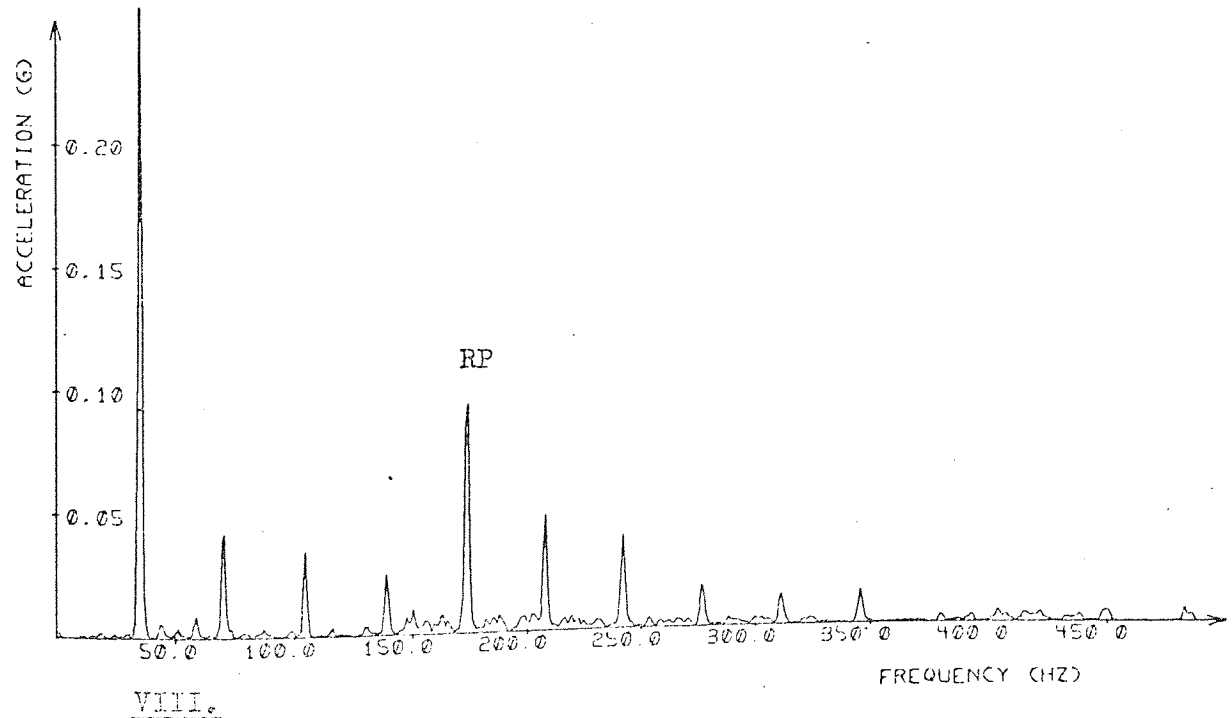

VIII.

Fig. 8.7.

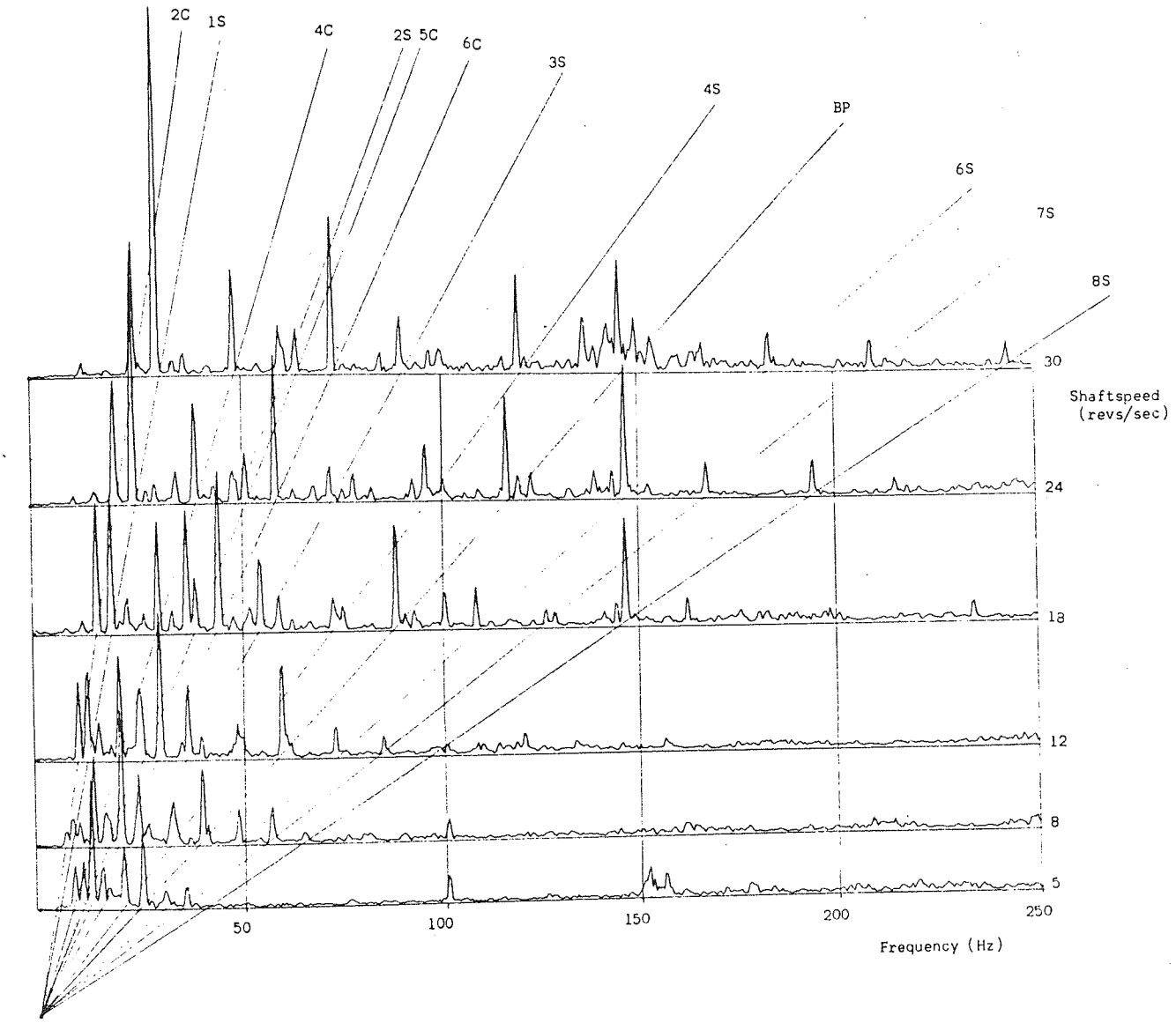

Fig. 8.8. Cambell type diagram of spherical roller bearing with 85 kg rotor mass.

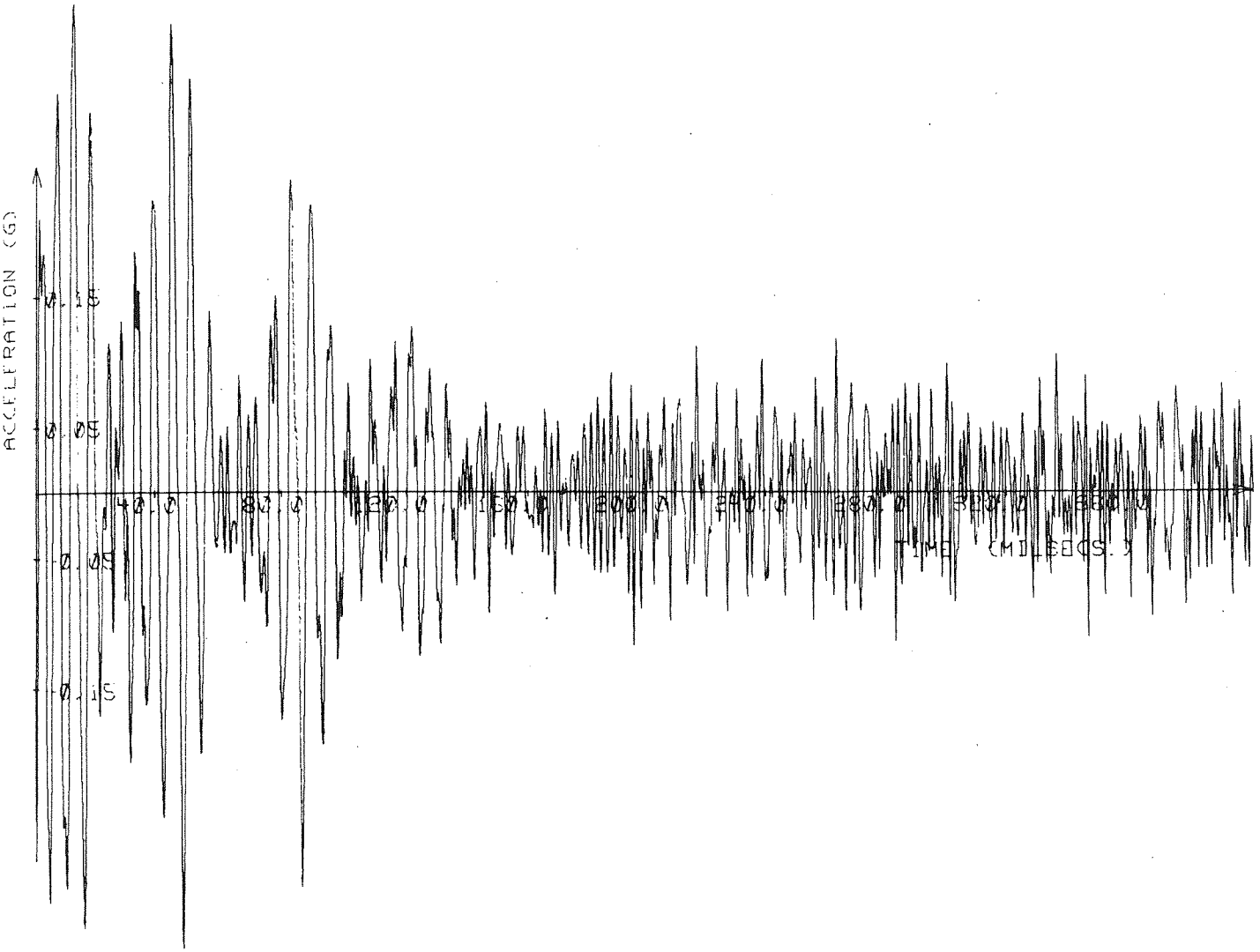

FIG. 8.9. SUDDEN REDUCTION OF VIBRATION LEVEL

AT 30.5 HZ SHAFT SPEED. TOTAL SWEEP TIME = 0.4 SECS.

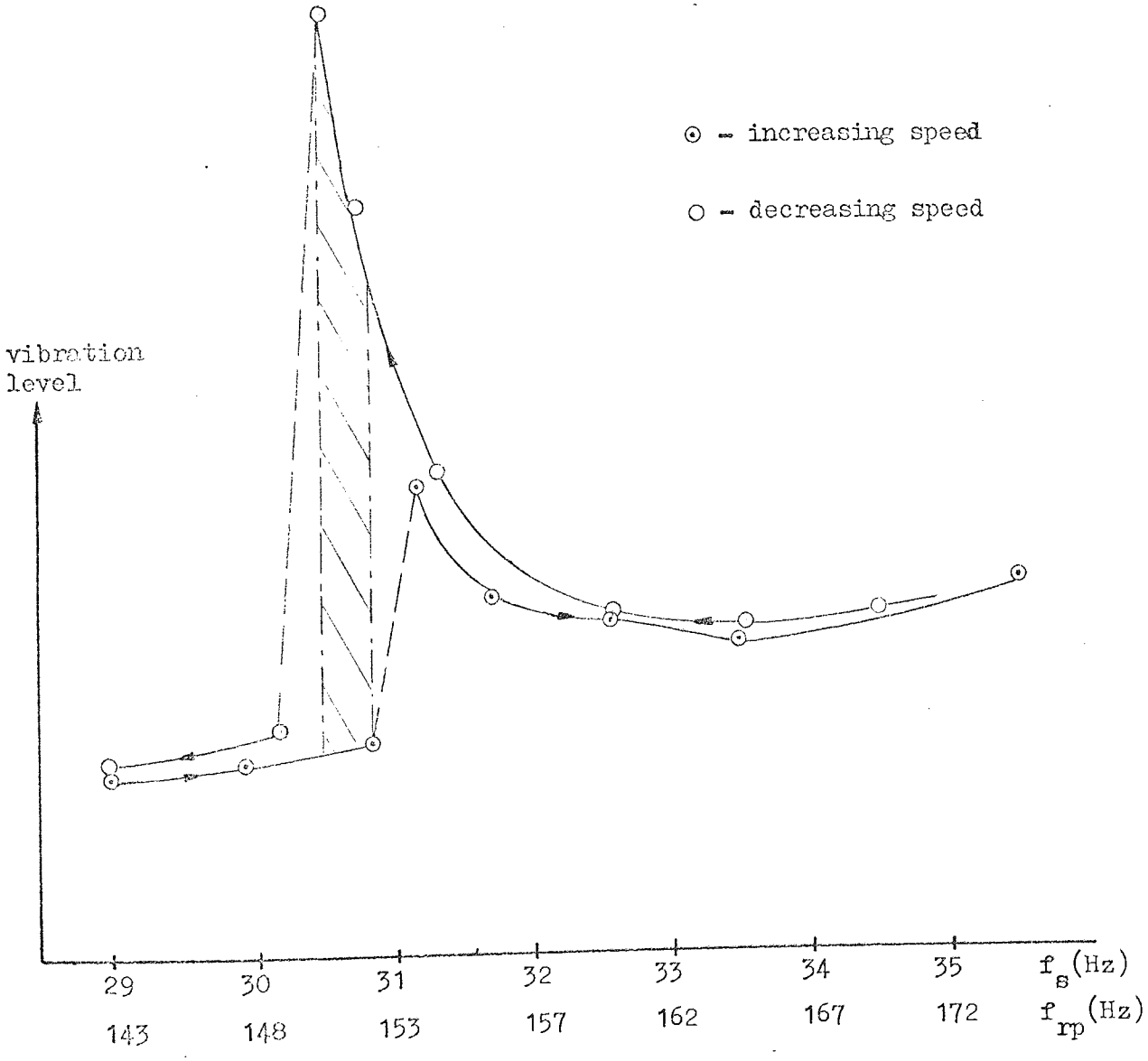

Fig. 8.10. Broadband RMS levels for increasing and decreasing speeds of spherical roller bearing with "soft" mounting and 12 kg rotor.

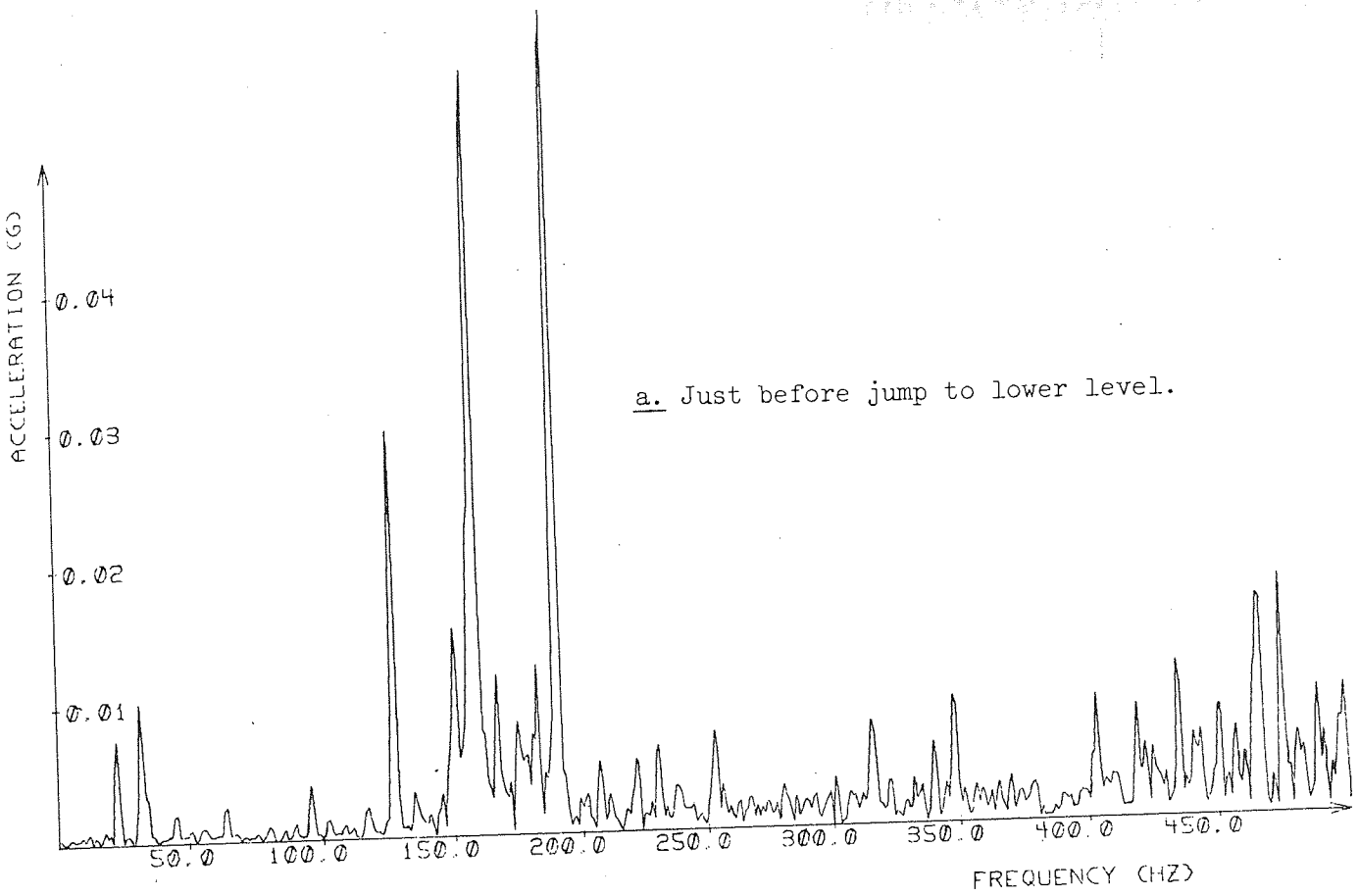

a. Just before jump to lower level.

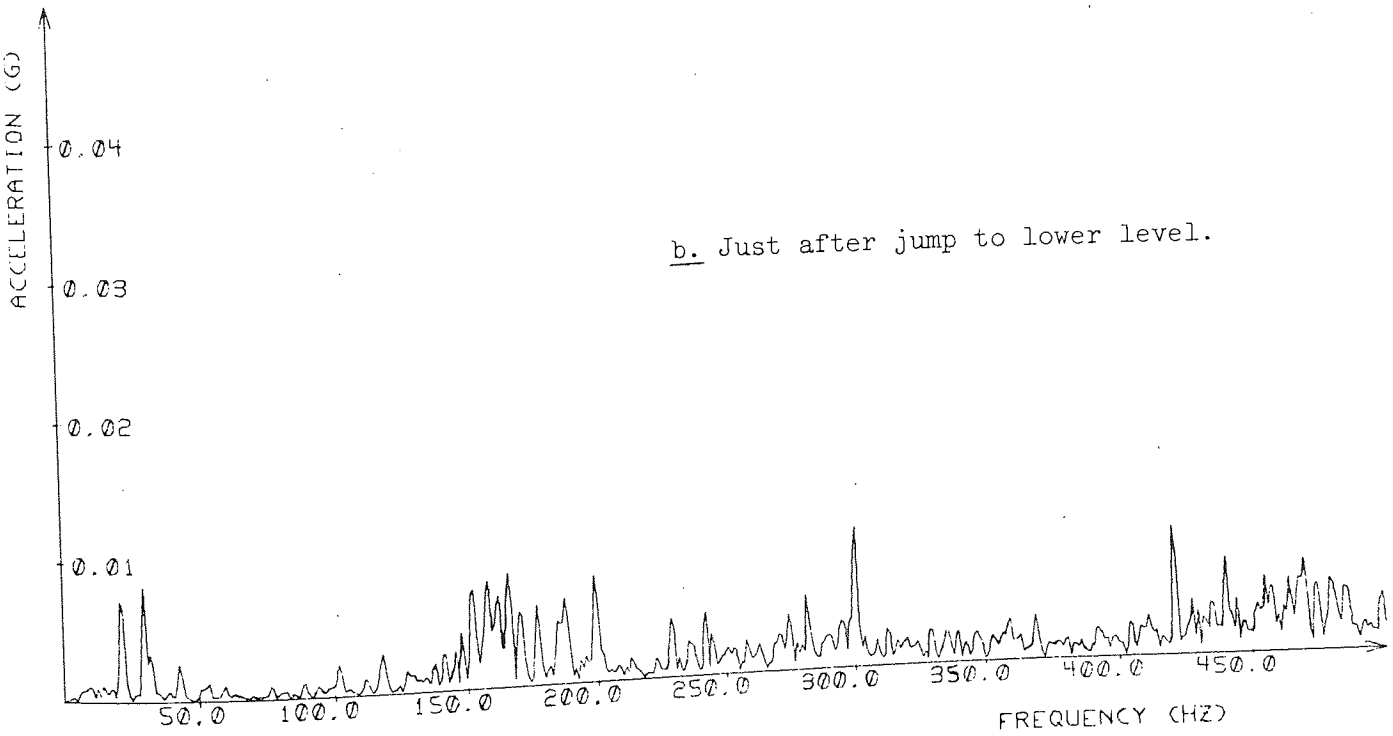

b. Just after jump to lower level.

Fig. 8.11. Spectrograms before and after the jump illustrated in Fig 8.10. Shaft speed approximatly 30.5 Hz.

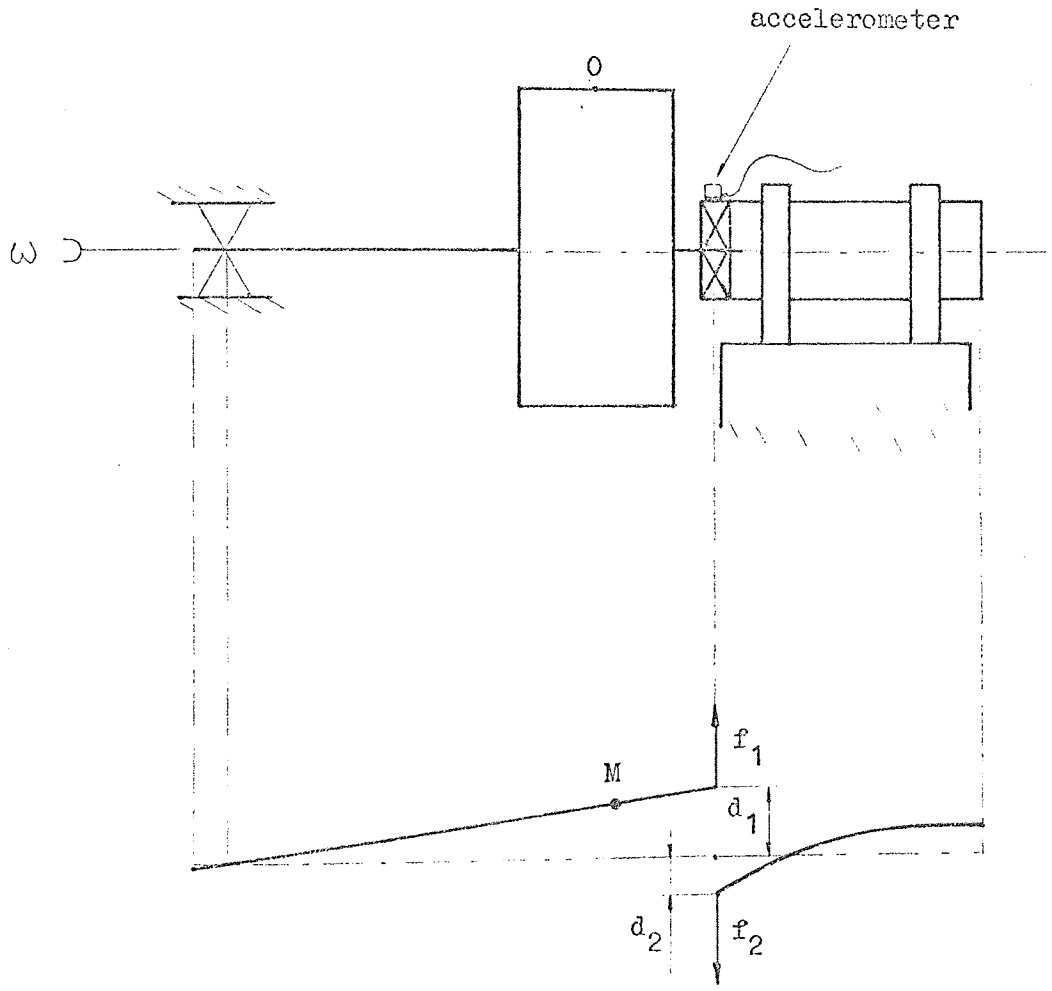

Fig. 8.12

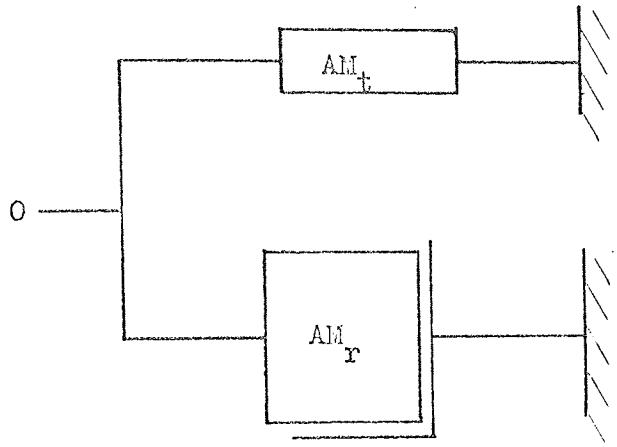

Fig. 8.13. Block diagram of sub impedances of test rig set up.

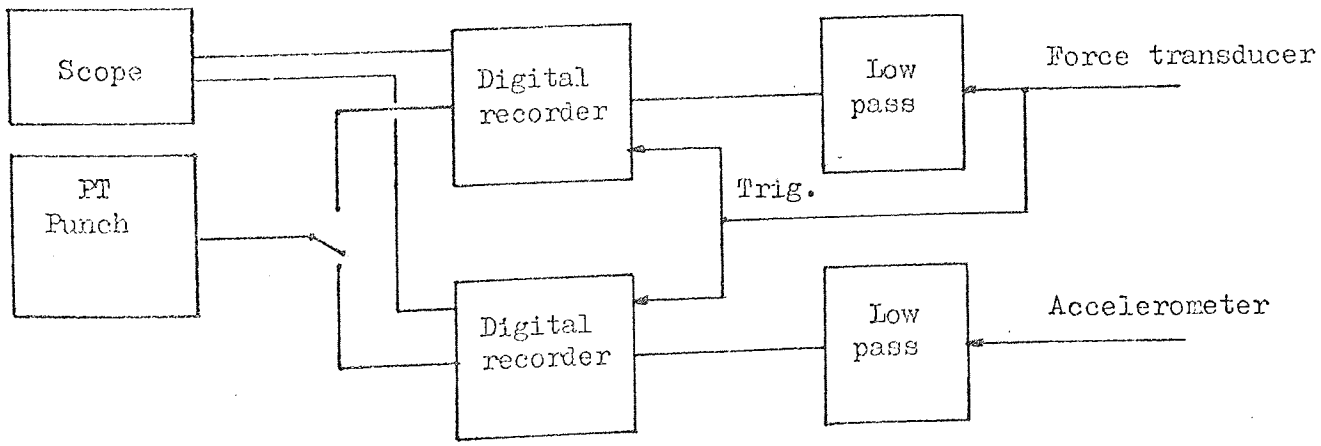

Fig. 8.14 Instrumentation set up for Mechanical Impedance testing by transient excitation.

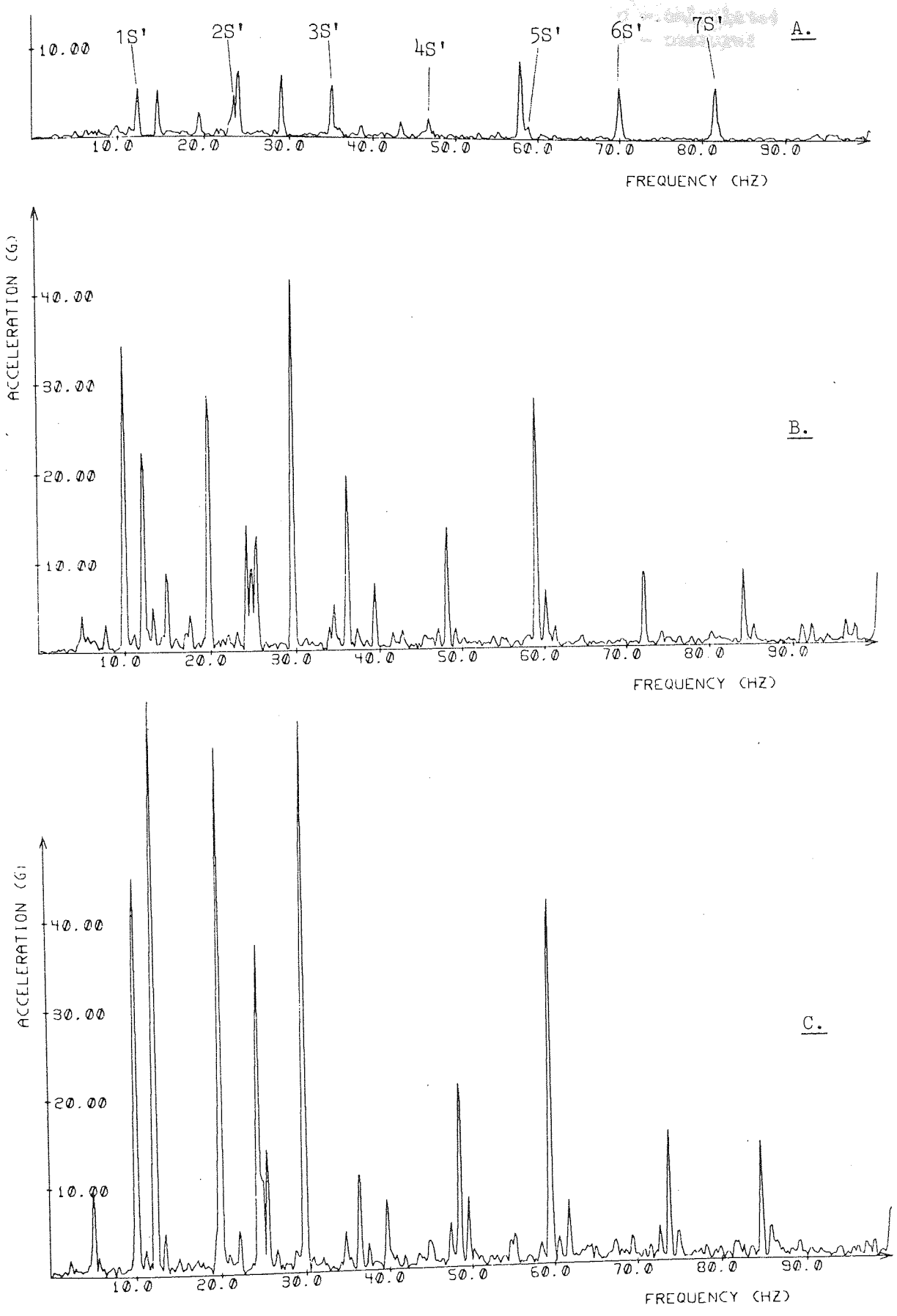

Fig. 8.15. Bearing A run at 12 Hz shaft speed with 12, 85 and 205 kg rotor in spectrograms A, B and C respectively.

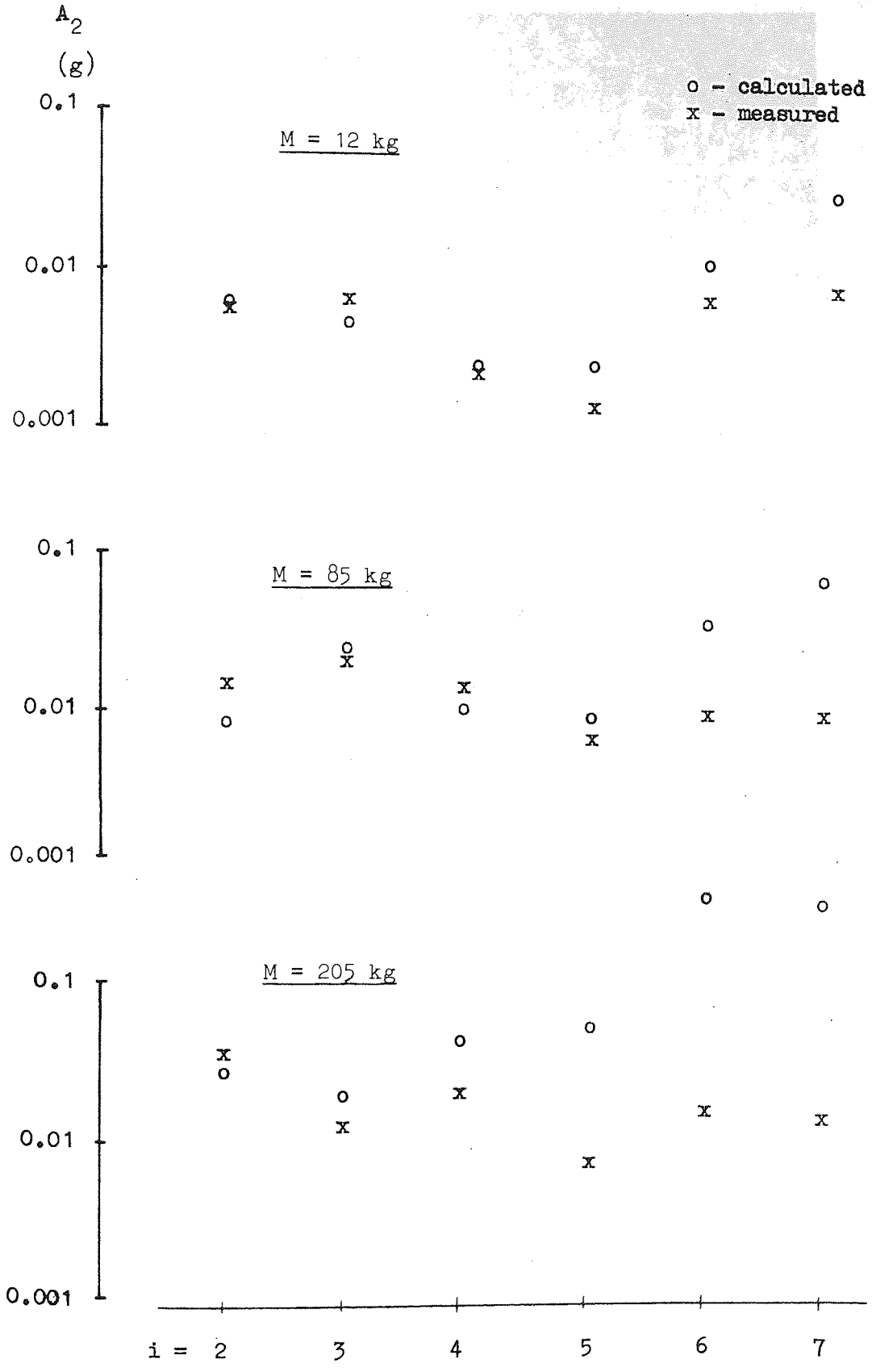

Fig. 8.16. Comparison of theoretical and experimental values for the amplitudes of vibration components due to inner ring lobes.

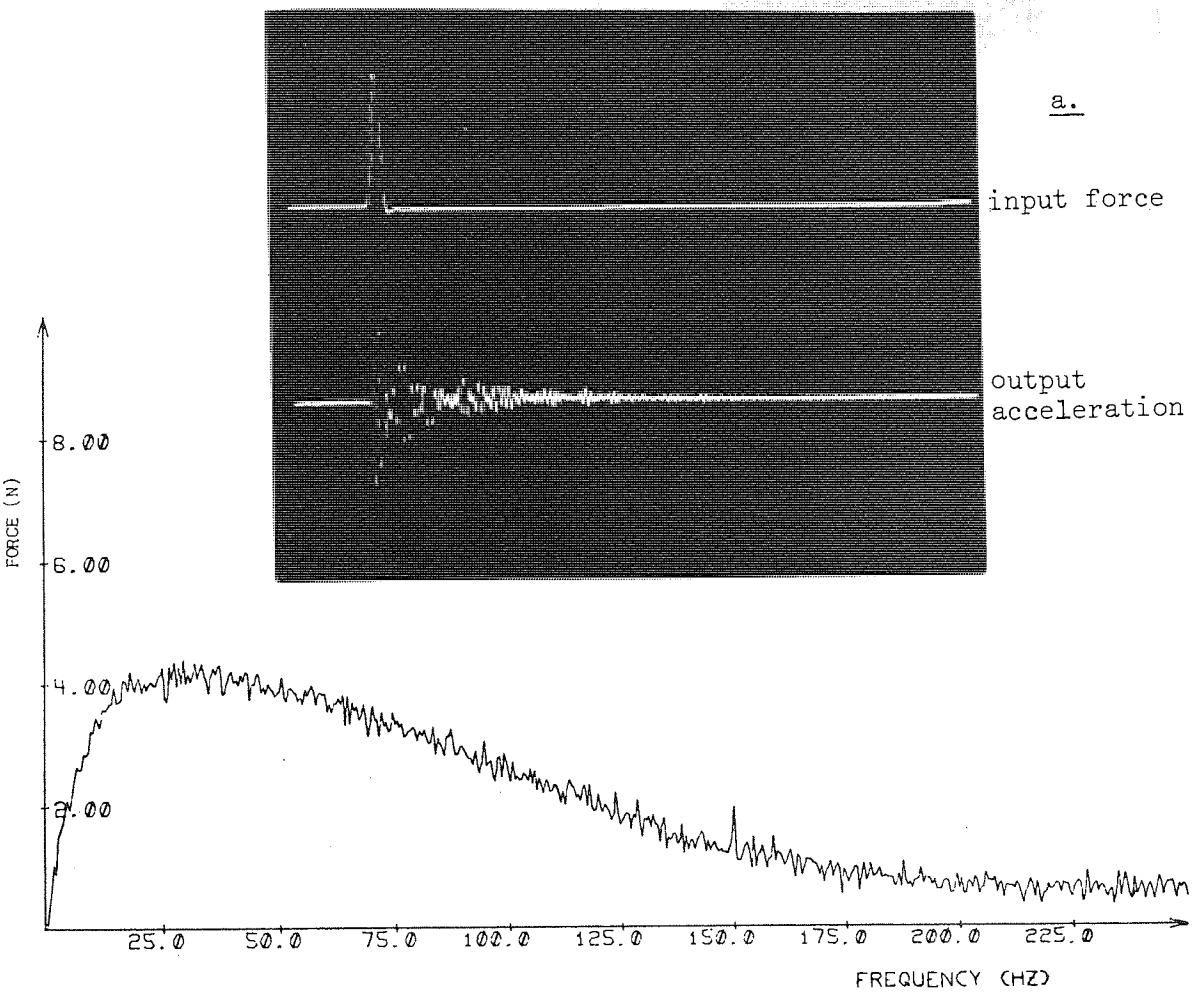

b. Fourier Transforms of input and output signals.

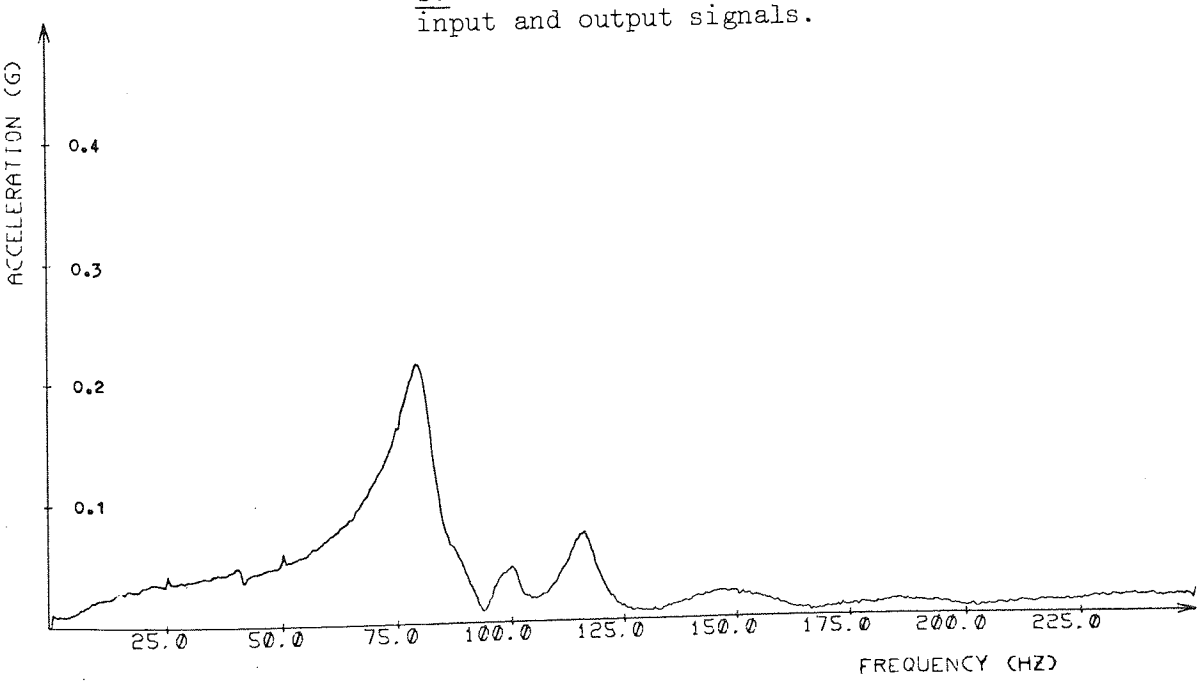

Fig. 8.17. Time and frequency domain representation of the input and output functions used to calculate the mechanical impedance of configuration A of fig. 8.1.

CHAPTER 9

ROLLING BEARING VIBRATIONS DUE TO WEAR

The components of rolling bearings undergo progressive surface and subsurface deterioration during operation. After a sufficient length of operating time, the accumulated damage renders the bearing incapable of performing its intended function. Bearing failure could, depending upon application, mean anything from actual breakdown with seizure to excessive noise and loss of accuracy due to slight abrasive wear. Increasing wear and fatigue will always be accompanied by some degree of change of the vibration characteristics of the bearing. There are significant differences in the progression of wear and fatigue, with the former developing in a continuous fashion and the latter causing a series of suddenly occurring depressions in the component surface (spalling). In previous chapters vibration phenomena in new bearings have been studied. Against this background knowledge, characteristic changes of bearing vibrations accompanying the development of two common modes of surface deterioration will be studied in this chapter, the practical objective being to facilitate condition monitoring and prediction of impending bearing failure by vibration analysis.

9.1 Failure modes of Rolling Bearings

A review of various types of rolling contact failure and their respective origins is given by Tallian in ref.(51), where rolling bearing failure modes are classified according to the table below.

TABLE 9.1

Mode:	Manifestation:
1 Wear type failure	1.1 Surface removal
	1.1.1 Removal of loose particles (wear)
	1.1.2 Chemical or electrical surface removal
	1.2 Cumulative material transfer between surfaces (smearing)
2 Plastic flow	2.1 Loss of contact geometry due to cold flow
	2.2 Destruction by material softening due to unstable overheating
3 Contact fatigue	3.1 Spalling fatigue
	3.2 Surface distress
4 Bulk failures	4.1 Overload cracking
	4.2 Overheat cracking
	4.3 Bulk fatigue
	4.4 Fretting of fit surfaces
	4.5 Permanent dimensional changes

Rolling bearings having a satisfactory lubrication, correct temperature, a suitable load and contacts with pure rolling motion, will after a sufficient length of operating time normally fail due to spalling fatigue (3.1). This is the classical mode of rolling contact failure and has been theoretically analysed in depth by Lundberg and Palmgren in ref. (5) where it is shown that the bearing life, L, is given by

$$L = (P/Q)^3 \cdot 10^6 \quad \ldots\ldots\ldots \quad (9.1)$$

where L is the number of revolutions after which there is a 90%

probability that no damage has occurred, P is the external load (or equivalent load) and Q is a factor characteristic for each bearing type and size called "Basic Dynamic Capacity". For a batch of bearings, L is dispersed over a wide range. It is assumed that the dispersion of life follows the dispersion of weak points of the material of the loaded components. The factor L therefore follows the Weibull distribution making

$$\log(\log(1/S)) = e \cdot \log L + \text{const} \qquad \ldots\ldots\ldots \quad (9.2)$$

where S is the probability that no damage has occurred after L million revolutions. The constant e is determined experimentally and is given to 1.1 for ball bearings and 1.5 for roller bearings. As indicated by equation (3.38), the maximum shear stress arises some distance below the surface. Consequently spalling fatigue is initiated subsurface, normally starting at a stress concentration around a microscopic slag inclusion. The crack propagates from the inclusion up to the surface so that a small splinter of metal becomes loose and is removed from the bearing. The effect of crack propagation time on failure distribution has been studied by Tallian in ref.(52), the main conclusion of which is that very heavily loaded bearings have a longer operational life than is predicted by equation (9.1). The damage is characterised by shallow, crater-like depressions with sharp edges and fracture type surfaces.

Spalling fatigue causes damage at certain discrete points of the component surfaces leaving the remaining surface intact. Other classes of failure modes like 1.1.1, 1.2, 3.2 cause damages, which are evenly

distributed over all loaded component surfaces. For these cases it is not easy to determine what failure mode is involved by inspection of the damage. Instead the conditions under which the bearing has been run usually indicate the cause of failure. Hence, traction forces preclude the occurrence of surface fatigue (3.2), which is therefore observed only in bearings having a pure rolling motion. Smearing (1.2) arises mainly in high speed bearings where the rolling bodies are violently accelerated as they enter the load carrying zone. Abrasive wear (1.1.1) finally occur in bearings having a mixed sliding-rolling motion of the contact points, i.e. bearings with close conformity between rolling elements and tracks.

In this study attention has been concentrated on two predominant failure modes, namely abrasive wear (1.1.1) and subsurface fatigue leading to spalling (3.1). From the point of view of monitoring, type 1.1.1 also covers classes 1.1.2, 1.2, 2.2 and 3.2, which exhibit similar surface changes. Other failure modes have been considered either rare or not requiring any sophisticated methods of detection.

9.2 Spalling fatigue monitoring

To obtain examples of spalling fatigue, spherical ball bearings were run under heavy load in the wear rig (see Chapter 4). Due to their low value of osculation these bearings have a pure rolling motion, which makes failure due to spalling fatigue probable. After 35 hours of operation with 600 kg load, 1750 RPM and a temperature around 80°C, damage of the outer ring at the point of maximum load occurred in the form of a crater-like depression typical for spalling fatigue. Using the

genuinely fatigued bearing as an example, spalling fatigue was simulated in new bearings by use of a spark erosion pen, which creates a similar type of depression with sharp edges. Comparisons between vibrations generated by the genuinely fatigued bearing and the bearings with simulated fatigue damage show similar vibration characteristics.

The fatigue crack is initiated subsurface and as long as the crack has not reached the surface of the component, the operation of the bearing is unaffected and the development of the damage cannot be monitored through vibration analysis. When the crack reaches the surface, a small metal chip is suddenly removed from the component and transient vibrations are excited each time a rolling element passes over the damage. Fig. 9.2 shows the distribution of transients in time for bearings with damage of outer ring, inner ring and rolling element. Compare 9.2a with 9.4b and 9.2c with 9.1, 1 - 3 KHz. The transformation from time domain to frequency domain of a comb of delta functions is another comb of delta functions as illustrated in fig. 9.3. Also the cases with modulated delta combs in fig. 9.2b and c will give delta combs in the frequency domain.

An experiment concerning spalling fatigue detection was carried out using a cylindrical roller bearing in which a fatigue type depression was simulated on the outer race. The bearing was mounted in the vibration test rig and run with 12 kg load at 10 Hz (600 RPM) shaft speed. By loosening the bolts, which through the brackets clamp the tube, the tube can be rotated 180°, so that the damage is either positioned right under the load or at the top of the bearing out of the load zone. Fig. 9.4

shows the vibration signal picked up on the bearing housing with the damage in and outside the load zone. Hence, fig. 9.4a represents a good bearing and fig. 9.4b a damaged bearing. The damaged bearing clearly has a higher overall level of vibrations and the predicted series of transients are clearly seen. The time between transients is $1/f_{rp}$, with f_{rp} for this bearing $10 \cdot 0.42\ 12 = 50.4$ Hz ($T_{rp} = 1/f_{rp} = 19.8$ msecs). The frequency spectrum of fig. 9.4b is shown in fig. 9.5 where the series of peaks spaced with f_{rp} is clearly seen between 250 and 700 Hz. Low frequency components have been filtered out to allow for a suitable scaling.

For the set up described it is obviously very easy to diagnose fatigue spalling, either directly from the time signal or from its spectrum. In a realistic monitoring situation the presence of noise from other vibration sources of the machinery raises complications. This effect was simulated in the test rig by attaching an electro-mechanical vibrator to the bearing housing. The direction of input force is shown in fig. 4.3a. The output of a white noise source is band filtered between 200 - 1000 Hz, fed through a power amplifier and then drives the 250 W vibrator. The RMS value of the vibrations generated with the bearing running with the crack under load was measured, the rig stopped and the power amplifier switched on and adjusted so that the vibrations generated had an RMS level twice that of the rig running without noise input. The rig was then started again and the vibrations from both bearing and noise source recorded with the crack in and out of the load zone. Fig. 9.6 shows the time signal for load free and loaded crack, where the previously obvious transients are buried in random noise. It is thus impossible to distinguish

directly from the time history plots which is the good bearing and which is the damaged bearing in the presence of a high level of external noise. Broadband RMS measurements were taken from the good and damaged bearing. The average RMS value for the good bearing was 0.631 and for the damaged bearing 0.755. The difference is consistent as will be demonstrated in section 9.4, but small for practical monitoring purposes. Fig. 9.7a and b shows the spectra from fig. 9.6a and b respectively. The spectra show distinct differences between the good and the damaged bearing and it would be possible to pick out the typical series of peaks at harmonics of f_{rp} in fig. 9.7b. The presence of noise however makes the interpretation of the spectrum more difficult and uncertain than was the case for the undisturbed bearing of fig. 9.5b. The signal to noise ratio can however be greatly improved by use of the averaging routine included in the DAS package. Fig. 9.7c is the result of 10 times averaging and shows the characteristic series of harmonics equally distinct as in fig. 9.5.

A problem when diagnosing spalling fatigue damage of the outer race by spectral analysis is that harmonics of f_{rp} occur due to VC also in good bearings as was predicted by the DYNSIM runs and also shown experimentally, see fig. 6.27. There are however differences in the amplitude distribution of these harmonics. While the components of VC origin decrease rather rapidly with the order of the harmonic, harmonics due to fatigue damage have a constant or increasing amplitude with frequency. The higher frequency contents of the transients is due to the sharp impact that occur when a roller hits the edge of the spalling crater. This conclusion is verified by spectrograms both from the genuinely fatigued bearing and from several bearings with simulated fatigue damage.

In the context of vibration components at RP frequency and harmonics thereof, a method of shaft-housing alignment, which has proved useful, should be mentioned. The Kinematic theory for VC vibrations showed that the amplitude of components at RP frequency and harmonics thereof increase in proportion to the radial clearance, see equation (7.38). Misalignment in the mounting of a bearing tends to close the radial clearance and also means that the local stiffness is reduced since only the edges of the rollers carry the load. Hence, shaft and housing should be adjusted so as to give maximum levels of VC vibrations to ensure that the bearing is running freely and with a proper load distribution. This somewhat paradoxical conclusion is supported by several alignments of the test rig where a good agreement between the described method and direct measurement of alignment was obtained.

Fatigue damage detection by auto correlation analysis has also been tried. For increasing time lags, auto correlation analysis will average out the random components of the signal while the harmonic components are sustained. The process thus has an ability to distinguish between random and harmonic components. As shown in fig. 9.3, the auto correlation of a comb of delta spikes is a similar comb of delta spikes, but with reduced level of random components if such were superimposed on the original comb. Hence the auto correlation of the time signal of fig. 9.4b should have a peak at $1/f_{rp}$ = 19.8 msecs. Such a peak also clearly occurs in fig. 9.8. The auto correlation functions of fig. 9.6a and b are shown in fig. 9.9a and b respectively. Obviously the auto correlation process like the spectrum averaging has the ability of revealing repeating components hidden in random noise.

Attempts at further processing of the output of the FFT routine using both further FFT processing and auto correlation analysis has been tried, but found not to be able to further improve the clarity of the results. The processing known as Summation analysis has not been attempted since it requires an elaborate triggering system giving a trig pulse per cage revolution. Summation analysis and auto correlation analysis have been further discussed in Appendix III.

Previously described diagnostic methods have made use of the repetitive nature of the transients. Another approach is to study only the high frequency components of the transients. Fig. 9.1 shows scope traces from a bearing with spalling fatigue on one roller, where the signal has been filtered through a sequence of frequency intervals. The first band, 1 - 3 KHz, shows regular series of peaks appearing each time the damaged roller passes through the load zone, compare fig. 9.2.6 Above 10 KHz it is no longer possible to see these regular series.

The filterwas then set at 25-50 kHz with the natural frequency of the accelerometer being 38 kHz, compate the SPM method described in Chapter 2. To investigate whether the number of peaks in this frequency region was correlated to the existence of damage, a bearing with a fatigue damage to the outer ring was fitted in the vibration test rig. A counter was linked to the output of the filter and counted all peaks exceeding a certain threshold level for periods of 60 secs. The rig was then run with the damage under load and outside the load zone. The ratio between counts of damaged bearing and good bearing are given in the table below.

Table 9.2

run	1	2	3	4
count ratio	1.37	5.15	1.87	2.43

In all four runs, consistently higher counts thus results for the damaged bearing compared to the good bearing, although there are large fluctuations of the count ratios. The number of counts seems a somewhat unstable measure of the state of the bearing. Peak counts for a bearing with a damage to the inner race was carried out with the same instrumentation. In this case the counter sampling was initiated by a trig pulse from the rotor shaft and the sampling time was chosen so as to allow the shaft to turn 60° during the time the gate was open. By moving the tooth on the rotor shaft, which initiates sampling, it is possible to compare peak counts with the crack in various positions of the bearing. The table below shows counts with the crack moving through circle segments positioned V degrees from the load line.

Table 9.3

V =	0	60	120	180	240	300
Counts =	831	794	774	752	771	771

Also this experiment shows an increase of counts when the crack is in the load zone, but the differences are small. In this case the shock wave will have to travel through the rolling element and the oil film interface before reaching the outer ring,which probably attenuates the high frequency components studied.

9.3 Abrasive Wear Monitoring

Due to their geometry spherical roller bearings have a mixed sliding and rolling motion of the roller-race contacts. This type of bearing is therefore prone to destruction through abrasive wear. The spherical roller bearing denoted A in Chapter 7 was run for 200 hours at 850 kg load and 90°C lubricant temperature in the wear rig. The wear process was speeded up by using a rather thin lubricant giving an oilfilm with a thickness of about one third of what is recommended by the manufacturer. The bearing was inspected every 50th hour and after 200 hours all load carrying surfaces had become considerably worn. At this stage the bearing was still fully functional in all respects. The impact of abrasive wear on the inner track surface is apparent from a comparison between fig. 7.10A showing the bearing when new and fig. 9.10a showing the bearing after 200 hours of operation. The frequency contents of respective race contours are given in fig. 7.11A and 9.10b (note the different frequency scales). Comparing first the size of the lobes it is apparent that the amplitudes of this low frequency out of roundness has diminished due to abrasive wear. The amplitude coefficients are given in the table below.

Table 9.4

i =	2	3	4	5	6	7
c_i, new bearing =	0.6	0.9	0.25	0.15	0.45	0.6
c_i, worn bearing =	0.52	0.85	0.21	0.04	0.19	0.42

This seems to be a logical result of the highest points of the race being the ones most severely worn, thereby evening out the lobes of the race.

Subsequent to inspection and measurement of the bearing components, the bearing was assembled and mounted in the vibration test rig. The effect of decreasing lobe sizes with wear does come through in the spectrograms from the rig runs, but is not drastic enough to form a basis for condition monitoring. Comparing the high frequency components of the surface spectrograms, it is apparent that these increase strongly with wear. Without making a detailed theoretical analysis as was done in Chapter 7 for the effects of low frequency out of roundness, one would expect an increased proportion of high frequency vibrations generated for the worn bearing compared to the new bearing. The existence of such an effect has also been established in the region 2.5-5.0 KHz shown in fig. 9.11 (M = 12 kg, f_s = 12 Hz) and fig. 9.12 (M = 85 kg, f_s = 24 Hz). Fig. 9.11 shows an increase of the overall vibration level with wear and the occurrence of frequencies above 2.5 KHz. In fig. 9.12 the overall level is not higher for the worn bearing, but the level of vibrations above 2.5 KHz has increased significantly. The level of high frequency vibrations in the context of abrasive wear is probably affected by things like the minimum oil film thickness and the size of the contact zone, but these effects have not been investigated in detail. For all trial runs with rotor weights 12, 85 and 205 kg and rotor speeds from 8 to 24 Hz, there is an appreciable increase of high frequency vibrations with wear. The difficulty of detecting wear condition by straightforward broad band RMS measurement is illustrated in the table below.

Table 9.5

Broadband RMS levels (G):

	$M=85;f_s=12.$	$M=85;f_s=24$	$M=12;f_s=12$	$M=205;f_s=12$
New bearing	0.18	0.48	0.12	0.083
Worn bearing	0.26	0.43	0.19	0.26

For the second example of table 9.5, the RMS value is actually lower for the worn bearing than for the new one. It is not surprising that this might occur since the low frequency vibrations due to lobes of the race give a significant contribution to the overall RMS level, and as was previously demonstrated, the abrasive wear tends to smooth out these lobes. Fig .9.12 shows a decrease with wear of components in the region 1.0 - 1.5 KHz. This is probably due to increased damping in the roller-race interface due to the roughening of the surfaces. If the knowledge of frequency distribution gained from the spectrograms is utilized and only the region most affected by track roughness is studied, a much improved reliability of RMS monitoring is gained.

Table 9.6

RMS of bandpass filtered (2.5 - 5.0 KHz) signal (G):

	$M=85;f_s=12$	$M=85;f_s=24$	$M=12;f_s=12$	$M=205;f_s=12$
New bearing	0.029	0.099	0.012	0.039
Worn bearing	0.083	0.29	0.073	0.099

The example shows the danger of over simplified monitoring approaches and demonstrates the advantages that can be won by studying the vibratory process and tailoring the monitoring system to the specific monitoring situation.

As has been mentioned previously, the auto correlation process has the ability of distinguishing between random and harmonic components of a signal. Usually this property is used to lift up and allow study of harmonic components buried in a noisy background, but it can also be used to study the nature of the random components. The way in which the random influence on the auto correlation function is attenuated with time lag is significative of the nature of the random components. The auto correlation function for band limited white noise is given by

$$C(\tau) = C_o \frac{\sin(2\pi f_c \tau)}{2\pi f_c \tau} \qquad \ldots\ldots\ldots \quad (9.3)$$

where f_c is the cut off frequency of the white noise. Hence, the higher the value for f_c is, the faster does the auto correlation function go to zero, e.g. the auto correlation of unlimited white noise is a delta spike at $\tau = 0$. For signals consisting of both random and harmonic components, the auto correlation function will stabilize around the harmonic components more quickly if the random component has a high proportion of high frequency vibrations. This phenomena is illustrated in fig.9.13, where the auto correlation from the worn bearing with high frequency noise (compare fig. 9.12) has stabilized at a time lag of about 15 msecs, while the new bearing stabilizes at about 35 msecs. Similar results were obtained for different loads and speeds of the bearing. This way of using auto correlation processing thus appears to be a practical way of monitoring developing abrasive wear.

9.4 Basic Monitoring Theory

The efficiency of a certain monitoring system is a concept worth a somewhat more detailed discussion. Clearly the user of such a system wants his system to trigger (give indication of malfunctioning) when, and only when, a fault in the monitored machinery has occurred. This means that the method of monitoring must be selective in its operation so as not to trigger for vibrations normally excited, or for vibrations, even if these are large, which are not associated with faults of the monitored system.

Comparing the spectrograms of good and fatigued bearings in fig.9.7a and c, it is immediately apparent which is the good and which is the damaged bearing. This is so for many methods of monitoring - the general character of the analysis makes it possible for an interpreter who knows what he is looking for to immediately tell whether the monitored machinery is faulty or not. Nevertheless, in many situations it is advantageous or even necessary to specify exactly which quantities are considered significant for the purpose of monitoring. This is obviously a necessity when the output of the monitoring system is interpreted by means of automatic data processing, but is useful also in other cases, because it allows for more systematic methods of monitoring to be used. Thus, for each monitoring situation a monitoring parameter, MPAR, should be determined and a rationally chosen trig level (TL) established, for which the machinery is considered faulty if MPAR>TL. This section is devoted to a discussion of these two monitoring parameters.

Going back to the demonstrated examples of bearing monitoring in section 9.2 and 9.3, the choice of MPAR is obvious for many cases, 1/ - 4/ of table 9.7, while for other cases, 5/ - 6/ of table 9.7, more consideration is required.

Table 9.7

1. Diagnosis of spalling fatigue by broad band RMS measurement, MPAR = RMS value.
2. Diagnosis of spalling fatigue by auto correlation analysis, MPAR = height of the peak at time lag = $1/f_{rp}$, (see fig. 9.9).
3. Diagnosis of fatigue spalling by counting high frequency transients, MPAR = number of counts during a specified length of time.
4. Diagnosis of abrasive wear by broadband and highpass RMS measurements, MPAR = measured RMS value.
5. Diagnosis of spalling fatigue by averaged frequency analysis. The peaks at RP frequency and its first few harmonics are more a function of VC vibrations than of damage. These should therefore not be included in MPAR. Judging from fig. 9.7c, the 5th - 15th harmonics of RP frequency are strongly affected by the occurrence of fatigue spalling of the outer race. Hence, choose MPAR = the mean value of the height of RP harmonics 5 - 15.
6. Diagnosis of abrasive wear by auto correlation analysis. Since the feature characteristic for abrasive wear is a quick stabilization of the auto correlation function, set MPAR = the time lag required for stable auto correlation function.

As a measure of the efficiency of the various monitoring methods exemplified, the ratio of MPAR for a damaged bearing and MPAR for a good bearing might be used,

$$q = MPAR_d/MPAR_g \quad \ldots\ldots\ldots \quad (9.4)$$

The q value is not representative for the monitoring method in a general sense, but only applies to the particular monitoring situation. The q values for the monitoring examples 1/ - 6/ of table 9.7 have been measured to,

Table 9.8

Example no.	q value	Comments
1/	1.20	Based on the mean value of 10 pairs of RMS readings.
2/	2.85	Measured directly from fig. 9.9a and b.
3/	2.70	Mean value of the ratios of table 9.2.
4/ broadband bandpass	1.41 3.6	Mean values from tables 9.5 and 9.6
5/	2.30	Obtained from direct measurement of the peaks of fig. 9.7a and c.
6/	2.33	Direct measurements from fig. 9.13a and b.

The q value is a simple and useful parameter describing the efficiency of a monitoring method applied to a specific monitoring situation. It is however a rather blunt instrument since it does not give any detailed information about the distribution of MPAR for good and damaged bearings. Further it does not determine an optimal trig level. A more sophisticated approach, although still very basic, is discussed below.

In a monitoring situation the monitored machinery is either fault free or faulty and the monitor is either triggered or not triggered. Hence, four events are possible

Table 9.9

System:	Monitor indication:
Fault free	Triggered (P_1)
	Not triggered (P_2)
Faulty	Triggered (P_3)
	Not triggered (P_4)

The probability of getting trigger indication if the bearing is fault free is P_1 and so on. Clearly an efficient monitoring system will trigger for faulty but not for fault free bearings. The probability of correct operation (PCO) is thus, the probability of not getting trigger indication for good bearing or, if the bearing is faulty, to get trigger indication. For the sake of simplicity assume that the probabilities for the bearing to be faulty or fault free are equal. The expression for PCO then becomes

$$PCO = (P_2 + P_3)/2 = (1 + P_3 - P_1)/2 \quad \ldots\ldots\ldots \quad (9.5)$$

For all TL, $P_3 \geq P_1$ for any meaningful monitoring system. Hence the minimum value og PCO is 0.5 and the maximum value is 1.0. For a given monitoring situation the probabilities P_1 and P_3 will be functions of the chosen value for TL. As is shown in fig. 9.14a, for a TL value below the normal vibration level of the bearing the monitor will always trigger ($P_1 = P_3 = 1$), while for a value of TL chosen too high, the monitor will never trigger ($P_1 = P_3 = 0$). Somewhere inbetween is the

TL value giving optimal performance. The functions for $P_1(TL)$ and $P_3(TL)$ can only be constructed from empirical data. P_1 and P_3 are plotted for two of the previously discussed monitoring methods (1/ and 2/ of Table 9.7) in fig. 9.14a and fig. 9.15a. The diagram in fig. 9.14a is based on 10 separate pairs of RMS readings from the time signals of fig. 9.6a and b and fig. 9.15 is based on five pairs of auto correlograms from the same signals. The resulting PCO profiles are plotted in figs. 9.14b and 9.15b. The abscissa axis of the probability diagrams are scaled in absolute units (RMS G and G^2), while the abscissa axis of the PCO diagrams have their zero point at the mean value of the MPAR readings and is scaled in percentage of this mean value. The PCO diagrams show immediately what the maximum PCO values are and at what TL values they are obtained. With RMS monitoring $PCO_{max} = 1$ for TL = 0.690 and with auto correlation monitoring $PCO_{max} = 0.98$ for TL = 0.107. It would however be unrealistic to use the value of PCO_{max} as the only measure of monitoring efficiency, because this presupposes that the P_1 and P_3 functions are completely known. In practice these functions are only known with a limited accuracy and might not take into account all possible events of the system. This is particularly so for a new monitoring situation when the operating experience is small. Another important requirement is thus that the monitoring system is stable, i.e. that TL can be chosen with a wide enough error margin (W), compare the previously discussed q value of table 9.8. As shown in fig. 9.14b and 9.15b 90% confidence of correct operation is obtained for TL levels within ±3.6% of the optimal value for RMS monitoring and within ±19.5% of the optimal TL value for Autocorrelation Monitoring. For the specific monitoring situation investigated having a high degree of noise

interference, the straightforward RMS method is hardly realistic because of its low W value. The auto correlation method on the other hand gives a good separation between readings from the good and damaged bearing with W = 39%. In many monitoring situations it is not equally damaging to get a false alarm as it is to miss an impending failure. Such considerations can be accounted for by a direct study of the P_1 and P_3 functions of figs.9.14a and 9.15a.

The method described is useful in highlighting the fundamental principals and objectives in the workings of a general monitoring system. In a practical application the usefulness of the method is entirely dependant on how well the P_1 and P_3 functions are known. These functions should include all the dispersion of the MPAR value that occurs in practice for various reasons (including human error) when using a specific monitoring system in a specific situation. Such information is best obtained by analysing historical data of monitor indications and failures from a system in practical use. Thus the method is practically useful only when a sufficient record of operating experience is available. In such a situation the operator of a monitoring system could benefit from reviewing the chosen trigger levels and general characteristics of his system according to the methods described.

Scope traces (50 mS/div.)

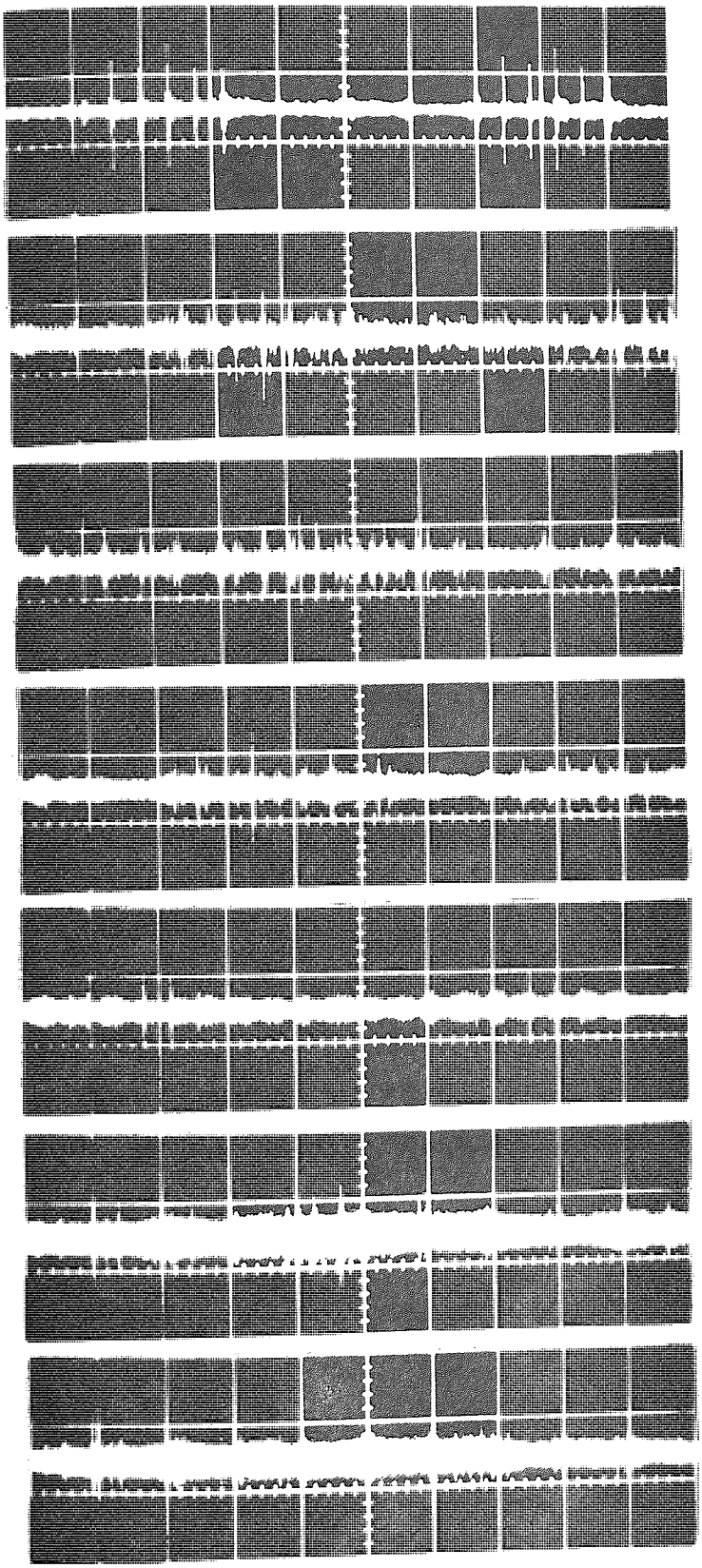

Cut-off frequencies for bandpass filter:

1 - 3 KHz

3 - 10 KHz

10 - 30 KHz

30 - 50 KHz

50 - 100 KHz

100 - 150 KHz

150 - 300 KHz

Fig 9.1

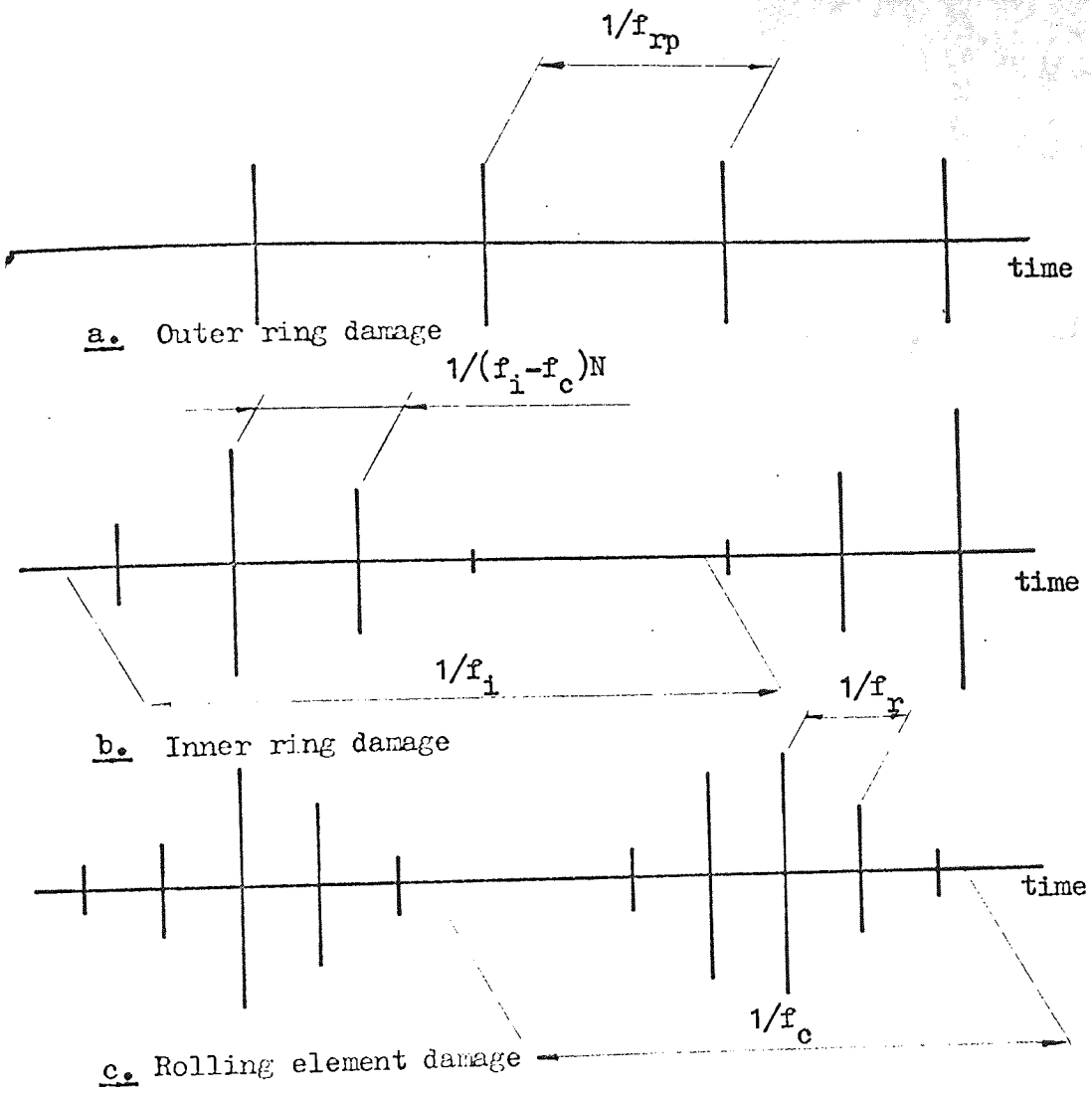
$1/f_{rp}$
time
a. Outer ring damage
$1/(f_i-f_c)N$
time
$1/f_i$
$1/f_r$
b. Inner ring damage
time
$1/f_c$
c. Rolling element damage

Fig. 9.2

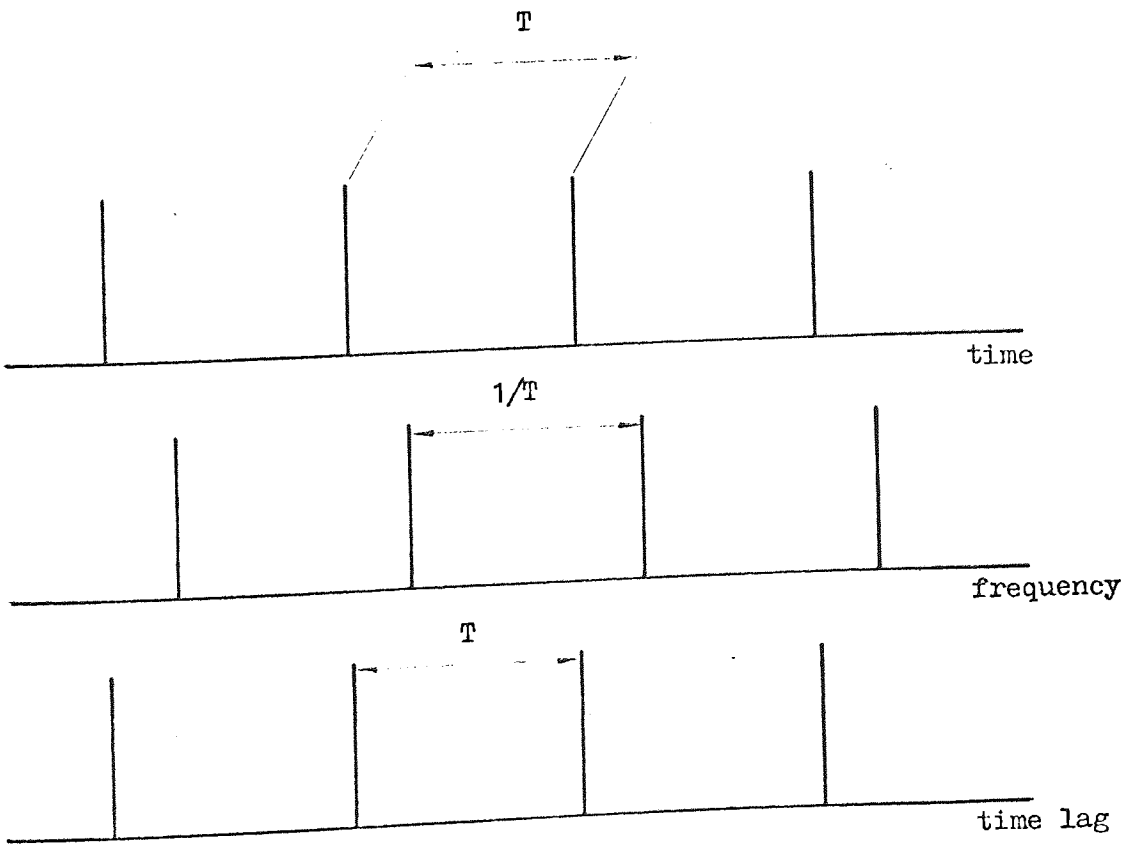
T
time
1/T
frequency
T
time lag

Fig. 9.3

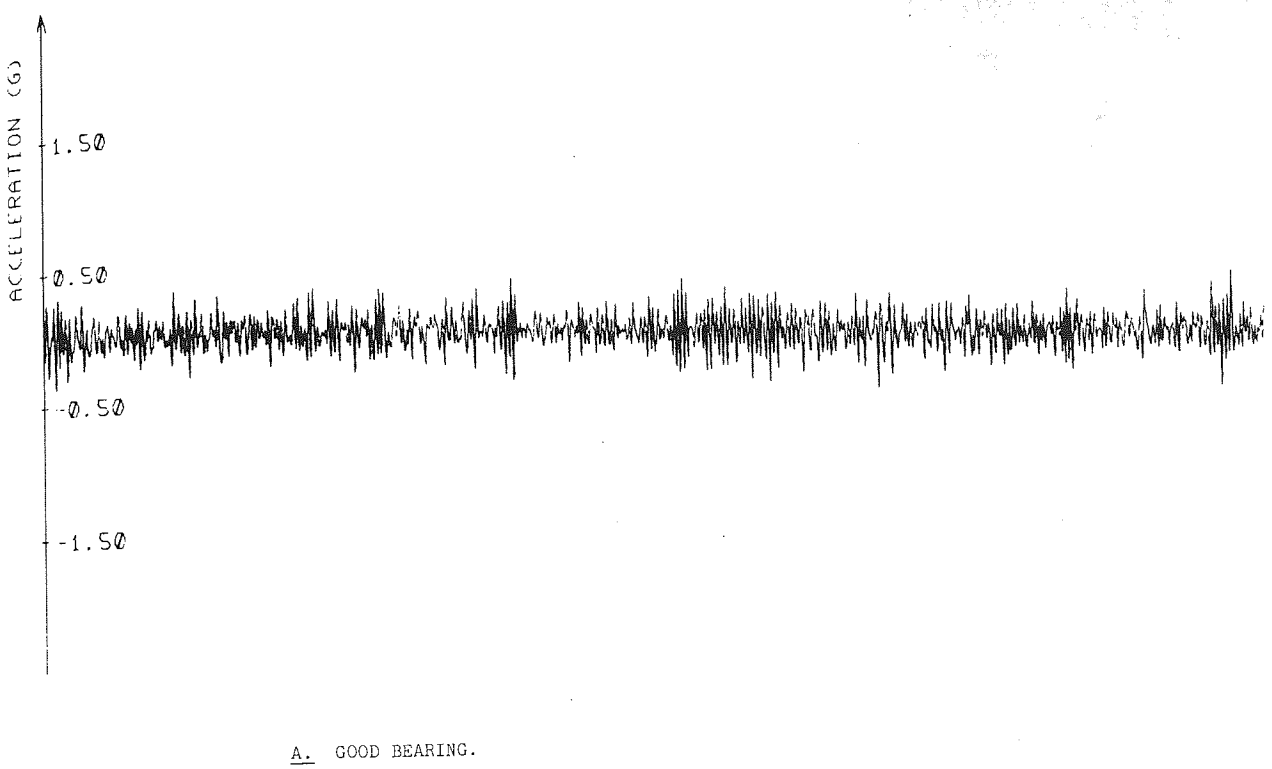

A. GOOD BEARING.

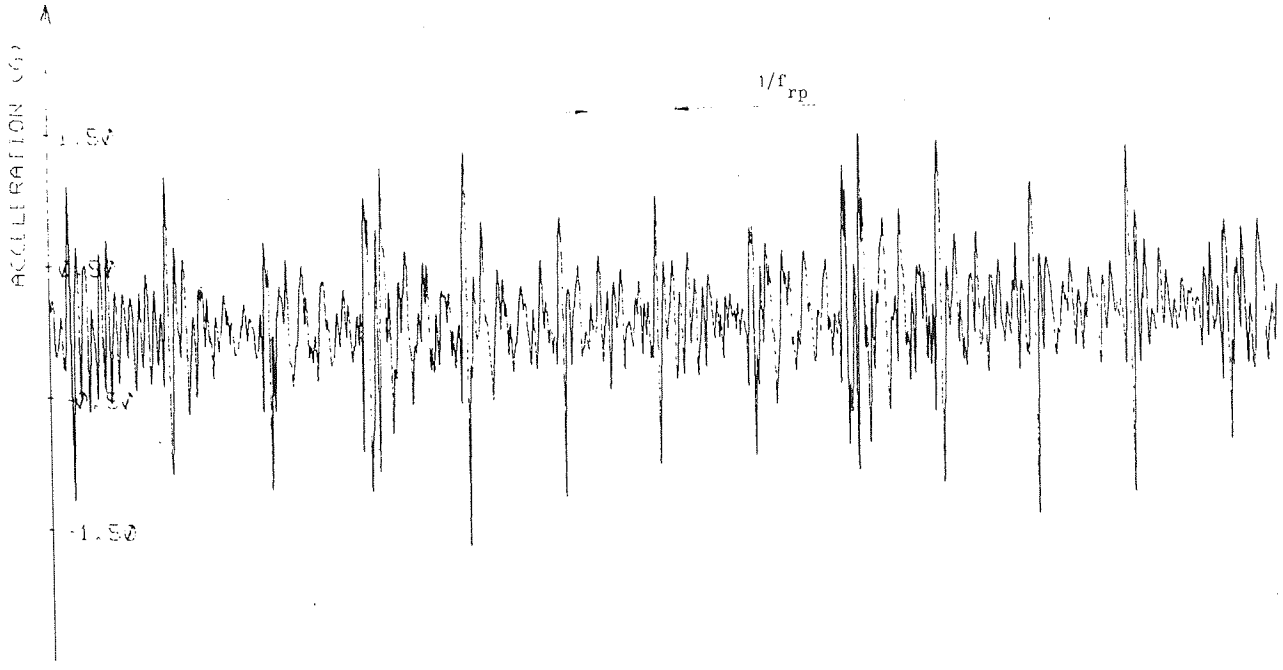

B. DAMAGED BEARING.

FIG 9.4

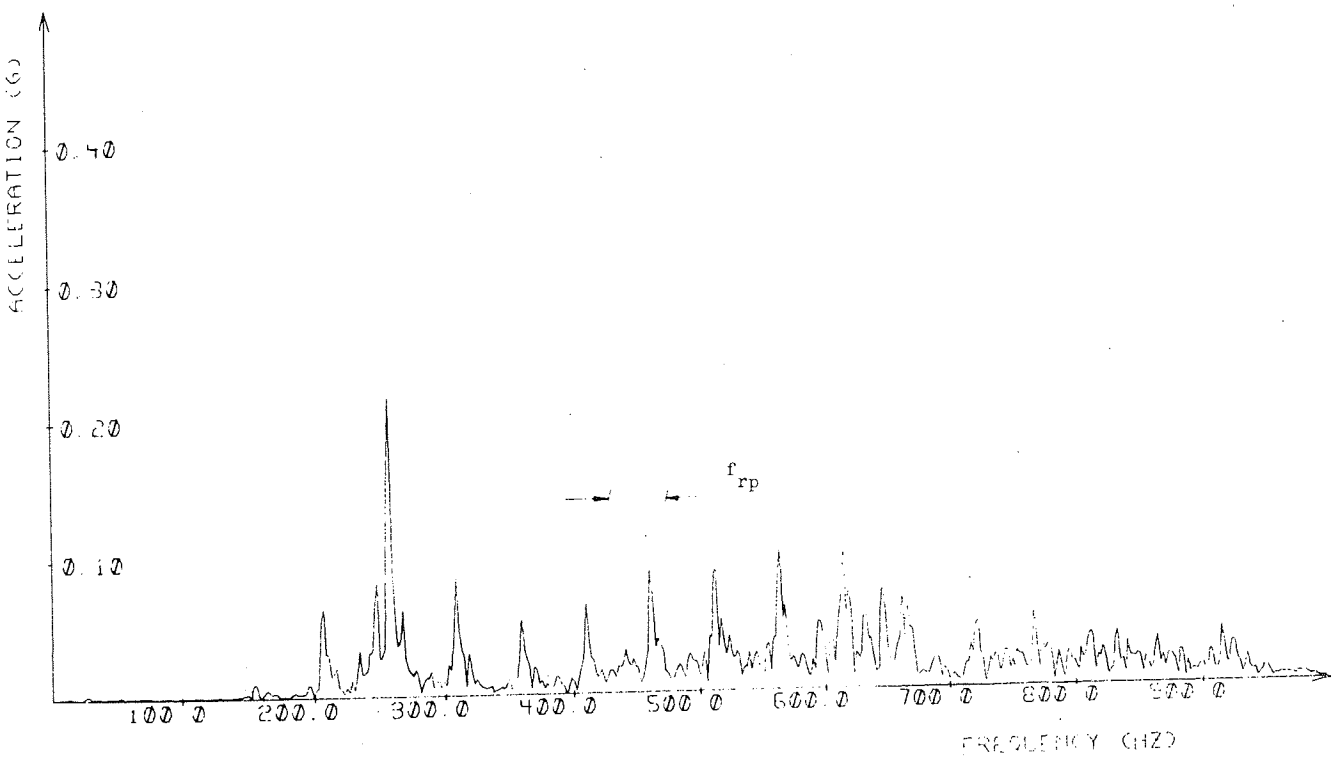
ACCELERATION (G)
0.40
0.30
0.20
0.10
f_{rp}
100.0
200.0
300.0
400.0
500.0
600.0
700.0
800.0
900.0
FREQUENCY (HZ)

FIG 9.5

A. GOOD BEARING.

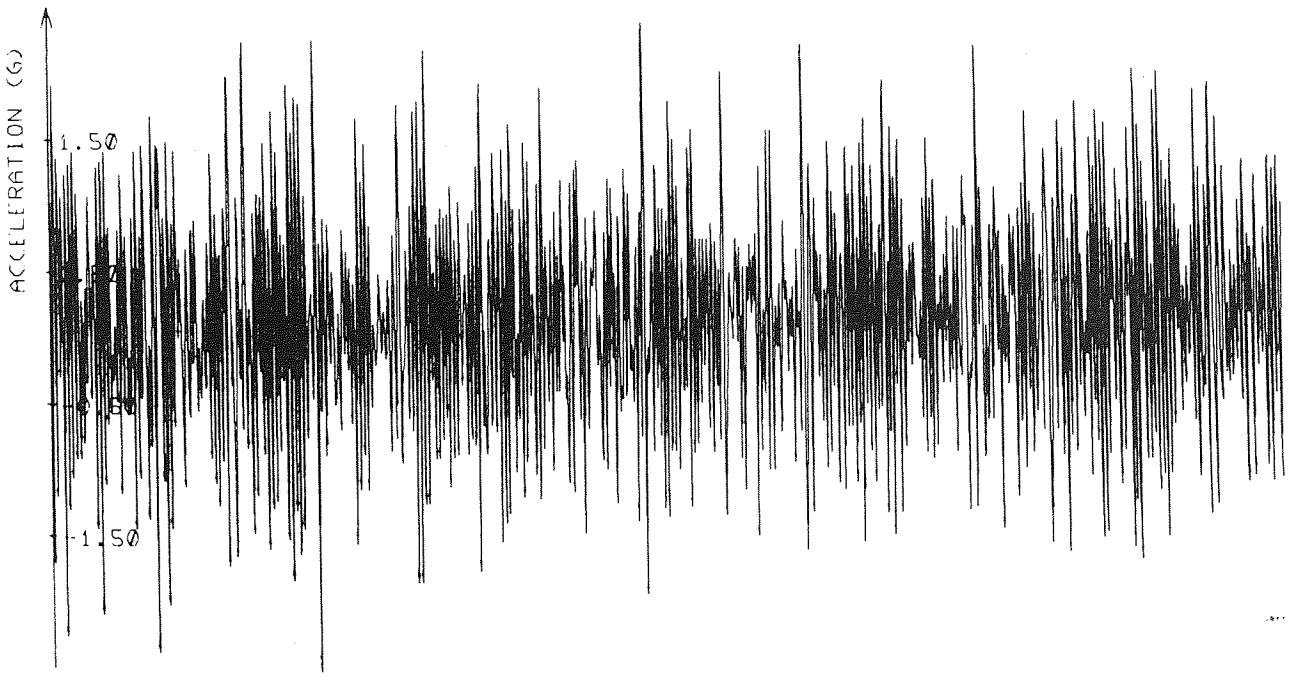

B. DAMAGED BEARING.

FIG 9.6

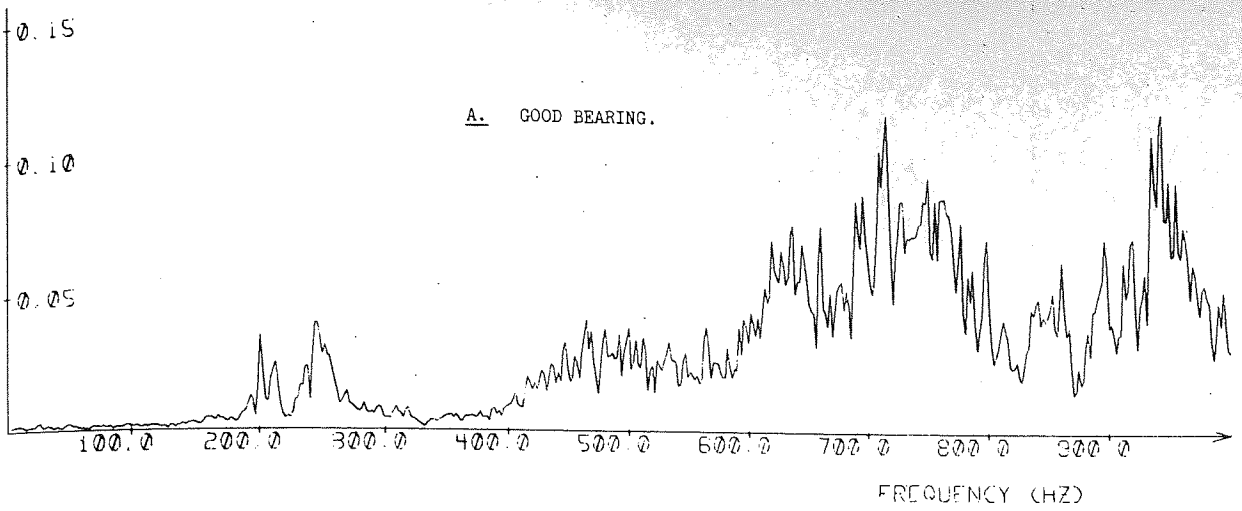
0.15
0.10
0.05
A. GOOD BEARING.
100.0
200.0
300.0
400.0
500.0
600.0
700.0
800.0
900.0
FREQUENCY (HZ)

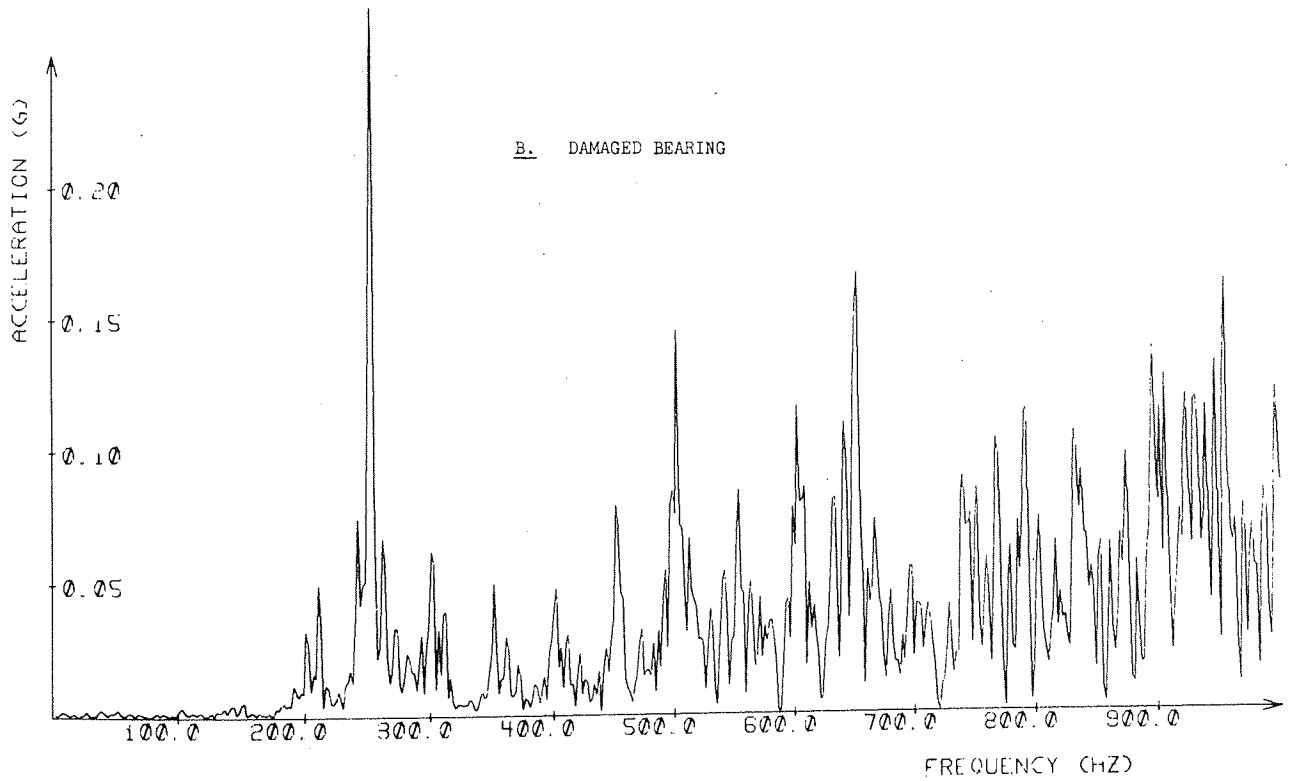
ACCELERATION (G)
0.20
0.15
0.10
0.05
B. DAMAGED BEARING
100.0
200.0
300.0
400.0
500.0
600.0
700.0
800.0
900.0
FREQUENCY (HZ)

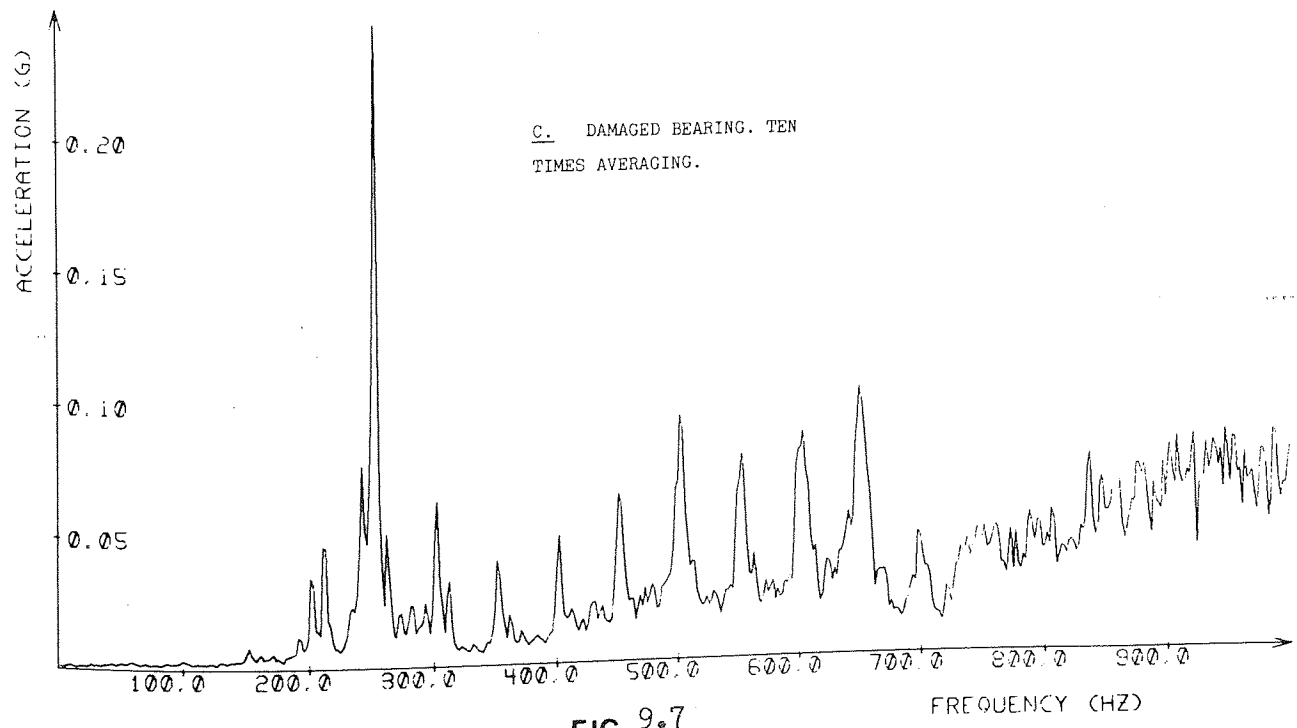
ACCELERATION (G)
0.20
0.15
0.10
0.05
C. DAMAGED BEARING. TEN TIMES AVERAGING.
100.0
200.0
300.0
400.0
500.0
600.0
700.0
800.0
900.0
FREQUENCY (HZ)

FIG 9.7

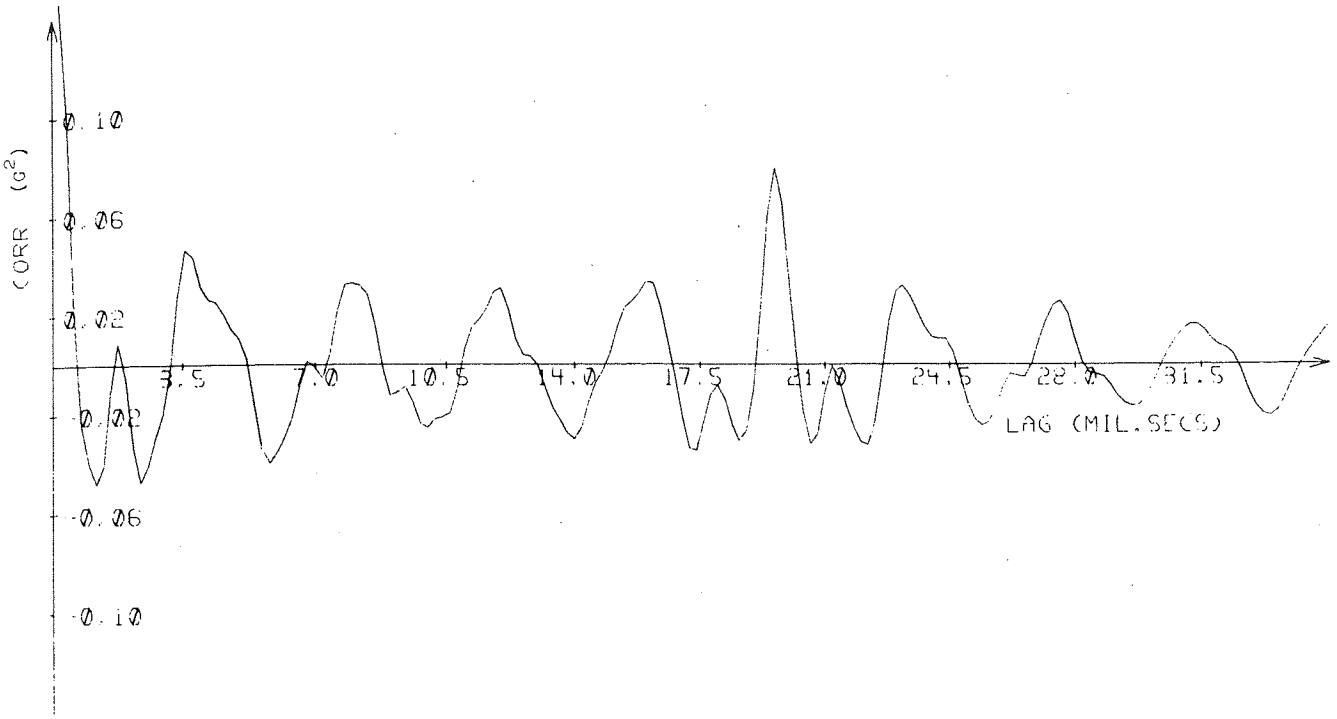

FIG. 9.8. AUTOCORRELATION OF THE TIME SIGNAL OF FIG. 9.4 B.

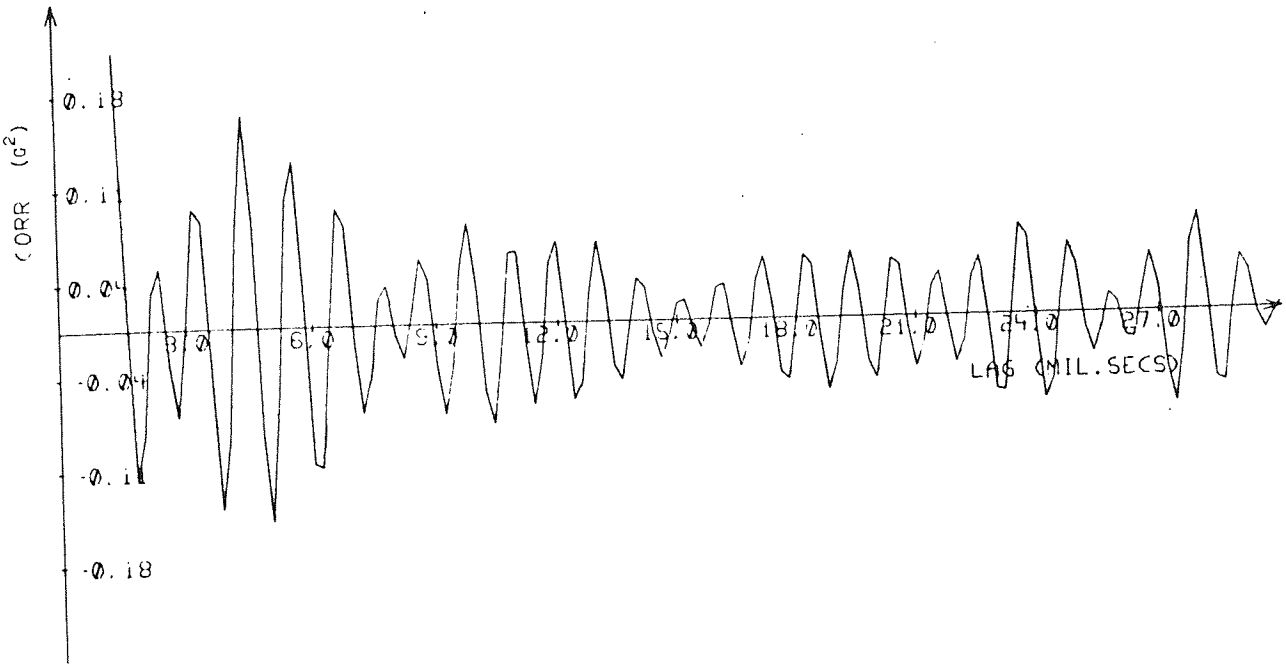

A. GOOD BEARING.

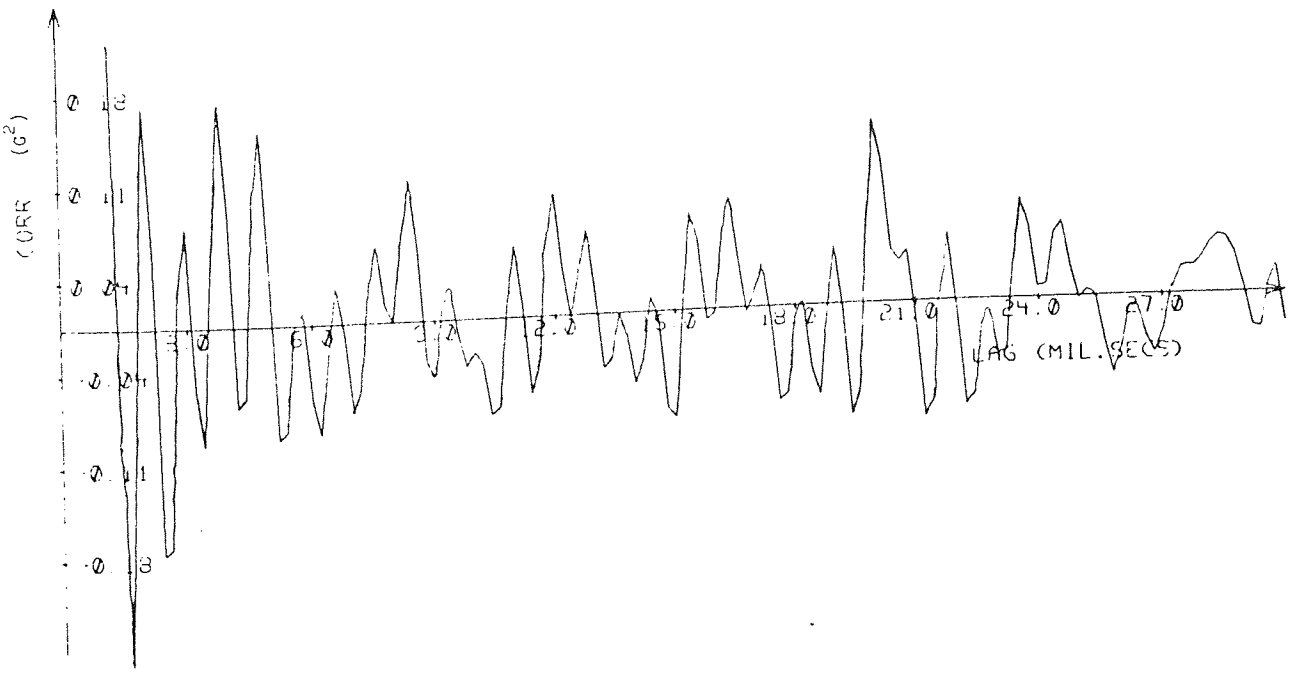

B. DAMAGED BEARING.

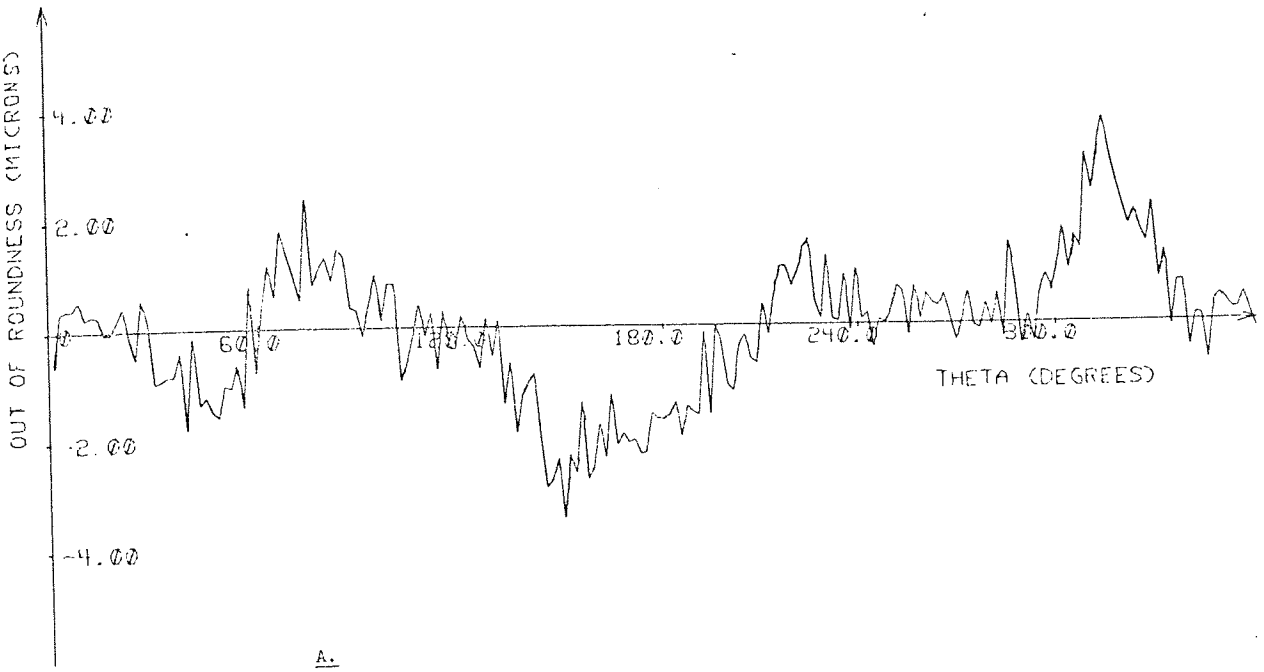
OUT OF ROUNDNESS (MICRONS)
4.00
2.00
-2.00
-4.00
60.0
180.0
240.0
THETA (DEGREES)

A.

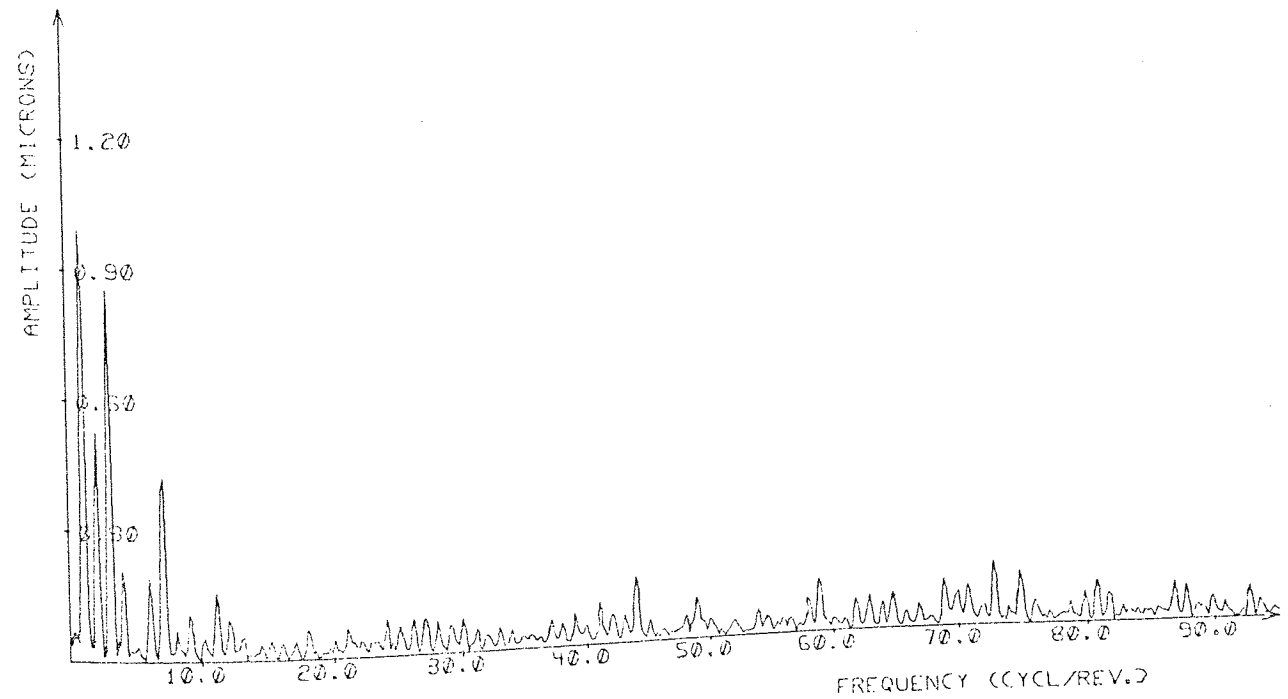
AMPLITUDE (MICRONS)
1.20
0.90
10.0
20.0
30.0
40.0
50.0
60.0
70.0
80.0
90.0
FREQUENCY (CYCL/REV.)

B.

FIG. 9.10

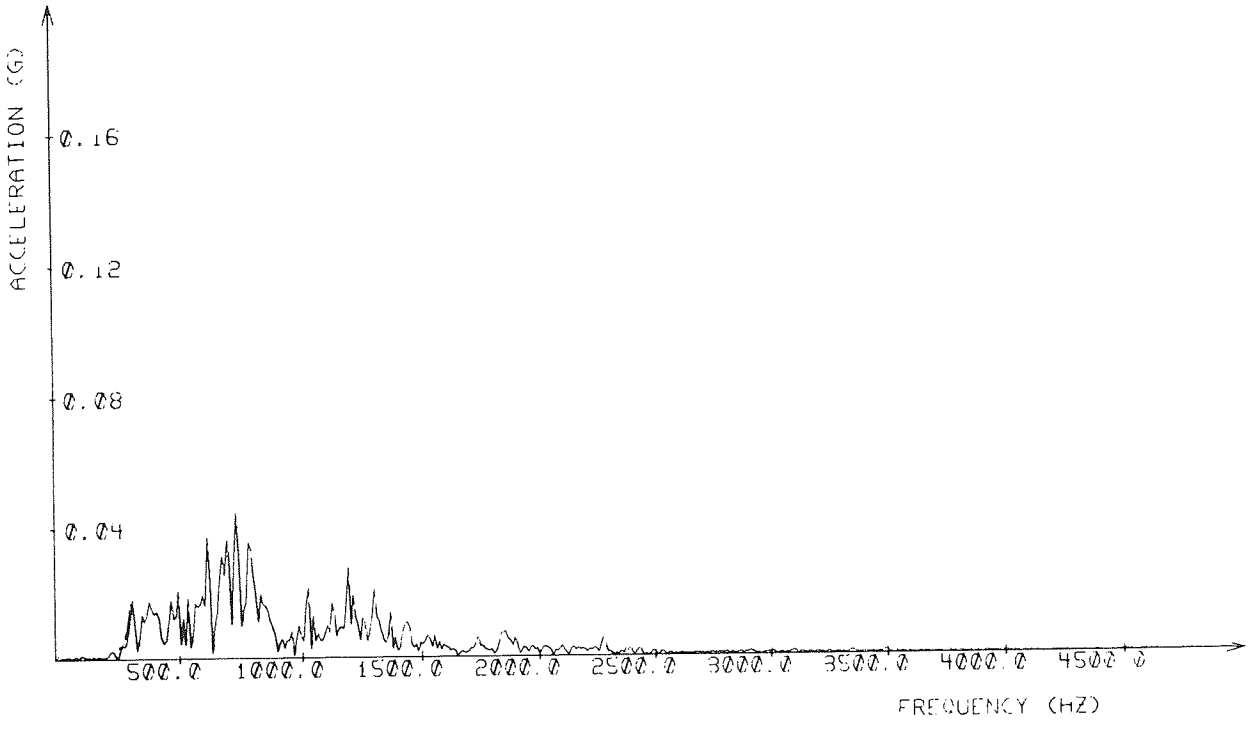

A. NEW BEARING.

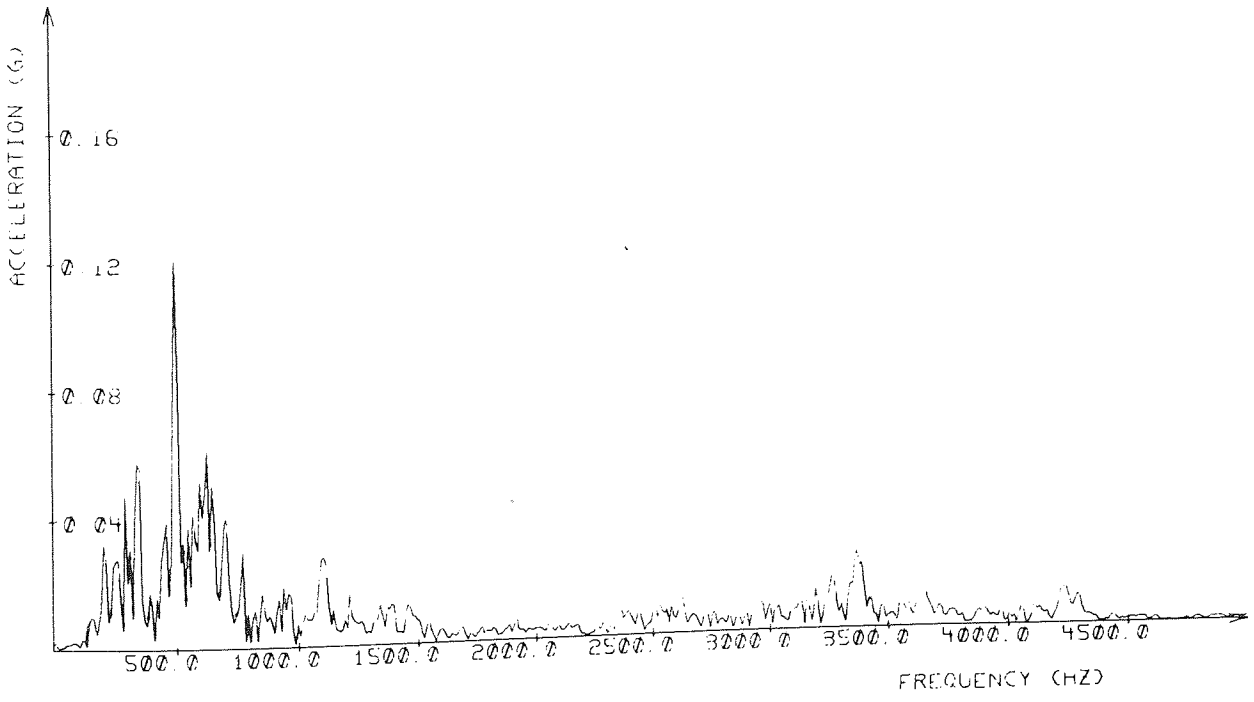

B. WORN BEARING.

FIG 9.11

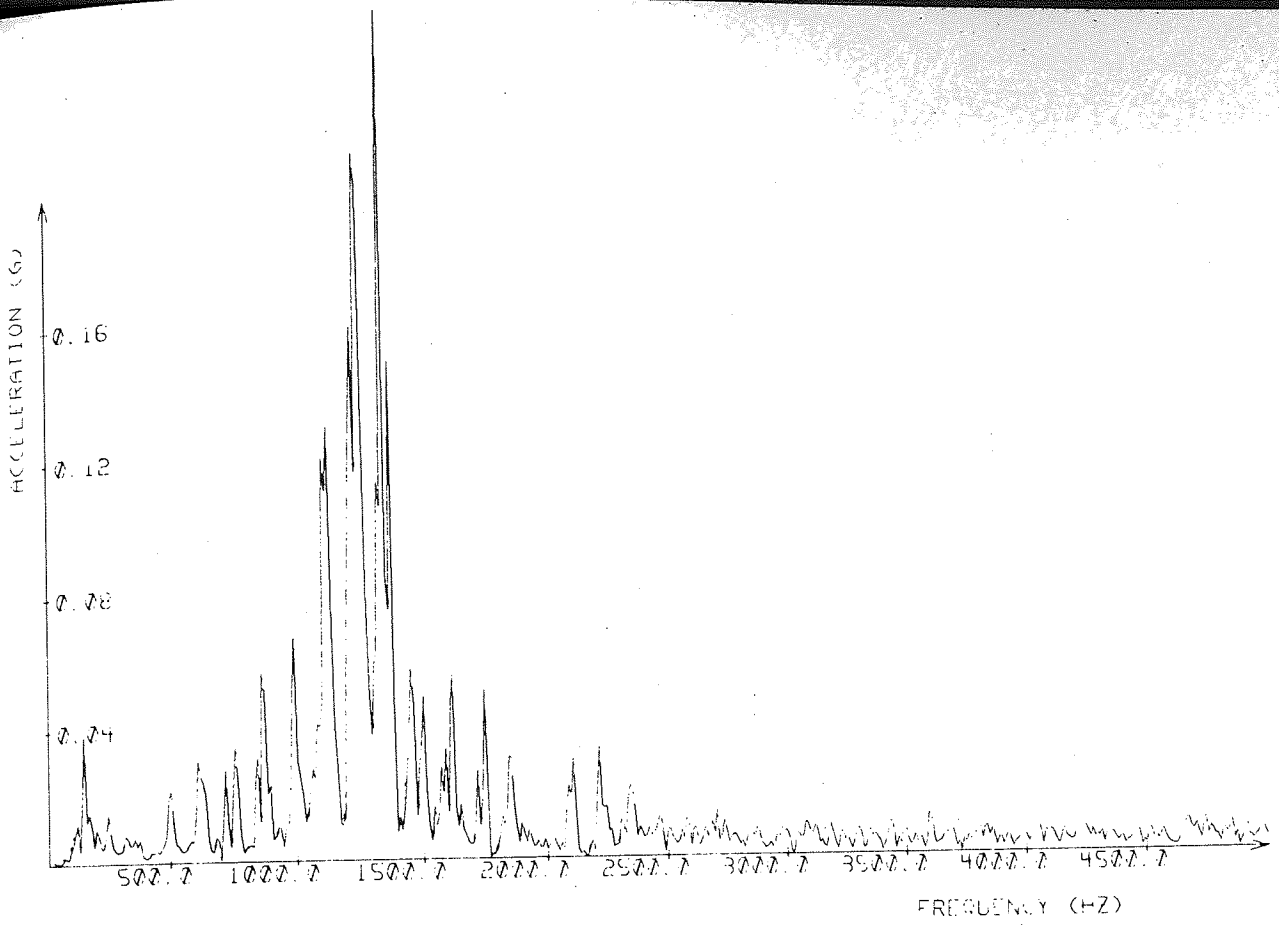

A. NEW BEARING.

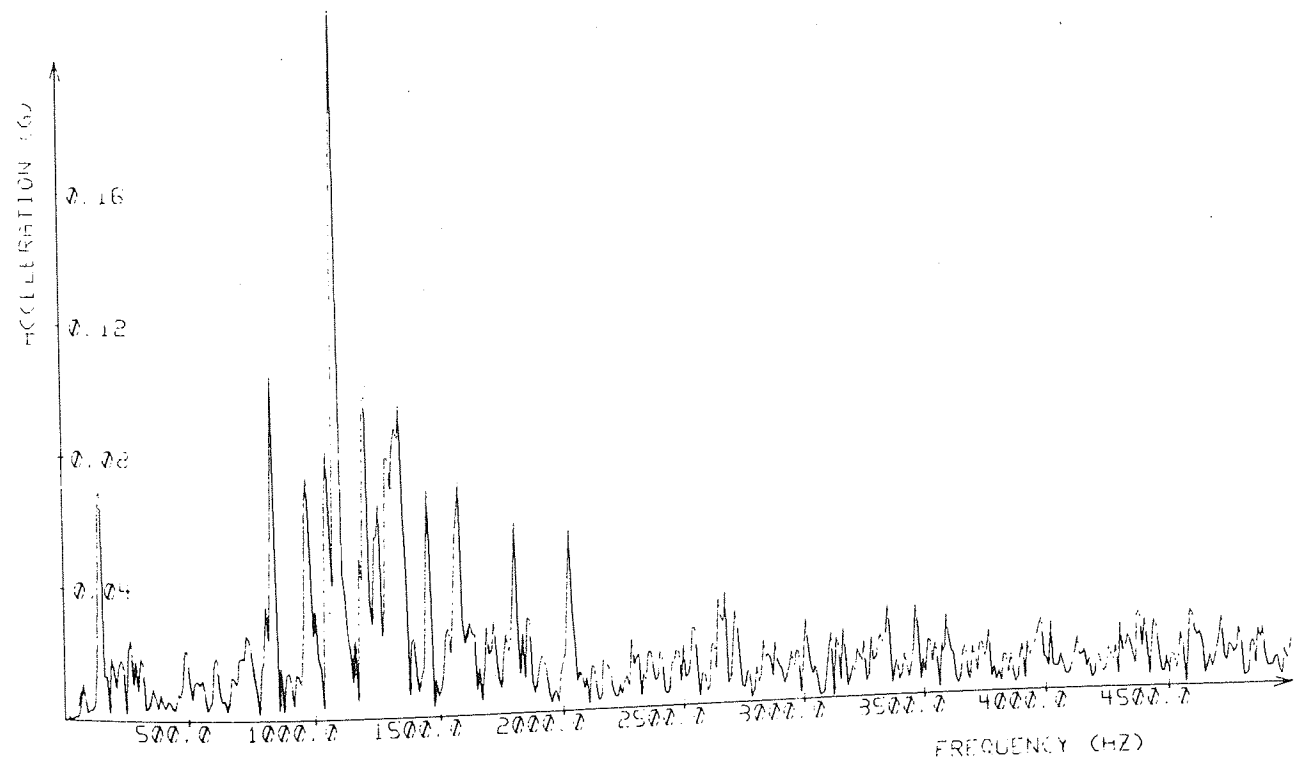

B. WORN BEARING.

FIG 9.12

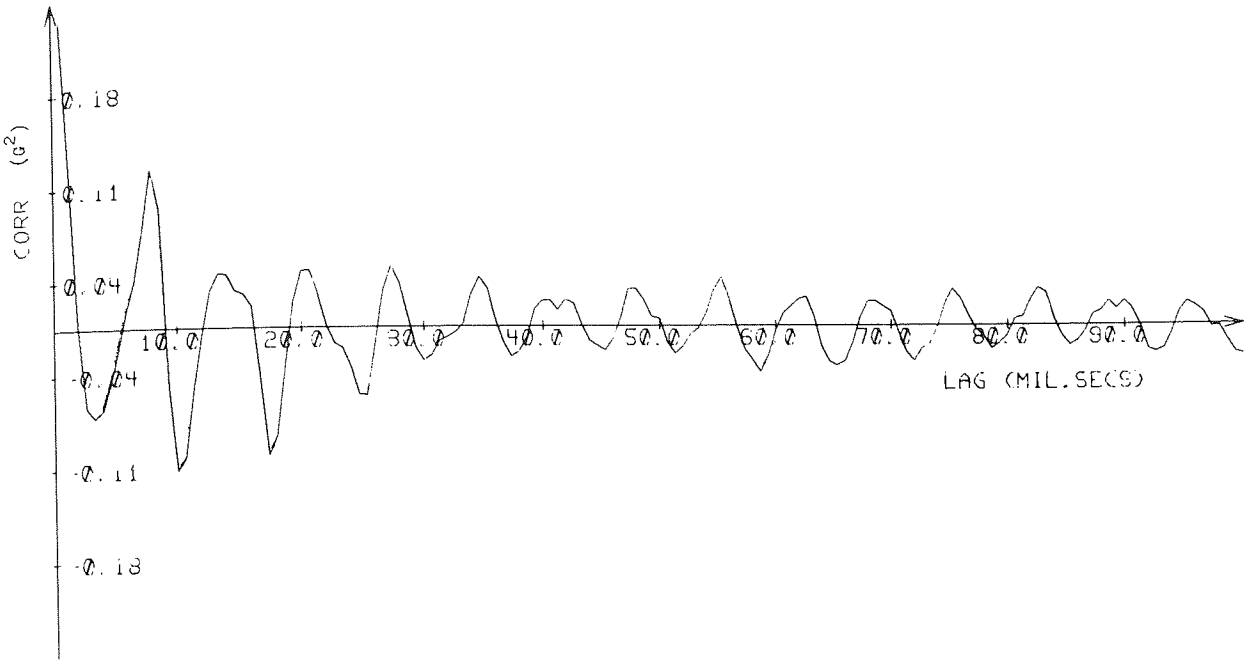

A. NEW BEARING.

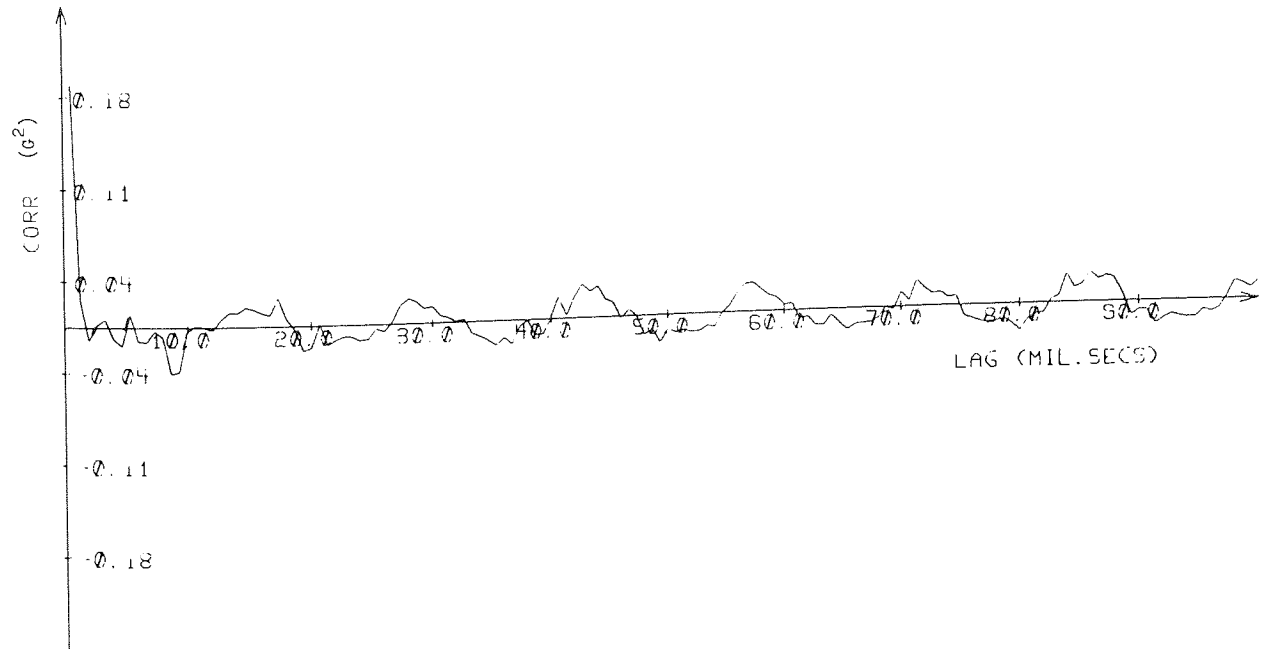

B. WORN BEARING.

FIG 9.13

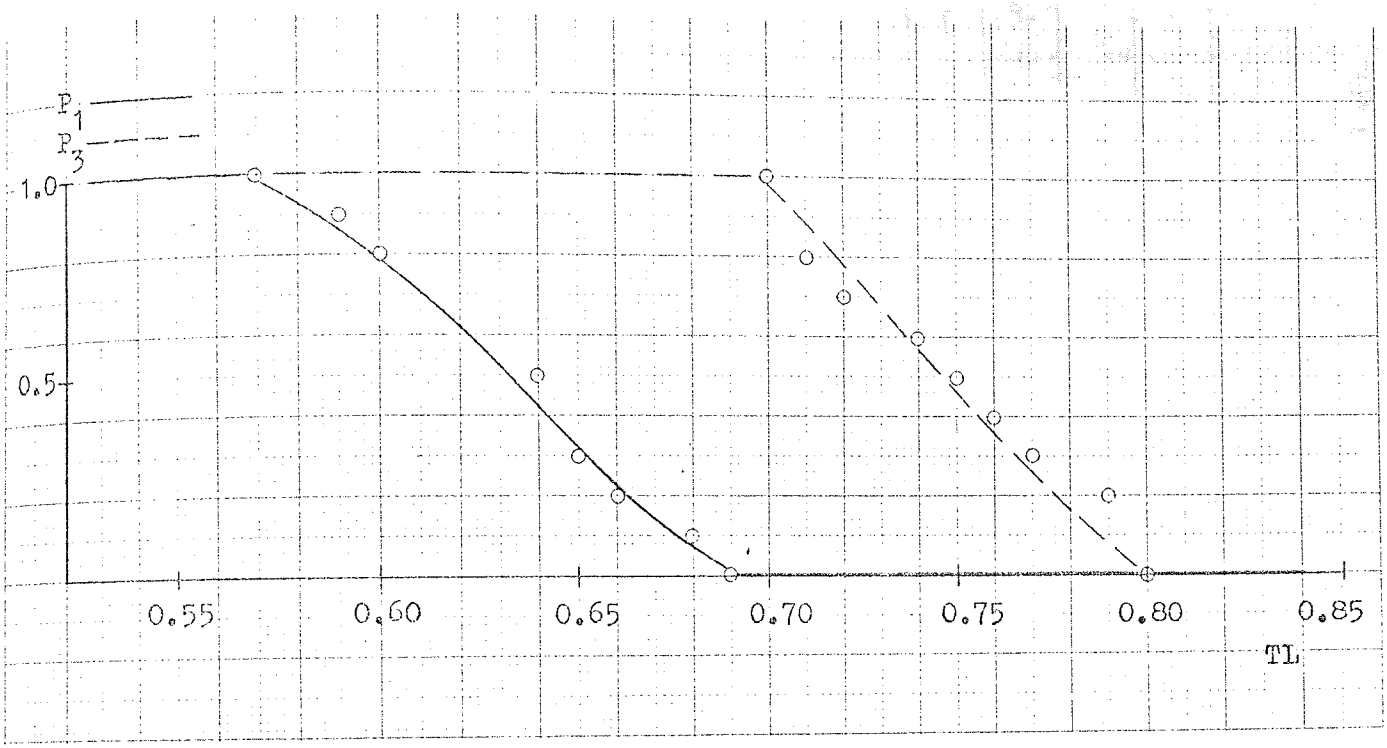

a.

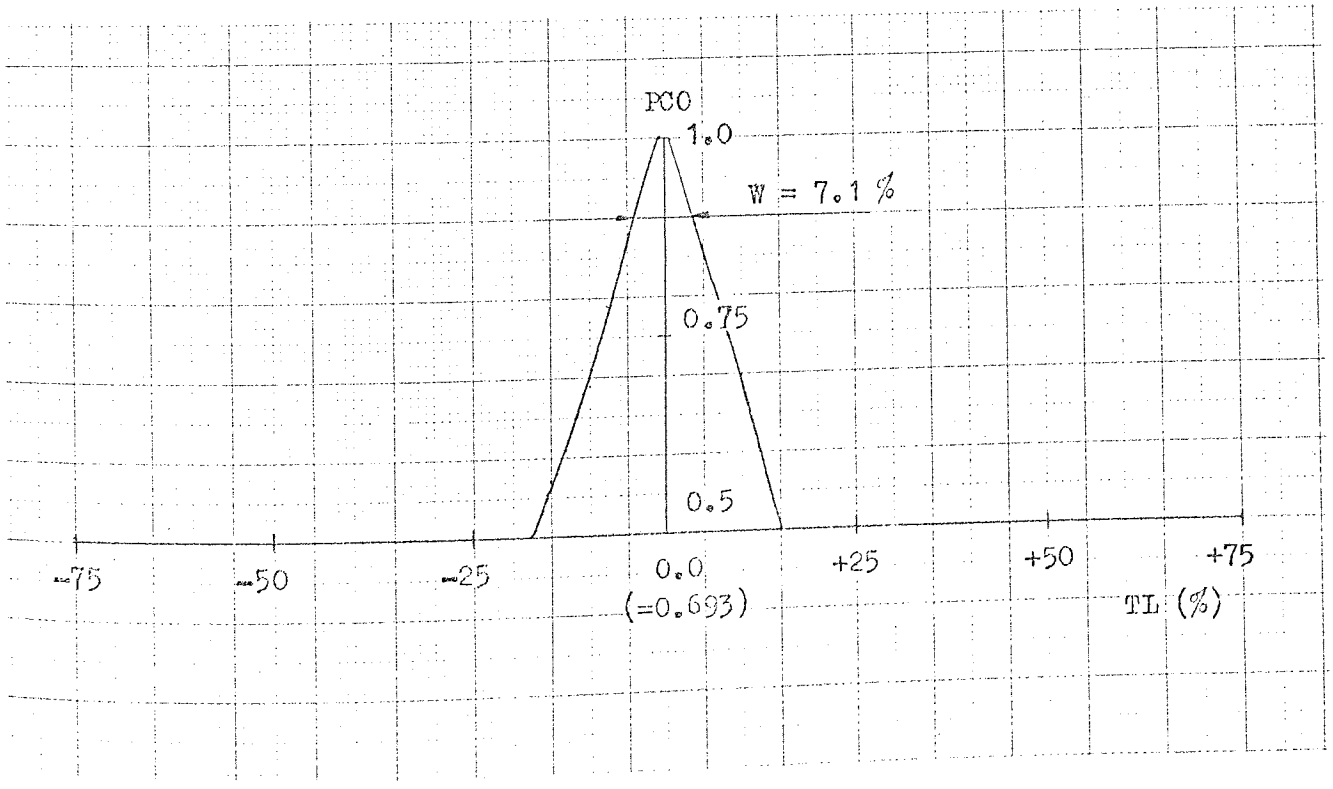

b.

Fig. 9.14 Characteristics of monitoring spalling fatigue by broadband RMS measurement.

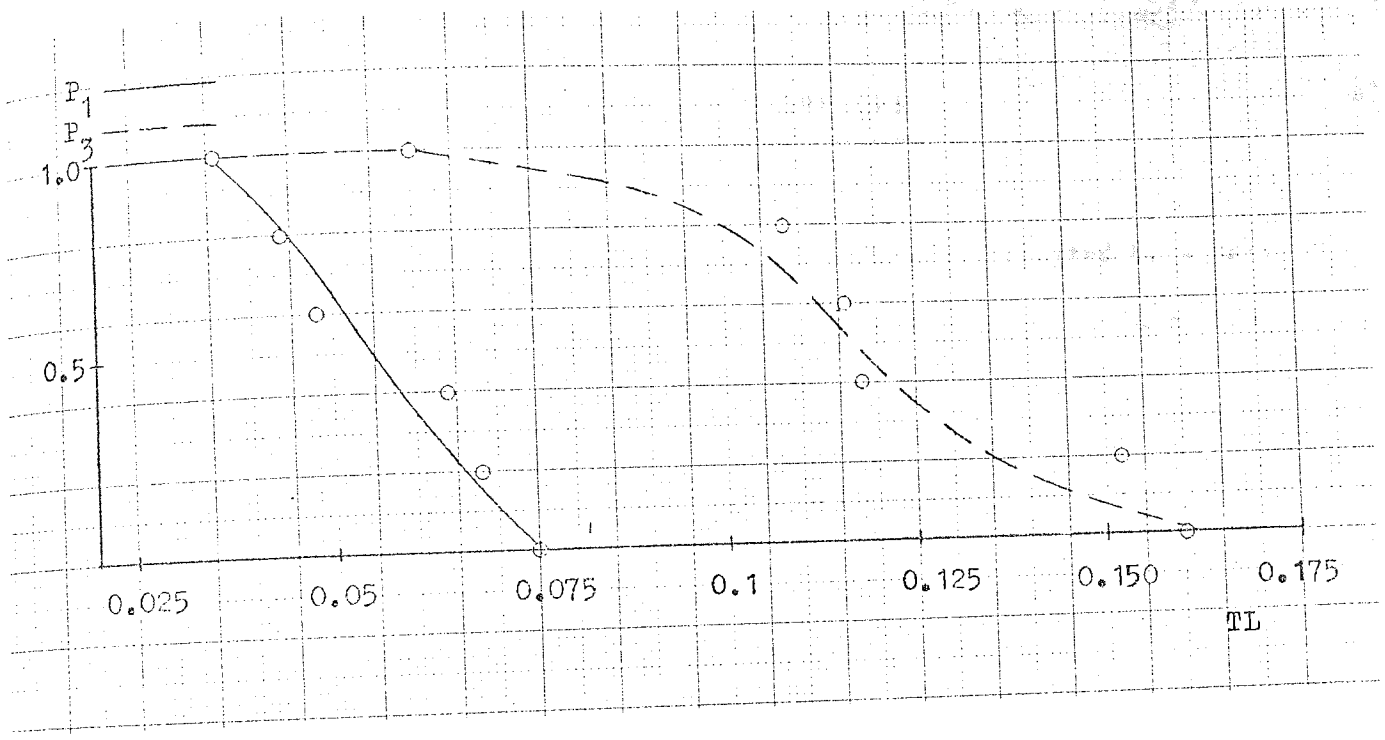

a.

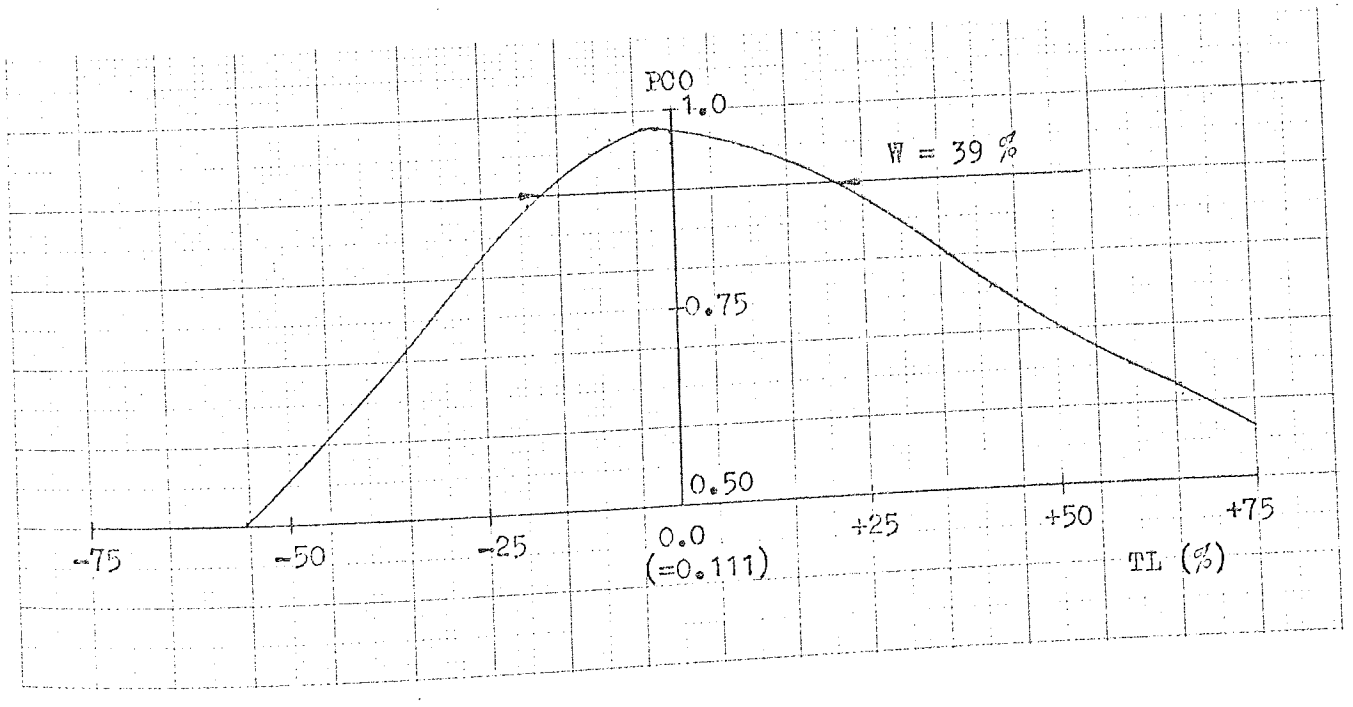

b.

Fig. 9.15 Characteristics of monitoring spalling fatigue by autocorrelation analysis.

LIST OF REFERENCES

1. Yamamoto T, "On Critical Speeds of a Shaft Sipported by a Ball Bearing", Journal of Applied Mechanics, June 1959.
2. Harris, T.A.,Roller Bearing Analysis, Wiley, 1966.
3. Eschmann, P., Ball and Roller Bearings, Heyden, 1958.
4. Dowson, D. and Higginson, G.R., "Theory of Roller Bearing Lubrication and Deformation", App.III, Lubrication and Wear Convention 1963, Inst.Mech.Engrs.
5. Lundberg, G. and Palmgren, A., "Dynamic Capacity of Rolling Bearings", Acta Polytechnica 1947, No.7.
6. Goodelle, R.A., Derner, W. and Root, L.E., "Determination of Static Load Distributions from Elastic Contacts in Rolling Element Bearings", ASLE trans. No 4, Vol.14.
7. Dowson, D. and Higginson, G.R., "Elasto Hydrodynamic Lubrication", Pergamon Press, 1965.
8. SLANG Manual, Hawker Siddely Dynamics Limited.
9. Miles, J.W., "Integral Transforms", Chapter 3 in "Modern Mathematics for the Engineer", Part 2, McGraw-Hill, 1956.
10. Pipes and Harvill, "Applied Mathematics for Engineers and Physicists", McGraw-Hill, 1970.
11. Champeney, D.C.,"Fourier Transforms and their Physical Applications" Academic Press, 1973.
12. Bendat, J. and Piersol, A., "Random Data: Analysis and Measurement Procedures", John Wiley & Sons Inc., 1971.
13. Edited by Harris and Crede, "The Shock and Vibration Handbook I-III" McGraw-Hill, 1961.

14. Hurty, W. and Rubinstein, M., "Dynamics of Structures", Prentice-Hall, 1964.

15. Meirowitch, L., "Analytical Methods in Vibrations", MacMillan,1967.

16. "How to use the NOVA and SUPER NOVA", Data General Corp.

17. "DOS Manual", Data General Corp.

18. "FORTRAN IV Manual", Data General Corp.

19. Perret, H., "Elastische Spielschwingungen konstant belasteter Wälzlager" (Elastic Clearance Vibrations of Roller Bearings having constant load), Werkstatt und Betrieb 8, 1950.

20. Meldau, E., "Die Bewegung der Achse von Wälzlagern bei geringen Drehzahlen" (Shaft movements of Roller Bearings at low speed), Werkstadt und Betrieb 7, 1951.

21. Perret, H., "Shwingungen in Wälzlagern bei statisch bestimmter Anstützung" (Vibrations of Roller Bearings being statically determinate), VDI Forschungsheft 434,1952.

22. Barakov and Shavrin., "Influence of Radial Clearance on Vibration Spectra of high speed ball bearings", Vestnik Mashinostroeniya, No.6, 1969, (in Russian).

23. Tallian, T. and Gustafsson, O., "Study of the Vibration Characteristics of Bearings", US Navy Contract NObs 78552, US Dept. of the Navy, Bureau of Ships, 1963.

24. Tallian, T. and Gustafsson, O., "Progress in Rolling Bearing Vibration Research and Control", ASLE - ASME Lubrication Conf. WAshington 1964, ASLE preprint No. 64-LC-27.

25. Tamura, A., "On the Vibrations caused by Ball Diameter Differences in a Ball Bearing", Trans.JSME, Vol.11, No.44, 1968.

26. Tamura, A. and Taniguchi, O., "Ball Bearing Vibrations - Second Report on the Subharmonic Vibration of order $\frac{1}{2}$ caused by Passing Balls", Trans.JSME 26, 1960.

27. Tamura, A. and Taniguchi, O., "Ball Bearing Vibrations - Third Report on the Axial Vibration caused by Passing Balls", Trans. JSME 26, 1960.

28. Tamura, A. and Taniguchi, O., "Ball Bearing Vibrations - Fourth report on the Non-linear Vibrations in Axial Direction", Trans.JSME 27, 1961.

29. Lohman, G., "Untersuchung des Laufgeräushes von Wälzlagern" (Investigation of running noise of Roller Bearings) Konstruktion 5, 1953.

30. Halm, G. and Woithe, H., "Untersuchungen über das Schwingungsverhalten von Radial - Rillenkugellagern" (Investigation of vibration characteristics of Radial Deep Groove Ball Bearings), Maschinbautautechnik 19, 1970, Part I Vol.10 and Part II of Vol.11.

31. Lura and Walker, "Bearing Noise Reduction", ASME Paper No.720733, 1972.

32. Kutchev and Pavlov, "Influence of Roller Bearing Clearance on Vibration", Russ.Eng.J. Part 9, 1974.

33. Yhland, E., "Waviness measurement - An Instrument for quality control in Rolling Bearing Industry", Inst.Mech.Eng. Conference on Properties and Metrology of Surfaces, 1968.

34. Yamamoto, T. and Ishida, Y., "The Particular Vibration Phenomena due to Ball Bearings at the Major Critical Speed",

35. Tamura, A., "On the Vibration Caused by Ball Diameter Differences in a Ball Bearing", Bull.JSME,Vol.11,1968.

36. Furness, "Vibration Monitoring", Industrial Electronics, Vol.5, 1967.

37. Balderstone, H., "The Detection of Incipient Failure in Bearings", J. of Materials Evaluation, June 1969.

38. Ballas, "Periodic Noise in Bearings", SAE Paper No.690756.

39. Yhland E., and Johansson, L., "Analysis of Bearing Vibration", Aircraft Eng., Vol.42, No.12, 1970.

40. Gustafsson, O. and Tallian, T., "Detection of Damage in Assembled Rolling Element Bearings", ASLE Trans.5, 1962.

41. Weichbrodt, B., "Mechanical Signature Analysis, a new tool for product assurance and early fault detection", 5th Reliability and Maintainability Conf.Proc., July 18 - 20 1966.

42. Gershman and Povarkov, "The Investigation of Spectral and Correlation Characteristics of Ball Bearing Vibrations", The 6th International Conf. on Acoustics, Tokyo, 1968.

43. Babkin, A. and Anderson, J., "Mechanical Signature Analysis of Ball Bearings by Real Time Spectrum Analysis", J. of Environmental Sciences, Jan.1973.

44. Bannister and Donato, "Signature Analysis of Turbomachinery", J. of Sound and Vibration, Sept.1971.

45. Botö P, "Detection of Bearing Damage by SPM", Ball and Roller Bearing Engineering No.167, 1971.

46. Howard, P., "Application of Shock Pulse Technology and Vibration Analysis to Rolling Bearing Condition Monitoring", Proc.20th International Symposium Albuquerque New Mexico, May 1974.

47. Broderick J., "Warning of Impending Bearing Failure", Techlink No.1397, Dept. of Trade and Industry.

48. Edited by Pilkey and Cohen, "System Identification of Vibrating Structures", ASME publication 1972.

49. Downham, E. and Woods, R., "The Rationale of Monitoring Vibration on Rotating Machinery in Continuously operating Process Plant", ASME Paper No. 71-Vibr-96.

50. Uhrich, M., "Fast Fourier Transforms without Sorting", IEEE Trans. on Audio and Electroacoustics, June 1969.

51. Tallian, T., "Rolling Contact Failure Controlled through Lubrication" Paper 14 of "Lubrication and Wear: Fundamentals and Application to design", The Inst.of Mech.Eng., Vol.182, Part 3A, 1967.

52. Tallian, T., "Weibull distribution of Rolling Contact Fatigue Life and Deviation thereform", ASLE, No.5, 1962.

53. Scanlan, "Noise in Rolling Element Bearings", ASME Paper 65-WA/MD-6.

APPENDIX I

THE MATHEMATICAL BASIS FOR SPECTRAL ANALYSIS

Fourier Transformation is used widely in this thesis for Spectral Analysis and Mechanical Impedance calculation purposes. Though a lot has been written on these subjects, no reference has been found that treats them in one concept and in a way that is suitable for practical engineering application. The fundamental concepts and relationships will therefore be discussed briefly in this Appendix.

1. INTEGRAL TRANSFORMS

The theory of Integral Transforms is founded on the works of Fourier, Laplace and Cauchy. It is however not until relatively recently that they have reached widespread use among engineers and then in particular for the purpose of operational calculus. The discovery of their potential in this context is due mainly to Heaviside who showed how transforms could be used to reduce several types of differential equations to equations which allowed algebraic manipulations. A readily understood review of the most commonly used Integral Transforms can be found in Chapter 3 of Ref.(9).

An Integral Transform has the general form

$$F(s) = \int_a^b K(s,x)f(x)dx \quad \ldots\ldots\ldots\ldots\ldots\ldots (I.1)$$

where F(s) is the transform of f(x) and K(s,x) is called the "kernel" (core) of the transform. It is thus clear that the characteristics of the transform is determined by the kernel, K, and the limits of integration, a and b.

Two important and closely related transforms are Laplace Transforms and Fourier Transforms with kernels e^{-sx} and e^{-jrx} and limits $a = 0$; $b = \infty$ and $a = -\infty$; $b = \infty$ respectively or

Laplace Transform $$F(s) = \int_0^\infty e^{-sx} f(x)dx \quad \text{.....(I.2)}$$

s complex

Fourier Transform $$F(r) = \int_{-\infty}^{\infty} e^{-jrx} f(x)dx \quad \text{.....(I.3)}$$

r real

The Fourier Transform is often looked upon as a special case of the Laplace Transform. The usefulness of the Laplace Transform lies to a great extent in the simple form into which its derivatives are transformed $(L(f^{(n)}(x)) = s^n F(s) - \sum_{i=1}^{n} s^{n-i} f^{(i-1)}(0))$ and the ease to incorporate initial values. It is therefore used as a standard operational method to solve differential equations. For the purpose of Spectral Analysis however, the Fourier Transform is used and it is with this Transform and its use that the rest of this Appendix will deal.

2. FOURIER SERIES AND THE FOURIER INTEGRAL

The use of Fourier Series to express almost arbitrary, periodic functions is a well known technique. The may be less common complex form of Fourier Series does, although fundamentally not different from the trigonometric form, offer not only the advantage of being more compact and convenient but it also clearly shows the relationship between Fourier Series and the Fourier Transform. Certain conditions must be fulfilled for a function to be expandable into a Fourier Series. It must be periodic ($f(t) = f(t+T)$) and it must be single valued, have a finite number of maxima and minima and have only finite discontinuities, although a finite number of delta functions are allowed. These are the Dirichlet conditions and obviously almost any periodic function that occurs

in practice will fulfil these conditions. If the conditions are fulfilled it can be shown that a sum of a series of harmonics (with the fundamental frequency equal to 1/T) exists and converges towards f(t) as the number of harmonics approaches infinity. Hence,

$$f(t) = \sum_{n=-\infty}^{n=\infty} a_n e^{jn \frac{2\pi}{T} \cdot t} \quad \ldots\ldots\ldots\ldots\ldots\ldots (I.4)$$

Where the Fourier coefficients, a_n, are given by

$$a_n = \frac{1}{T} \int_0^T f(u) e^{-jn \frac{2\pi}{T} \cdot u} du \quad \ldots\ldots\ldots\ldots\ldots (I.5)$$

For derivations see for instance Appendix C of Ref.(10). If there is a discontinuity in f(t) the expansion will take a value at this point which is the mean value of the values at both sides of the discontinuity.

Due to the periodicity the limits of integration of Equation (I.5) may be changed to -T/2 to T/2, thus

$$a_n = \frac{1}{T} \int_{-T/2}^{T/2} f(u) e^{-jn \frac{2\pi}{T} \cdot u} du \quad \ldots\ldots\ldots\ldots (I.6)$$

Combine (I.4) and (I.6) gives

$$f(t) = \sum_{n=-\infty}^{n=\infty} \frac{1}{T} \int_{-T/2}^{T/2} f(u) e^{jn \frac{2\pi}{T}(t-u)} du \ldots\ldots (I.7)$$

Substitute $\Delta s = \frac{1}{T}$ which gives

$$f(t) = \sum_{n=-\infty}^{n=\infty} \Delta s \int_{-T/2}^{T/2} f(u) e^{2\pi jn\Delta s\,(t-u)} du \ldots\ldots (1.8)$$

It can then be shown (see Appendix C, Ref.(10)) that if T increases towards infinity, Equation (I.8) will pass over into

$$f(t) = \int_{-\infty}^{\infty} ds \int_{-\infty}^{\infty} f(u)e^{2\pi js(t-u)}du$$

$$= \int_{-\infty}^{\infty} e^{2\pi jst}\, ds \int_{-\infty}^{\infty} f(u)e^{-2\pi jsu}\, du \quad \ldots\ldots\ldots\ldots\ldots (I.9)$$

Equation (I.9) is known as the Fourier Integral and it gives an expression for f(t) by extending the Fourier Series representation to a case where the period of the function f(t) becomes infinity long, i.e. f(t) becomes non-periodic.

3. FOURIER TRANSFORMS

By substituting $\omega = 2\pi s$ and $t = u$, equation (I.9) is rewritten-

$$f(t) = \frac{1}{2\pi} \int_{-\infty}^{\infty} e^{j\omega t}\, d\omega \int_{-\infty}^{\infty} f(t)\, e^{-j\omega t}\, dt \quad \ldots\ldots (I.10)$$

where the last integral is known as the forward Fourier Transform of f or

$$F(\omega) = \frac{1}{2\pi} \int_{-\infty}^{\infty} f(t)\, e^{-j\omega t}\, dt \quad \ldots\ldots\ldots\ldots\ldots (I.11)$$

To obtain the inverse Fourier Transform of $F(\omega)$, insert equation (I.11) into the Fourier Integral formula (I.10)

$$f(t) = \int_{-\infty}^{\infty} F(\omega)e^{j\omega t}\, d\omega \quad \ldots\ldots\ldots\ldots\ldots\ldots (I.12)$$

The two equations (I.11) and (I.12) are known as a Fourier Transform pair. Whether the constant of $\frac{1}{2\pi}$ is positioned in front of the forward or inverse

Transform does not make any difference in principal (Ref.(11) puts the constant in front of the inverse transform),but the form used here highlights the similarities with the Fourier coefficients and the physical interpretation of the Fourier Transform.

The Fourier Transform (I.11) of nonperiodic functions and the Fourier coefficients from Equation (I.4) of periodic functions makes up the frequency domain representation discussed in Chapter 5 for their respective classes of functions. However, as has been indicated in the derivation of the Fourier Integral, the Fourier Transform is a generalisation of the Fourier coefficients to functions of infinite period and thus Fourier series expansion is a subset of Fourier Integral representation. Therefore although $F(\omega)$ is a continuous function in the general case of a nonperiodic function, for a periodic function the Transform will degenerate into discrete delta functions, which occur at the same frequencies in the spectrogram as the harmonics of the Fourier Series. Further, the areas under the delta functions are equal to the modulus of the corresponding Fourier coefficients. Hence the Fourier Transform transforms all functions that fulfil the Dirichlet conditions from time domain to frequency domain or, by using the inverse Transform, from frequency domain to time domain. The presence of peaks of infinite height in the spectrogram of a periodic, stationary function is however inconvenient. To overcome this problem one must start by considering the function that is to be transferred. Functions, or signals, that have finite energy contents (basically transients) will produce a Fourier Transform, the modulus of which is finite for all frequencies. Other signals, like periodic signals or stationary random signals, have a total energy content which increases with time but has a finite energy transfer rate (energy transferred per

unit of time) or in other words, they are finite power signals. For this class of functions the Fourier Transform version below gives finite values also for signals with periodic components

$$F(\omega) = \lim_{T\to\infty} \frac{1}{2\pi T} \int_{-T/2}^{T/2} f(t)e^{-j\omega t}dt \quad \ldots\ldots\ldots\ldots (I.13)$$

$F(\omega)$ is a continuous function which corresponds to the sequence of coefficients of Equation (I.5). If $f(t)$ is purely harmonic, then

$$\begin{cases} F(\omega) = a_n ; \ \omega = n \cdot \frac{2\pi}{T} \\ F(\omega) = 0 \ ; \ \omega \neq n \cdot \frac{2\pi}{T} \end{cases} \quad \ldots\ldots\ldots\ldots\ldots\ldots (I.14)$$

The Transforms can in practice be obtained

1. From published tables (Ref. (11) has a rather large table) provided $f(t)$ has a common, analytical expression, or
2. By evaluating the integrals of Equation (I.11) if $f(t)$ has an analytical expression (residual calculus is often used), or
3. If $f(t)$ does not have an analytical expression or if this is too complicated to be evaluated the integral can be calculated by use of numerical methods.

In the first two cases an analytical expression of the Transform is obtained while in the third case the result will be in the form of a table of figures. If the Transform is used in a physical application the phenomena will be more easily understood and the influence of the parameters will be made clear if $F(\omega)$ has an analytical form. This is however not always possible. If, for instance, $f(t)$ is a measured signal of some kind then numerical methods will have to be employed to evaluate the transform.

4. FAST FOURIER TRANSFORM

Assume that f(t) is a signal the value of which is known only at discrete, equally spaced points, $t = K \cdot \Delta t$; $K = 1,2,.....N$. This is the situation that arises in practise when samples are taken of a signal by scanning it with a Digital Event Recorder or the A/D converter of a computer. Providing Δt is chosen according to certain rules (see Chapter 5) an estimate of a_n can then be calculated. The discrete analogue to Equation (II.5) is thus

$$a_n = \frac{1}{N} \cdot \sum_{K=0}^{K=N-1} f(K\Delta t)\ e^{-2\pi jnK\Delta t} \quad \text{.....(I.15)}$$

Consider the equality of (I.14). For a nonperiodic signal the factor T does not exist. However by making T very large, the increments of $\omega = n \frac{2\pi}{T}$ will become very small and the resulting sequence of $a_0, a_1, a_2, ...a_n, ...a_p$ will be so closely spaced that they will form an adequate estimate of $F(\omega)$. The choice of T in this case is not bound to a fundamental frequency of the signal as is the case in normal Fourier Series expansion, but is only chosen to give a sufficiently closely spaced estimate. Thus, Equation (I.15) can be used as a numerical method of calculating $F(\omega)$ in Equation (I.13). If T is large then P (in the sequence above) will also have to be large to cover a sufficient frequency range. This method is therefore practical only when a high speed digital computer is used. However, the evaluation of the sum will be very time-consuming if P is large, since it involves calculation of trigonometric functions, which is a slow process on computers. This originally prohibited extensive use of digital computers for Frequency Analysis. Around 1965 however, Cooley and Tukey published an algorithm for calculation of the Fourier Series coefficients using a method that is much

more efficient in terms of computer time than the straightforward evaluation of Equation (I.15). There have since been a number of routines designed on similar basic principles but with different characteristics as regards speed, storage requirement and so on. All FFT routines are based on a technique of dividing the sum of Equation (I.15) into a number of sums, each being summed over one of the composite factors of N. These sums can then be used in an iterative way to build up all coefficients a_n. The theory behind this is complicated and will not be described here. For a detailed account see Chapter 9 of Ref.(12). If the condition $N = 2^k$, where k is an integer, is put on the number of samples, the FFT routine becomes particularly efficient and many FFT routines work only with values of N that fulfil this condition. For such a routine the speed of the FFT computation compared with the straightforward summation analysis is at least as good as given below,

$$\frac{\text{(FFT speed)}}{\text{(summation technique speed)}} = \frac{N}{4 \cdot k} \quad \ldots\ldots\ldots\ldots (I.16)$$

For N = 1024 the speed ratio becomes 25.6 .

5. SPECTRAL ANALYSIS BY FOURIER TRANSFORM

In practical analysis of signals associated with vibrations, it is often important to determine the frequency distribution of the signal. For virtually all signals that occur in practice, be they transient, periodic, almost periodic, random, stationary, nonstationary or a mixture of functions belonging to these classes, the Fourier Transform of the signal will yield a function which describes the average frequency composition of the part of the signal that is transformed. Usually the relative phase between the harmonic components are not important for the

interpretation of the Frequency Spectrum and therefore only the modulus of the Fourier Transform is studied. From Equation (I.4) it is apparent that the modulus of the coefficients a_n are in a physical sense the amplitudes of the sinewaves that together form the signal f(t). Bearing in mind that the sequence a_0, a_1, a_2,.....a_N approaches F(ω), the ability of the Fourier Transform to resolve the frequency composition of f(t) becomes evident. Obviously the process of Fourier Analysis much resembles analog, narrowband filtering and it is also, together with other digital filtering methods, sometimes referred to as synthetic filtering. Since Fourier Analysis yields a set of discrete points to form the Frequency Spectrum it resembles an analog, narrowband filter bank rather than the usual analog, narrowband sweep.

6. MECHANICAL IMPEDANCE

Fourier Transforms are used in a context seemingly quite different from Spectral Analysis, namely when used to describe the dynamic characteristics of a mechanical system in terms of the system's Mechanical Impedance. The Mechanical Impedance method provides a black box model for a mechanical system. The Transfer Function of the box relates input force to output displacement, velocity or acceleration. Impedance is defined as the ratio between input force and output velocity in frequency domain. The inverse of Impedance is called Mobility or Admittance while the ratio between force and acceleration is called Apparent Mass.

The Mechanical Impedance function can be based either on theoretical calculations or on experimental measurements. One of the attractions of the method lies in the fact that a complicated system can be divided into elements, the Impedances of which can be obtained independently through

theoretical calculations or experimental measurements, whichever is the most suitable for that particular element, and then combined to give the total Impedance of the system. The total Impedance for a series of sub Impedances is

$$\frac{1}{Z_{tot}} = \sum_{i=1}^{i=n} \frac{1}{Z_i} \quad \text{.....(I.17)}$$

and for parallel sub Impedances

$$Z_{tot} = \sum_{i=1}^{i=n} Z_i \quad \text{.....(I.18)}$$

Chapter 10 of Ref.(13) has an extensive table of Impedances for many common combinations of masses, springs and dampers.

If a reliable, theoretical model exists for the system, the Mechanical Impedance can be derived from the ordinary, differential equations of motion of the system. For instance for the single degree of freedom system defined by the equation of motion below

$$m\ddot{x} + c\dot{x} + kx = f(t) \quad \text{.....(I.19)}$$

the Impedance is obtained by first Laplace Transforming it, assuming zero initial displacement and velocity,

$$ms^2X(s) + scX(s) + kX(s) = F(s) \quad \text{.....(I.20)}$$

Where F(s) is the Laplace Transform of the forcing function and X(s) is the Laplace Transform of the displacement function. Rewrite (I.20) as

$$X(s)\,[ms^2 + cs + k] = F(s) \quad \text{.....(I.21)}$$

By differentiating the displacement function the velocity function is obtained

$$V(s) = s \cdot X(s) \quad \text{.....(I.22)}$$

Substitute V(s) into (I.21)

$$V(s)[ms^2 + cs + k] = s \cdot F(s) \quad \ldots\ldots\ldots\ldots\ldots\ldots (I.23)$$

For Mechanical Impedance application purposes, only the oscillatory case is of interest, thus, substitute $s = j\omega$ in Equation (I.23) which makes the Laplace Transform pass over into a Fourier Transform (see Section I.1).

$$V(\omega)[-m\omega^2 + cj\omega + k] = j\omega \cdot F(\omega) \quad \ldots\ldots\ldots\ldots\ldots\ldots (I.24)$$

The Mechanical Impedance is defined as

$$Z(\omega) = \frac{F(\omega)}{V(\omega)} \quad \ldots\ldots\ldots\ldots\ldots\ldots (I.25)$$

Where $F(\omega)$ is the Fourier Transform of the input forcing function and $V(\omega)$ is the Fourier Transform of the output velocity function. By comparing Equation (I.24) and Equation (I.25) it becomes clear that for this single degree of freedom system the Impedance becomes

$$Z(\omega) = \frac{-m\omega^2 + cj\omega + k}{j\omega} \quad \ldots\ldots\ldots\ldots\ldots\ldots (I.26)$$

or

$$Z(\omega) = c + j\left(m\omega - {}^{k}/_{\omega}\right) \quad \ldots\ldots\ldots\ldots\ldots\ldots (I.27)$$

For complicated mechanical systems it is often not practical to try to establish a mathematical model in this fashion. The shapes of the components of the structure might be too complicated, the boundary conditions not well defined and so on. The accuracy of the results will then be poor in relation to the effort required to obtain them. There are however well established methods to measure the Impedance experimentally. It will now be shown how the Impedance can be calculated from the response of the system when excited by a known forcing function. The forcing function f(t) is an arbitrary function that complies with the Dirichlet conditions. Divide f(t) into very narrow

segments with a width $\Delta\tau$ and height $f(\tau)$. Now define $h(t-\tau)$ as the response of the system at time t after it has been excited by a delta function at time τ. The delta function is a mathematical abstraction which has the value zero for $t \neq \tau$ and infinity for $t = \tau$ and the area between $\delta(t-\tau)$ and the time axis is one. If the system is instead excited by one of the segments of $f(t)$ the system response will be approximately $h(t-\tau) \cdot f(\tau) \cdot \Delta\tau$. The smaller $\Delta\tau$ is, the more accurate is this approximation. If the system is linear the law of superposition holds true and the response at time t of all the segments can be obtained by adding the momentary values of their respective impulse responses up. By letting $\Delta\tau$ approach zero the sum passes over into an integral and the well known Convolution Integral is obtained.

$$x(t) = \int_0^t h(t-\tau) \cdot f(\tau) d\tau \quad \ldots\ldots\ldots\ldots\ldots\ldots (I.28)$$

A more complete derivation can be found in for instance Ref.(14) or Ref.(15). From Equation (I.28) the input-output relationship for the system in frequency domain can easily be obtained. The Fourier Transform of the Convolution Integral namely takes on a particularly simple form and can be found in any Fourier Transform table,

$$FT(x(t)) = FT\left(\int_0^t h(t-\tau) \cdot f(\tau) d\tau\right)$$

becomes

$$X(\omega) = H(\omega) \cdot F(\omega) \quad \ldots\ldots\ldots\ldots\ldots\ldots (I.29)$$

where $X(\omega)$, $F(\omega)$ and $H(\omega)$ are the Fourier Transforms of $x(t)$, $f(t)$ and $h(t)$ respectively. By differentiating both membra of Equation (I.29) and replacing $j \cdot \omega \cdot X(\omega)$ by $V(\omega)$ Equation (I.29) can be written as

$$\frac{F(\omega)}{V(\omega)} = \frac{j\omega}{H(\omega)} \quad \ldots\ldots\ldots\ldots\ldots\ldots (I.30)$$

By comparison with Equation (I.25) it is evident that the Impedance of a linear system can be calculated from the Fourier Transform of the impulse response of the system. In practice it is seldom possible to create a shockpulse that is short and high enough to resemble a delta function but $H(\omega)$ can then instead be obtained from the input and output signals by use of Equation (I.29). If the Impedance function of a system is known, the output from the system when excited by a known forcing function can be obtained from Equation (I.30).

To further clarify the physical interpretation of the Transfer Function $H(\omega)$, assume that the forcing function is a sinewave function, $f(t) = A(\omega_o)\sin\omega_o t$. If the system is linear it will have a particular solution representing steady state response $B(\omega_o)\cdot\sin(\omega_o t - \phi)$. These functions, Fourier Transformed and put into Equation (I.29), gives

$$B(\omega_o)[\delta(\omega-\omega_o)-\delta(\omega+\omega_o)]\cdot e^{j\omega\phi} = H(\omega_o)\cdot A(\omega_o)[\delta(\omega-\omega_o)-\delta(\omega+\omega_o)] \quad .....(I.31)$$

or

$$H(\omega_o) = \frac{B(\omega_o)}{A(\omega_o)}\, e^{j\omega\phi} \quad .....(I.32)$$

The modulus of $H(\omega)$ is

$$|H(\omega_o)| = B(\omega_o)/A(\omega_o) \quad .....(I.33)$$

Which is simply the ratio between the amplitudes of the input and output signals, i.e. the magnification of the system. The argument of $H(\omega)$ is

$$\arg(H(\omega)) = \phi \quad .....(I.34)$$

which is the phase difference between input and output signal or, the phase shift of the system.

It is now possible to get a more intuitive idea of how the knowledge of the Impedance of a system makes it possible to calculate the output signal if the input signal is known, or vice versa, by use of Fourier Transforms of these signals. Each point $(\omega_o; F(\omega_o))$ of the Transform of, say, the output signal, represents a sinewave component of this signal, with amplitude $|V(\omega_o)|$ and phase lag $\arg(V(\omega_o))$. According to the previous paragraph, the response at this particular frequency is created by an input signal, which has the shape of a sinewave with amplitude $|F(\omega_o)| = |V(\omega_o)| \cdot |Z(\omega_o)|$ and a phase lag $\arg(F(\omega_o)) = \arg(V(\omega_o)) + \arg(Z(\omega_o))$. By allowing ω_o to assume all values in the frequency range of interest, the input function is determined. Hence, when Fourier Analysis is used to obtain the Impedance of a system, its function is, as was the case of Spectral Analysis, to determine the frequency distribution of the signals involved.

APPENDIX II

A SYSTEM FOR DIGITAL ANALYSIS OF SIGNALS (DAS).

DAS consists of a suite of programs designed for general purpose signal processing on a high speed, digital minicomputer. The system performs many of the commonly used vibration analysing procedures (previously discussed in Chapter 5 and Appendix I) and it includes, apart from the actual processing algorithms, also all necessary input, output and preprocessing routines. Flexibility and versatility of the system together with ease of operation have been regarded as first priorities but it has also been possible to achieve good efficiency as regards speed and storage capacity.

1. DESCRIPTION OF HARDWARE

The computer used for this work is a so called minicomputer, Data General's Nova 1200, which is shown with its peripherals in picture II.1 and the whole hardware arrangement on a block diagram in Fig. II.2. It is equipped with 24K core memory in its central processor (point 1 in picture II.1) and with a 256K disk (2) and twin magnetic tape cassettes (3) as backing up storage capacity. The computer runs under a Disk Operating System (DOS 05) and the operator controls it from a Teletype (4) keyboard. The machine has a 10 bit A/D converter (5) and an eight channel multiplexer (5). For the use of the DAS program package, only one of the available eight channels is used (channel No. 0, point 9). The A/D converter works with an accuracy of within 0.5%. The peaks of the analog input signal should be in the range ± 5 Volts (peak) but it has an overload

protection up to 10 Volts RMS. In principal the analog signal could come directly from the vibration pick up and the system could be run on line, but for practical reasons the vibration signal is instead recorded on a FM tape recorder (6) and later played back into the A/D converter. To comply with the rules given in Chapter 5, concerning sampling frequency versus frequency contents of the signal, the analog signal is passed through an adjustable bandpass filter (7). The filtered signal is monitored on an oscilloscope (8). The rate at which samples are taken from the input is determined by an external triggering device (9), a tunable "flip-flop", which produces a square-wave signal of about 6.5 Volts (peak). The frequency of the trigger signal can be adjusted with a potentiometer to the desired sampling frequency while being monitored by the counter (10) connected to the count/trig socket. If the data is already digitized and punched on papertape it can be loaded into the system with the fast, optical reader (11). Plotting facilities are provided by the digital plotter, Houston incremental 8" x 11", (12), and for printouts the fast character printer (13) is used. Further information on machine and peripherals is given in Ref. (16).

2. ORGANISATION AND OPERATION OF THE SOFTWAVE

The program package consists of a set of 16 complete ("main") programs, stored on disk in relocatable, binary form, i.e. they can be transferred directly into the central processor without previous compiling and linking. The source programs are written in DGC Fortran IV, see Ref. (18). The DAS system works in an interactive way, making it possible for the operator to control the processing by giving instructions on the Teletype keyboard. The programs can be divided into two categories:

Administrative programs and dataprocessing programs. The administrative programs (DAS, PLOT1) set labels and parameters necessary for the operation of the dataprocessing programs. They do not handle any data and the corespace thus made available is instead used for program instructions. The dataprocessing programs (SAMPLE, PTAPE, CAS, WINDOW, MRVS, PROBDENS, PROBDISTR, AUTOCORR, FFT, PSD, PLOT2, DFPO, ORDAPLOT, AVERAGER) generally have rather few program instructions in order to leave space for sufficient amount of data. The requirements for storage space for data can be quite large even for rather modest amounts of ordinates. For instance, suppose that 1024 ordinates are read into a program. These 1024 datapoints might produce 1024 y-axis coordinates and 1024 x-axis coordinates, in all 3072 (3K) datapoints. If the datapoints are declared as real numbers each data occupies 2 words, i.e. the total space requirement is 6144 words (6K). If the data is complex (which is the case for the FFT routine) each real, complex datapoint occupies 4 words making the total storage requirement 4K + 4K In addition the FFT routine needs 4·NOS K space for intermediate data, in all 12K of the storage space is occupied by data. Since the total available memory space is about 23.5K (the DOS 05 system occupies about 0.5K) it is obvious that the dataprocessing programs have to be short and efficient.

There is only space enough in the central processor for one program at a time. Therefore the whole set of program is stored on disk and programs loaded into core when required. When the system is activated DAS is read into core and started. The program presently in core in relocatable form constitutes the "core image". DAS then lists the routines with code numbers to be used by the operator when calling a routine.

When the operator has given instructions on the Teletype, DAS will call up and activate the wanted routine or routines in sequence. This "calling up" is done in the following manner: The program in the central processor (DAS), is deleted, the wanted program is loaded into core from its diskfile and executed, the core image is again deleted and DAS is again read into core and started at the point where the program swap was initiated. DAS then either calls up a new program, thus going through a sequence of programs, or returns control to the operator at the Teletype keyboard. This technique of swapping programs between core and disk is known as overlaying, see Ref. (17). There are in principal two ways of storing intermediate data during an overlay. For small amounts of data the common block in core is used and is therefore left intact when the rest of the core image is deleted. For bulk storage of data, diskfiles are used. Though they have much longer access time, they have a greater capacity than the common block in core. Thus, the ordinates read from A/D converter or papertape, are stored on diskfile ORDA, the calculated x-axis and y-axis coordinates are stored on diskfiles XAX and YAX and during the averaging process diskfile RYAX is used. All data diskfiles are written in binary code to shorten the access time. As will be described in the next section under GRAPHPLOT, the common block is used to store labels and operating parameters during program swaps.

3. THE PROGRAM UNITS

A sample program is included at the end of this Appendix. Underlined figures are specified by the operator. Questions from the computer are answered with 1 for Yes and 0 for No. The arrangement of software is shown in Fig. (II.3).

Main Program:

DAS

DAS is a fairly large program (about 20K) which administers the system without itself handling any data. It supplies the other programs with instructions and enables the operator to use the system in an interactive way and with a minimum of operating instructions to be typed on the Teletype.

Input Routines:

1. SAMPLE

$NOS_{max} = 5000$

functions: ORDA(J) = ADC(J)· CF

This program handles the A/D conversion, i.e. it digitizes the analog input signal into a sequence of samples. The sampling frequency is set on the external triggering oscillator and is also specified on the Teletype for scaling purposes. Note that if the magnetic tape is speeded up or slowed down, the sampling frequency specified on the Teletype should be (the actual sampling frequency)· (recording speed)/(playback speed). The calfactor transfers the readings from the A/D converter into suitable units. When NOS, CALFACT and SFREQ are specified the computer responds by printing PAUSE and the execution is halted. The operator can now start the tape-recorder and check on the monitoring oscilloscope that the recording is free from "drop outs" and other disturbances. When the carriage return key on the Teletype is pressed, an assembler subroutine activates the A/D converter and for each pulse from the external trigger one sample is taken from the analog input and transferred into core. When the specified number of samples (NOS) have been read, each sample is multiplied with the calibration factor whereafter the sequence of samples is written on diskfile ORDA.

2. PTAPE

NOS_{max} = 5000

function: ORDA(J) = PTAPE(J)·CF

Data already digitized and stored on papertape can be loaded into the computer using this routine. The data should be punched on the tape in ASCII code and in the following sequence: Integers, carriage return, line feed, integers, carriage return, line feed, and so on. A parity check on mispunching is automatically done and if an error is detected the execution of the program is halted.

Preprocessing Routines:

3. CAS

function: ORDA(J) = (ORDA(J)-MEAN)/RANGE

The contents of diskfile ORDA is read into core and the file is deleted. The original ordinates are then normalised (centered and scaled) and the normalised ordinates are written back on diskfile ORDA. RANGE should be specified as the upper limit of the data minus the lower limit of the data.

4. WINDOW

$NODS_{max}$ = 1024

function: ORDA(J)=(1+SIN(J·2·π/NODS-π/2))·ORDA(J)

With this program the ordinates on diskfile ORDA are read into core and multiplied with the Hanning window function described in Chapter 5. The original content of the diskfile is deleted and the new ordinates are written back on ORDA.

Processing Routines:

Before using any processing routines (except MRVS) the ordinates must be centered and scaled by the use of CAS.

5. MRVS

$$\text{function: MEAN} = \frac{1}{NOS} \sum_{J=1}^{NOS} ORDA(J) \qquad VAR = \sum_{J=1}^{NOS} \frac{(ORDA(J)-MEAN)^2}{NOS}$$

$$RMS = \sqrt{\sum_{J=1}^{NOS} \frac{ORDA(J)^2}{NOS}} \qquad SDEV = \sqrt{VAR}$$

This routine reads the contents of diskfile ORDA and calculates the mean value, the root mean square, the variance and the standard-deviation of the ordinates. The result is printed on the Teletype. Note that this program should normally be used before using CAS or WINDOW.

6. PROBDENS

function: YAX(J)=(number of ordinates falling between XAX(J) and XAX(J+1)$\cdot \frac{100}{NOS}$

The probability Density function is calculated using this routine. The range of data (specified in CAS) is divided into 64 intervals and the number of ordinates falling within each interval makes, after being divided by NOS and multiplied with 100, up the y-coordinates of the histogram. The corresponding x-axis coordinates are also calculated and the coordinates of the two axis are then written separately on the two diskfiles XAX and YAX.

7. PROBDISTR

$$\text{function: } YAX(J) = \sum_{K=1}^{J} YAX(K); \quad J = 1,2,.....64$$

The Probability Distribution Function is the cumulative histogram of the Probability Density Function and is thus calculated using the contents of diskfile YAX created by PROBDENS. Hence, before calling PROBDISTR, PROBDENS must have been executed as the preceding program. PROBDISTR then reads diskfile YAX, calculates the cumulative values and writes them back on YAX.

8. AUTOCORR

$$NODS_{max} = 3000$$

$$\text{function: } YAX(J) = \frac{1}{NODS-LAG} \sum_{L=1}^{NODS-LAG} ORDA(L) \cdot ORDA(L+J)$$

When the operator has specified NODS and LAG (expressed in number or ordinates) the contents of ORDA are read into core, the Autocorrelation function is calculated and written on YAX and the corresponding x-coordinates calculated and written on XAX. The computation is rather time consuming so LAG and NODS should not be chosen unnecessarily large.

9. FFT

$$NODS_{max} = 1024$$

$$\text{function: } C(J) = \frac{1}{NODS} \sum_{K=0}^{NODS} ORDA(K)\, e^{\pm j 2\pi JK/NODS}$$

$$YAX(J) = 2 \cdot |C(J)|$$

This program calculates the Fourier coefficients of the ordinates. Forward or inverse transform can be chosen by the operator. If the signal is a non transient the ordinates should first be weighted using the window routine. The first NODS ordinates are read into core from ORDA and their

complex Fourier Transform is calculated. The transformation is carried out by a Fourier Transform subroutine described by M. Uhrich in Ref. (50) This routine is unusually compact but is not very fast, 1024 ordinates take about 90 seconds to transform. The output of the subroutine consists of complex numbers but for most vibration analysis work the phase is not interesting and therefore the modulus of the transform is calculated and written on diskfile YAX and corresponding x-axis co-ordinates on XAX. Note that the program works only if NODS = 2^N with N = 1,2,.....10.

10. PSD

function: YAX(J) = YAX(J)^2/2

The Power Spectral Density function is calculated using the results from the FFT routine. Hence PSD can only be called immediately after FFT.

Output Routines:

11. GRAPHPLOT

When GRAPHPLOT is called, PLOT1 is first read into core and started. The operator can then specify a graph number which will be drawn on the graph, thus helping to identify the plot with the computer printout. When the carriage return key is pressed the plotter will start working and the operator should before doing this have positioned the pen at the top left corner of the graph-sheet. PLOT1 will then draw and tick the axis and write the proper labels. The information required to do this is given from previous stages of the processing as the sequence of programs is gone through. For instance when a Fourier Analysis is carried out the following sequence is gone through: When SAMPLE is

called the label "A/D-CONV" is set and the value assigned to SFREQ is used for scaling of the x-axis. The setting of RANGE in CAS gives the correct scaling of the y-axis whereas when FFT is called the label "MOD OF FFT" and the axis labels "frequency (Hz)" and "acceleration (g)" is set and the positioning of the axis on the graph sheet is determined. Hence when the chosen sequence of programs is gone through all information that is required for the plotting will be available for PLOT1 in the commonblock. When labels and axis are drawn the pen is positioned at the origin, PLOT1 is deleted and PLOT2 is read into core. The pen position is defined as zero-zero and YAX and XAX are read into core, scaled and plotted. A new graph sheet is then put into position.

12. ORDAPLOT

NODS ≤ NOS

This program is used to plot the first NODS ordinates of diskfile ORDA. The ordinates are read into core and written back on diskfile YAX and the corresponding x-axis coordinates are created and written on XAX. PLOT1 and PLOT2 are then called in sequence.

13. DFPO

To obtain more accurate outputs than are possible on a graphplot the program DFPO (diskfile printout) can be used. ORDA, XAX and YAX are read into core and printed. Note that the autocorrelation y-axis values will be biased with $+(\text{RANGE})^2/4$.

Auxillary Routines:

14. REPETITION (included in DAS but calling the separate program AVERAGER)

For averaging purposes some of the program sequences can be repeated automatically and the average of the results taken. The following sequencies can be repeated in this way by use of REPETITION: 1/SAMPLE, CAS, WINDOW, FFT, AVERAGER; 2/SAMPLE, CAS, PROBDENS, AVERAGER; 3/SAMPLE, CAS, AUTOCORR, AVERAGER. To set the parameters required for these functions (NOS, RANGE, NODS and so on) the operator first goes through the wanted sequence in the usual way and sets the parameters. These are then stored in the commonblock and can be used when needed during the repetition of the program. The number of repetitions and the sequence wanted is set by the operator in REPETITION. When the sequence is gone through, AVERAGER is called up and adds the coordinates in YAX to the coordinates in RYAX, the latter being set at zero when the first sequence is started. When the sequence is gone through the specified number of times each y-axis coordinate in RYAX is divided by the number of repetitions and written back to YAX thus making them available for the output routines. No separate sequences are available for obtaining averaged results from PROBDISTR and PSD but since these functions use the output of PROBDENS and FFT such results can also be obtained by calling respective programs up after the repetitions have been gone through.

15,16,17/DUMMY1, DUMMY2, DUMMY3

These dummy file names makes it possible to link additional routines to the system simply by transferring them to diskfiles with the names IOTHER.SV;IIOTHER.SV;IIIOTHER.SV; respectively. The program must be written in Fortran or Assembler language and must be complete (main) programs, compiled and linked. They must have a commonblock identical with the other programs in the system.

18. STOP

When the operator wishes to leave DAS and return control to the computer's normal operating system this function is used.

Examples of printouts from DAS runs are given on pages II.13 - II.18 with the associated graphs on pages II.19 - II.27.

```
R
DAS


DIGITAL ANALYSIS ØF SIGNALS

INPUT:
READ A/D-CØNVERTER (1)
READ PAPERTAPE (2)
PREPRØCESSING:
CENTER AND SCALE DATA (3)
WINDØW (4)
PRØCESSING:
MRVS (5)
PRØBABILITY DENSITY FUNCTIØN (6)
PRØBABILITY DISTRIBUTIØN FUNCTIØN (7)
AUTØCØRRELATION FUNCTIØN (8)
FØURIER TRANSFØRMATIØN (9)
PØWER SPECTRAL DENSITY FUNCTIØN (10)
ØUTPUT:
GRAPHPLØT (11)
PLØT ØRDINATES (12)
PRINT (13)
AUXILLARY:
REPETITIVE PRØCESSING (14)
DUMMY1 (15)
DUMMY2 (16)
DUMMY3 (17)
STØP (18)


RØUTINE NØ=1

SAMPLE
CALFACTØR=0.00957
NØS=3500
SAMPLING FREQ=10000
PAUSE
STØP


RØUTINE NØ=5

MRVS
MEAN=   0.0016    RMS=    0.7084    VAR=     0.5019    SDEV=    0.7084
STØP


RØUTINE NØ=3

CENTER AND SCALE
RANGE=5
STØP
```

COMMENTS:

The letter "R" implies that the computer is operating under its normal operating system. To activate the DAS-system, type DAS

Listing of available routines

Chose routine

Input signal is a sine wave of 1 units amplitude at 250 Hz frequency

Set y-axis scale

```
RØUTINE NØ=12

ØRDAPLØT
NØ. ØF DATAPØINTS=2000
STØP

GRAPH PLØT
GRAPH NØ=1
STØP
STØP
```

COMMENTS:

The x-axis scale is calculated from sampling frequency and number of data points

```
RØUTINE NØ=8

AUTØCØRR
LAG-RANGE=200
NØ.ØF DATAPØINTS=1000
STØP
```

Note that autocorr(0)= =VAR=0.5

```
RØUTINE NØ=11

GRAPH PLØT
GRAPH NØ=2
STØP
STØP
```

```
RØUTINE NØ=6

PRØBDENS
STØP
```

```
RØUTINE NØ=11

GRAPH PLØT
GRAPH NØ=3
STØP
STØP
```

For PROBDENS and PROBDISTR the previous y-axis scale now becomes the x-axis scale

```
RØUTINE NØ=7

PRØBDISTR
STØP
```

```
RØUTINE NØ=11

GRAPH PLØT
GRAPH NØ=4
STØP
STØP
```

COMMENT:

```
RØUTINE NØ=1

SAMPLE
CALFACTØR=0.00957
NØS=1024
SAMPLING FREQ=1000
PAUSE
STØP
```

Take a new series of samples

```
RØUTINE NØ=3

CENTER AND SCALE
RANGE=5
STØP

RØUTINE NØ=9

FFT
NUMBER ØF DATAPØINTS=1024
FØRWARD?=1
INVERSE?=0
STØP
```

FFT without previous hanning. Note the broad base of the peak at 150 Hz

```
RØUTINE NØ=11

GRAPH PLØT
GRAPH NØ=5
STØP
STØP

RØUTINE NØ=4

HANNING WINDØW
NØ. ØF DATAPØINTS=1024
STØP

RØUTINE NØ=12

ØRDAPLØT
NØ. ØF DATAPØINTS=1024
STØP

GRAPH PLØT
GRAPH NØ=6
STØP
STØP

RØUTINE NØ=9

FFT
NUMBER ØF DATAPØINTS=1024
FØRWARD?=1
INVERSE?=0
STØP
```

Shows the effect of the window function

COMMENTS:

```
ROUTINE NO=11

GRAPH PLOT
GRAPH NO=7
STOP
STOP
```

Compare with graph 5

```
ROUTINE NO=1

SAMPLE
CALFACTOR=0.00957
NOS=512
SAMPLING FREQ=1000
PAUSE
STOP
```

Take a new sample

with only 512 points

```
ROUTINE NO=3

CENTER AND SCALE
RANGE=2.5
STOP
```

```
ROUTINE NO=4

HANNING WINDOW
NO. OF DATAPOINTS=512
STOP
```

```
ROUTINE NO=9

FFT
NUMBER OF DATAPOINTS=512
FORWARD?=1
INVERSE?=0
STOP
```

```
ROUTINE NO=11

GRAPH PLOT
GRAPH NO=8
STOP
STOP
```

This smaller sample

gives a broader peak -

i.e. poorer frequency

resolution

```
ROUTINE NO=10

P.S.D.
STOP
```

```
ROUTINE NO=11

GRAPH PLOT
GRAPH NO=9
STOP
```

The height of the peak

at 150 Hz represents

the Mean Square (VAR) value

of the component at this

frequency

```
ROUTINE N0=1

SAMPLE
CALFACTOR=0.00957
NOS=1024
SAMPLING FREQ=1000
PAUSE
STOP

ROUTINE N0=3

CENTER AND SCALE
RANGE=5
STOP

ROUTINE N0=4

HANNING WINDOW
NO. OF DATAPOINTS=1024
STOP

ROUTINE N0=9

FFT
NUMBER OF DATAPOINTS=1024
FORWARD?=1
INVERSE?=0
STOP

ROUTINE N0=14

AVERAGING ROUTINE
NUMBER OF REPETITIONS=2
FFT?=1

SAMPLE
CALFACTOR=0.00957
PAUSE
STOP

CENTER AND SCALE
STOP

HANNING WINDOW
STOP

FFT
STOP

AVERAGING SUB
STOP

SAMPLE
CALFACTOR=0.0
PAUSE
STOP
CENTER AND SCALE
STOP

HANNING WINDOW
STOP

FFT
STOP
```

COMMENTS:

Before calling "Repetetive Processing", call the required sequence of routines to set operating parameters

Since the cal.factor is set to zero in the second loop, the average amplitude of the signal is 0.5 units

RØUTINE NØ=13

COMMENTS:

DISKFILE PRINTØUT

ØRDA	XAX	YAX
0.00000	0.97656	0.00006
0.00000	1.95312	0.00010
0.00000	2.92968	0.00004
0.00000	3.90625	0.00004
0.00000	4.88281	0
0.00000	5.85937	
0.00000		
0.00		0.00058
	137.69500	0.00087
0000	138.67100	0.00119
0.00000	139.64800	0.00178
0.00000	140.62500	0.00102
0.00000	141.60100	0.00072
0.00000	142.57800	0.00116
0.00000	143.55400	0.00277
0.00000	144.53100	0.00422
0.00000	145.50700	0.00788
0.00000	146.48400	0.22464
0.00000	147.46000	0.50318
0.00000	148.43700	0.27997
0.00000	149.41400	0.00910
0.00000	150.39000	0.00389
0.00000	151.36700	0.00317
0.00000	152.34300	0.00214
0.00000	153.32000	0.00110
0.00000	154.29600	0.00127
0.00000	155.27300	0.00128
0.00000	156.25000	0.00039
0.00000	157.22600	0.00005
0.00000	158.20300	0.00034
0.00000	159.17900	0.00061
0.00000	160.15600	0
0.00000	161.13200	
0.00000	162	
0.00000		0.00012
0	.00	0.00026
	496.09300	0.00024
000	497.07000	0.00014
0.00000	498.04600	0.00035
0.00000	499.02300	0.00023
0.00000	500.00000	0.00039
0.00000		
0.00000		
0.00000		
0.00000		
0.00000		
0.00000		
0.00000		
0.00000		
0.00		

As shown by the printout, the actual frequency of the analysed signal is 147.5 Hz

RØUTINE NØ=18
STØP
R

The "R" implies that control is now returned to the computer's normal operating system

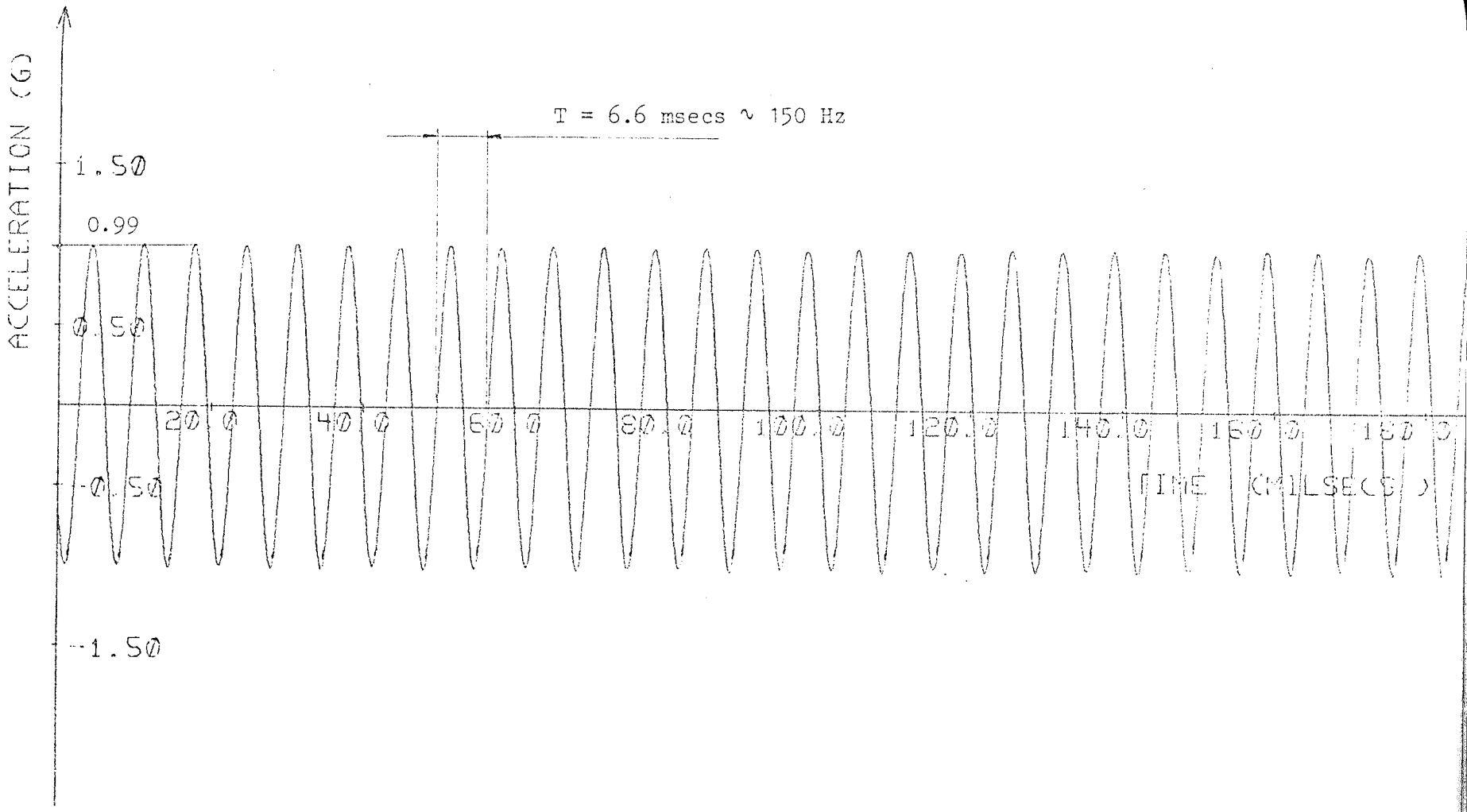

A/D--CONV. ORDINATES GRAPH NO: 1

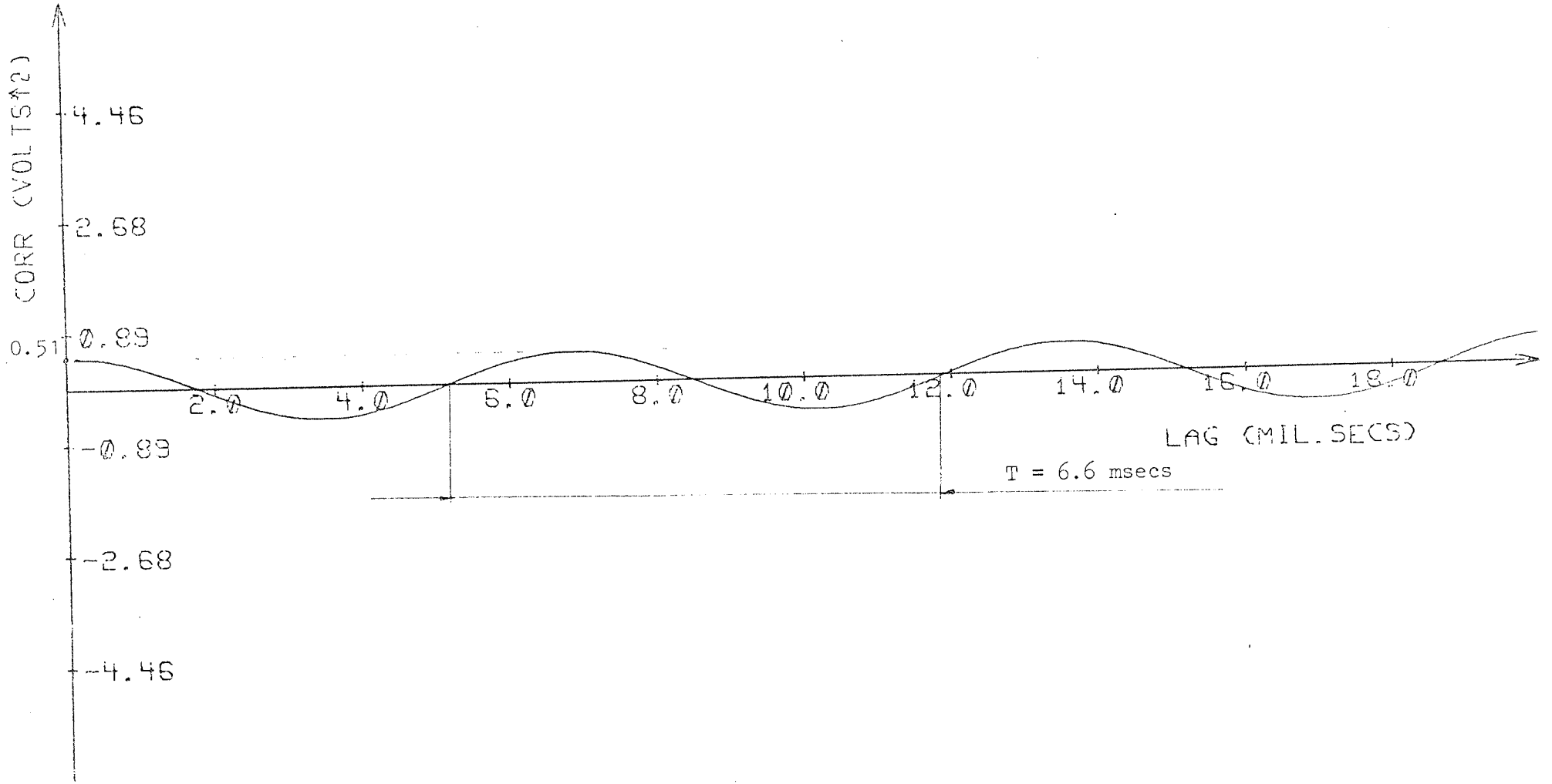

A/D-CONV. AUTOCORR

GRAPH NO: 2.

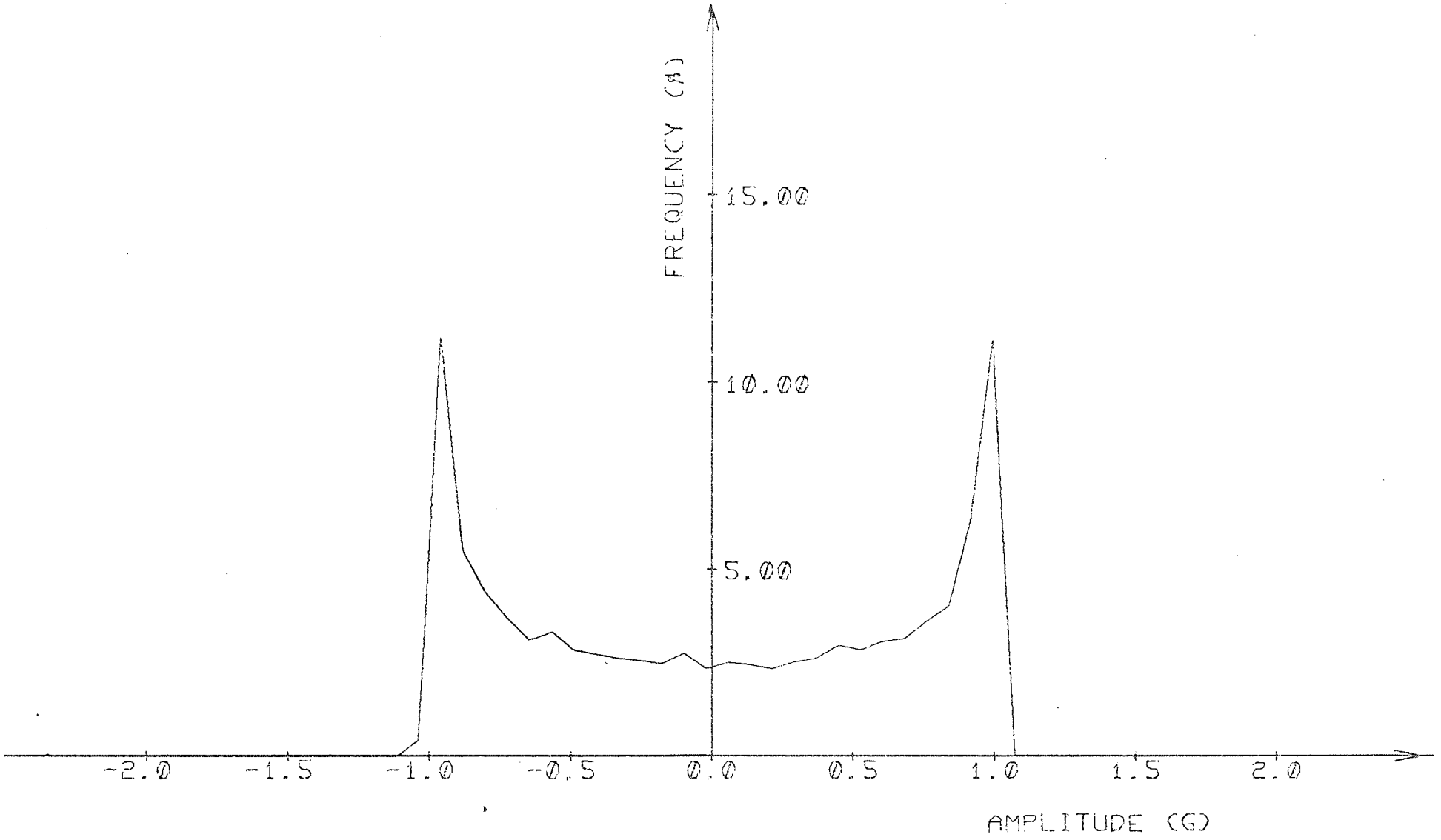

A/D-CONV. PROBDENS GRAPH NO: 3.

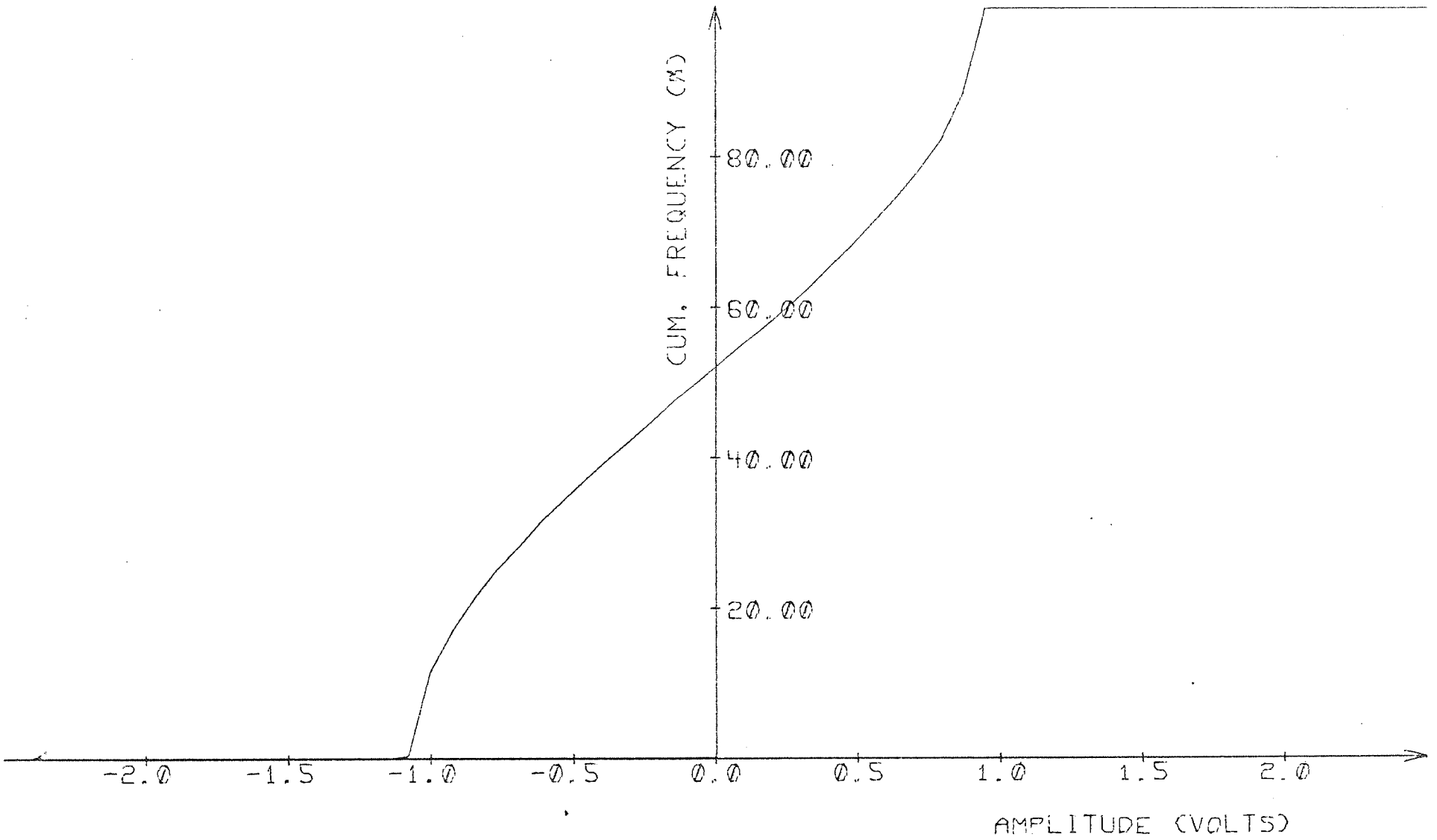

A/D-CONV. PROBDISTR GRAPH NO: 4.

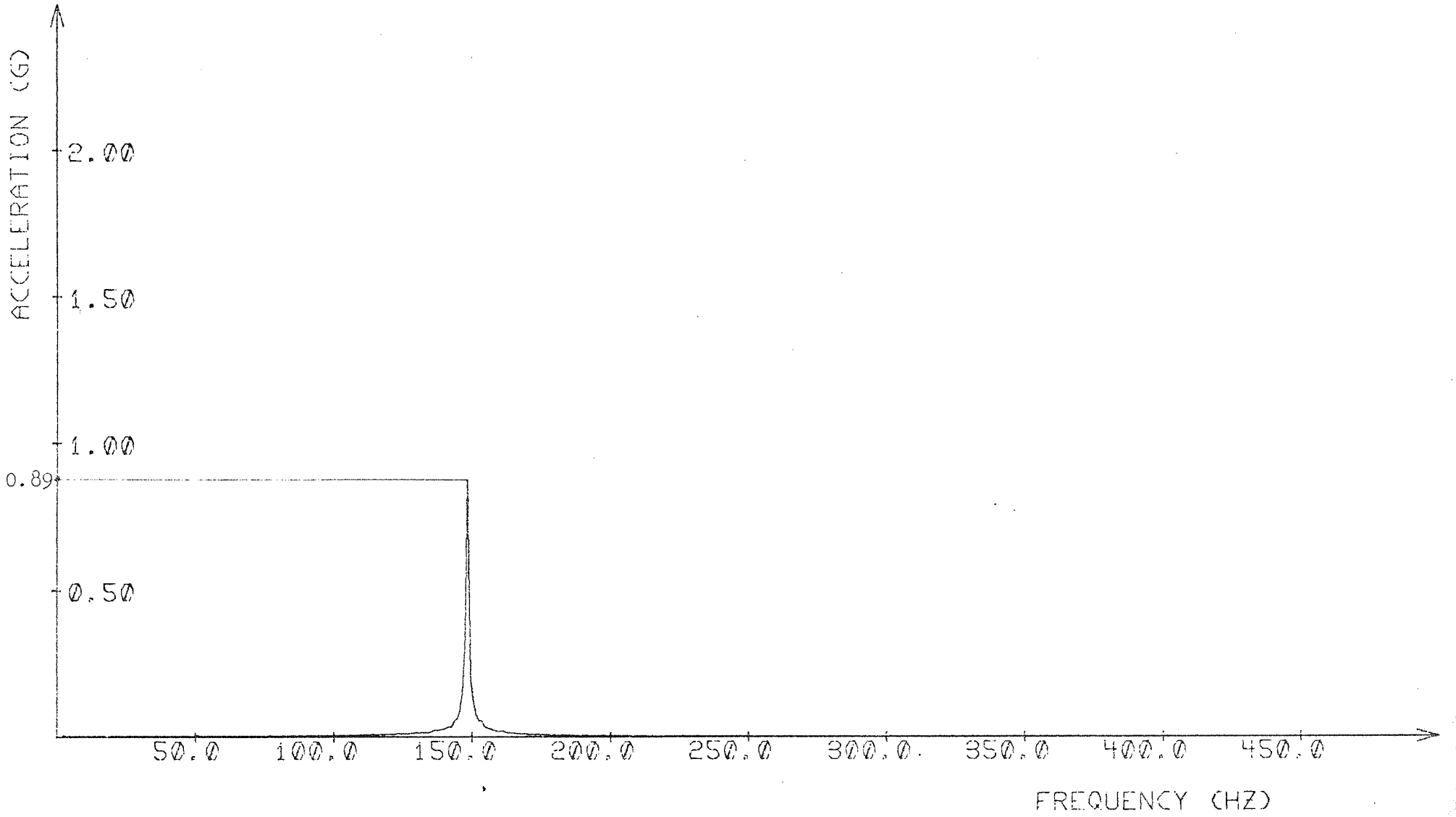

A/D-CONV. MOD OF FFT GRAPH NO: 5.

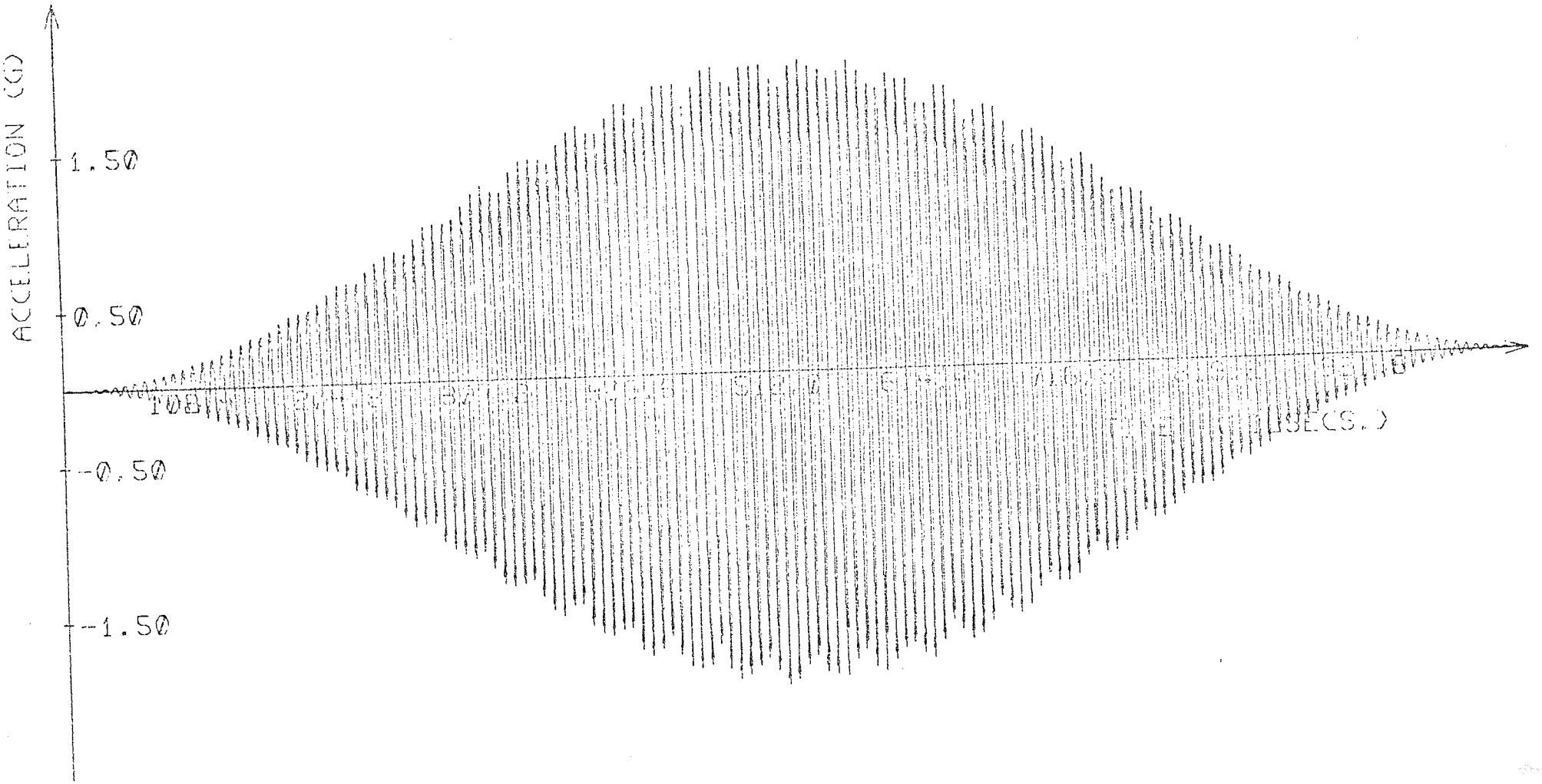

A/D-CONV. ORDINATES

GRAPH NO: 6.

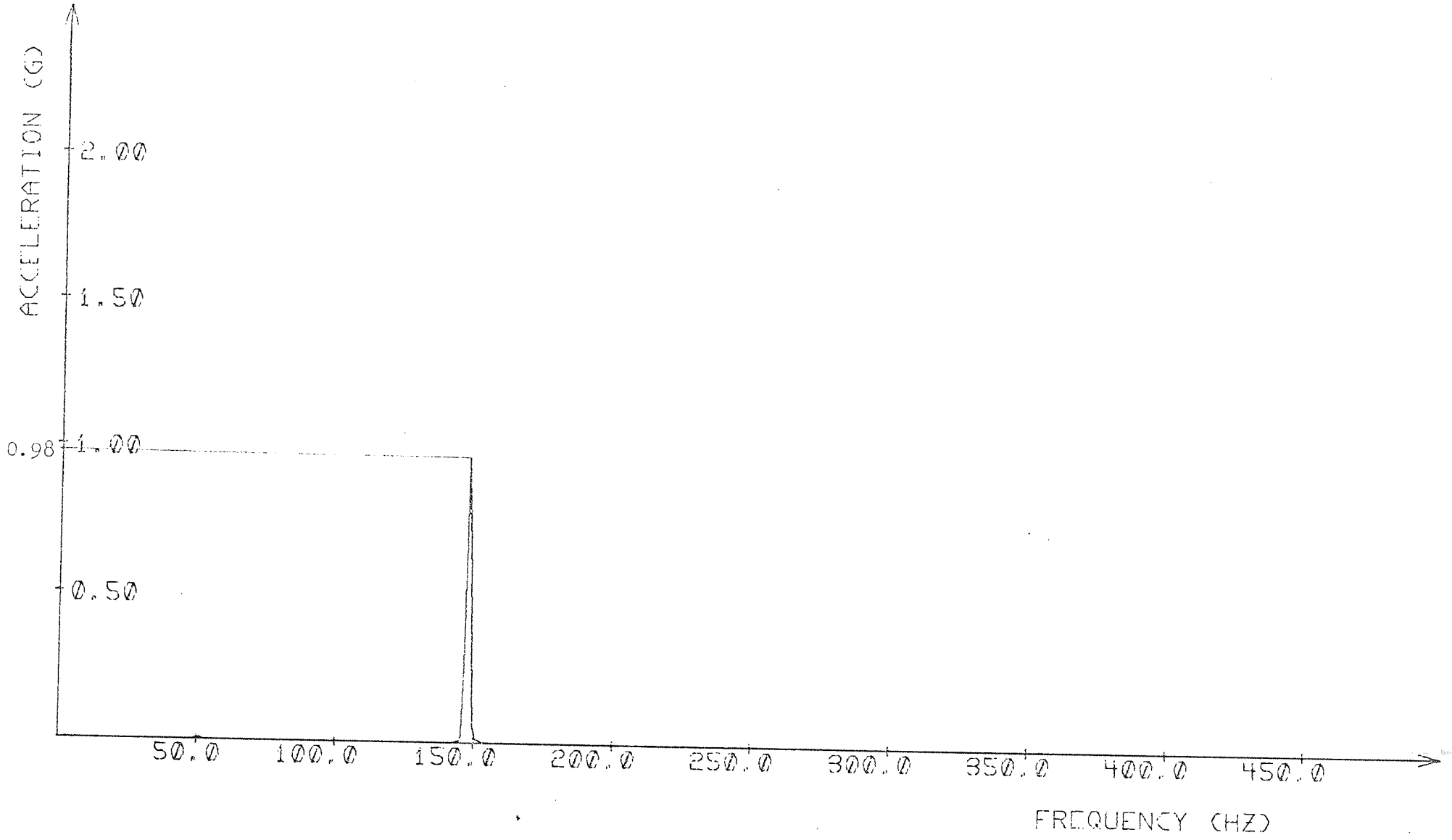

A/D-CONV. MOD OF FFT

GRAPH NO: 7.

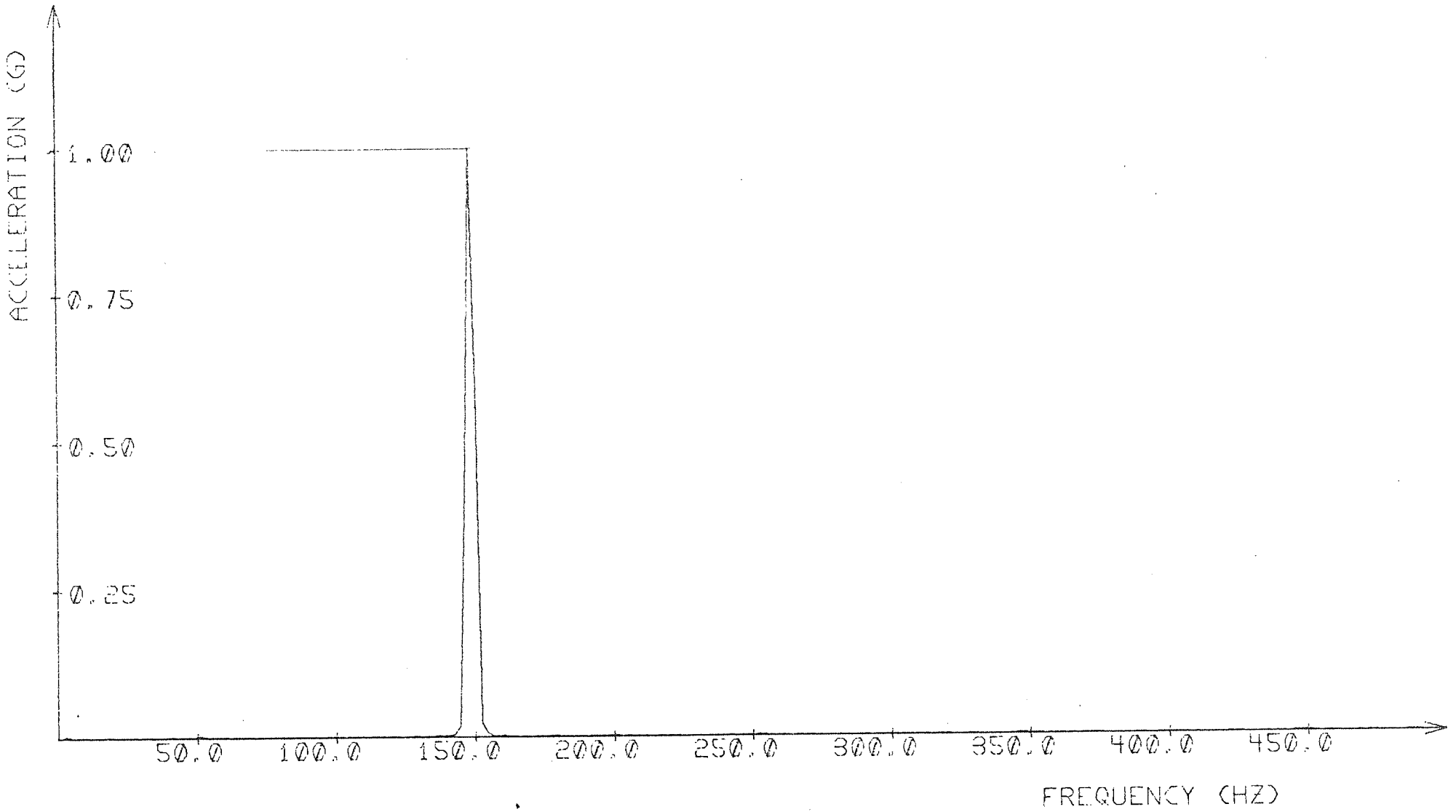

- 92'11 -

A/D-CONV. MOD OF FFT GRAPH NO: 8.

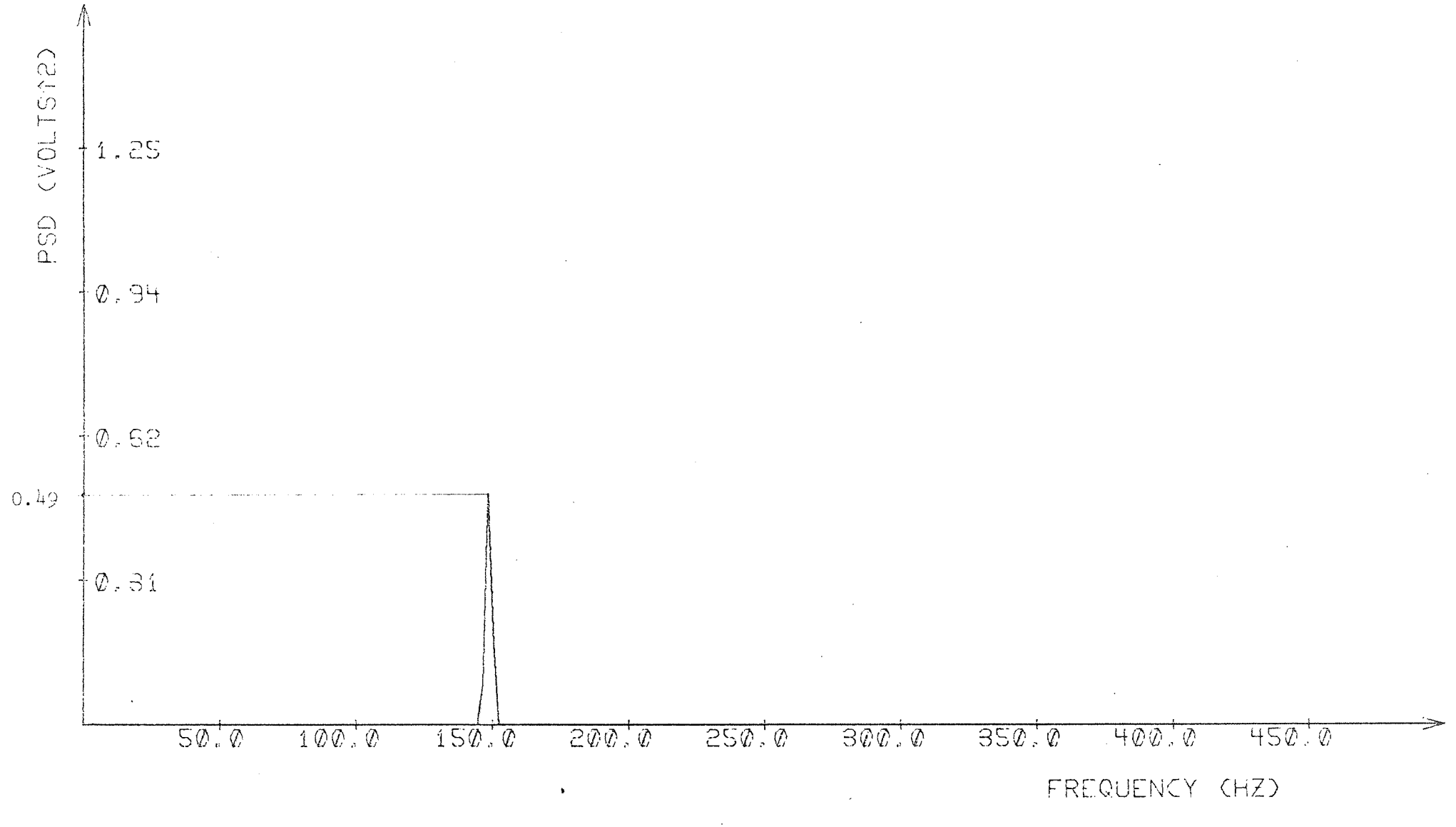

A/D-CONV. P.S.D. GRAPH NO: 9.

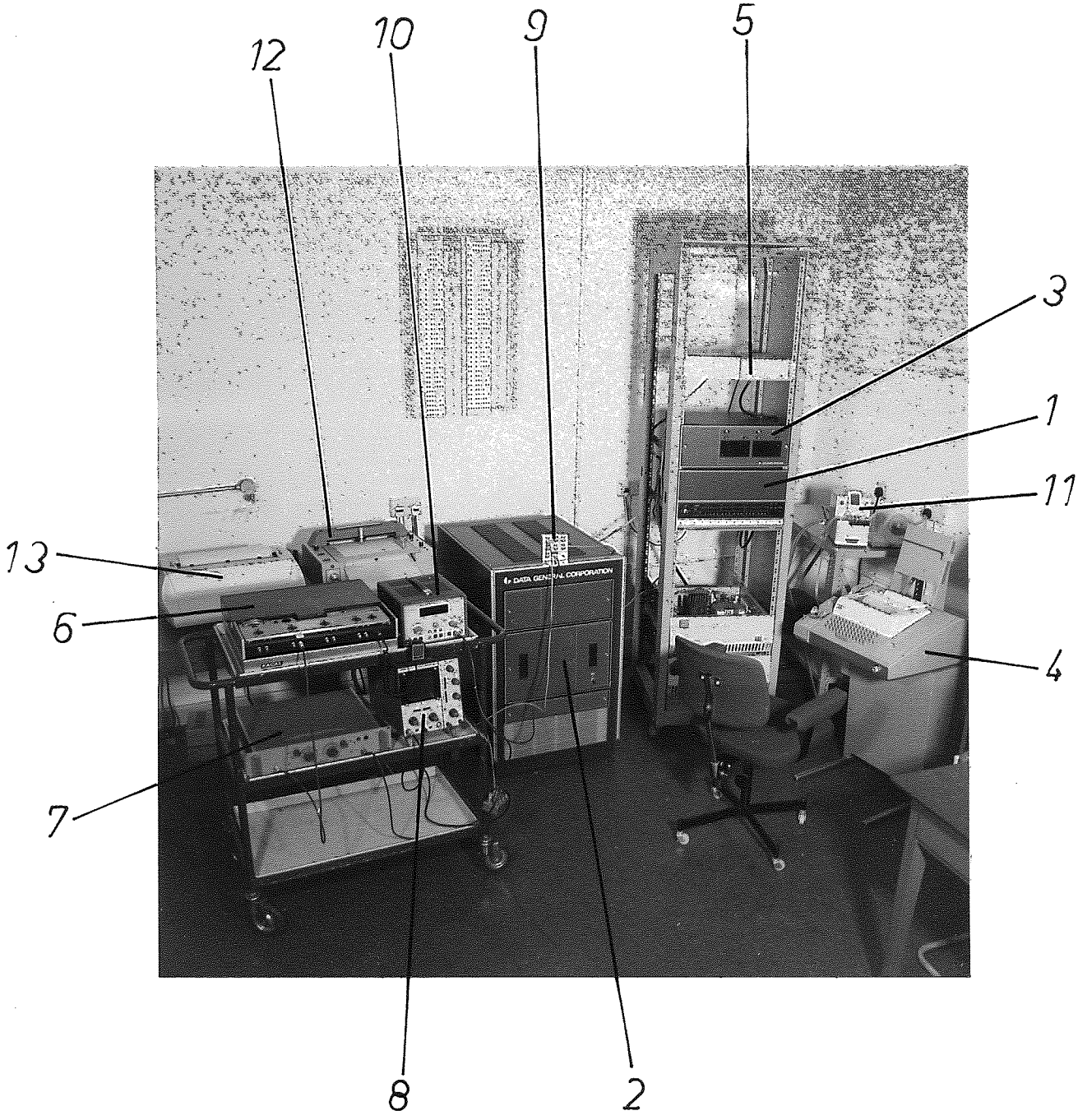

FIG II.1

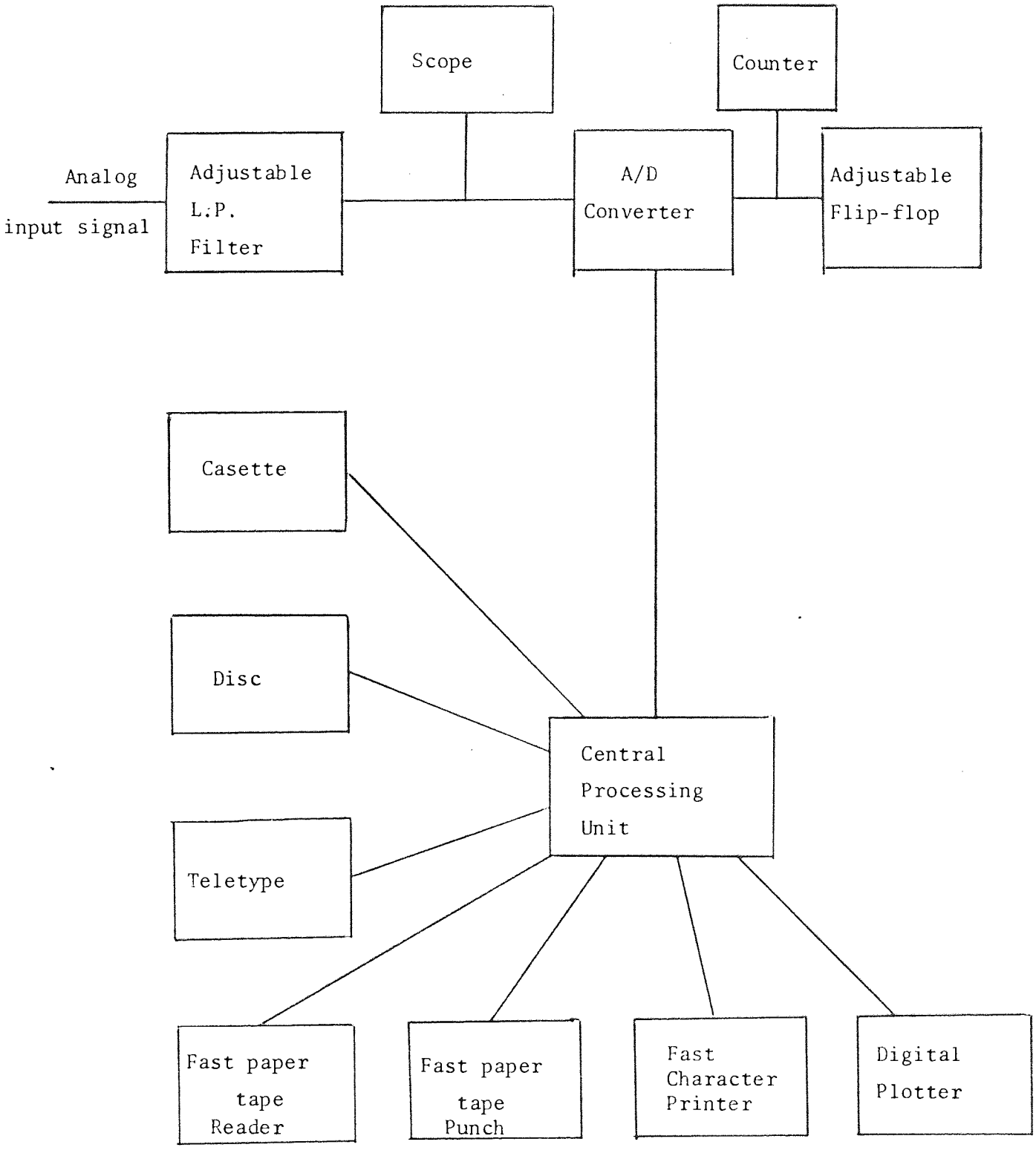

Fig. II.2 Hardware Layout.

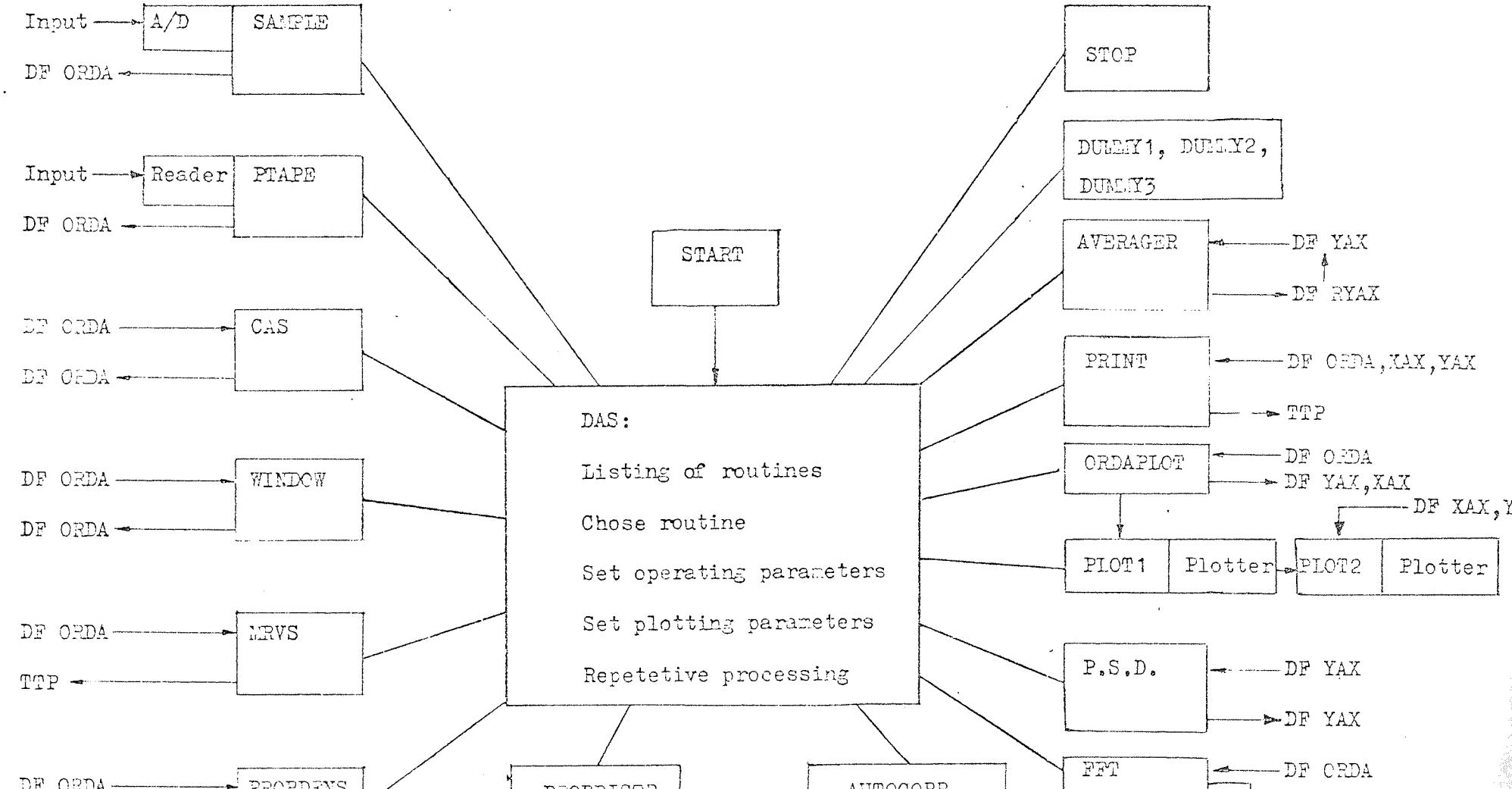

Fig. II.3. Arrangement of software for the DAS system.

DF stands for disk file and TTP for Teletype printer

APPENDIX III

AUTOCORRELATION AND SUMMATION ANALYSIS - A COMPARISON OF NOISE SUPPRESSION POWER

Consider a time varying function given by

$$Z(t) = A \cdot X(t) + B \cdot \sin\omega t \qquad \ldots\ldots\ldots \quad (III.1)$$

where $X(t)$ is white noise with an upper cut off frequency f_c. When the function $Z(t)$ is processed by Autocorrelation or Summation analysis, the resulting function will generally consist of a harmonic term, H, and a random term, R. Hence

$$\text{Autocorr } [Z(t)] = C(T,\tau) = H_1(\tau) + R_1(\tau) \ldots\ldots \quad (III.2)$$

and

$$\text{Sum } [Z(t)] = S(T,\tau) = H_2(\tau) + R_2(\tau) \ldots\ldots\ldots \quad (III.3)$$

where T is the averaging time of the processing. For both types of analysis, the R terms will approach zero as T goes to infinity. Since there is no practical problem in choosing the value for τ freely, τ (or for the discrete version, L) is henceforth assumed to be sufficiently large. Thus,

$$\lim_{T \to \infty} C(T,\tau) = H_1(\tau) = \frac{B^2}{2} \cos\omega\tau \qquad \ldots\ldots\ldots \quad (III.4)$$

τ large

and

$$\lim_{T \to \infty} S(T,\tau) = H_2(\tau) = B\sin\omega\tau \qquad \ldots\ldots\ldots \quad (III.5)$$

In practical analysis however, T will always have a finite value and the way in which R approaches zero is therefore determinative for the efficiency of the respective methods. Therefore define the signal to noise ratio of the Autocorrelation function and Summation function for Z(t) as

$$Q_c(T) = \frac{\text{Var}^{\dagger}[H_1]}{\text{Var}\ [R_1]} \quad \ldots\ldots\ldots \quad \text{(III.6)}$$

and

$$Q_s(T) = \frac{\text{Var}\ [H_2]}{\text{Var}\ [R_2]} \quad \ldots\ldots\ldots \quad \text{(III.7)}$$

respectively. For digital analysis the Z(t) function is assumed to be sampled at N equidistant points during time T. N is thus the discrete counterpart to T. We now want to compare the values of Q_c and Q_s for the averaging time T_o (or number of samples N_o).

Autocorrelation

From equation (III.4),

$$\text{Var}^*[H_1(\tau)] = \frac{B^4}{4} \cdot \text{Var}[\cos\omega\tau] = B^4/8 \quad \ldots\ldots\ldots \quad \text{(III.8)}$$

From equation (III.2)

$$R_1(\tau) = C(T_o,\tau) - H_1(\tau) \quad \ldots\ldots\ldots \quad \text{(III.9)}$$

To calculate the R_1 term, first set up the expression for the C term,

---

† The variance of a function is the mean square value of the function provided the function has first been made to have a zero mean value.

* $\text{Var}[A \cdot f(t)] = A^2 \cdot \text{Var}[f(t)]$

$$C(T_o,\tau)^* = \frac{1}{T_o}\int_o^{T_o} [A\cdot X(t) + B\cdot\sin\omega t]\cdot[A\cdot X(t+\tau) + B\cdot\sin\omega(t+\tau)]dt = \frac{A^2}{T_o}\int_o^{T_o} X(t)\cdot X(t+\tau)dt + \frac{AB}{T_o}\left[\int_o^{T_o} X(t)\cdot\sin\omega(t+\tau)dt + X(t+\tau)\cdot\sin\omega t\right] + \frac{B^2}{T_o}\int_o^{T_o}\sin\omega t\cdot\sin\omega(t+\tau)dt \quad \ldots\ldots\ldots \quad (III.10)$$

The last term of equation (III.10) is equal to H_1. R_1 is thus the first two terms of equation (III.10). The variance of these terms are calculated separately.

$$\mathrm{Var}\left[\frac{A^2}{T_o}\int_o^{T_o} X(t)\cdot X(t+\tau)dt\right] =$$

$$A^4\mathrm{Var}\left[\frac{1}{T_o}\int_o^{T_o} X(t)\cdot X(t+\tau)dt\right] \quad \ldots\ldots\ldots \quad (III.11)$$

The expression within the brackets is simply the autocorrelation of white noise. According to Chapter 6 of ref.(12), the variance of the estimate of the value for autocorrelation at lag τ for white noise band limited to f_c is

---

* $\mathrm{Autocorr}[f(t)] = C(T_o,\tau) = \frac{1}{T_o}\int_o^{T_o} f(t)\cdot f(t+\tau)dt$

The discrete counterpart is

$$C(N,L) = \frac{1}{N}\sum_{k=1}^{N} X(k)\cdot X(k+L)$$

$$\mathrm{Var}[C(T_o,\tau)] = \frac{1}{2f_cT_o}\,[C^2(0) + C^2(\tau)] \quad \ldots\ldots\ldots \quad (III.12)$$

With τ chosen sufficiently large, equation (III.12) simplifies to

$$\mathrm{Var}[C(T_o)] = \frac{C^2(0)}{2f_cT_o} = \frac{1}{2f_cT_o} \quad \ldots\ldots\ldots \quad (III.13)$$

Hence the variance of the first term is

$$\mathrm{Var}_1 = \frac{A^4}{2f_cT_o} \quad \ldots\ldots\ldots \quad (III.14)$$

The second term of equation (III.10) is then considered,

$$\mathrm{Var}_2 = A^2B^2\mathrm{Var}\left[\frac{1}{T_o}\int_o^{T_o} X(t)\cdot\mathrm{Sin}\omega(t+\tau)dt + \right.$$

$$\left. + \frac{1}{T_o}\int_o^{T_o} X(t+\tau)\mathrm{Sin}\omega t\,dt\right] \quad \ldots\ldots\ldots \quad (III.15)$$

The two integrals of this expression are the mean value of the respective products after the integration signs. According to Chapter 6 of ref.(12) the variance of the estimate of the mean value of a band limited white noise signal is

$$\mathrm{Var}[X(t)] = 1/2f_cT_o \quad \ldots\ldots\ldots \quad (III.16)$$

The X(t) term in equation (III.15) are weighted with on the average $1/\sqrt{2}$ during one cycle of the sine function. Hence the variance of each of the two terms of equation (III.15) is $1/4f_cT_o$ and

$$\mathrm{Var}_2 = A^2B^2/2f_cT_o \quad \ldots\ldots\ldots \quad (III.17)$$

Thus

$$\mathrm{Var}[R_1] = \mathrm{Var}_1 + \mathrm{Var}_2 = A^2(A^2 + B^2)/2f_cT_o \quad \ldots\ldots\ldots \quad (III.18)$$

Combining equations (III.8) and (III.18) then gives the signal to noise ratio for autocorrelation analysis,

$$Q_c = \frac{B^4 f_c T_o}{4A^2(A^2 + B^2)} \quad \ldots\ldots\ldots \quad (III.19)$$

Summation*

From equation (III.5)

$$\mathrm{Var}[H_2] = B^2/2 \quad \ldots\ldots\ldots \quad (III.20)$$

From equation (III.3)

$$R_2(\tau) = S(T_o,\tau) - H_2(\tau) \quad \ldots\ldots\ldots \quad (III.21)$$

From equation (III.21) it is clear that R_2 is the estimate of the mean value of X(t). By use of equation (III.16) the variance of the R_2 term then becomes

$$\mathrm{Var}[R_2] = A^2/2f_cT_o \quad \ldots\ldots\ldots \quad (III.22)$$

---

* In Summation analysis sampling sequences are initiated at the same points of the period of H_2. The samples are stored and the process repeated a number of times. Subsequently corresponding points of each sequence are added togcther thereby averaging out random components.

Equations (III.20) and (III.22) then give the signal to noise ratio for Summation analysis

$$Q_s = B^2 f_c T_o / A^2 \qquad \ldots\ldots\ldots \quad (III.23)$$

The relative efficiency of the two methods as regards noise suppression power then becomes

$$\frac{Q_c}{Q_s} = \frac{1}{4[(A/B)^2+1]} \qquad \ldots\ldots\ldots \quad (III.24)$$

Hence the value for Q_c/Q_s depends on the proportions of random and deterministic components of the time signal. For only a small contribution of noise the ratio is about 1/4. For equal proportions the ratio is 1/8 and for very high noise levels, Summation analysis has a much higher efficiency than Autocorrelation analysis.